NASA-CR-72588

FINAL REPORT

on

TECHNIQUES FOR FABRICATING ROCKET ENGINE COMPONENTS CONTAINING INTRICATE FLOW CHANNELS

by

A. N. Ashurst, M. Goldstein, and M. J. Ryan
BATTELLE MEMORIAL INSTITUTE
Columbus Laboratories
505 King Avenue
Columbus, Ohio 43201

prepared for

NATIONAL AERONAUTICS AND SPACE ADMINISTRATION
Lewis Research Center

August 1, 1969

Contract NAS3-11189

NASA Lewis Research Center
Cleveland, Ohio
John Kazaroff, Project Manager
Chemical Rockets Division

NASA-CR-72588

FINAL REPORT

on

TECHNIQUES FOR FABRICATING ROCKET ENGINE COMPONENTS CONTAINING INTRICATE FLOW CHANNELS

by

A. N. Ashurst, M. Goldstein, and M. J. Ryan
BATTELLE MEMORIAL INSTITUTE
Columbus Laboratories
505 King Avenue
Columbus, Ohio 43201

prepared for

NATIONAL AERONAUTICS AND SPACE ADMINISTRATION
Lewis Research Center

August 1, 1969

Contract NAS3-11189

NASA Lewis Research Center
Cleveland, Ohio
John Kazaroff, Project Manager
Chemical Rockets Division

TABLE OF CONTENTS

TABLE OF CONTENTS (Continued)

LIST OF TABLES

LIST OF TABLES (Continued)

LIST OF ILLUSTRATIONS

LIST OF ILLUSTRATIONS (Continued)

LIST OF ILLUSTRATIONS (Continued)

LIST OF ILLUSTRATIONS (Continued)

LIST OF ILLUSTRATIONS (Continued)

FOREWORD

The research described herein was conducted by Battelle Memorial Institute, Materials Design and Fabrication Division, and performed under NASA Contract NAS3-11189. The work was done under the management of the NASA Project Manager, Mr. John Kazaroff, Chemical Rockets Division, NASA-Lewis Research Center. The hot-pressing data for the densification rate curves shown in Figures I-7 through I-10 were generously supplied by Mr. E. G. Smith of Battelle. Program management during the Task I phase of work by Mr. D. C. Carmichael of Battelle is recognized, and conduction of portions of the Task I studies, particularly the thermochemical calculations and development of the borosilicate glass tooling by Dr. Darrell Ownby, is gratefully acknowledged.

ABSTRACT

Powder metallurgy techniques were developed to fabricate simulated rocket engine components having intricate internal flow channels. To demonstrate these techniques, two simulated components of different and complex design were fabricated. One consisted of a copper baffle component of the "film and convection" cooling design concept. The other component was a nickel injector having a "shower head" design with fuel and oxidizer ports separated at the injector face.

The components were fabricated by consolidating powder around compatible and selectively leachable tooling using the hot-isostatic-compaction process. The dimension, alignments, and contours of the tooling representing the internal flow channels were maintained with high precision during powder densification and bonding. The tooling was removed solely by chemical dissolution; no machining other than to expose the tooling at the surface of the components was required.

Pressure testing of simulated copper baffles was accomplished with hydrostatic pressures of 700 psi and higher for 5 min. The copper powder achieved densities higher than 98 percent of theoretical densities and mechanical properties that were equivalent or better than commercially pure wrought and annealed copper products. Helium leak testing of the simulated nickel injectors was accomplished with no detectable leakage between the bipropellant channel systems. The nickel powder achieved densities higher than 97 percent of theoretical density.

SUMMARY

Powder metallurgy techniques were developed to fabricate rocket engine components containing intricate internal flow channels. The technique involves consolidating and bonding powder materials around selectively removable tooling by the hot-isostatic compaction process.

The tooling for each component was selected based on known physical and metallurgical properties, thermochemical calculations, and compatibility with component materials. The final selection was made after compatibility and leachability tests were conducted on fabricated samples. A borosilicate glass was chosen for the tooling in the copper baffles. The glass was compatible with copper and was selectively removed with a $67HF\text{-}33H_2O$ solution. Two tooling materials, 1018 steel and 1100 aluminum, were found desirable for the nickel injectors. Aluminum formed NiAl intermetallics at the interface during hot-isostatic compaction and prevented further reaction between aluminum and nickel. However, the brittle intermetallics were considered to be possible sources of cracks during injector operation. Therefore, the 1018 steel tooling material was selected over aluminum. The steel was selectively removed with a $25H_2SO_4\text{-}75H_2O$ solution. The aluminum can be quickly removed with either a 8M NaOH solution or a dilute HCl solution.

During compatibility testing and powder process development, copper powder was consolidated around glass tooling by hydropressing at 20,000 psi without fracturing or displacing the tooling provided the tooling was located geometrically on a plane of equal pressure. The copper was then densified to better than 98 percent of its theoretical density by hot-isostatic compaction at 1000 F and 10,000 psi for 3 hr. Nickel powder was consolidated around steel tooling and around aluminum tooling by hydropressing at 80,000 psi followed by hot-isostatic compaction at 1200 F and 10,000 psi for 3 hr to better than 98 percent of theoretical density. After modifying the design of the nickel injector, the hydropressing was unnecessary and was eliminated.

Full scale baffle components were fabricated from copper powder using the borosilicate glass tooling. Complete densification to near theoretical density was achieved and the baffle was successfully hydrotested at 700 psig for 5 min. The glass tooling maintained dimensions and alignment to within ±0.01 in. Surface finish within the channels was smooth, and flow channels were unimpeded. Mechanical properties of the densified copper powder were comparable or better than wrought and annealed commercial copper products. Grain sizes were very fine owing to the initial powder size and limited grain growth at the low bonding temperatures.

Full size injector components were fabricated from nickel powder using low carbon steel for the tooling. To maintain the alignment of the two different, bi-propellent flow systems within the injector, one set of tooling, representing the oxidizer flow channels, was first fixed in position by consolidating nickel powder around this system of tooling. The other tooling system, representing the fuel channels, was then assembled onto the first set. Nickel powder was consolidated around the second tooling system while simultaneously bonding it to the nickel around the first set of tooling. By this technique, the nickel powder achieved densities of about 97 percent of theoretical while maintaining alignment and dimensional control of the flow channels to within ±0.01 in. of specified tolerances except for a few tooling pins near the outer edge. These pins were distorted out of tolerance because the powder was compacted nonuniformly and tended to flow preferentially towards the edges. Helium leak tests of the injector was accomplished with no detectable leakage between the bi-propellant channel systems.

The successful fabrication of these components demonstrated the feasibility of fabricating complex hardware containing intricate internal flow channels by hot isostatically compacting powder metals.

INTRODUCTION

Background

Rocket engine components which contain intricate and complex internal flow passages are difficult and costly to produce. The components require close dimensional control that necessitates accurate and usually extensive machining. In many cases, these components cannot be made in one piece and require the joining of two or more subassemblies. The joining processes generally used to bond various components, such as brazing, soldering, fusion welding, or solid-state bonding, have a number of problems associated with them, including plugging of internal passages, internal burrs which can impede flow, and warpage. Many of these difficulties can be eliminated and a savings in cost realized by fabricating such components as a single piece from powder.

Scope of Work

The present effort was initiated to develop powder metallurgy techniques for fabricating structures containing intricate internal flow systems that require close dimensional control.

The two components selected for this program to demonstrate these powder metallurgy techniques were the copper straight component test sample or baffle as redrawn in Figure I-1 from NASA Drawing No. CF620868, and a simulated nickel injector test piece redrawn in Figure I-2 from NASA Drawing CF620867. The baffle design chosen for this effort is of the "film and convection" cooling scheme which was identical to baffles fabricated and used for M-1 engine development. The baffle is incorporated with the injector to reduce the possibility of deleterious instability. The simulated injector is typical of a "shower-head" design having

B

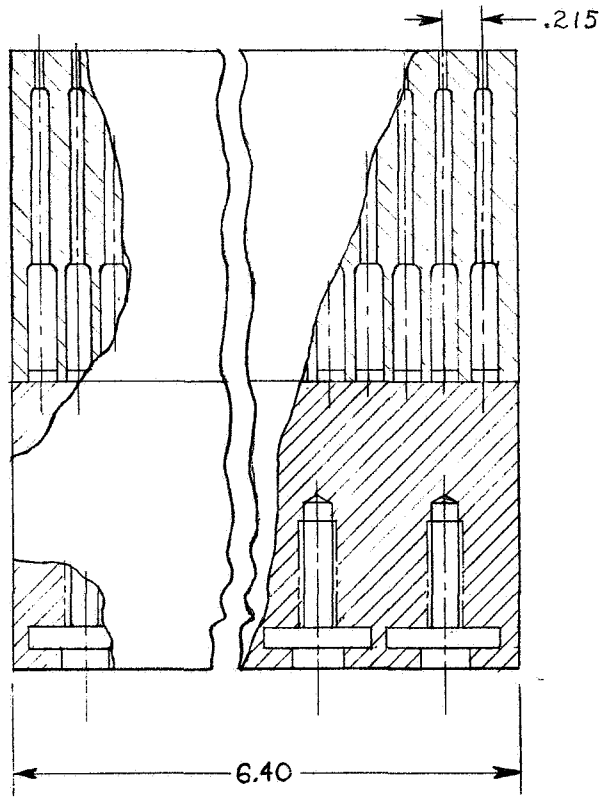

SECTION D-D

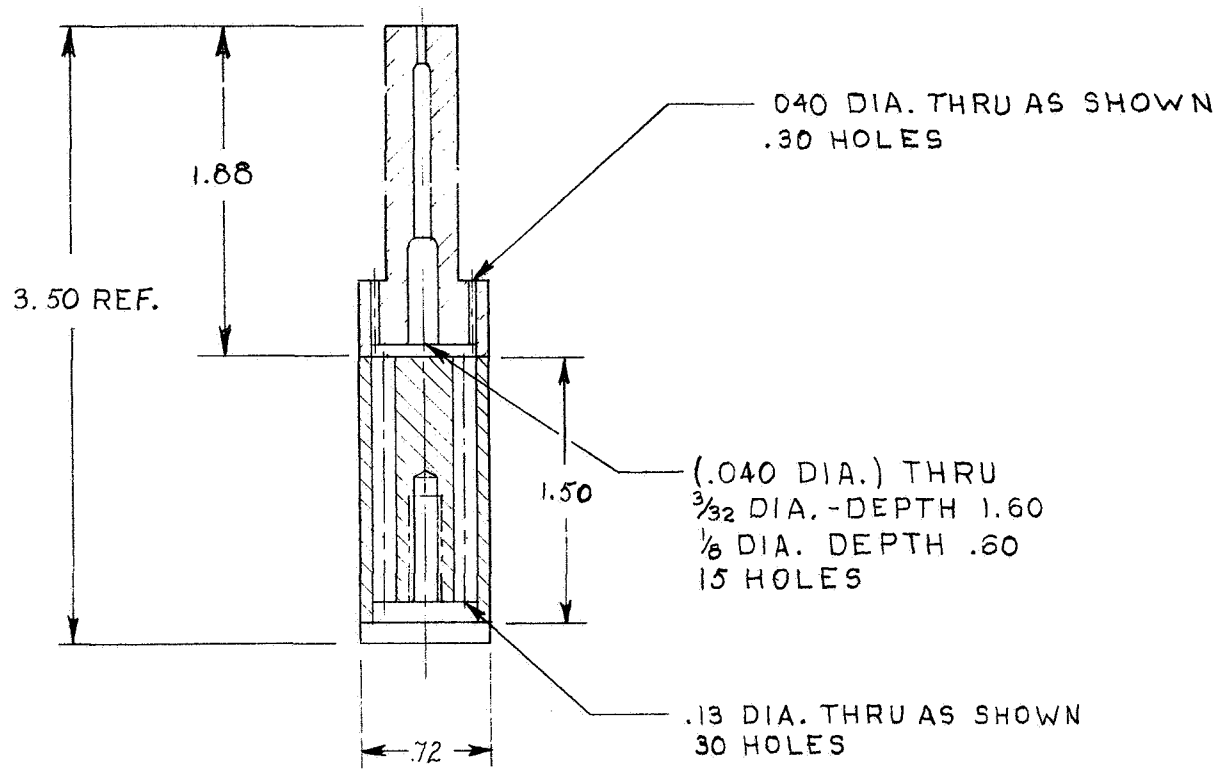

SECTION B-B

NOTE:

SECTIONS SHOWN ARE REDRAWN FROM NASA-LEWIS REVISED DRAWING NO. CF 620868 DATED 6-23-67

ZONE	REV. LET.	REVISIONS	BY	DATE

MAT'L. (COMMERCIAL TOLERANCES APPLY)

OFHC COPPER

TOLERANCE UNLESS OTHERWISE NOTED		
FRAC. ±	ANG. ±	DEC.

	DRAWN	CHECKED	PROJ. APP.
BY			
DATE			
DIV.			

NEXT ASSY.	NO. REQ'D.

SCALE	K-G

BATTELLE MEMORIAL INSTITUTE
505 KING AVE.
COLUMBUS 1, OHIO

TITLE
STRAIGHT COMPONENT
COPPER BAFFLE

ACCT. NO.

DWG. NO. Figure I-1

B

B

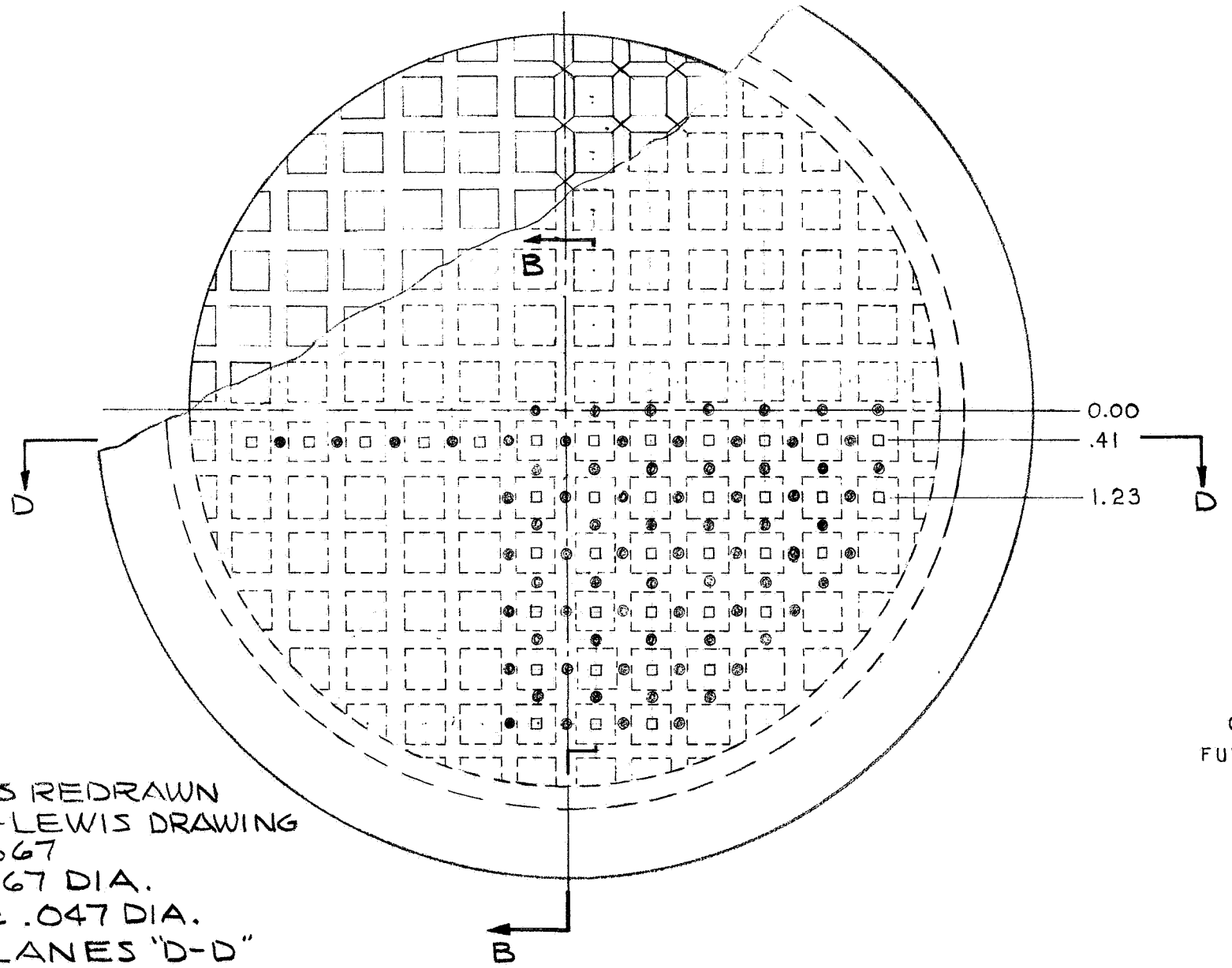

SECTION B-B

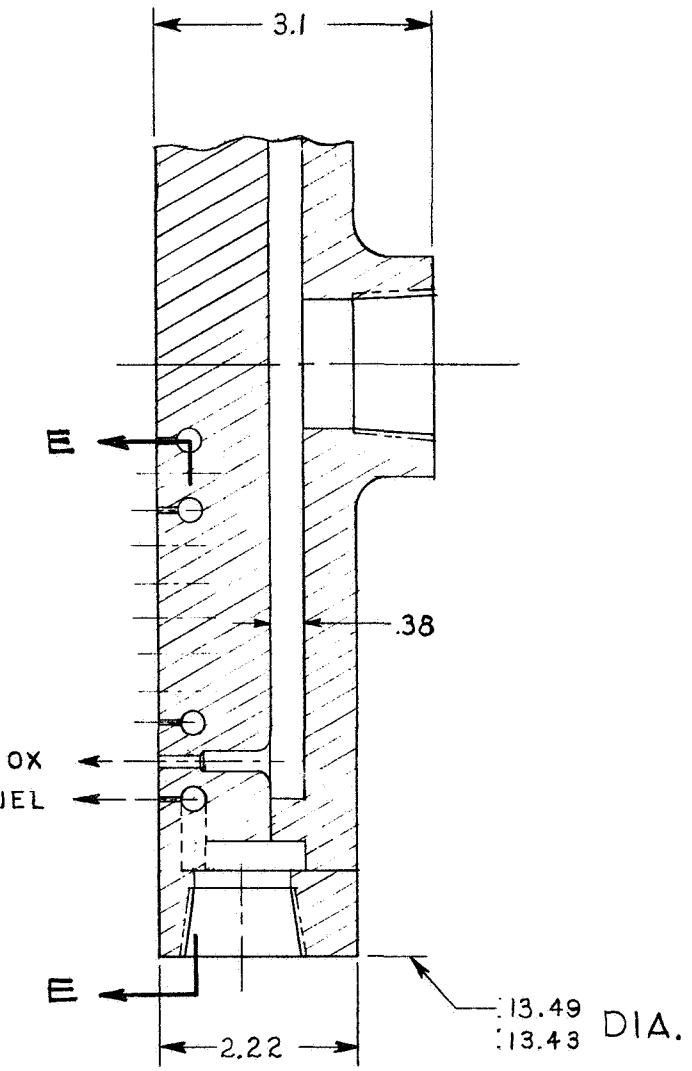

NOTE:

1. THIS SKETCH IS REDRAWN FROM NASA-LEWIS DRAWING NO. CF 620867
2. OX HOLE .067 DIA.
3. FUEL HOLE .047 DIA.
4. SECTION PLANES "D-D" AND "EE" SHOWN IN THIS FIGURE ARE THE SECTIONS REFERRED TO IN REPORT ON WHICH TESTING AND INSPECTION OF TEST SAMPLE NO. 1 WAS ACCOMPLISHED.

ZONE	REV. LET.	REVISIONS	BY	DATE

MAT'L. (COMMERCIAL TOLERANCES APPLY)
NICKEL

TOLERANCE UNLESS OTHERWISE NOTED		
FRAC. ±	ANG. ±	DEC.

	DRAWN	CHECKED	PROJ. APP.
BY			
DATE			
DIV.			

NEXT ASSY.	NO. REQ'D.

SCALE | K-G

BATTELLE MEMORIAL INSTITUTE
505 KING AVE.
COLUMBUS 1, OHIO

TITLE
SIMULATED NICKEL INJECTOR TEST SAMPLE

ACCT. NO.

DWG. NO. Figure I-2

B

HILLS CO.—10-5155—1000—10-68

separated fuel and oxygen systems into the face plate. These two components typify the complexity of the flow system required in many mixing, combustion, and cooling systems and thus are well suited to demonstrate the feasibility of using powder fabrication techniques to produce these and similar structures containing intricate internal flow channels.

Special Facility Used in Program

The hot-isostatic-compaction process was selected as the approach for making components of these complex shapes. The principal technical requirements of the process, which are all met by the hot-isostatic-compaction method are:

(1) Use of the lowest possible compaction temperature to minimize tooling compatibility problems and permit the widest possible selection of tooling materials.

(2) Application of uniform, isostatic, high pressure to obtain maximum densification in all regions of complex shapes and to avoid tooling distortion during densification.

The Hot-Isostatic-Compaction Process

Basically, the hot-isostatic compaction technique is an idealized hot-pressing operation performed in a high-pressure autoclave in which a compaction force is applied by a high pressure of inert gas at elevated temperatures. The isostatic pressurizing medium is the unique character of this technique as compared to conventional methods.

In this process, a large cold-wall autoclave containing a resistance heater is used to attain the high gas pressures and temperatures required for compaction or bonding. Insulating material is located between the wire-wound

resistance heater and the inside wall and heads of the high-pressure autoclave to prevent appreciable heating of the cold-wall vessel. A sectional view of the autoclave used in the program is shown in Figure I-3. To prepare assemblies for processing, the powders to be densified are preformed by vibratory packing and/or hydropressing, assembled into a thin metal container, then evacuated and sealed. The sealed assemblies are then placed in the heater inside the autoclave and the temperature and pressure required for compaction and bonding are applied. At temperature, the high gas pressure in the system is uniformly transmitted through the container walls from all directions to the contained material. The powder particles to be compacted are deformed, and complete surface contact and solid-state bonding of the particles occurs.

Selection of the metal to be used for the container is based upon the following factors: compatibility with the material being processed, the relative thermal expansions of the materials, forming and welding characteristics, ability to be removed after processing, and ability to deform plastically at the processing temperature. A slight reaction of the container with the powder material is tolerable since the exterior surface can be machined after hot-isostatic compaction.

Purpose of Program

The objectives of the program are:

(1) To develop expendable tooling for powder metal systems

(2) To investigate process variables and optimize the fabrication process

(3) To fabricate and test subscale components containing intricate internal flow channels using the optimum powder metallurgy techniques with the developed tooling.

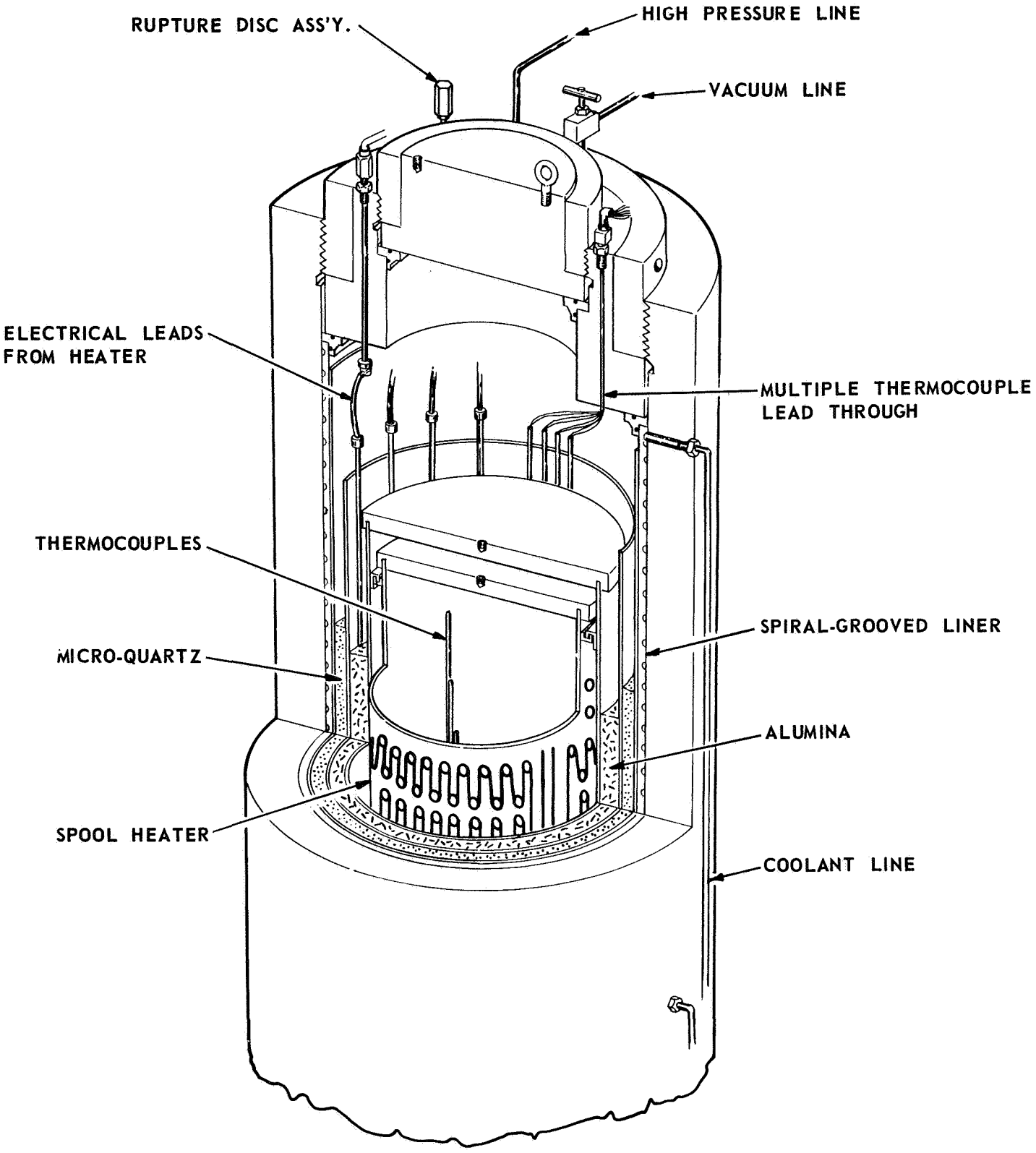

FIGURE I-3. COLD WALL HOT-ISOSTATIC COMPACTION AUTOCLAVE

Definition of Task Work

The program was divided into three tasks:

Task I. Tooling Development, Process Optimization, and Inspection Techniques

Task II. Fabrication and Testing of Simulated Copper Baffles

Task III. Fabrication and Testing of Simulated Nickel Injectors.

Task I studies involved three subtasks. In Subtask A, expendable tooling materials were selected by thermochemical calculations, compatibility data analyses, determination of solubility rates, and ease of fabrication. Tests to verify suitability and compatibility of candidate tooling materials were conducted. In Subtask B, powder-fabrication techniques and parameters were developed using powder samples of simplified designs. Subscale components were fabricated to optimize the tooling and compaction processes. In Subtask C, techniques were established to evaluate these samples nondestructively by radiographic inspection and flow tests. The samples were also examined destructively by sectioning.

Task II studies were divided into two subtasks. In Subtask A, baffle component test pieces were fabricated from copper powder utilizing the internal tooling, powder metallurgy techniques, and processing methods developed in Task I. The principal parts required to fabricate this rocket engine component consisted of the internal tooling, two solid copper fixtures, copper powder, and a rigid external frame made of steel. In Subtask B, the fabricated baffle was evaluated by nondestructive tests developed in Task I and by a hydrostatic pressure test at 700 psig for 5 min. The components were then destructively examined by sectioning, metallographic analysis, tensile tests, and dimensional inspections.

Task III studies involved two subtasks. Subtask A required the fabrication of prototype injector component test pieces by the methods and processes developed in Task I. The principal parts of this component consisted of the tooling, a

nickel base support and nickel powder. In Subtask B, the injectors were tested nondestructively by flow tests and helium leak tests to verify nonleakage between the bi-propellant flow systems. Additional nondestructive tests were made by techniques developed in Task I and then the injectors were inspected destructively by sectioning.

TASK I STUDIES: FABRICATION AND TESTING OF SUBSCALE PROTOTYPES

Subtask I-A: Compatibility Testing and Development of Expendable Tooling

The objective of this subtask was to select and develop expendable tooling required for the fabrication of copper and nickel components.

A survey of the literature on physical, metallurgical, and thermochemical properties of materials was conducted to screen candidate materials from several classes of materials, including metals, salts, soluble glasses, and composites. Candidate materials were chosen on the basis of their melting points and the temperature at which adverse reactions occurred with the base metals. Candidate tooling materials considered in the metals class are listed in Table I-1. Binary and ternary compounds considered for tooling applications are listed in Table I-2 along with available physical properties and results of thermochemical calculations.

Those materials that were costly, difficult and expensive to fabricate, and toxic were eliminated. Many of the ternary compounds tended to absorb or react with water from the atmosphere and would make the fabrication of sound tooling from these materials difficult and expensive. The compatibility of the remaining materials was examined for adverse reactions at about 1350 F, slightly higher than the maximum temperature that was used for hot-isostatic compaction. Those materials showing a negative change in the free energy of formation with the base metals were eliminated. Materials that were going to be difficult to remove from the components were also eliminated from further consideration.

One of the candidate materials that proved to have substantial promise was graphite. Experiments were conducted late in the program and the results were not available until recently. Several rods and a ring of ATJ graphite were machined, coated with a thin layer of nickel by electroless coating techniques, then assembled into nickel powder and sealed in low carbon steel containers.

TABLE I-1. CANDIDATE TOOLING MATERIALS: METALS

Metal	Eutectic Reactions with Copper, C	Eutectic Reactions with Nickel, C
Ag	779	960
Al	548	640
Au	889	950
B	1060	990
Ba	550	None
Be	1512	1157
C	None	None
Ca	560	--
Co	None	None
Cr	1075	1345
Fe	None	None(a)
Ge	640	775
Mg	485	507
Mn	870	(b)
Mo	--	1315
Nb	--	1175
Ni	None	--
Os	None	None
Pt	None	None
Re	None	None(c)
Rh	None	--
Ru	None	(d)
Sb	526	626
Si	802	964
Ta	None	1360
Th	881	1000
Ti	885	942
U	950	740
V	None	1203
W	None	None
Zn	(e)	(e)
Zr	885	961

(a) Fe-Ni system has a minimum of 1440 C.
(b) Mn-Ni system has a minimum at 1018 C.
(c) Re-Ni system alloys easily.
(d) Ru-Ni system is probably a solid solution, but amounts of solubility not known.
(e) Zn melting point of 419 C is too low for tooling use.

TABLE I-2. CANDIDATE TOOLING MATERIALS: COMPOUNDS

Compound	Melting or Sublimation Point, C	ΔF of Formation at 1000 K (kcal/gram-atom) With Cu	With Ni
Na_2O	1275	+43.0	+28.5
CdO	900 d.	+15.5	+1.0
ZnO	1975	+36.5	+22.0
MgO	2800	+96.5	+82.0
CaO	2580	+105.0	+80.5
Al_2O_3	2045	+86.5	+72.0
SnO_2	1127	+22.0	+8.5
SiO_2	1610	+60.5	+46.0
TiO_2	1825	+68.5	+54.0
ZrO_2	2715	+85.5	+71.0
HfO_2	2812	+97.5	+83.0
Cr_2O_3	2435	+46.5	+32.0
NiO	1990	+14.5	--
CoO	1935	+14.0	-0.5(a)
Fe_3O_4	1538 d.	+25.0	+10.5
BaO	1923	+88.5	+74.0
Li_2O	1700	+87.5	+73.0
MoO_3	795	+17.5	+3.0
WO_3	1473	+25.0	+8.5
Mn_2O_3	1080	+34.5	+20.0
NaCl	801	+55.0	+57.5
$CaCl_2$	772	+57.0	+59.5
$BaCl_2$	925 tr.	+63.0	+65.5
$CrCl_2$	824	+11.5	+14.0
$NiCl_2$	1001	+2.5(a)	--
KF	880	+62.0	+48.5
NaF	980	+64.0	+50.5
LiF	870	+75.0	+61.5
CdF_2	1040	+15.0	+1.5
ZnF	872	+19.5	+6.0
MgF_2	1266	+63.0	+49.5
CaF_2	1360	+77.0	+63.5
AlF_3	1040	+41.0	+27.5
TiF_3	1200	+39.0	+25.5
PbF_2	855	+12.0	-1.5(a)
CrF_2	1100	+26.5	+13.0
FeF_2	> 1000 (?)	+19.5	+6.0
CoF_2	1200	+14.0	+0.5
MnF_2	856	+30.5	+17.0

TABLE I-2. (Continued)

Compound	Melting or Sublimation Point, C
(b)	
$BaBr_2$	847
NiB_2	963
BeC	2100
LiH	1239
K_2S	840
Ag_2S	825
Na_2S	1180
$LiBO_4$	840
$CdSO_4$	1000
$CoSO_4$	989
$PbSO_4$	1000 d.
$LiSO_4$	860
$MgSO_4$	1124 d.
K_2CO_3	891
K_2CrO_4	968
K_2GeO_3	823
$K_2Ge_4O_9$	1033
$K_2MoO_4 \cdot H_2O$	919
Ag_3PO_4	849
$NaAlO_2$	1650
$NaBO_2$	966
$NaCO_3$	851
Na_3AlF_6	1000
Na_2SO_4	884
$Na_4P_2O_7$	880
$Zn_3B_4O_9$	980

d. = decomposes
tr. = transforms

(a) Tentatively eliminated due to possible reaction.

(b) Thermochemical calculations were not required on the following compounds. These materials were eliminated for other reasons.

The ring specimen was sintered at 2100 F in vacuum for approximately 50 hr. The rod specimens were hot-isostarically compacted at 1300 F and 10,000 psi for 4 hr.

The graphite rods were exposed on each end by cutting through the surrounding dense nickel. Three techniques were attempted to selectively remove the graphite from the nickel matrix. In one, the specimen was placed in a muffle furnace, heated to 1400 F, and the graphite recession rate in air determined. In the second, the specimen was placed in a gas furnace, heated to 1400 F, and the graphite recession rate in the gas atmosphere measured. The third technique involved the use of a copper nozzle directed at the exposed graphite surface. The specimen was placed in a gas furnace heated to 1400 F, and superheated steam was injected through the nozzle into the hole channel containing the graphite rod. The graphite recession rate was determined to be higher with this third technique than in the other experiments. A comparison of recession rates is shown in Figure I-4.

The ring specimen was then placed in a gas furnace, heated to 1400 F, and the graphite removed by the steam injection technique. It was noted that the use of demineralized water during steam production prevented a buildup of scale on the surfaces that otherwise retarded the graphite recession rate. After partially removing the graphite, the ring specimen was examined by radiography. A radiograph of the specimen is shown in Figure I-5. The specimen was sectioned to examine the internal channels. A photograph of the sectioned ring specimen is included in Figure I-6.

Graphite can be easily machined into suitable tooling configurations, it is compatible with the base metals at high temperatures, and it can be rapidly removed from consolidated powder matrices. The use of graphite for selectively removable tooling is thus shown to be very promising.

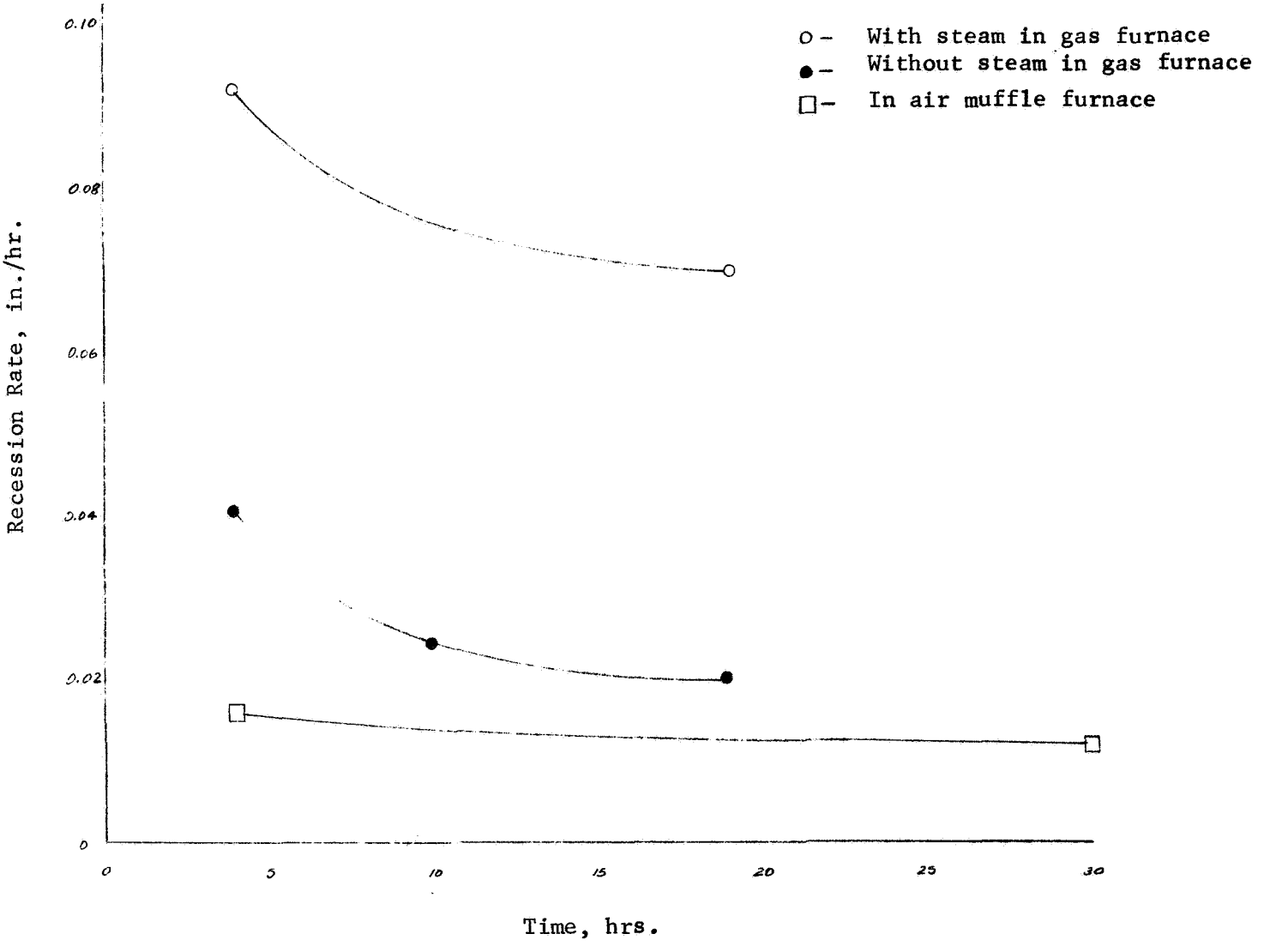

FIGURE I-4. GRAPHITE RECESSION RATE AT 1400 F

Each specimen consisted of a 1/4 in. diameter ATJ rod in hot-isostatically compacted nickel powder.

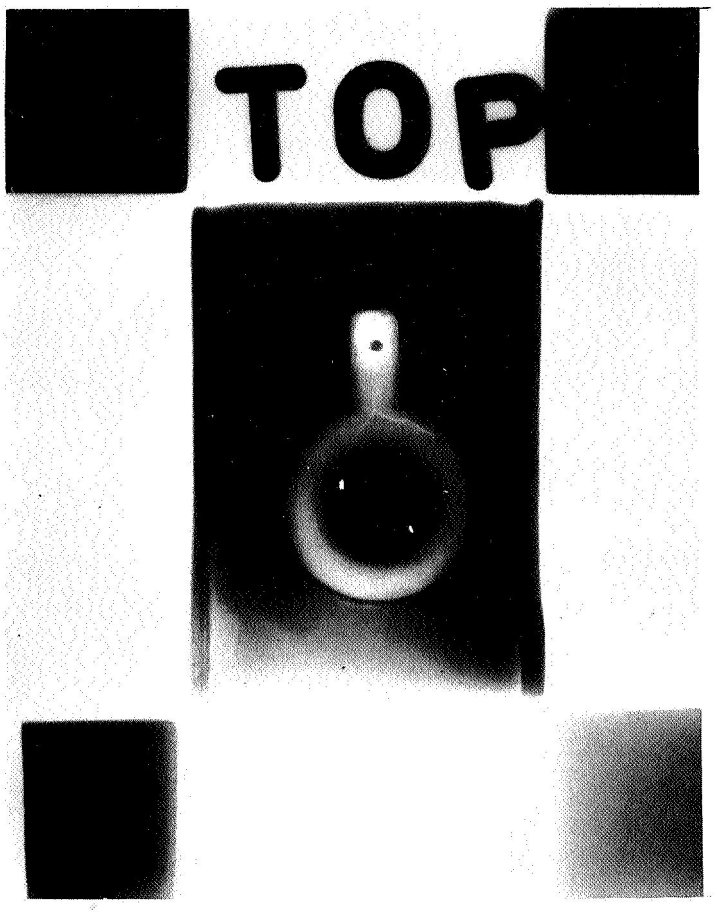

FIGURE I-5. RADIOGRAPH OF GRAPHITE RING SPECIMEN

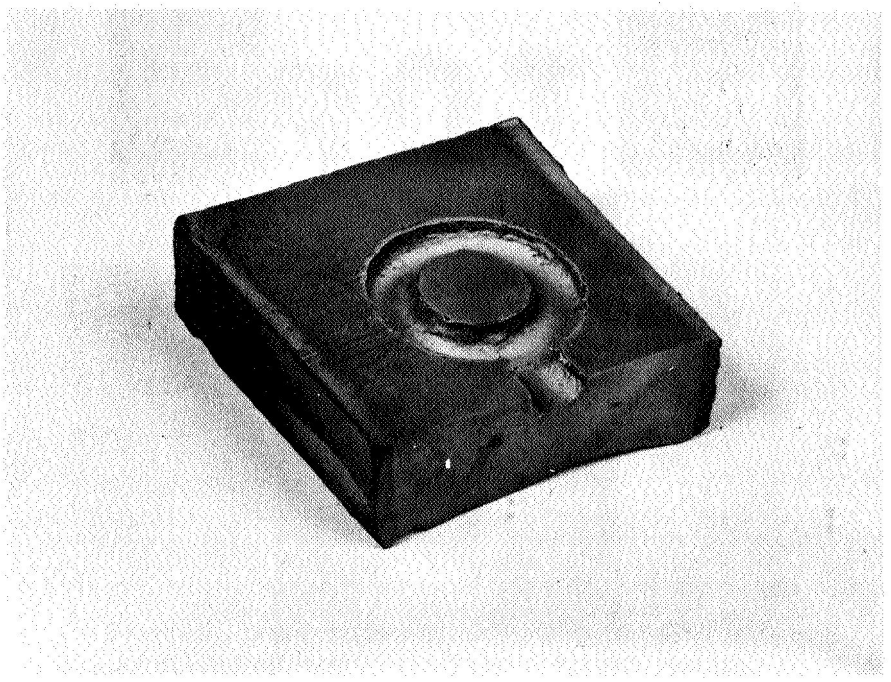

FIGURE I-6. PHOTOGRAPH OF SECTIONED GRAPHITE RING SPECIMEN

Compatibility and leachability tests were conducted on other potential tooling materials. These consisted of 1018 steel, 1100 aluminum coated with a thin layer of chromium, calcium encapsulated in a thin iron sheath, and three types of glass (borosilicate, lead, and pure silica). Three metal oxides (NiO, ZnO, and MgO) were also studied but subsequently dropped because of negligible leaching rates. Aluminum was coated with a thin layer of chromium to reduce reactions between the base metal and the aluminum. Without the protective coating on aluminum, gross alloying and eutectic reactions were expected during hot-isostatic compaction. Likewise, calcium was protected by a thin iron or steel sheath to prevent adverse reactions between the calcium and base metals. Even though calcium and aluminum had to be protected with barrier coatings, their use as tooling was still considered practical since both metals could be quickly removed in various solutions or could be melted out after consolidation of the base metal powders around the tooling. Both materials are inexpensive. Both could be fabricated into the complex tooling shapes by casting techniques or by machining. While neither metal was subsequently chosen as the tooling material to prepare full size components in Tasks II and III, these investigations showed that their use was feasible.

Compatibility test specimens were prepared by incorporating cylinders of the candidate materials in specimens of the base metal powders. The 1018 steel and the three glasses were machined or ground to cylindrical shapes and assembled in the base metal powders by vibratory packing the powder around the cylinders. Two techniques were attempted to fabricate calcium into suitable shapes. The ingot was encapsulated in a thin steel tube and swaged to about 1/8 in. diameter. In another experiment, the ingot was kept lubricated with mineral oil and swaged to 1/8 in. diameter without using a steel container. Calcium was fabricated by this latter technique into the desired shapes, then following the swaging of calcium,

the metal was cleaned with acetone and encapsulated in a thin steel tube for assembly into compatibility specimens. Aluminum cylinders were cut and machined from 1100 stock. Several different coating techniques were attempted to coat the aluminum with a thin film on chromium. Two of these coating techniques proved to be satisfactory and are summarized in Table I-3. The most suitable technique for circular pieces was found to be barrel tumble plating, while for the square and irregular shaped tooling, the zincate dip technique proved to be best.

The compatibility specimens were hydropressed and hot-isostatically compacted at the optimum conditions determined during the powder metallurgy process development subtask (see Subtask I-B). Specimens with copper powder were hydropressed at 20,000 psi and hot-isostatically compacted at 1000 F and 10,000 psi for 3 hr. Specimens with nickel powder were hydropressed at 80,000 psi and hot-isostatically compacted at 1200 F and 10,000 psi for 3 hr. The specimens were sectioned for metallographic examination and leach tests.

No significant interdiffusion of the steel tooling into copper or nickel was detected. The chromium barrier layer was effective in preventing diffusion of aluminum into copper at 1000 F for 3 hr. Above that temperature, interdiffusion and reaction of aluminum in copper was observed. The chromium barrier layer was likewise ineffective in preventing diffusion between aluminum and nickel. However, gross reactions and alloying did not occur in this system because of the formation of intermetallics at the nickel-aluminum interface. Although the eutectic reaction for aluminum-nickel occurs at about 640 C (1190 F), the diffusion of aluminum into nickel is retarded by the formation of hard intermetallic compounds at the interface. These compounds act very effectively as diffusion barriers and prevent further reactions between aluminum and nickel. No reactions or significant diffusion occurred between the 7052 glass and copper or between SiO_2 and copper. Significant diffusion did occur between the 0120 lead glass and copper

TABLE I-3. DEPOSITION TECHNIQUES USED TO COAT 1100 ALUMINUM TOOLING

Al-Ni-Cr (Barrel Tumble Plating)	Al-Zincate dip-Cr (Rack Plating)
1. Degrease Al in methyl-ethyl-ketone	1. Degrease Al in methyl-ethyl-ketone
2. Rinse in ethanol	2. Rinse in ethanol
3. Rinse in water	3. Rinse in water
4. Chemically polish 1 min. at R.T. in 750 ml HNO_3-220 ml HF-720 ml H_2O	4. Chemically polish 1 min. at R.T. in 750 ml HNO_3-220 ml HF-720 ml H_2O
5. Rinse in water	5. Rinse in water
6. Plate in nickel sulfamate bath at 40 ASF for 30 min. at 120 F (a)	6. Immerse in commercial zincate dip for 30 sec.
7. Rinse in water	7. Dip in chemical polish (Step 4)(c)
8. Plate in acid chromium bath at 250 ASF for 80 min. at 120 F (b)	8. Rinse in water
9. Rinse in water	9. Repeat Step 6
	10. Repeat Steps 7 through 9 until a uniform coating is achieved
	11. Plate in acid chromium bath at 500 ASF for 20 min. at 120 F (d)
	12. Rinse in water

(a) Produces a nickel intermediate layer about 0.001 in. thick.
(b) Produces a chromium coating about 0.0005 in. thick.
(c) Chemically strips the zincate coating.
(d) Produces a chromium coating about 0.0005 in. thick.

which resulted in a rough, porous surface layer in the copper. Calcium was effectively encapsulated in the steel and no reaction or significant diffusion was observed with the nickel.

Tests were performed on the materials to determine leach rates, effects of fabrication techniques on leaching behavior, effect of the leaching solution on the surface finish of the base material, and to determine if residue products of leaching were left behind that would impair the flow through the internal channels of the components. The results of leach tests on these materials are presented in Table I-4. Attempts to leach sintered metal oxides at any appreciable rate were unsuccessful. The glass was leached at a significant rate which was found to be comparable to that for aluminum and faster than the leach rate for steel. Calcium metal was removed easily and quickly in tap water or in a slightly acidic aqueous solution. Aluminum likewise was removed quickly in various leaching solutions. Two leaching solutions were found that could remove 1018 steel at a reasonable rate from the powder metallurgy components without attacking the base metals significantly; these were concentrated phosphoric acid and 25 percent sulphuric acid. Surface finish measurements were taken on consolidated copper and nickel powder surfaces before and after leaching. Estimated leach rates and the resulting surface finishes are summarized in Table I-5. The leach rates are approximated due to the irregular chemical attack of surfaces. The selection of the leaching solution for a particular tooling material is indicated in Table I-6. It was found that the glass tooling in preliminary cylindrical specimens contained numerous cracks but remained well-aligned in the structure. Cracking in the glass occurred during the room-temperature hydropressing cycle. The copper powder near these cracked regions had a tendency to extrude into the void space during hot-isostatic compaction and produce defects within the leached-out channels that

TABLE I-4. RESULTS OF LEACH TESTS ON CANDIDATE TOOLING MATERIALS

Material	Leaching Solution	Solution Temperature	Average Leach Rate(b)	Remarks
1018 Steel	25% HCl	R.T.	0.215 g/hr	
1018 Steel	50% HCl	R.T.	0.050 g/hr	
1018 Steel	100% HCl	R.T.	0.130 g/hr	
1018 Steel	100% H_3PO_4	R.T.	0.142 g/hr	
1018 Steel	25% H_2SO_4	R.T.	0.055 g/hr	
1100 Aluminum	50% HCl	100 C	0.176 g/hr	
1100 Aluminum	50% H_2SO_4	R.T.	0.004 g/hr	
1100 Aluminum	8M NaOH	R.T.	0.105 g/hr	
1100 Aluminum	$FeCl_3$ + HCl(a)	R.T.	0.073 g/hr	
Cast Calcium	H_2O	R.T.	~3 g/hr	
Swaged Calcium	H_2O + 10% HCl	R.T.	--	Black layer on surface also dissolved, but leaching was periodically inhibited by the layer.
Swaged Calcium	H_2O + 10% HNO_3	R.T.	--	
0120 Lead Glass	67% HF	R.T.	~0.3 g/hr(c)	Formed white layer which retarded leaching rate.
7052 Borosilicate Glass	67% HF	R.T.	~0.7 g/hr	
Silica, SiO_2	67% HF	R.T.	~0.2 g/hr	
NiO	Various acids, bases, and salts	--	--(d)	Generally much slower than glasses above. Residue powder left behind.
ZnO	"	--	--(d)	
MgO	"	--	--(d)	

(a) One gallon $FeCl_3$ solution plus 12 oz of 38 percent HCl.

(b) After 29 hr of leaching on pellets about 1/4-in. diameter by 1-in. long.

(c) Leaching of glasses was conducted for 4-1/2 hr.

(d) Leach rate could not be determined due to disintegration of pellets into fine powder.

TABLE I-5. RESULTS OF LEACH TESTS ON COMPATIBILITY SPECIMENS

System				
Base Metal	Tooling Material	Leaching Solution(a) Concentration	Average Leach Rate(c)	Surface Finish (μ-in., RMS) of Base Metal
Cu	1018 Steel	25% H_2SO_4	0.006 in./hr	25
		100% H_3PO_4	0.008 in./hr	17
Cu	Cr/1100 Al	1N NaOH	0.007 in./hr	18
		50% HCl	0.033 in./hr	115
Cu	Steel/Ca	H_2O	--(d)	16
		10% HCl	0.042 in./hr	60
Cu	7052 Glass	67% HF	0.019 in./hr	16
Cu	0120 Glass	67% HF	0.009 in./hr	300(e)
Cu	SiO_2	67% HF	0.008 in./hr	18
Ni	1018 Steel	25% H_2SO_4	0.008 in./hr	180
		100% H_3PO_4	0.006 in./hr	180
Ni	1100 Al	8M NaOH	0.046 in./hr	38
		$FeCl_3$ + HCl(b)	0.011 in./hr	240

(a) Leaching solutions were kept at a constant temperature of 26 C.
(b) Solution of $FeCl_3$ + HCl prepared by mixing 12 oz of 38 percent HCl to 1 gallon $FeCl_3$.
(c) Leach rates were determined by measuring changes in lengths of the tooling per unit time.
(d) Leaching of calcium was periodically inhibited by scale formation on the metal.
(e) Surface roughness of copper was caused by reaction with 0120 glass during hot-isostatic compaction at 1000 F.

TABLE I-6. SELECTION OF LEACHING SOLUTION FOR REMOVAL OF TOOLING FROM NICKEL AND COPPER COMPONENTS

Component Material	Tooling Material	Leaching Solution
Copper	1018 Steel	100% H_3PO_4 or 25% H_2SO_4
	Cr-Coated Aluminum	50% HCl
	7052 Glass	67% HF
	Fe-Encapsulated Calcium	10% HCl or H_2O Followed by 25% H_2SO_4
Nickel	1018 Steel	25% H_2SO_4
	Cr-Coated Aluminum	8M NaOH

impeded fluid flow. By performing the hydropressing step at the lowest possible pressure that would still give sufficient green strength, it was possible to eliminate the cracking of the glass. During hot-isostatic compaction, the glass becomes soft enough to resist fracturing, and the flow channels generated from glass tooling were continuous and relatively free of defects. Calcium metal was not used in subsequent fabrication experiments for several reasons. Shaping the calcium to the desired tooling configurations was complicated by the need for a protective environment and liner. By shaping in air, the calcium reacted slowly with moisture and with nitrogen to form a friable black surface scale. While the calcium can be protected in an iron sheath or with an iron coating, this technology was not developed far enough to satisfy program requirements. Also, calcium was not available in suitable shapes to make the desired tooling for the subscale or full-scale components.

In summary, the tooling materials that appeared to have the greatest promise after the screening process and these preliminary tests were:

For the Copper Baffle	For the Nickel Injector
(1) 7052 Borosilicate glass	(1) 1100-aluminum
(2) 1018 steel	(2) 1018 steel
(3) Cr-coated 1100-aluminum (provided process temperature was kept to 1000 F or below).	(3) Iron-encapsulated calcium.

Subtask I-B: Powder Metallurgy Process Optimization

The objective of this subtask was to investigate powder-metallurgy fabrication techniques and conditions to develop the process which will be used for fabrication of rocket engine components in Tasks II and III.

The primary problem area regarding powder compaction was the establishment of the optimum conditions as dictated by tooling material compatibility.

In hot-pressing studies conducted on copper and nickel powders, data was produced showing the dependence of densification on time at constant temperature and various pressures. These data, shown in Figures I-7 through I-10, were used as a guide to determine the conditions for hot-isostatic compaction at 10,000 psi during the experimental determination of the other parameters (time and temperature).

From the graphs, the densification rates for copper were determined at 650 psi and at 15,300 psi. These curves start to converge as the end-point density is approached, and the time required to reach comparable densities at 10,000 psi was averaged between these two pressures. Densification rates for nickel powder were determined at 10,200 psi, and the time to reach comparable densities at 10,000 psi were close enough to be taken directly from the 10,200 isolar. Consolidation occurs by bulk plastic deformation of copper and nickel powders during densification to 90 percent density. Above 90 percent, densification rates decrease, but the density continues to rise slowly due to further consolidation and closure of voids by creep and/or diffusion processes. Although high densities can be achieved solely by plastic deformation, it was desirable to achieve densities near or above 98 percent for several reasons. High mechanical properties in the fabricated metal powder were required, interconnected porosity that could cause leaks through the microstructure had to be prevented, and metallurgical bonding of the powder to solid sections was desired. The end-point densities achieved during bulk plastic deformation by both copper and nickel powders are less than 100 percent as indicated in Table I-7. To promote densification to 98 percent and better in copper a 60 minute dwell time was estimated as the minimum to achieve relatively significant densification by creep and diffusion in copper; for nickel, a minimum dwell time for 30 minutes was assumed. Hot-isopressing conditions for the initial experiments

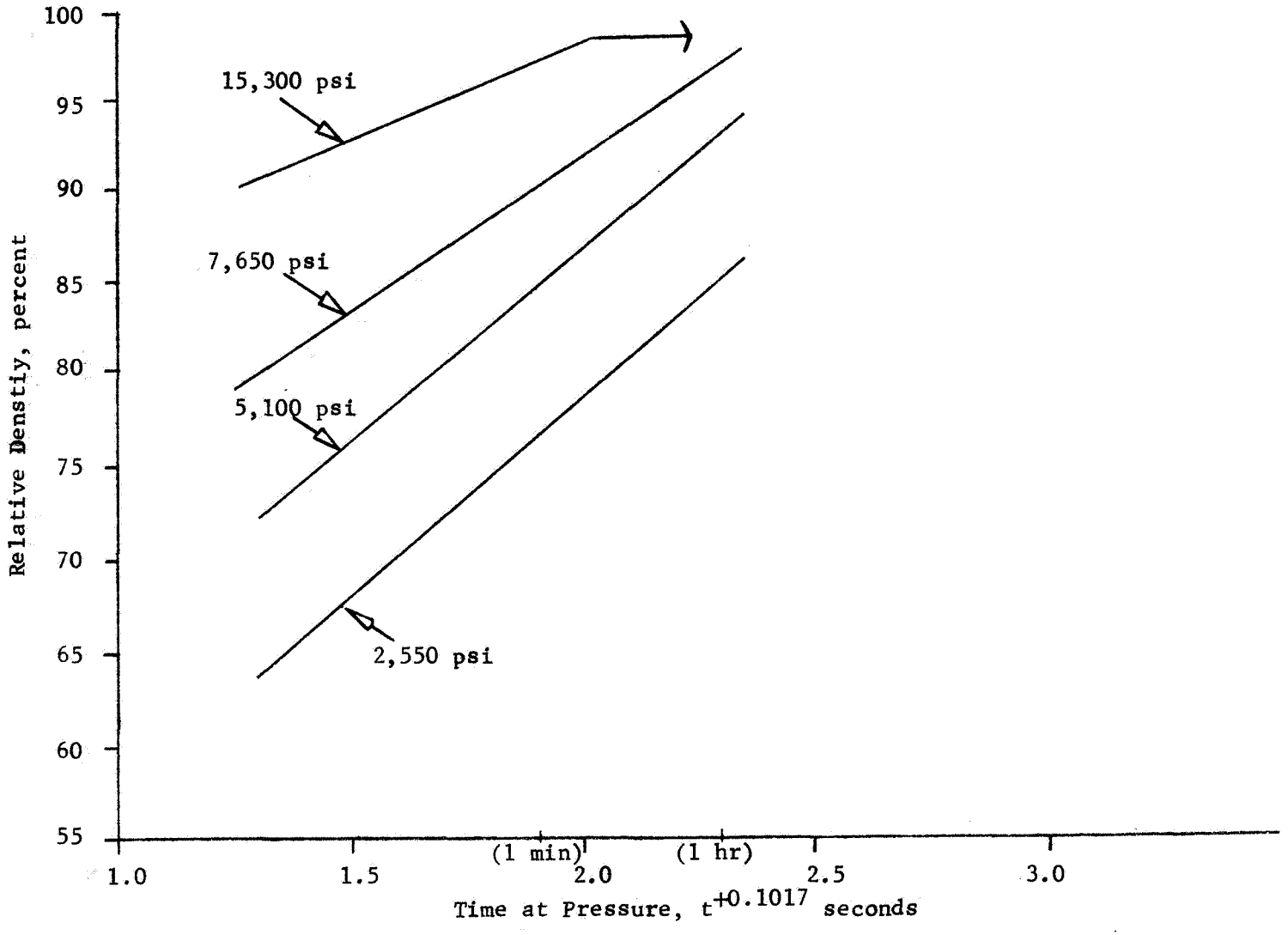

FIGURE I-7. RELATIVE DENSITY-TIME-AT-PRESSURE CURVES FOR -270 +325 MESH COPPER POWDER HOT PRESSED AT 1000 F[1]

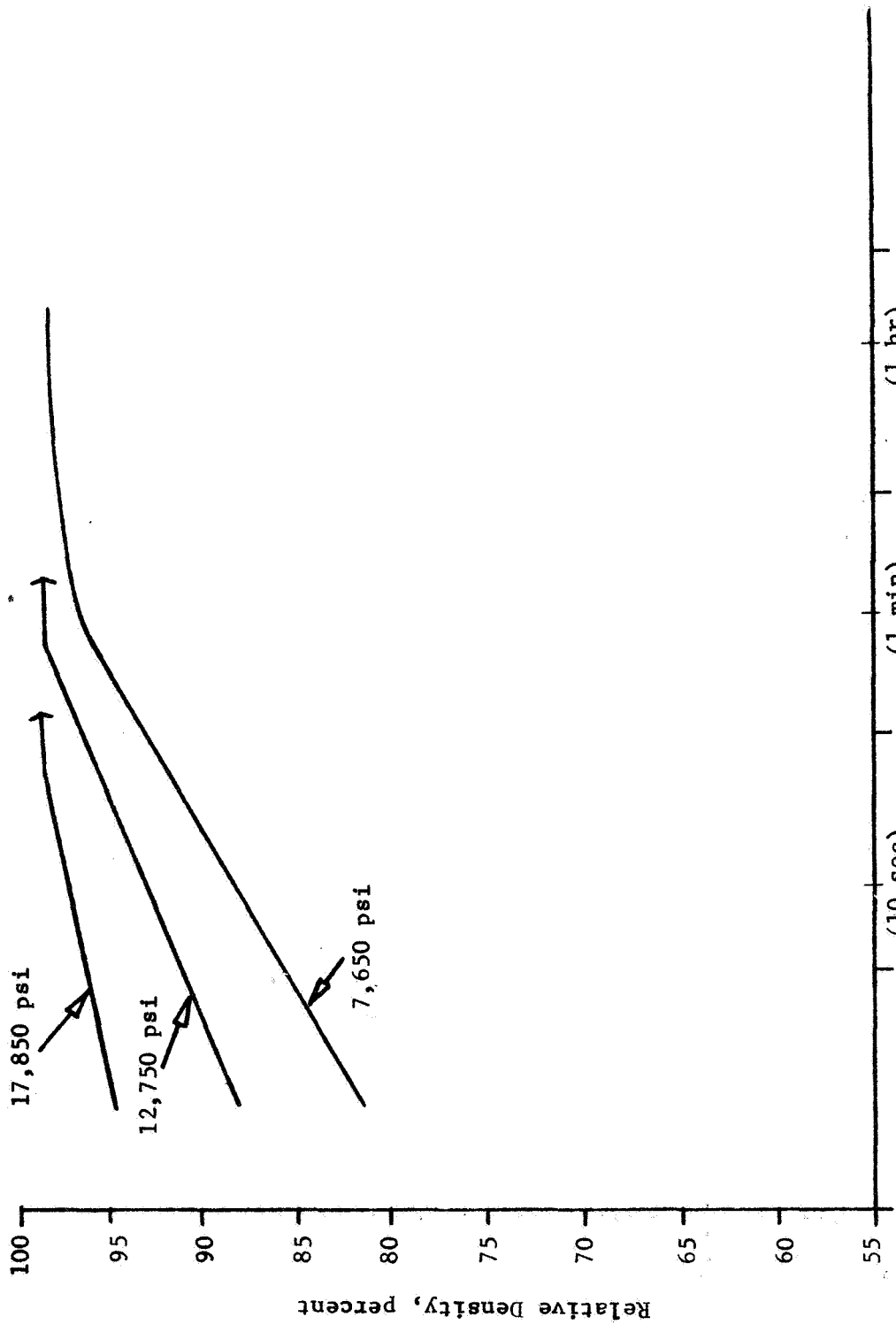

FIGURE I-8. RELATIVE DENSITY-TIME-AT-PRESSURE CURVES FOR -270 +325 MESH COPPER POWDER HOT PRESSED AT 1200 F (1)

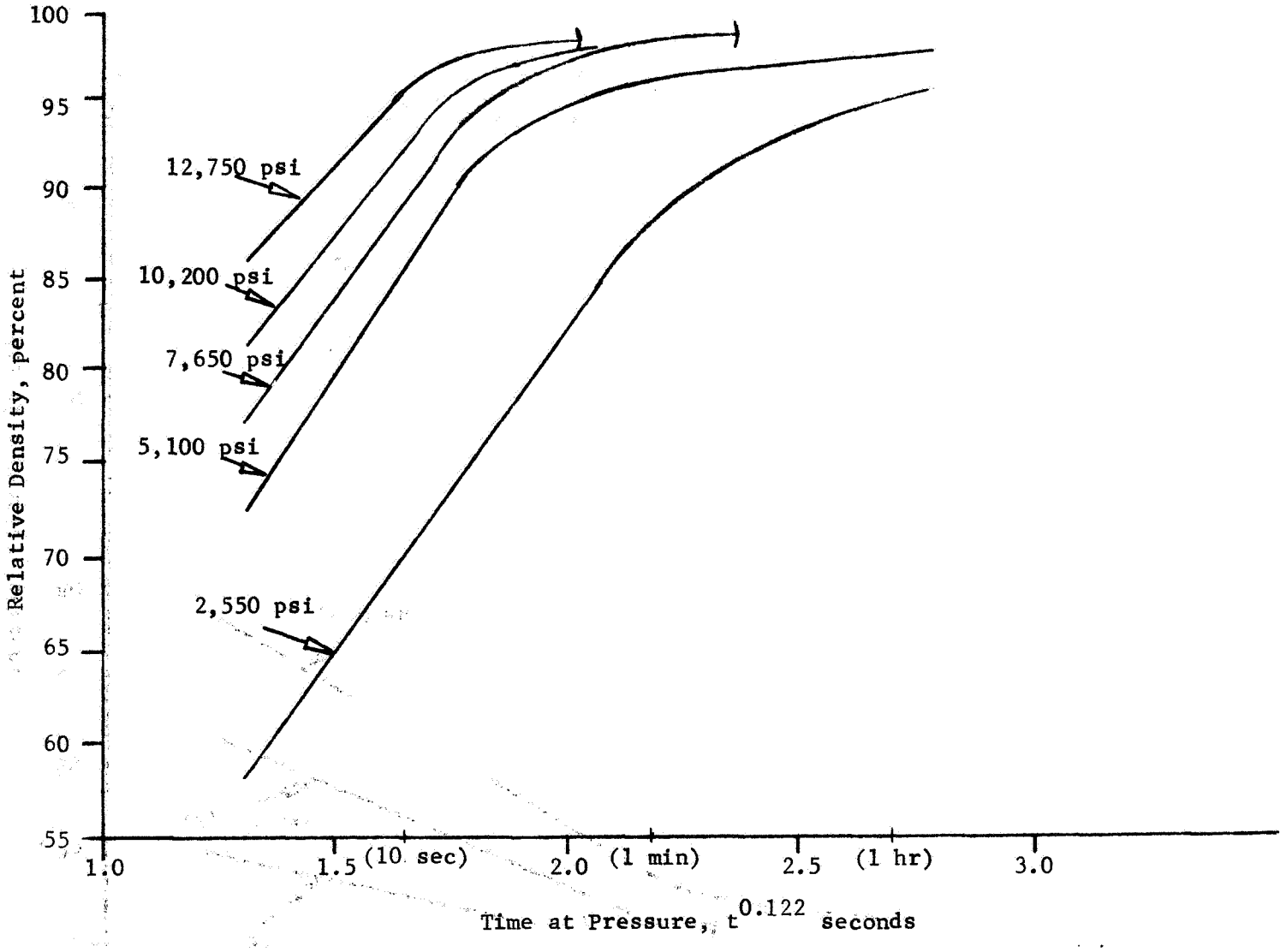

FIGURE I-9. RELATIVE DENSITY-TIME-AT-PRESSURE CURVES FOR -270 +325 MESH NICKEL POWDER HOT PRESSED (1) AT 1000 F

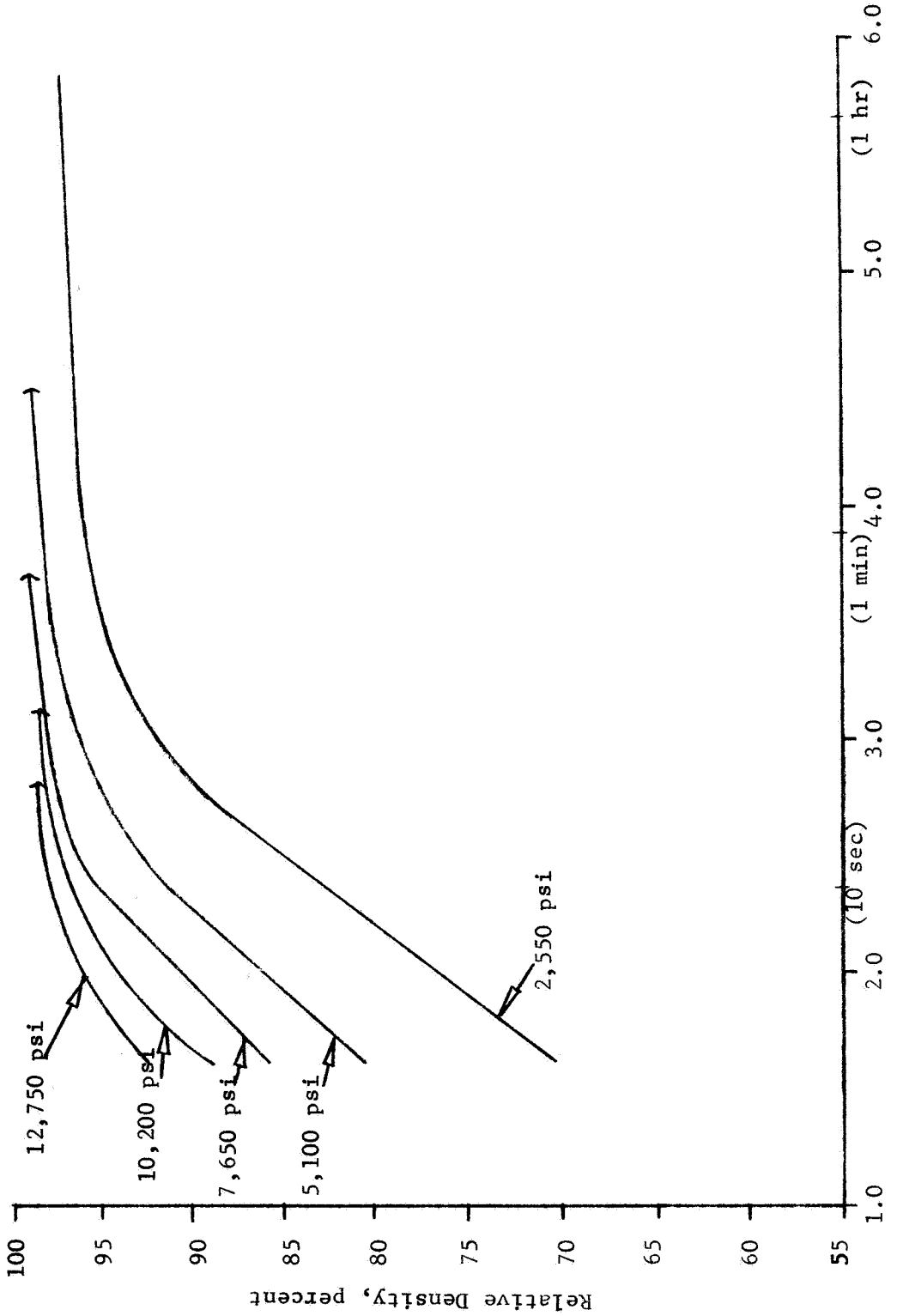

FIGURE I-10. RELATIVE DENSITY-TIME-AT-PRESSURE CURVES FOR -270 +325 MESH NICKEL POWDER HOT PRESSED AT 1200 F (1)

TABLE I-7. DENSIFICATION OF Cu AND Ni POWDERS AS PREDICTED BY HOT-PRESSED DATA

(Pressure constant at 10,000 psi)

Metal Powder	Temperature, F	End-Point Density, %	Time to Reach End-Point Density
Cu	1000	98	1.5 hr
Cu	1200	98	40 min
Ni	1000	97	35 min
Ni	1200	95	0.5 min

were made in the range of 1000 to 1200 F, and 1 to 3 hr, with pressure of 10,000 psi remaining constant. The hot-isostatic pressing experiments were conducted on solid, cylindrical parts prepared from nickel and copper powder as follows:

Cycle	Pressure	Temperature	Time
(1)	10,000 psi	1000 F	1 hr
(2)	10,000 psi	1200 F	1 hr
(3)	10,000 psi	1000 F	3 hr
(4)	10,000 psi	1200 F	3 hr .

Three different copper powders and three different nickel powders were selected for investigations. A simple numbering system was adopted to identify specimens. Specimens were numbered and lettered according to the powder tested (copper or nickel), type of powder, hydropressing pressure, and the hot-isostatic compaction cycle. Table I-8 summarizes the specimen identification system and the pertinent parameters. Samples of powder were characterized for oxygen content, particle size distribution, particle shape, and internal porosity. Identification and analyses of the powders are contained in Table I-9. Particle shapes and porosity in the particles as received from the vendors are shown in Figures I-11 through I-16.

The apparent densities, vibratory pack densities, and hydropress densities were determined for each powder, and are summarized in Figures I-17 and I-18. The bulk and vibratory packed densities of C1-type copper powder was much lower than either C2 or C3 and was due to its very fine, irregularly shaped particles. During hydropressing, however, the C1 type powder achieved high densities. All the copper powder types were 60 percent dense or better after hydropressing at 10 tsi and had sufficient green strength for handling and rough machining after-

TABLE I-8. SPECIMEN IDENTIFICATION

Number or Letter	Identification and Meaning
Letter Prefix	Denotes metal powder
C	Copper
N	Nickel
First Digit	Identifies type of powder as listed in Table I-9
N1	-200 mesh nickel powder
N2	K-3603C, -200 mesh nickel powder
N3	K-3603B, -200 mesh spherical nickel powder
C1	Electrolytic fines, -140 mesh copper powder
C2	Electrolytic fines, -200 mesh copper powder
C3	K-1433, -100 mesh copper powder
Second Digit	Denotes the hydropressing pressure used to cold compact the powder
1	10 tsi
2	20 tsi
3	30 tsi
4	40 tsi
V	Vibratory packed only, not hydropressed
Third Digit	Denotes which hot-isostatic compaction cycle the powder was processed in
1	First cycle: 1000 F, 10,000 psi, 1 hr
2	Second cycle: 1200 F, 10,000 psi, 1 hr
3	Third cycle: 1000 F, 10,000 psi, 3 hr
4	Fourth cycle: 1200 F, 10,000 psi, 3 hr

TABLE I-9. POWDER IDENTIFICATION AND CHARACTERIZATION

A. Identification and Oxygen Analyses

Powder:	Copper	Copper	Copper	Nickel	Nickel	Nickel
Vendor's Identification:	Electrolytic Fines	Electrolytic -200 Mesh	K-1433 -100 Mesh	-- -200 Mesh	K-3603 C -200 Mesh	K-3603 B -200 Mesh
BMI's Identification:	C1	C2	C3	N1	N2	N3
Oxygen Analysis, %:	0.68	0.42	0.18	0.29	0.26	0.28

B. Vendor's Certified Typical Elemental Analysis of Copper and Nickel Powder, PPM

C3		N2 and N3	
Ag	30	Co	540
Pb	10	Cu	38
Fe	30	Fe	20
Ni	20	S	170
Sb	5	C	40
Ca	5		
Bi	5		
Si	15		
Sn	20		

C. Particle Size Distributions (weight percents)

	Copper Powder			Nickel Powder		
Mesh	C1	C2	C3	N1	N2	N3
+100	0	0.04	0	0	0	0
-100, +140	0.96	5.05	3.11	0	0.06	91.91
-140, +170	5.10	21.63	5.15	0.1	23.19	7.96
-170, +200	3.99	8.85	2.45	0.1	28.47	0
-200, +230	3.72	11.05	3.17	0.5	21.92	0
-230, +270	4.55	10.80	5.22	6.6	10.77	0
-270, +325	9.64	16.93	12.89	19.0	10.65	0
-325	71.21	25.00	67.68	73.5	4.77	0
losses	0.83	0.65	0.33	0.2	0.17	0.13

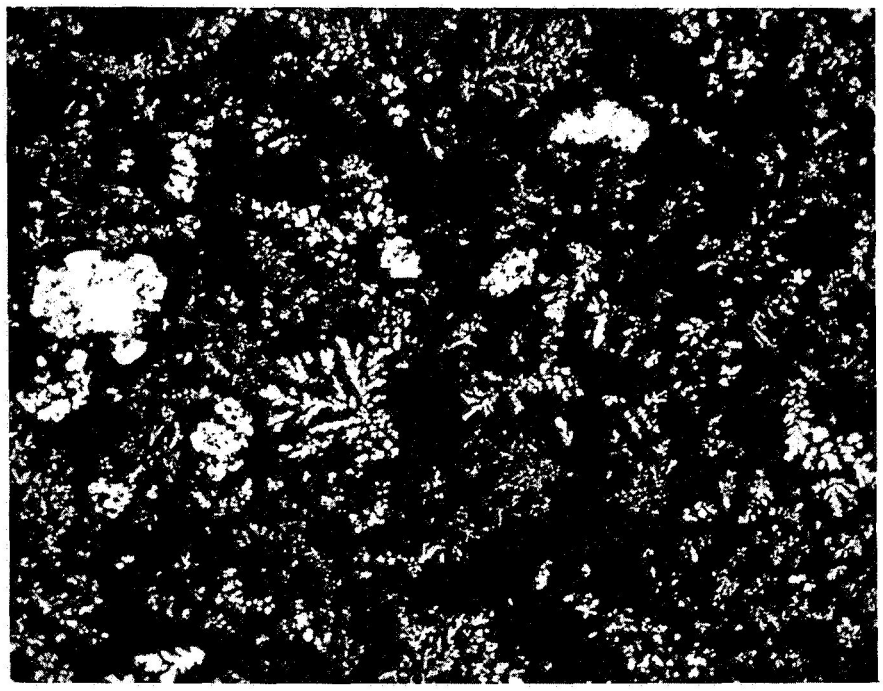

150X 3C588

FIGURE I-11. C1-TYPE COPPER POWDER

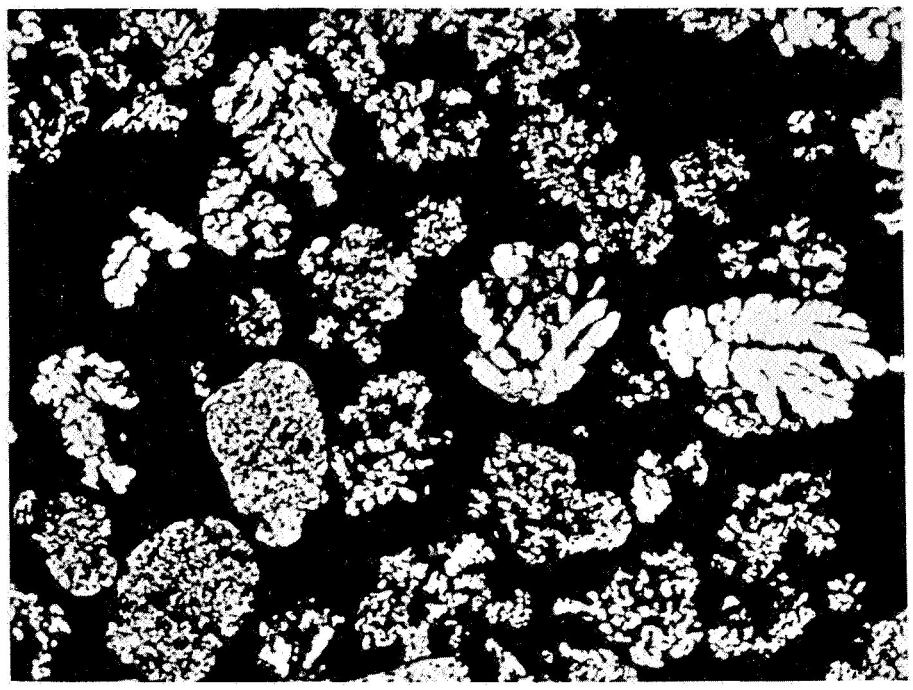

150X 3C589

FIGURE I-12. C2-TYPE COPPER POWDER

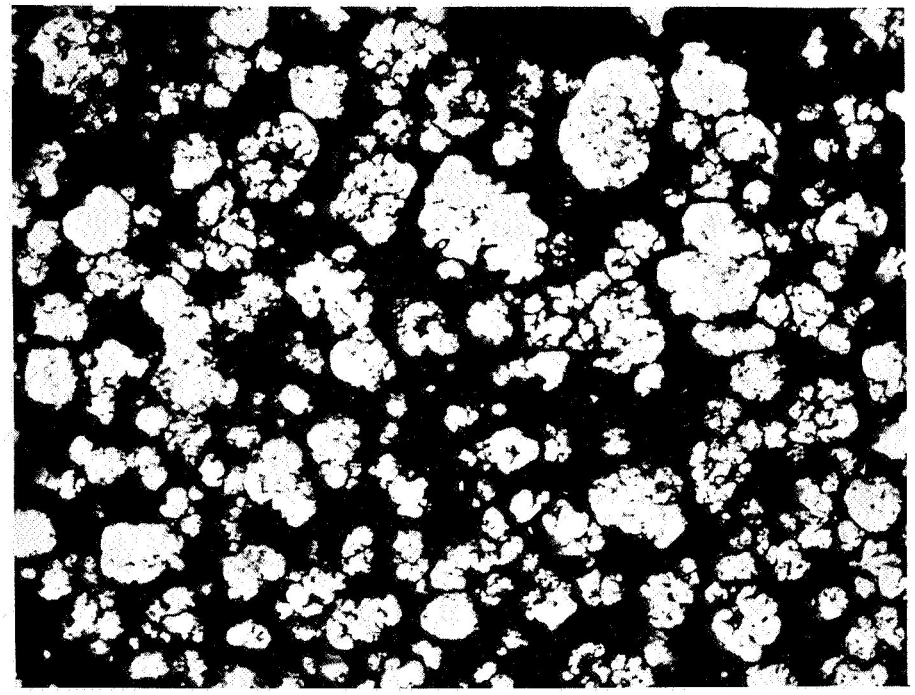

150X OC843

FIGURE I-13. C3-TYPE COPPER POWDER

150X 3C590

FIGURE I-14. N1-TYPE NICKEL POWDER

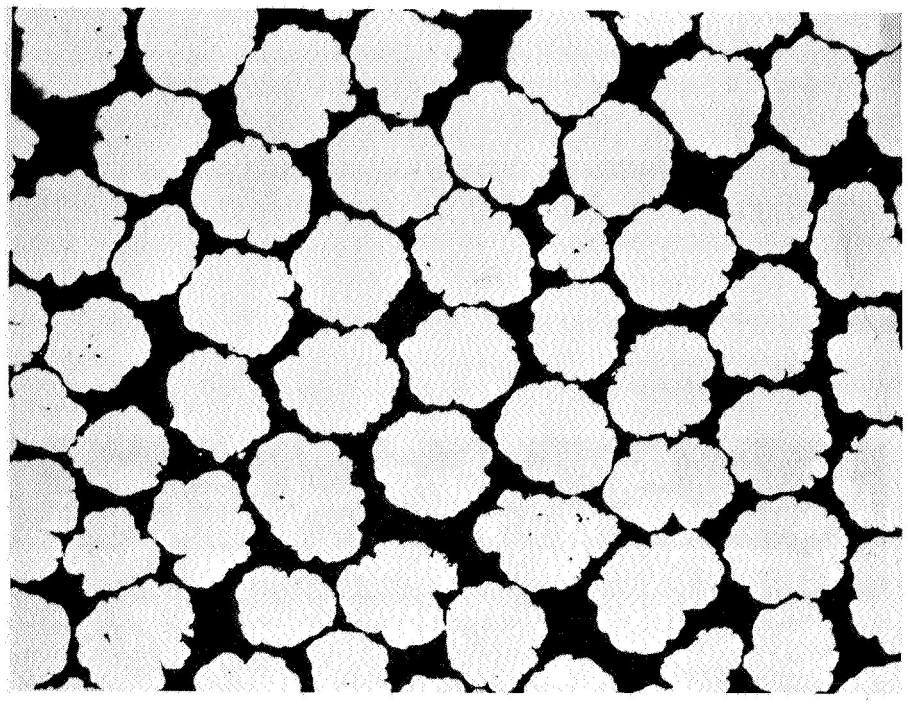

150X (a) Polished 0C837

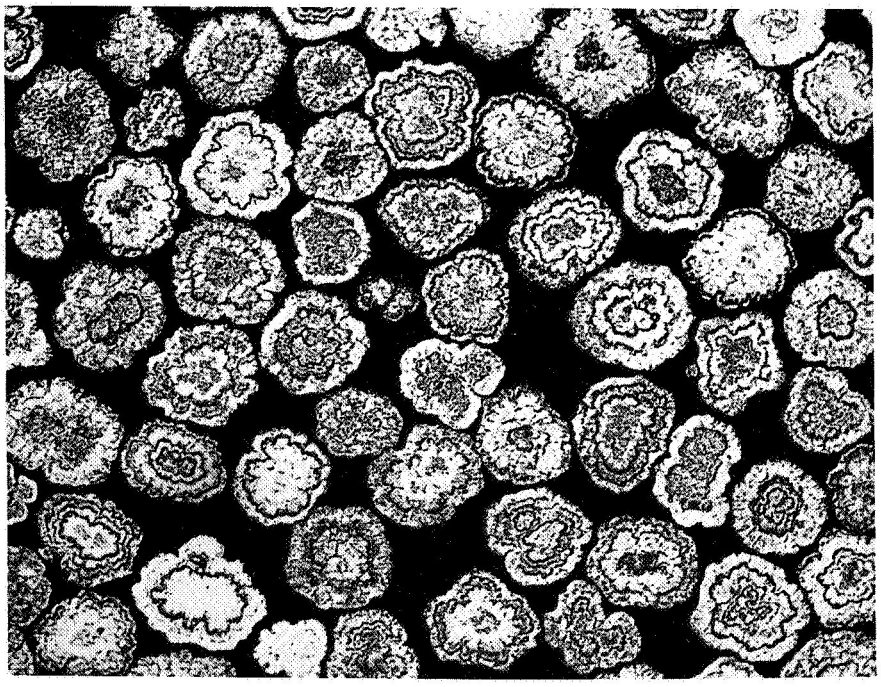

150X (b) Etched 3C881

FIGURE I-15. N2-TYPE NICKEL POWDER

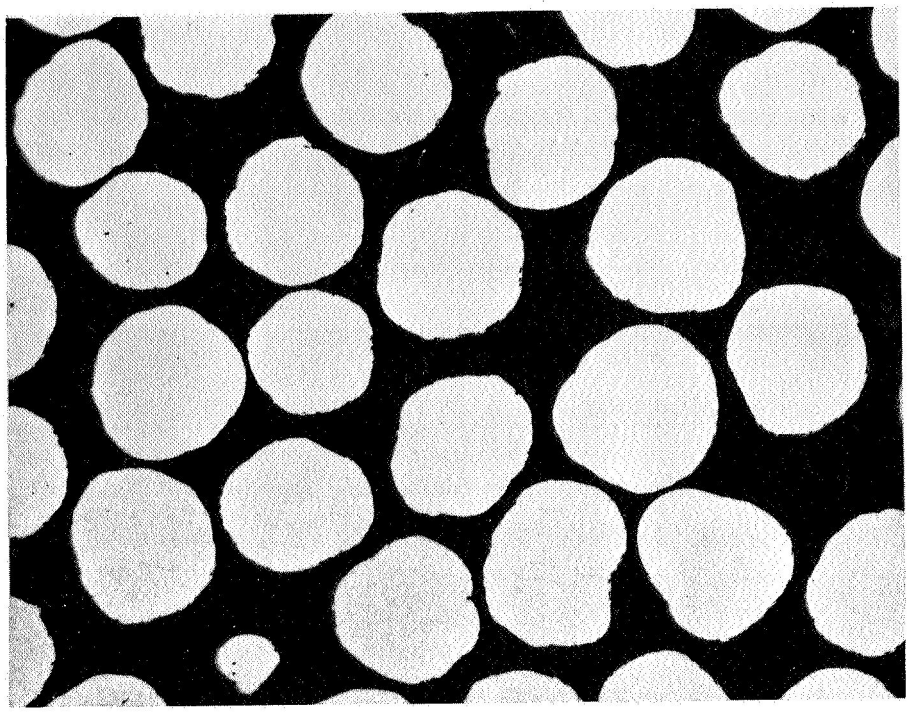

150X (a) Polished 0C840

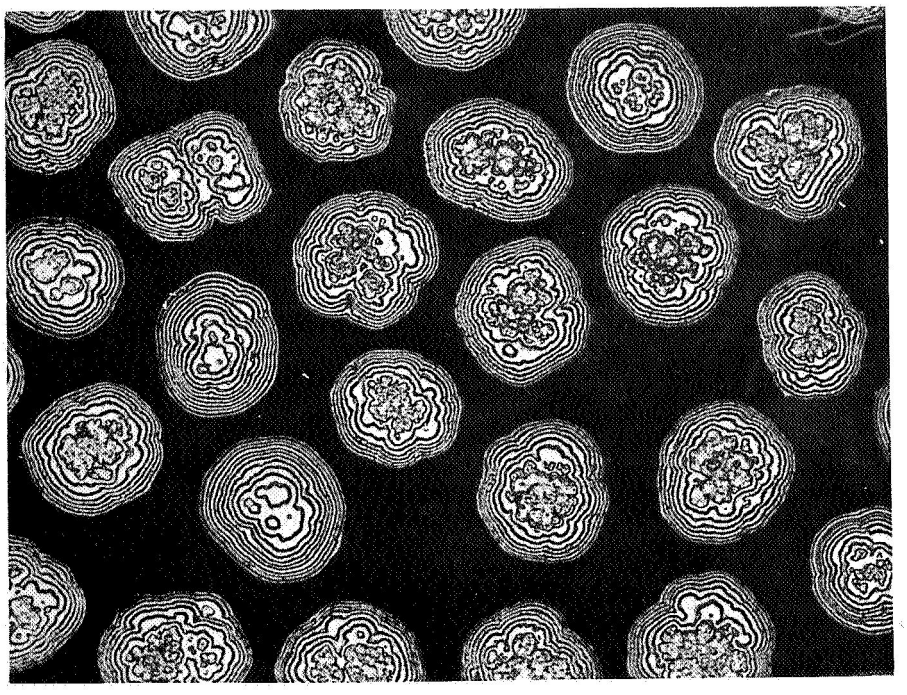

150X (b) Etched 3C882

FIGURE I-16. N3-TYPE NICKEL POWDER

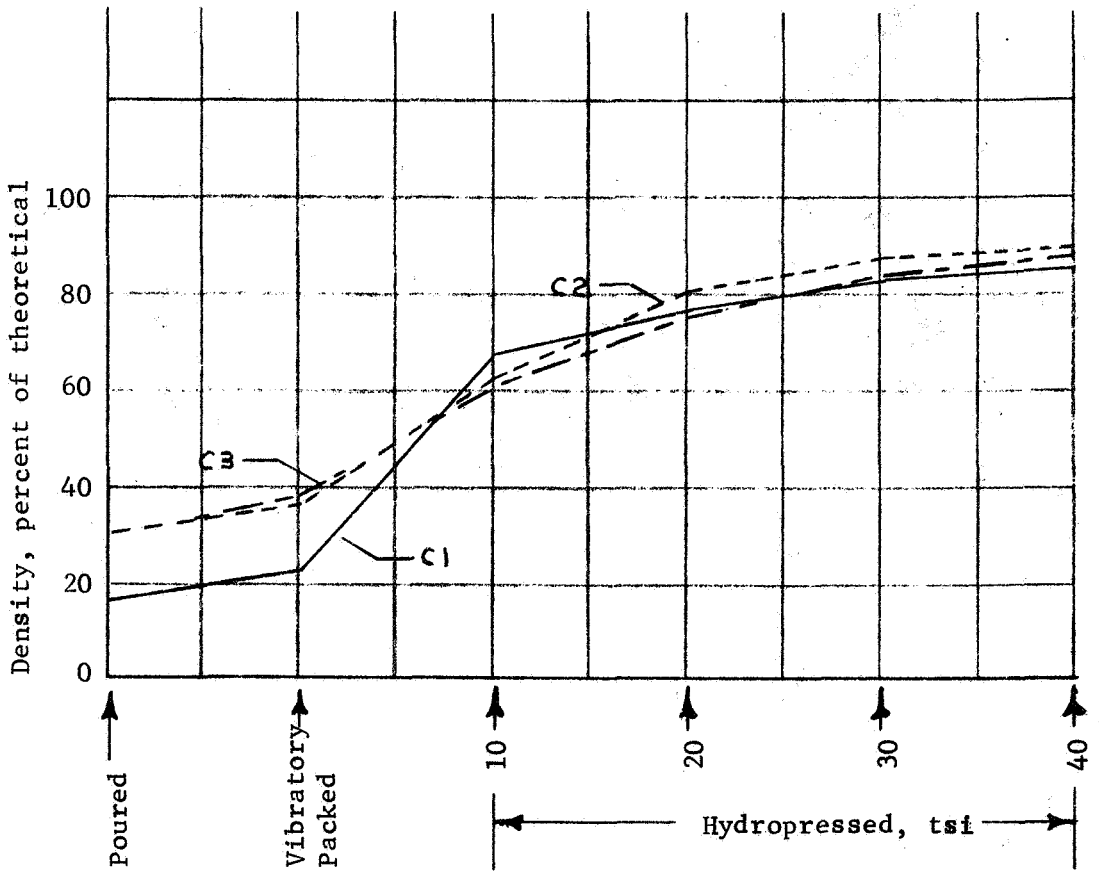

FIGURE I-17. DENSITIES ACHIEVED BY COPPER POWDERS DURING VARIOUS PRECOMPACTION PROCESS STEPS

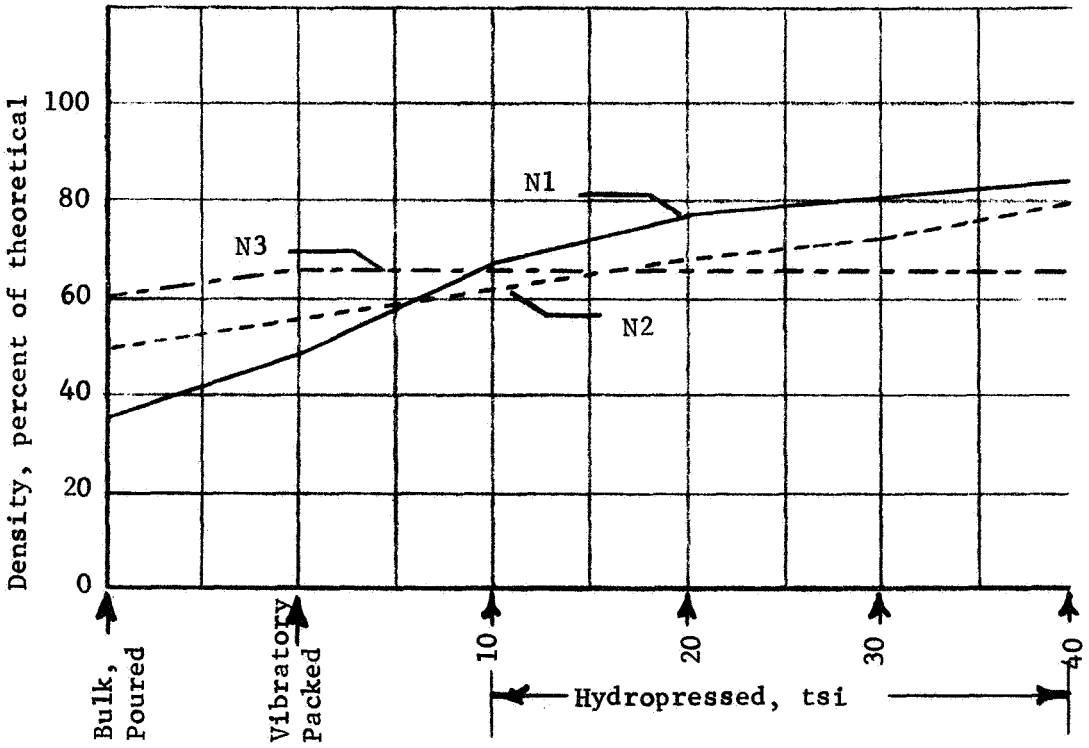

FIGURE I-18. DENSITIES ACHIEVED BY NICKEL POWDERS DURING VARIOUS PRECOMPACTION PROCESS STEPS

wards. The large increase in density of C1 powder from vibratory packing to hydropressing was considered a disadvantage from the standpoint of dimensional control.

The use of N1 powder was also considered detrimental to dimensional control due to the large amount of shrinkage that occurred between vibratory packing and hydropressing. TheN2-type powder followed a nearly linear relationship between hydropressing pressure and density. Below 30 tsi, however, the N2-type powder had little green strength and could not be handled or rough machined. The N3-type spherical nickel powder achieved the highest vibratory packed densities which is characteristic of vibratory packed spheres provided the porosity within the particles is negligible. However, another characteristic of these spherical particles was its inability to achieve suitable green strength unless very high pressures are used. The N3-type powder could not be given sufficient green strength even after hydropressing at pressures up to 50 tsi.

Hydropressed pellets were hot isostatically compacted at the conditions indicated earlier. Comparison of the effects of hot-isostatic compaction on density are illustrated in Figure I-19. Due to the large number of process variables involved, the number of specimens studied for each parameter was necessarily small, but several trends were noted. As expected, slightly higher densities of copper powder were achieved by hot isostatically compacting for 3 hr rather than 1 hr at the same temperature and similar results were achieved by compacting at 1200 F compared to 1000 F in autoclave cycles having the same hold time. The densities were near theoretical even after compacting at 1000 F, and the lower temperature cycling could be utilized if adverse reactions between the copper powder and the tooling materials were likely to occur at the higher temperature. Higher densities of nickel powder appeared to be achieved after hot isostatic compacting when hydropressing was done above 20 tsi. Also, use of higher temperatures resulted in higher densities for the same cycling times when the nickel powder had been precompacted at hydropressures of more than 20 tsi.

	Cycle No.	Temp., F	Time, hr	Pressure, ksi
⬡ – C1-Type Copper	1	1000	1	10
○ – C2-Type Copper	2	1200	1	10
□ – C3-Type Copper	3	1000	3	10
▽ – N1-Type Nickel	4	1200	3	10
⌓ – N2-Type Nickel				

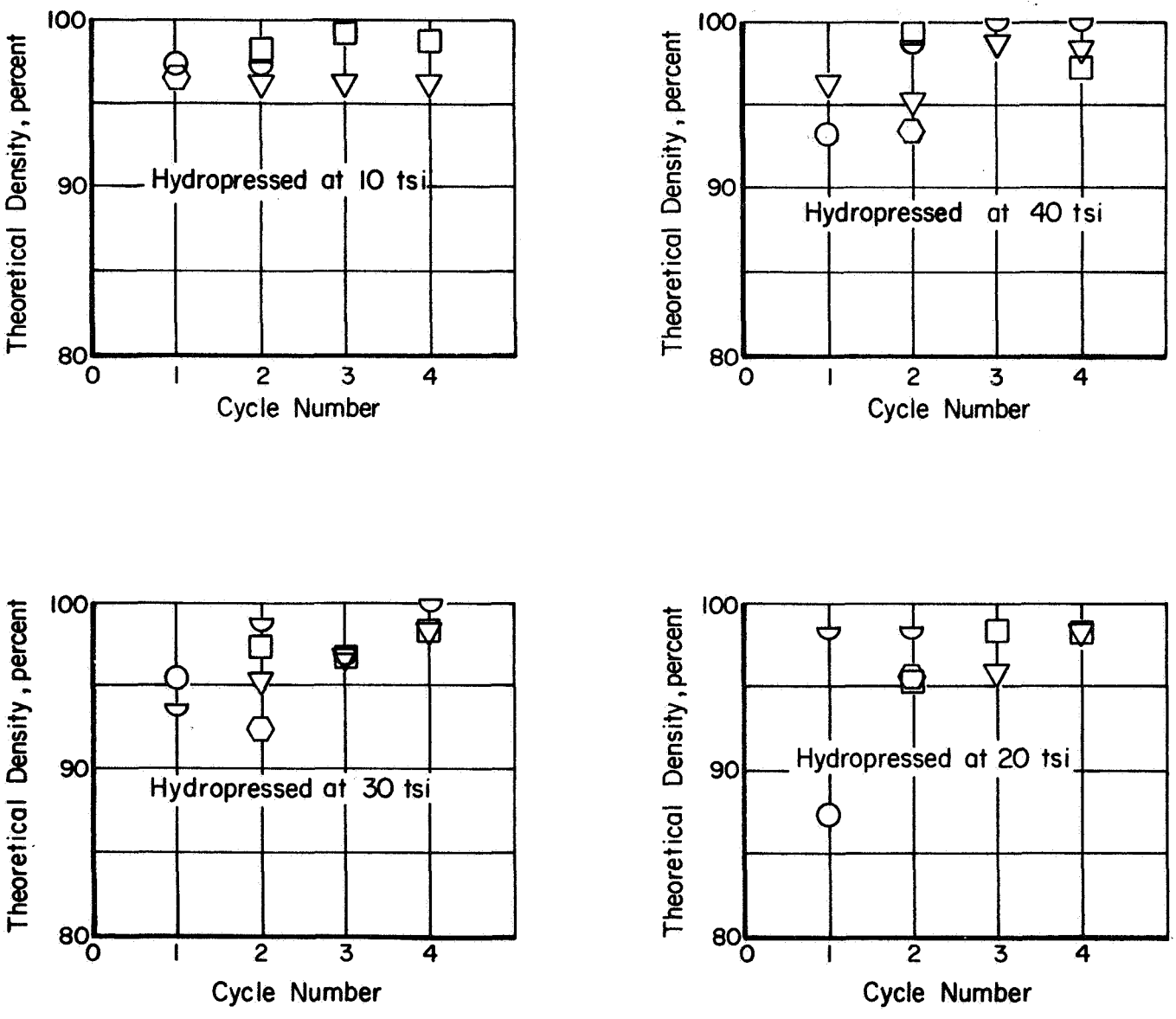

FIGURE I-19. EFFECTS OF HOT-ISOSTATIC COMPACTION CONDITIONS ON DENSITIES OF COPPER AND NICKEL POWDERS

Hardness measurements were taken on selected samples for comparison with the hardness on commercially pure wrought and annealed copper and nickel products and are shown in Figures I-20 and I-21. The hardness measurements on consolidated nickel powders compared well with commercially pure nickel products. Measurements on consolidated copper powders of the C3-type were generally higher than OFHC copper products, and this is attributed to the much finer grain size in the hot isostatically compacted copper powders. Metallographic examination of the compacted copper powder specimens indicated that the average grain size in all the copper specimens was less than 10μ. Little or no grain growth occurred in specimens compacted at 1000 F; a slight amount of grain growth was apparent in copper powder specimens compacted at 1200 F. The C1 and C2-type copper powders contained a relatively wide range of grain sizes, but the C3-type powder maintained a nearly uniform grain size. The C1 copper powder achieved high densities, had very little interconnected porosity, but contained somewhat more impurity artifacts than C2 or C3, and the final grain size distribution covered a wide range. The C2 powder was not much different in its microstructure than C1. The C3 powder achieved the highest densities and very little porosity could be detected. The final grain size was quite fine, and the size distribution was relatively uniform. Typical microstructure was shown in Figures I-22 through I-24. Because of its ability to densify nearly completely at lower temperatures, the C3-type copper powder was selected for fabrication of the subscale and full-size baffles.

Typical microstructures of compacted nickel powders are shown in Figures I-25 through I-28. The N1 nickel powder achieved high densities but not as high, generally, as N2 or N3; impurities in the microstructure were slightly greater than in N2 or N3. The final grain size and shape in N1 varied greatly.

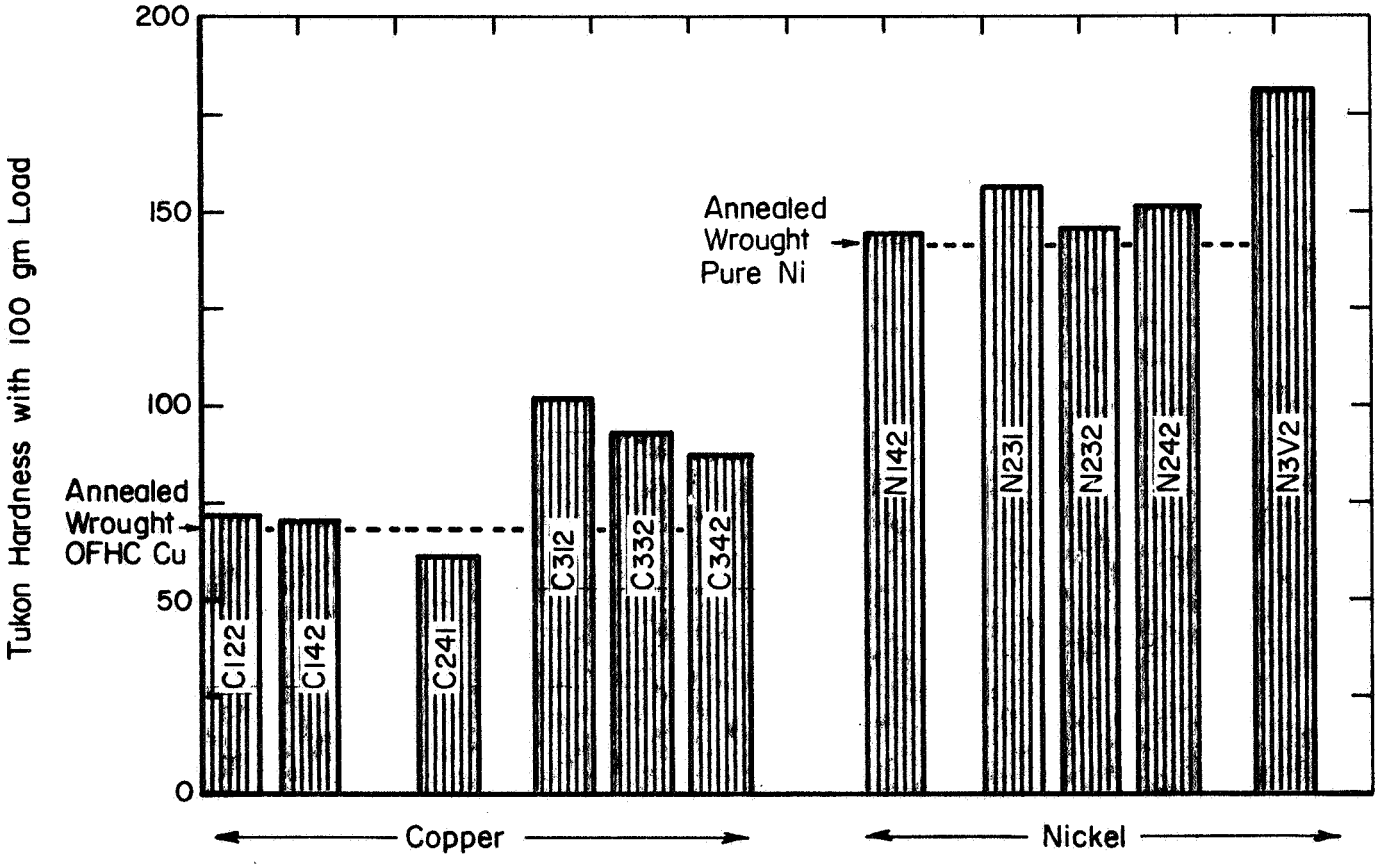

FIGURE I-20. RESULTS OF HARDNESS TESTS ON NICKEL AND COPPER POWDERS HOT-ISOSTATICALLY COMPACTED IN CYCLES 1 AND 2

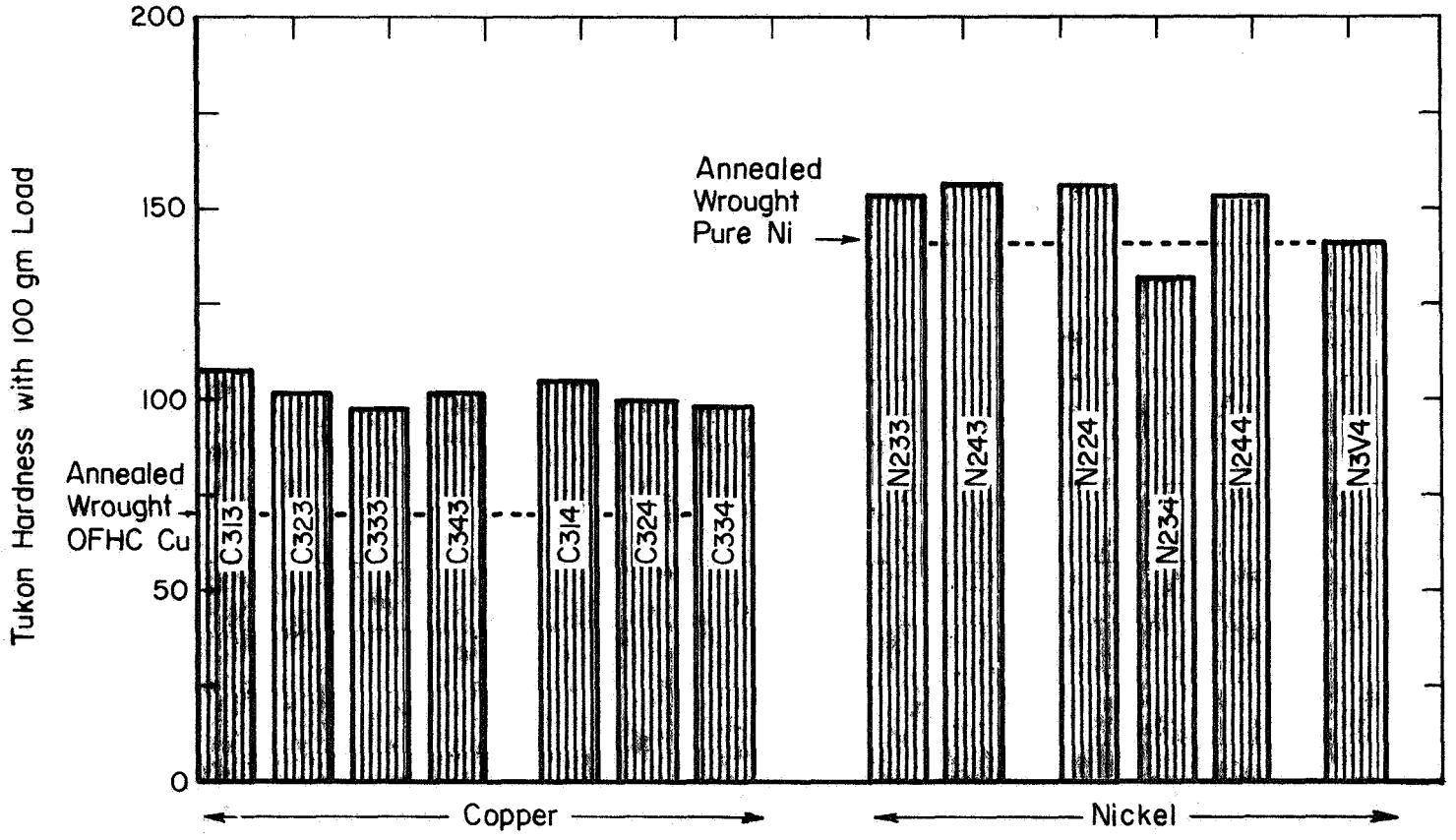

FIGURE I-21. RESULTS OF HARDNESS TESTS ON NICKEL AND COPPER POWDERS HOT-ISOSTATICALLY COMPACTED IN CYCLES 3 AND 4

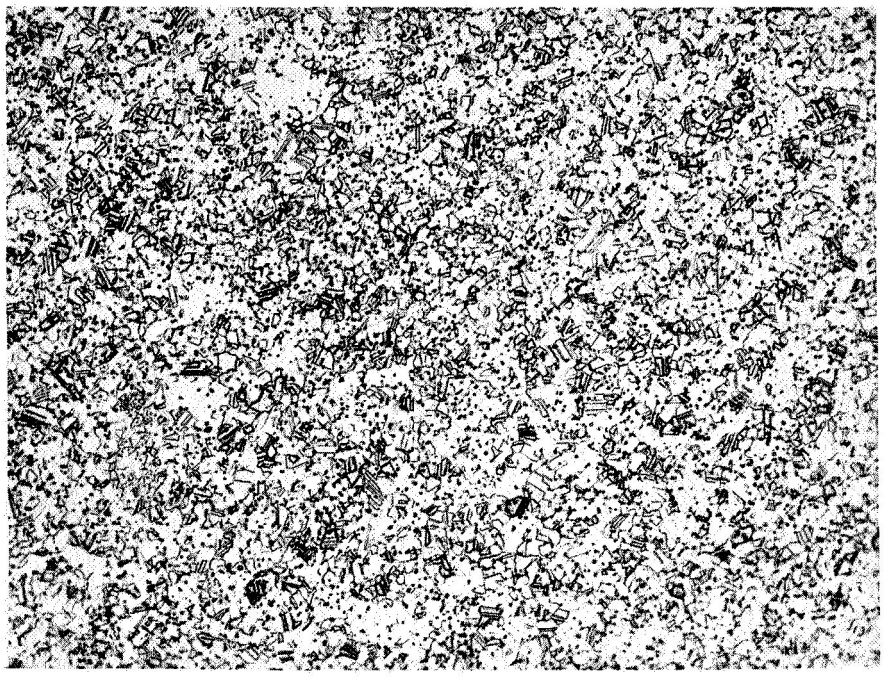

250X Etched 4C024

FIGURE I-22. MICROSTRUCTURE OF HOT ISOSTATICALLY COMPACTED C1-TYPE COPPER POWDER

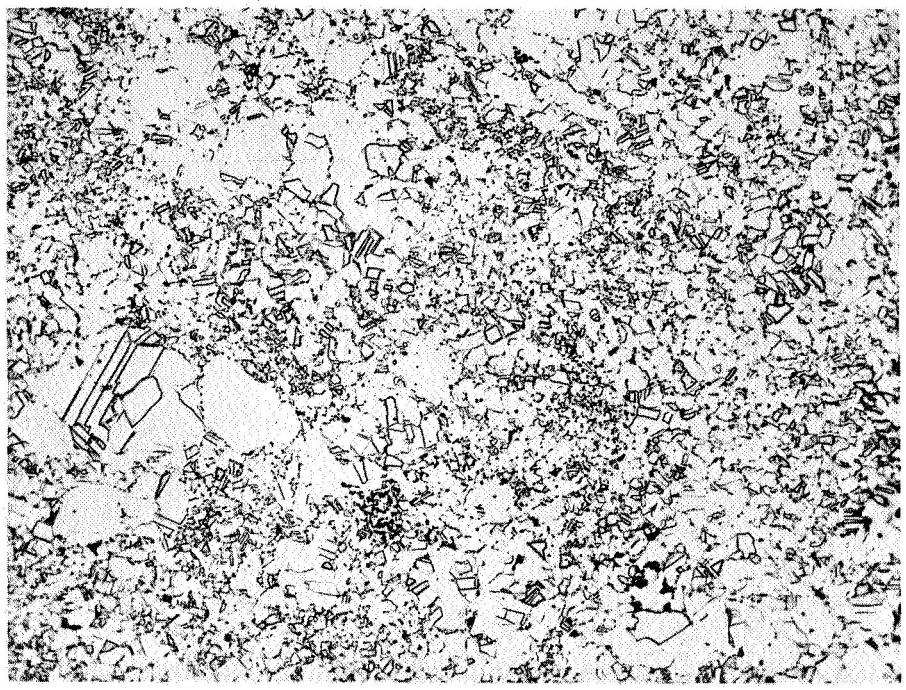

250X Etched 4C035

FIGURE I-23. MICROSTRUCTURE OF HOT ISOSTATICALLY COMPACTED C2-TYPE COPPER POWDER

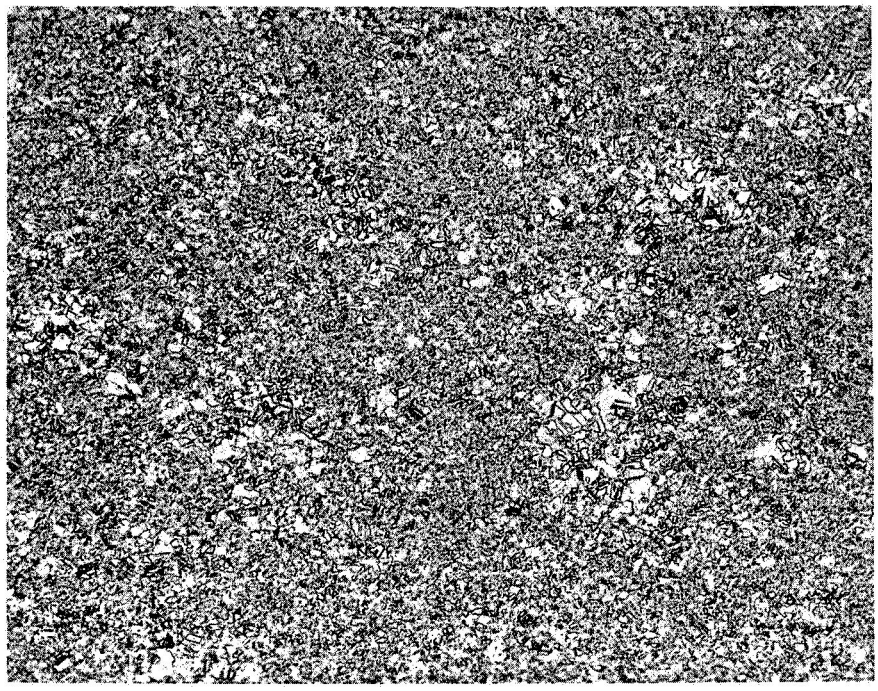

250X Etched 4C513

FIGURE I-24. MICROSTRUCTURE OF HOT ISOSTATICALLY COMPACTED C3-TYPE COPPER POWDER

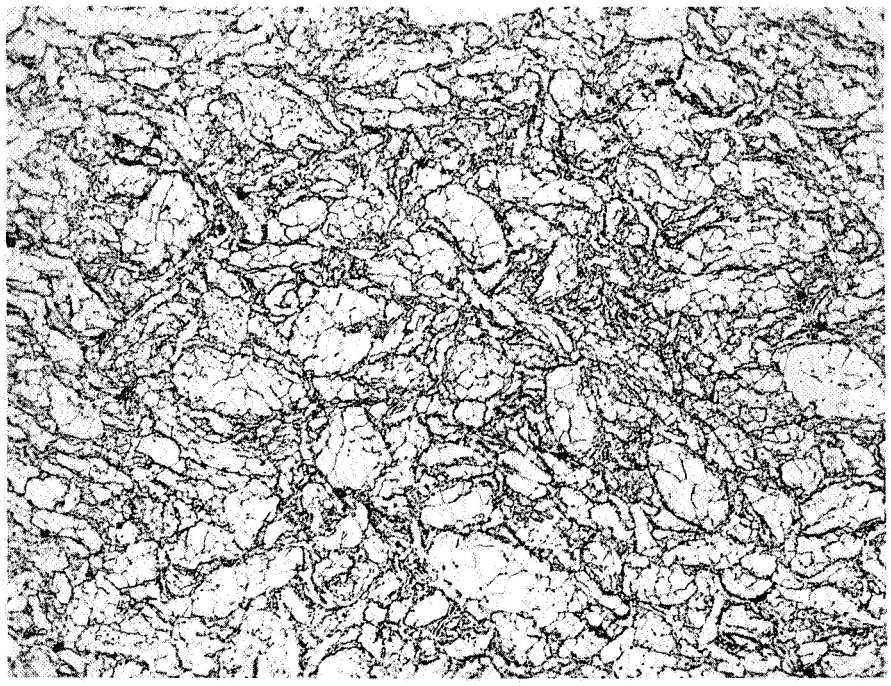

250X Etched 4C072

FIGURE I-25. MICROSTRUCTURE OF HOT ISOSTATICALLY COMPACTED N1-TYPE NICKEL POWDER

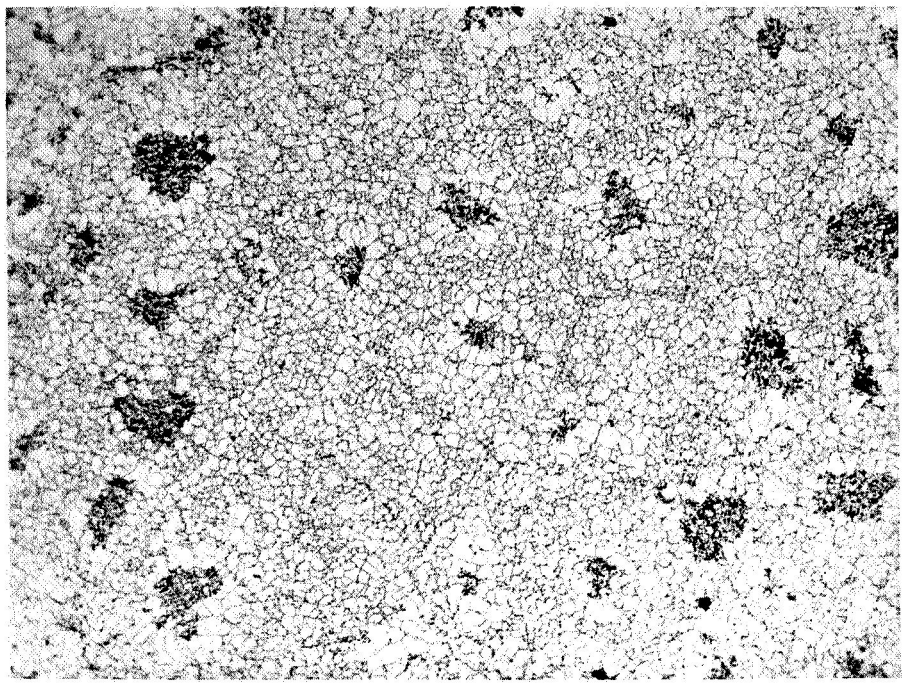

250X Etched 4C084

FIGURE I-26. MICROSTRUCTURE OF HOT ISOSTATICALLY COMPACTED N2-TYPE NICKEL POWDER

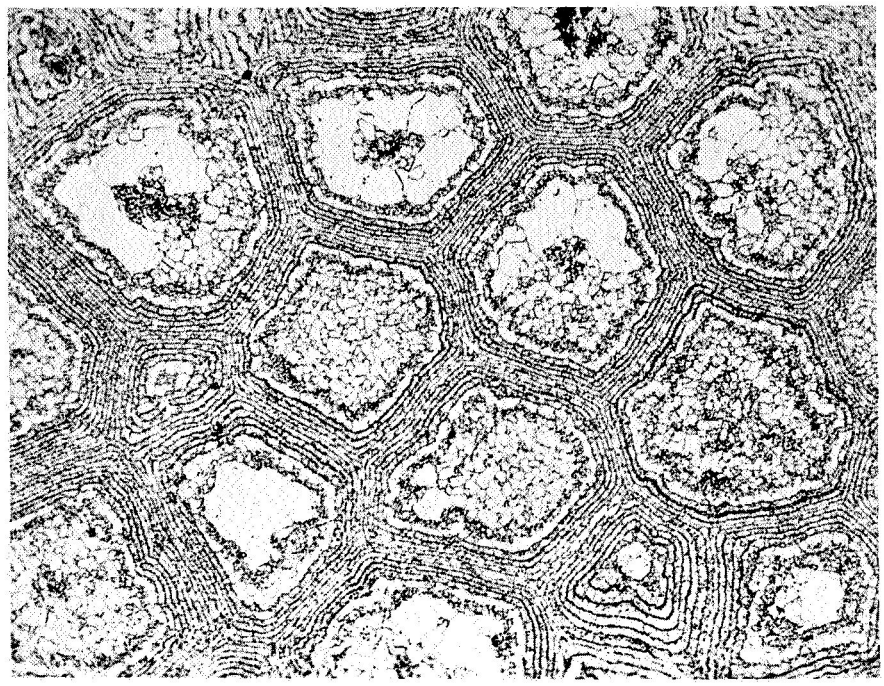

250X Etched 4C101

FIGURE I-27. MICROSTRUCTURE OF HOT ISOSTATICALLY COMPACTED N3-TYPE NICKEL POWDER

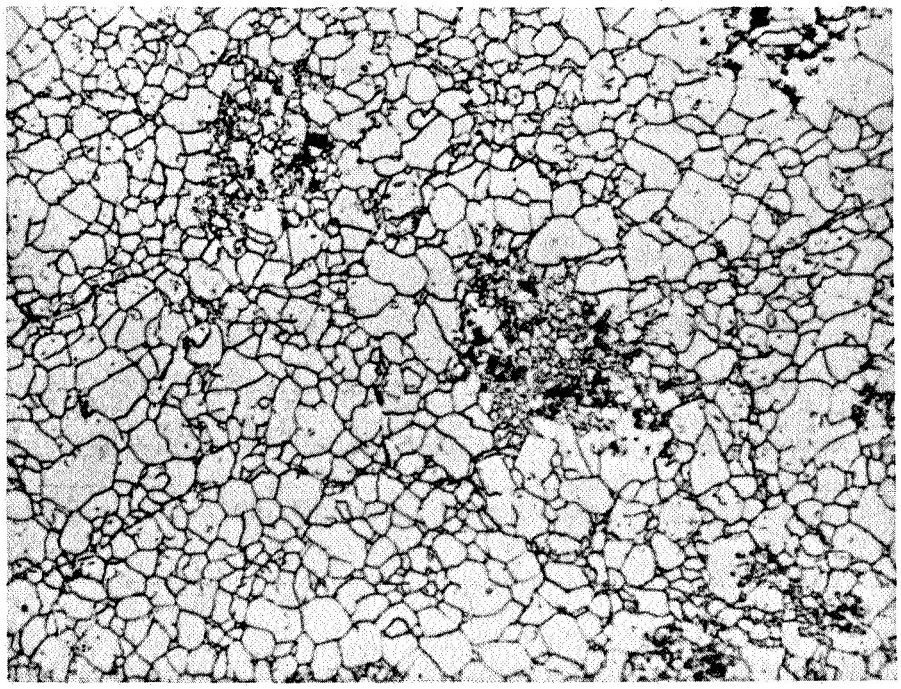

750X Etched 4C553

FIGURE I-28. HIGHER MAGNIFICATION OF HOT ISOSTATICALLY COMPACTED N2-TYPE NICKEL POWDER SHOWING HIGH DENSITY AND VERY FINE GRAIN SIZE ACHIEVED BY THIS MATERIAL

The N2 microstructures contained little porosity or impurities. The final grain size was fine and very uniform in size distribution. The N3 microstructures retained the original lamellar ring configuration. These layers, however, were broken up into finer grains during hot-isostatic compaction, and the interfaces of the particles that came into contact showed a uniform, fine grained structure. Densification of the spherical N3-type powder at 1200 F and 10,000 psi for 3 hr to better than 98 percent of theoretical density was achieved. In all of the microstructures, including those that did not achieve high densities, good bonding between particles was evident wherever the surfaces came into contact. The powder chosen in this program for subscale and full size injector fabrication was the N2-type nickel powder because of its better response to hydropressing and its better density and microstructural characteristics after hot-isostatic compaction.

After an evaluation of the process parameters for C3-type copper powder, the optimum properties appeared to be achieved by hydropressing at 10 tsi, then hot isostatically compacting at 1000 F and 10,000 psi for 3 hr. The N2-type nickel powder appeared to achieve optimal properties by hydropressing at 40 tsi followed by hot-isostatic compaction at 1200 F and 10,000 psi for 3 hr. These parameters are considered to be the minimum conditions that will achieve adequate densification and bonding of the powders. Higher temperatures and longer times of hot-isostatic compaction can be used provided the effects on tooling compatibility with the base metals are minimal. Higher temperatures were eventually used in Task II and Task III studies.

Additional experiments were made with the tooling materials in an effort to prevent the breakage of the glass tooling and to reduce or eliminate bending of the tooling materials in general during the hydropressing cycle. These experiments consisted of placing the tooling rods in a stainless steel picture

frame and packing copper powder around and into this assembly. Radiographic examination of the rods after hydropressing showed very little bending and no indication of other defects; an x-ray of the fabricated assembly is shown in Figure I-29. Since the frame assembly closely simulated the tooling design for copper baffle, dimensional control to close tolerances during fabrication of the baffles appeared feasible.

Picture frame supports for the subscale copper baffles were cut and machined from 304 stainless steel. Sections of the frames were held in place with screws. An OFHC copper plate was machined to close tolerances and inserted between the legs of the separated tooling. This plate was held with side screws through the picture frame. An assembled baffle with tooling incorporated prior to powder packing is shown in Figure I-30.

The subscale copper baffle assemblies were placed in rectangular rubber bags, copper powder vibratory packed around the tooling, and the bag sealed. Hydropressing was accomplished at 10 tsi. Radiographic inspection of the tooling in the baffle components showed that the tooling maintanned its position in the frame with very little bending. Radiographs of two hydropressed baffle components are shown in Figures I-31 and I-32. After hydropressing, the bags were removed and thin steel sheet formed to enclose the baffle assembly. The edges of the sheet were heliarc welded, then a 1/8-in.-diameter 304-type stainless steel evacuation stem welded to one end. The assembly was then outgassed in vacuum at 500 F for about 4 hr to remove moisture and adsorbed gases. The assembly was sealed under a vacuum of about 10^{-3} torr. The sealed baffle components were hot isostatically compacted at 1000 F and 10,000 psi for 3 hr. Considerable deformation of the containers around the components was observed, as shown in Figure I-33. Figure I-34 shows the three subscale baffle components after decanning.

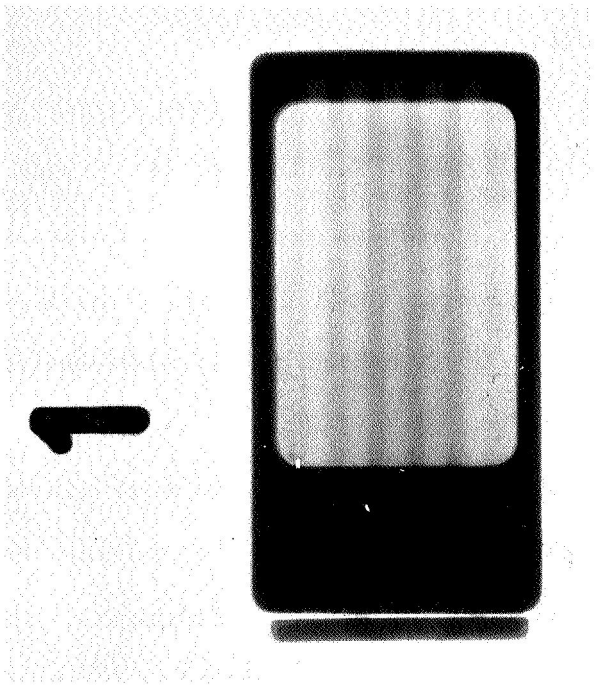

FIGURE I-29. RADIOGRAPH OF INTERNAL TOOLING IN HYDROPRESSED COPPER POWDER

The dark frame is the stainless steel picture frame.

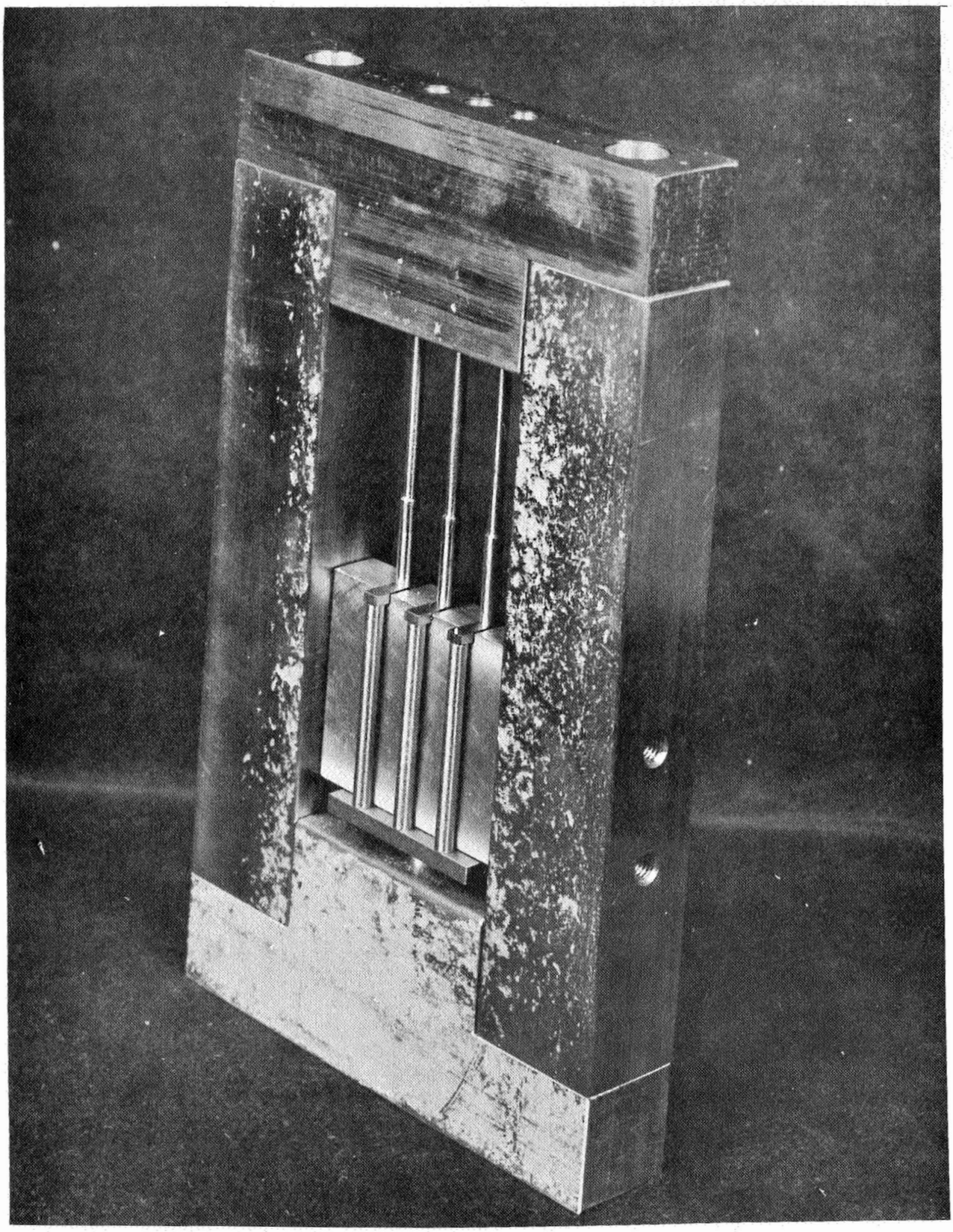

40830

FIGURE I-30. ASSEMBLY OF SUBSCALE COPPER BAFFLE WITH STEEL TOOLING

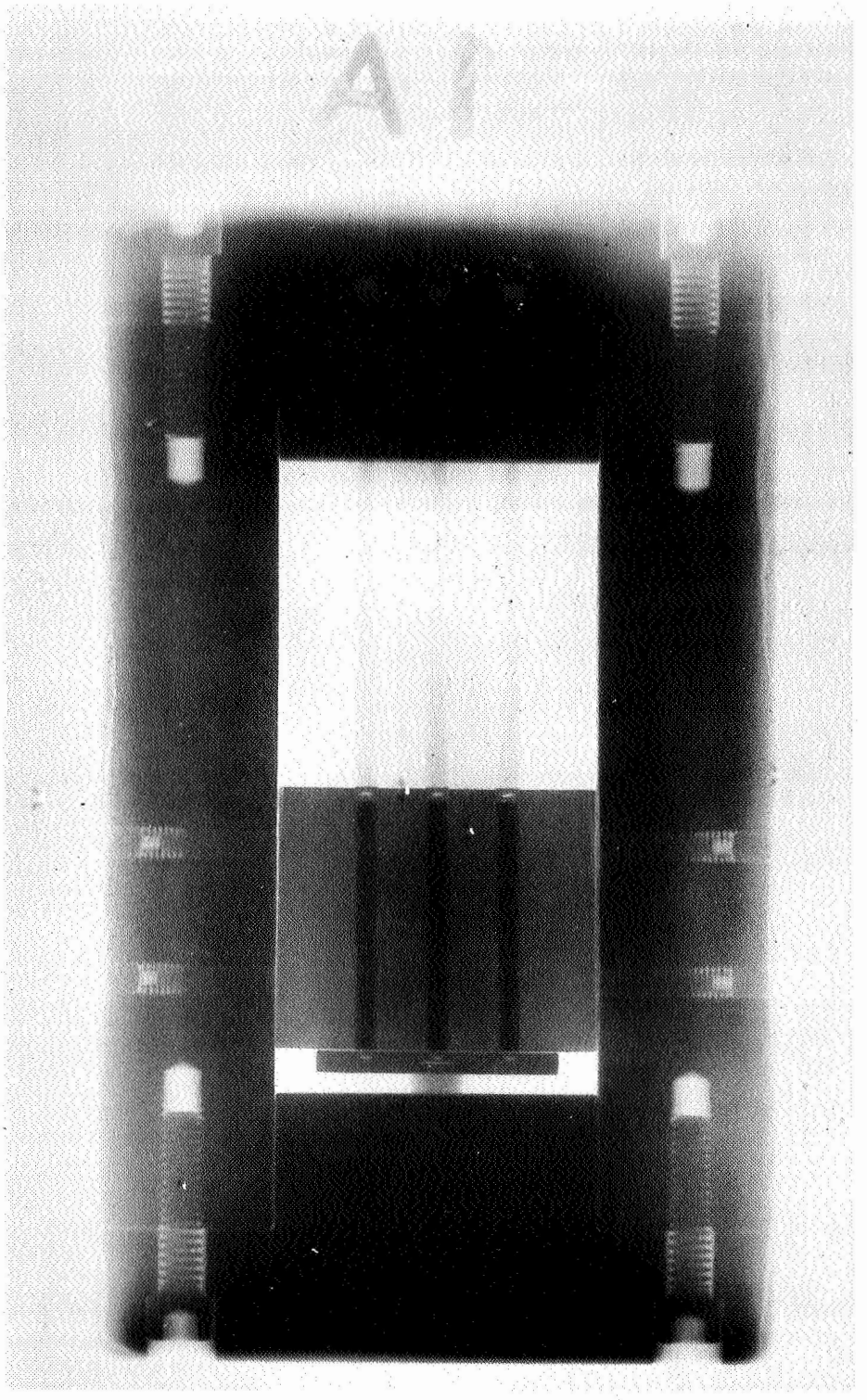

FIGURE I-31. RADIOGRAPH OF SUBSCALE COPPER BAFFLE WITH TOOLING AFTER HYDROPRESSING AT 10 TSI

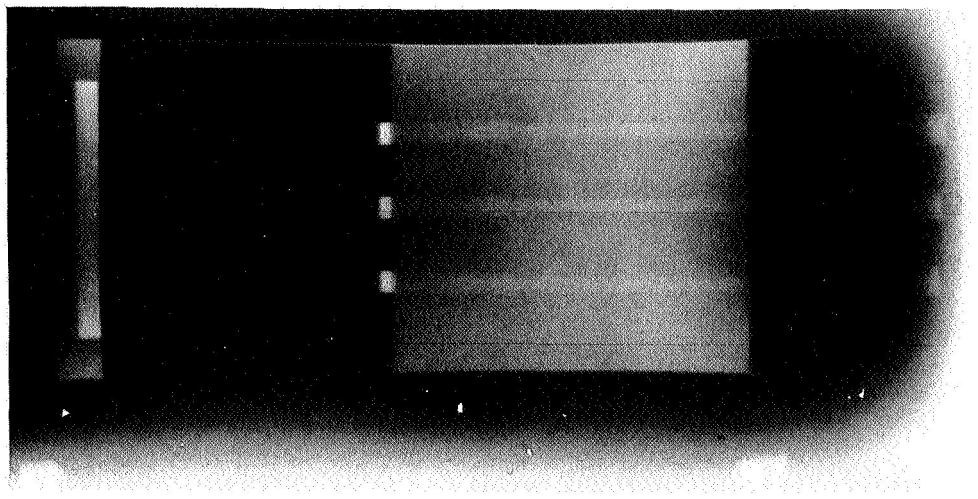

FIGURE I-32. RADIOGRAPH OF SUBSCALE COPPER BAFFLE WITH ALUMINUM TOOLING AFTER HYDROPRESSING AT 10 TSI

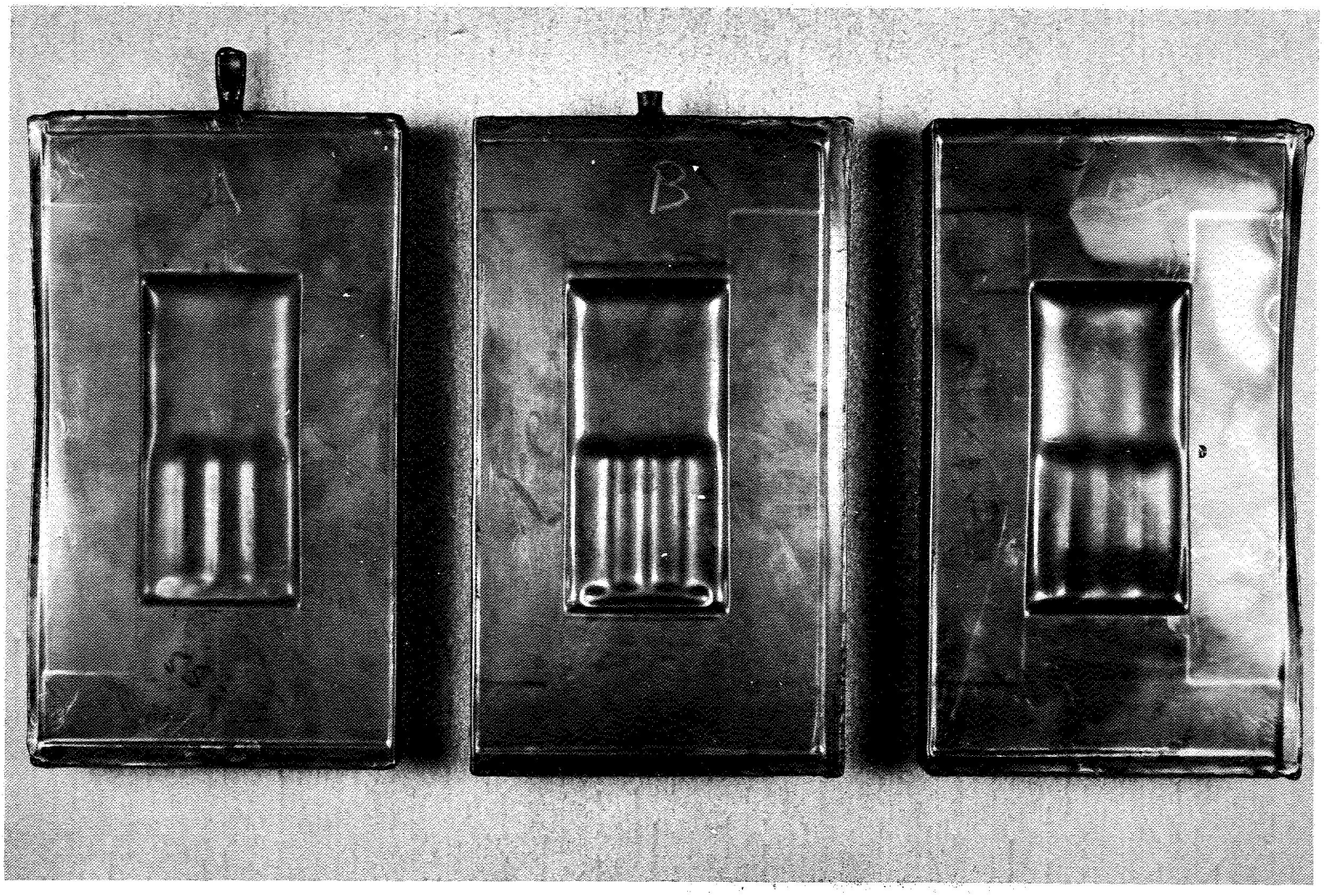

41039

Glass Tooling 1018 Steel Tooling Cr-Coated Aluminum Tooling

FIGURE I-33. SUBSCALE COPPER BAFFLES IN STEEL CONTAINERS AFTER HOT-ISOSTATIC COMPACTION

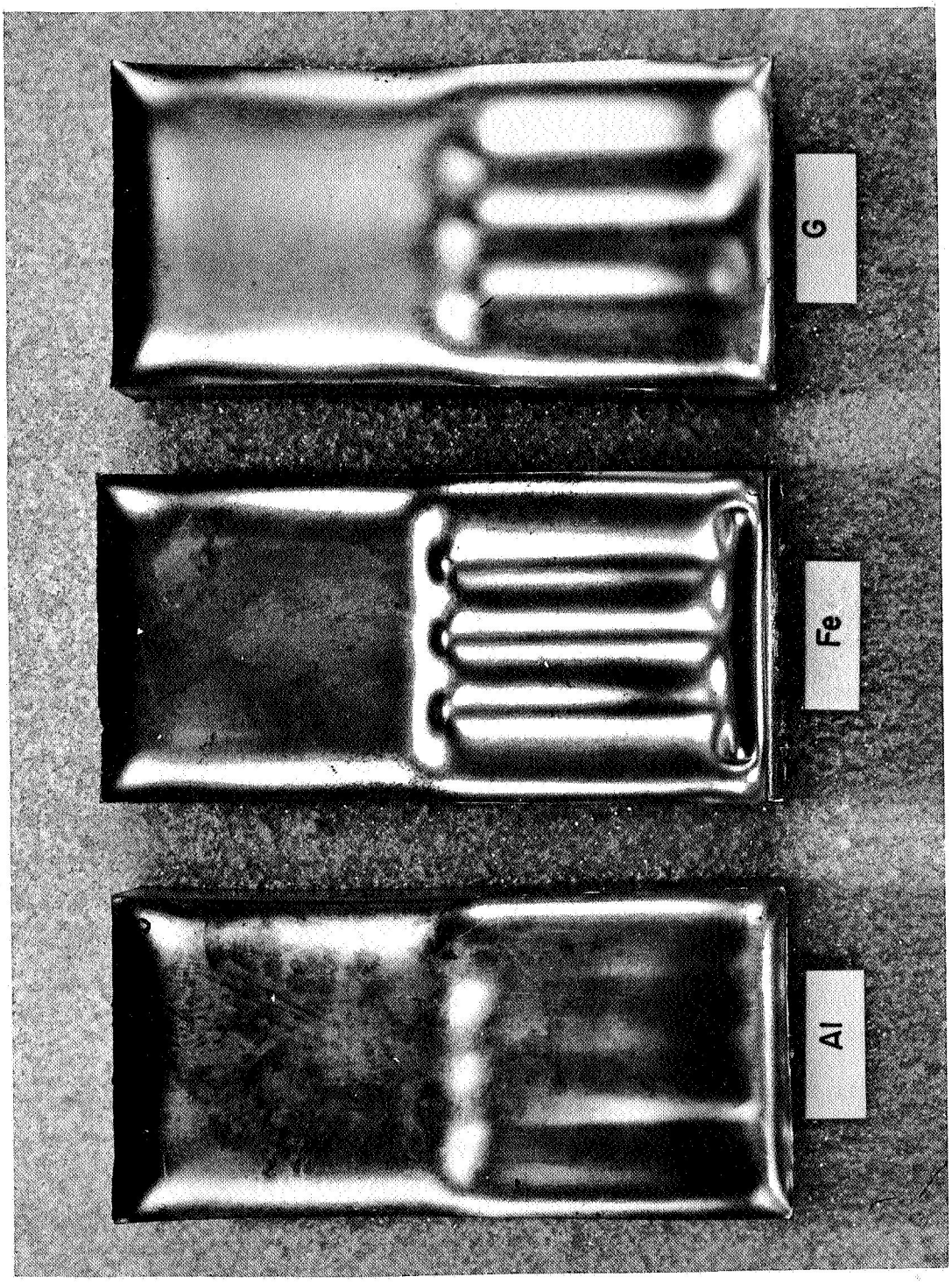

FIGURE I-34. SUBSCALE COPPER BAFFLES AFTER REMOVING STEEL CONTAINERS

The components were inspected by x-ray radiography then placed in leaching solutions to remove the tooling. The steel tooling was completely removed in concentrated H_3PO_4 solution. The aluminum tooling was partially removed in 1N NaOH solution. The glass tooling was completely removed in a $67HF\text{-}33H_2O$ solution. After removing a portion of the aluminum tooling from the subscale component, it became evident that extensive alloying had occurred between the aluminum and copper during hot-isostatic compaction. The aluminum could not be completely removed because of the gross alloying with the copper. These anomalies were sufficient to eliminate aluminum as a candidate tooling material for the copper baffles.

Nondestructive and destructive evaluations of the other two subscale baffle components were conducted after the tooling was removed. These techniques are discussed in a following section (Subtask I-C).

Two types of tooling were prepared for the subscale nickel injectors. One set was prepared from 1018 carbon steel. The other set consisted of 1100-aluminum tooling. Each set consisted of two separate tooling pieces, one tooling piece representing the fuel channels and the other tooling piece representing the oxidizer channels. Drawings of the two tooling pieces are shown in Figures I-35 and I-36. When assembled and consolidated, the two tooling pieces remain separated by nickel powder. A sectional view of the subscale nickel injector assembly design is sketched in Figure I-37.

The outer shell container for the subscale nickel injector was machined from 304 stainless steel. The inner shell retaining ring was machined from pure nickel and was tight-fitted to the I.D. of the outer container. To fix the tooling in the injector and prevent movement or rotation of the tooling during processing, nickel pins were press-fitted to the nickel base plate and tooling shaft at the bottom of the injector. Another nickel pin was inserted through the

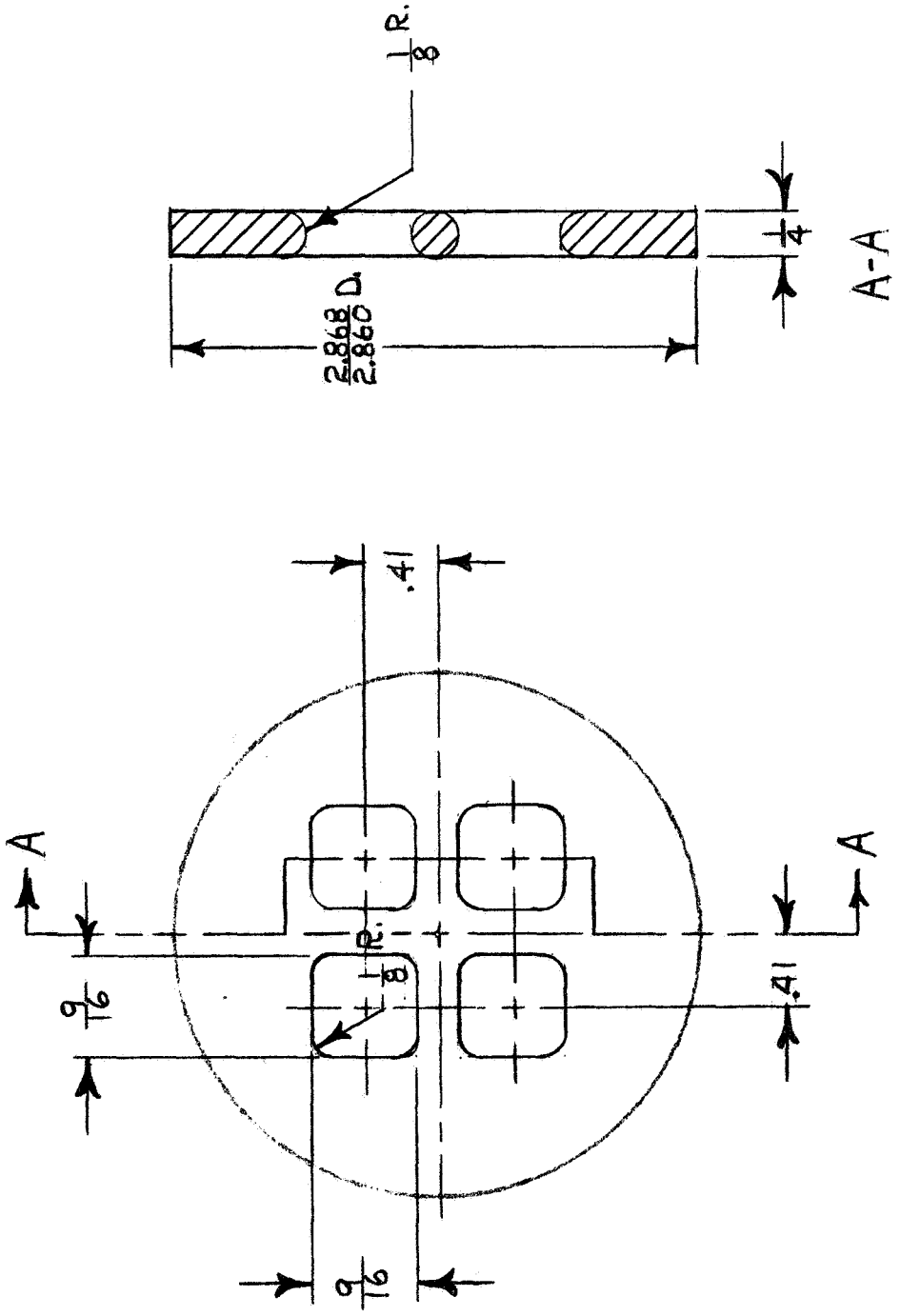

FIGURE I-35. TOOLING DESIGN FOR FUEL CHANNELS IN SUBSCALE INJECTOR

A steel ring was welded to the periphery of the piece above to complete the tooling.

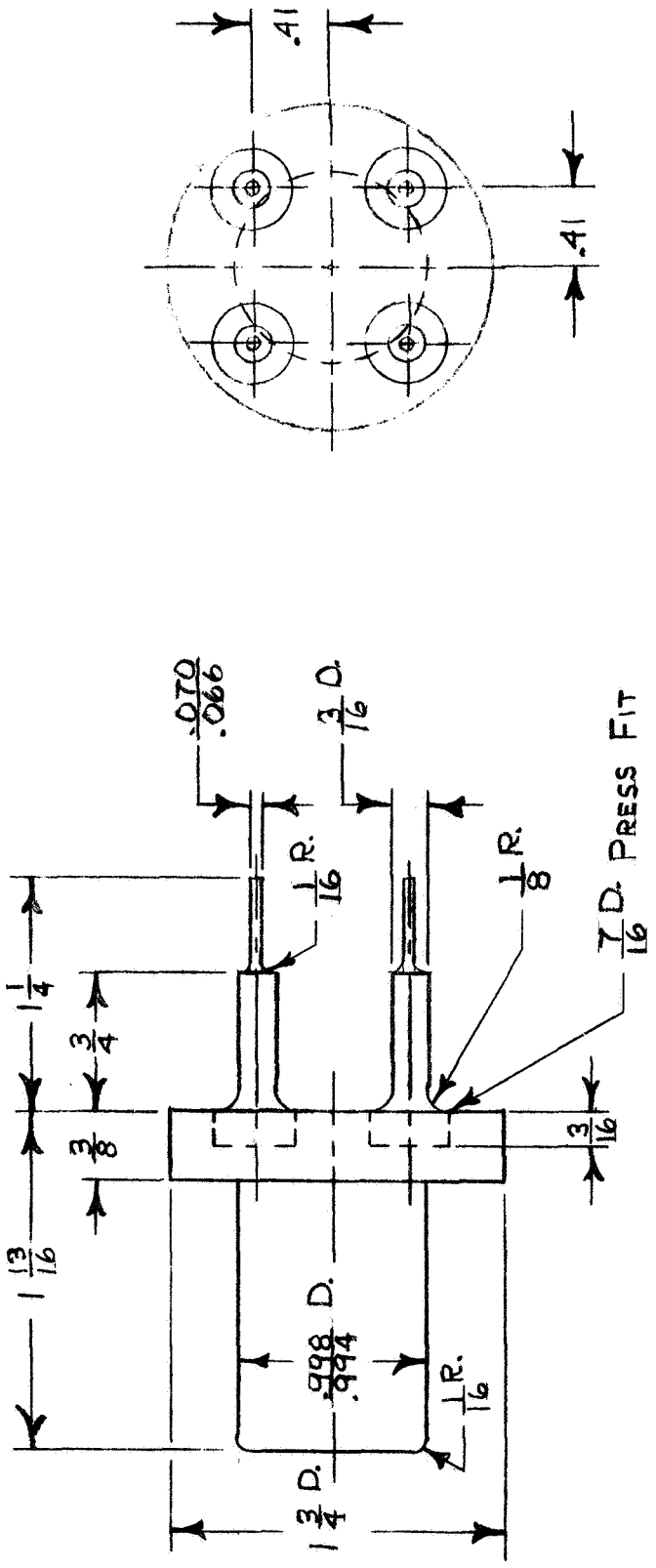

FIGURE I-36. TOOLING DESIGN FOR OXIDIZER CHANNELS IN SUBSCALE INJECTOR

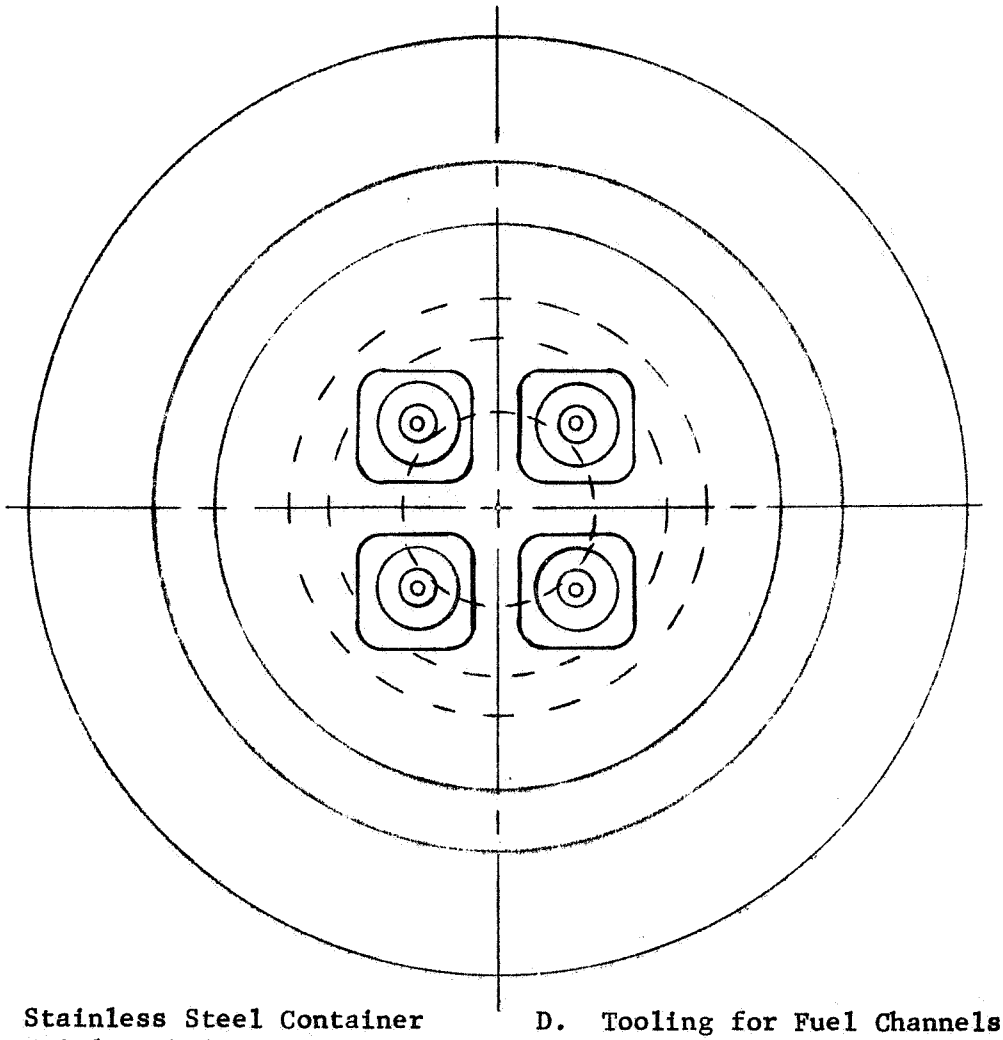

A. Stainless Steel Container
B. Solid Nickel Retaining Ring
C. Nickel Powder
D. Tooling for Fuel Channels
E. Tooling for Oxidizer Channels
F. Nickel Base Plate

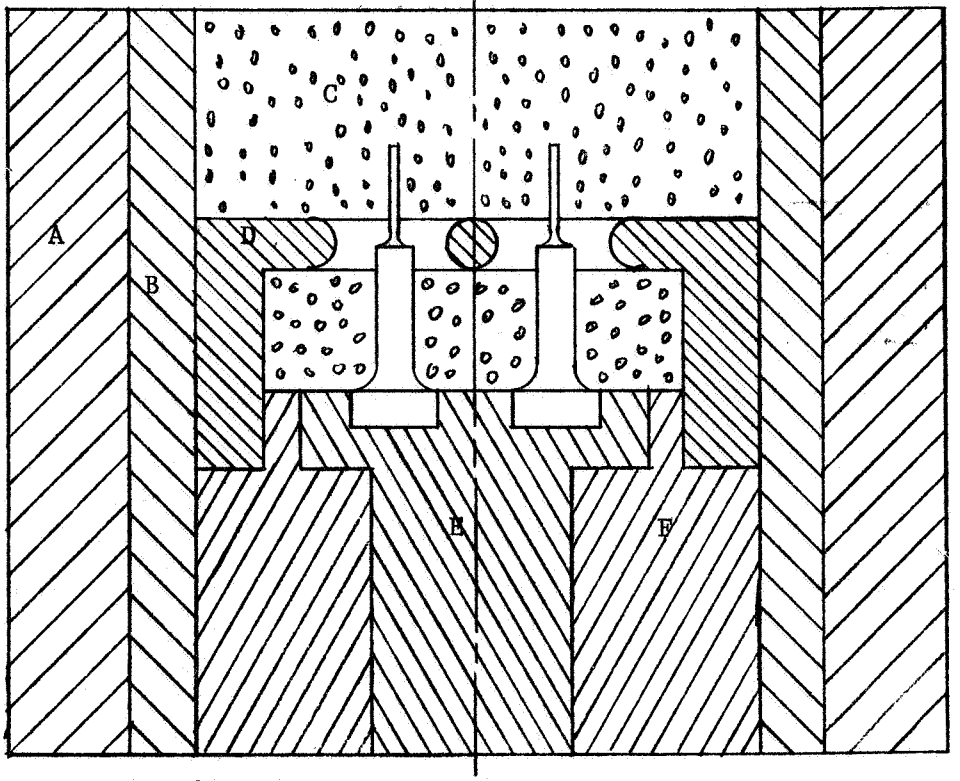

FIGURE I-37. SKETCH OF SUBSCALE NICKEL INJECTOR DESIGN

stainless steel container and nickel retaining ring to fix the position of the fuel-channel tooling. In one injector specimen, a solid nickel base plate was fabricated to hold the tooling plate and pins while in the other injector, a 75 percent dense nickel base plate was fabricated from powder by hydropressing and placed below the oxidizer channel tooling. This was incorporated to determine if the nickel powder could be fully densified below as well as above the tooling parts and to compare the dimensional control of the tooling using these two different designs.

After assembling the tooling in the subscale nickel injectors, the nickel pins were placed through the stainless steel retaining shell to fix the positions and prevent any movement of the tooling during vibratory packing and subsequent fabrication steps. The N2 nickel powder was vibratory packed into the assembly, and several cylindrical rubber bags were used to seal the assembly. Hydropressing was accomplished at 40 + si. Radiographic examination of the tooling in the injectors after hydropressing was not possible due to the large thickness of the injector and stainless steel assembly. After the bags were removed, the hydropressed parts were placed in steel containers 5 in. diameter by 1/8-in.-thick wall 1018 steel tubing for the sides, and 5 in. diameter by 1/8 in. thick spun stainless steel plates for the end lids. The injector components were vacuum outgassed at 500 F for 4 hr. The containers were sealed in a vacuum of about 10^{-3} torr. The sealed specimens were hot isostatically compacted at 1200 F and 10,000 psi for about 4 hr. The soak time was increased 1 hr to ensure that the large mass of material in the subscale injector achieved a temperature of 1200 F and was held at 1200 F for at least 3 hr. After the compaction cycle, the injectors were visually inspected, then each was decanned by machining. The component with aluminum tooling was sectioned across one of the tooling pins to examine the interface as-bonded. The component was then placed in a bath of 1N NaOH to remove the tooling.

Subtask I-C-1: Inspection Techniques

The objective of this subtask was to develop nondestructive inspection techniques and to destructively inspect components fabricated in Task I. Inspection techniques developed in this task were subsequently utilized on full scale components fabricated in Tasks II and III to determine tooling location, completion of the tooling removal process and control of dimensions and alignment of the internal flow channels.

Radiographs examination of components and flow tests were the primary nondestructive tests used. Ultrasonic tests were eliminated as a possible inspection tool due to the thicknesses and complexity of the internal structures encountered in the components.

Subscale copper baffles were inspected by x-ray radiography at several points in the fabrication process. X-ray inspection was performed after hydropressing copper powder around the tooling and was described earlier with reference to Figures I-29, -31, and -32. Similar inspections were made of the subscale baffle components after removing the tooling. The radiographs showed in good detail the position and alignment of the tooling in the baffles. The tooling placed adjacent to the solid OFHC copper plates (denoted as "lower tooling region with split legs" in the next figure) maintained their position and alignment through the fabrication process as is illustrated in Figure I-38. The tooling in the upper region was well positioned and straight in the center section but near the ends some bending of the tooling was observed. The baffle containing steel tooling was sectioned after leaching was completed and is shown in Figure I-39. Density measurements and hardness tests on local sections of the baffle with steel tooling were measured. Densities in the subscale copper baffle averaged 98.4 percent of theoretical with less than ±0.4 percent variance in any localized

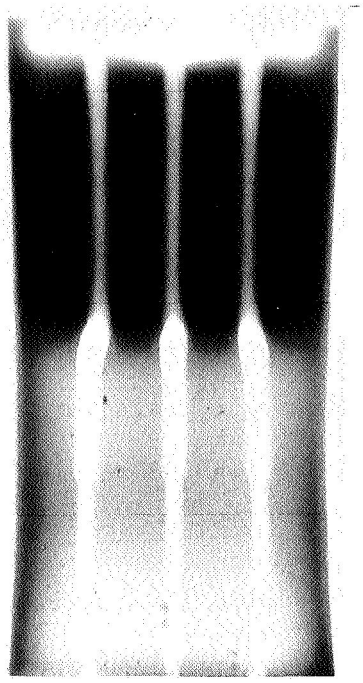

FIGURE I-38. RADIOGRAPH OF HOT ISOSTATICALLY COMPACTED SUBSCALE COPPER BAFFLE WITH GLASS TOOLING COMPLETELY REMOVED

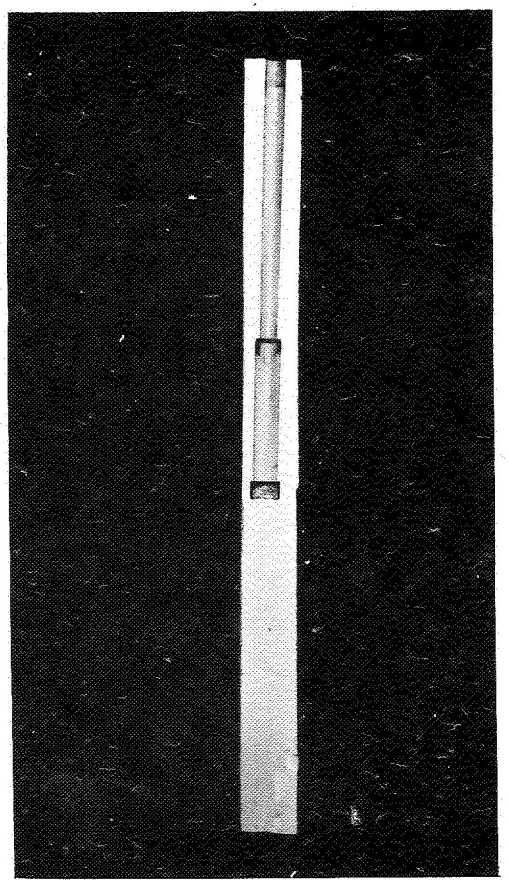

41549

(a) Sectioned copper baffle showing alignment and dimensional control in center region.

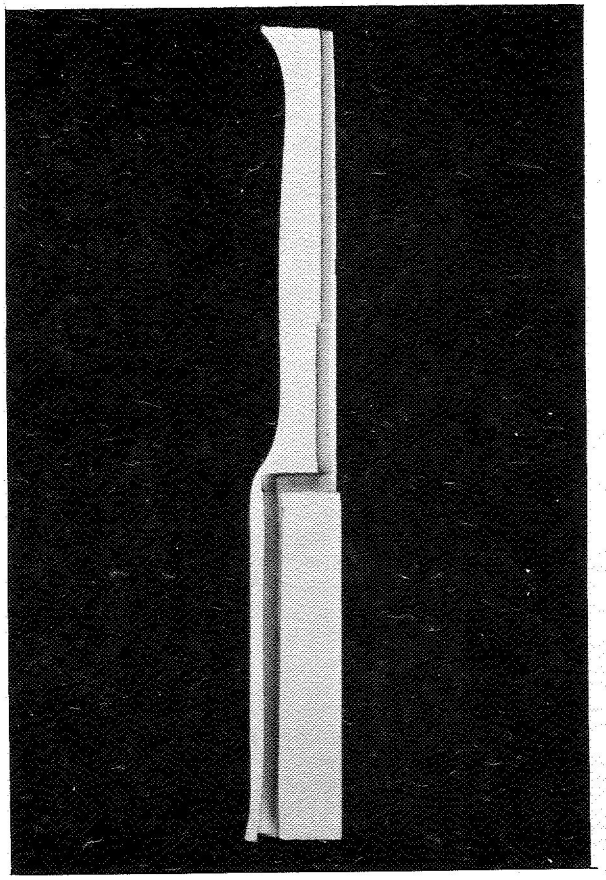

41647

(b) Sectioned copper baffle showing continuity and dimensional control of flow channels.

FIGURE I-39. SECTIONED SUBSCALE BAFFLE WITH STEEL TOOLING REMOVED

section. Localized hardness measurements were taken across nine different copper/tooling interfaces, and no gradients in hardness were detected. The hardness values compared almost identically with those taken on fully dense copper powder specimens fabricated earlier.

Because of the small sized sections taken from the subscale copper baffles, it was not possible to obtain suitable tensile test bars from these sections. Instead, representative tensile tests were conducted on solid cylindrical samples that had been processed from the C3-type copper powder at the same conditions as the subscale copper baffles. These samples were evaluated for density, hardness, and microstructural characteristics so that a direct comparison could be made between the representative samples and the subscale components. The results of these tests are summarized in Table I-10.

Metallographic examination of the nickel in the subscale injectors indicated that a density variation existed from the outer regions of high density to the central regions of low density. The particles were well-bonded but the high porosity (about 15 percent) in the central regions caused some deterioration of the nickel structure in this section. Also of interest was the nickel-aluminum interface in the subscale injector containing aluminum tooling. The interface diffusion zone and intermetallics formed at the interface during hot-isostatic compaction are shown in Figure I-40. Microhardness traverses were conducted across this interface and the results are tabulated in Table I-11.

Attempts were made to x-ray the internal structure of the hot isostatically compacted subscale nickel injectors after removing the steel container and thick retaining rings. Resolution of the steel tooling was fuzzy due to the large penetration thickness and small differences in densities between the steel and nickel. Some detail was resolved in the x-rays of the injectors containing aluminum tooling. Radiographs of the subscale nickel injectors are shown in

TABLE I-10. COMPARISON OF MECHANICAL PROPERTIES OF HOT ISOSTATICALLY COMPACTED C3-TYPE COPPER POWDER AND COMMERCIAL WROUGHT AND ANNEALED PRODUCTS

	C3	Annealed Commercial Copper
0.2% Offset Yield, psi	13,700	10,000
σ_{μ}, psi	32,000	32,000
Elongation, %	31	45
Red. in Area, %	22	--
E, 10^6 psi	18.9	17.0
Knoop Hardness, 100g	104	--
R_B Hardness, 100Kg	58	42

Note: Specimens were tested on Instron Testing Machine with cross-head speed of 0.005 in. per minute up to the 0.2 percent offset yield point, then cross-head speed was 0.05 in. per minute to fracture. All specimens were standard 1/4 in. gage diameter, 1.0 in. gage length, threaded end tensile bars.

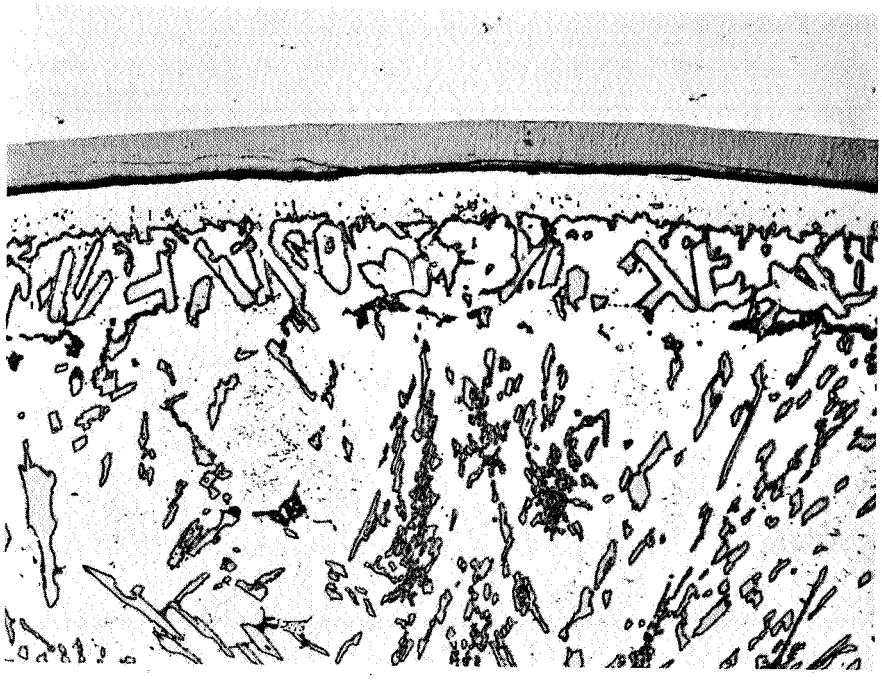

FIGURE I-40. MICROSTRUCTURE OF NICKEL-ALUMINUM INTERFACE AFTER HOT-ISOSTATIC COMPACTION AT 1200 F AND 10,000 PSI FOR 3 HR

TABLE I-11. RESULTS OF HARDNESS TESTS ON NICKEL-ALUMINUM BONDED INTERFACE

Zone	Average KHN, 100 g	No. of Indents
Nickel	147	4
Ni_3Al	1082	3
NiAl	692	3
Al	57	3

Figure I-41. In both specimens, the fuel-channel tooling appeared to be excessively deformed. The oxidizer channel tooling could not be adequately resolved in the radiographs for determinations of position and alignment. The steel tooling in the subscale injector was examined destructively by sectioning the injector. Localized density measurements on compacted nickel powder sections were taken. The density of the nickel powder above the fuel-channel tooling on the outer periphery was better than 98 percent dense. Below the oxidizer-channel tooling, the density was about 89 to 90 percent dense. The low density, in the region between the tooling pieces, was due to the restricted motion of the powder. This anomaly and methods for eliminating the low density regions and improving dimensional control are described in the following section on process optimization.

Despite the fact that the aluminum was molten during the hot-isostatic compaction cycle the molten metal did not extrude or penetrate into the nickel matrix. The total nickel-aluminum reaction zone was narrow, and the hole enlargement due to loss of nickel into the aluminum was negligible, less than 0.002 in. on the radius. This enlargement could be compensated for by making the tooling about 2 to 3 mils undersize on the diameter. At least two hard brittle intermetallic compounds formed at the interface. A portion of this brittle layer was removed during leaching in 8M NaOH; a tenacious layer of Ni-rich remained as shown in Figure I-42. The gray, Ni-rich compound, which was retained after leaching the aluminum in 8M NaOH, was ten times harder than nickel. If this brittle layer is left on the surfaces of the internal channels, it may adversely affect the behavior of the injector during its operation. Cracks formed in the layer could propagate into the nickel when the injector is in a stressed condition. Also, thermal cycling from room temperature to cryogenic temperatures may loosen particles of the brittle layer, and subsequent flow through the internal channels may break off pieces that could reduce or impede the flow of oxidizer or fuel.

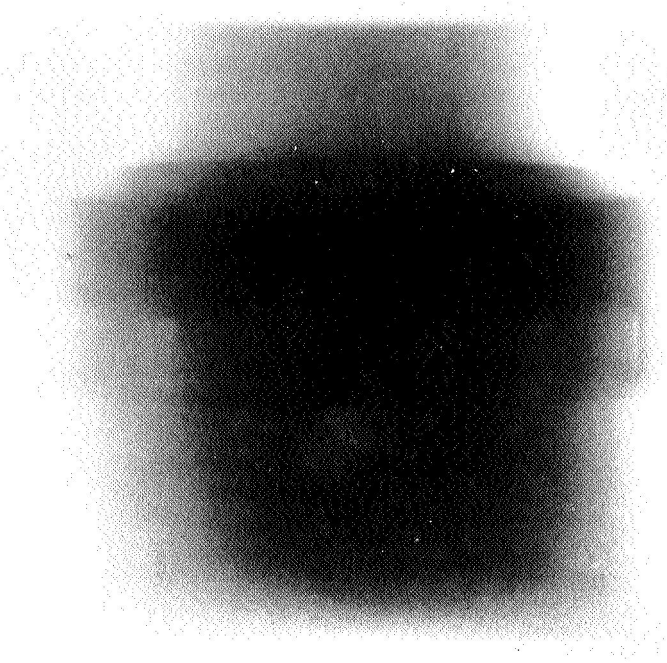

(a) Injector with aluminum tooling.

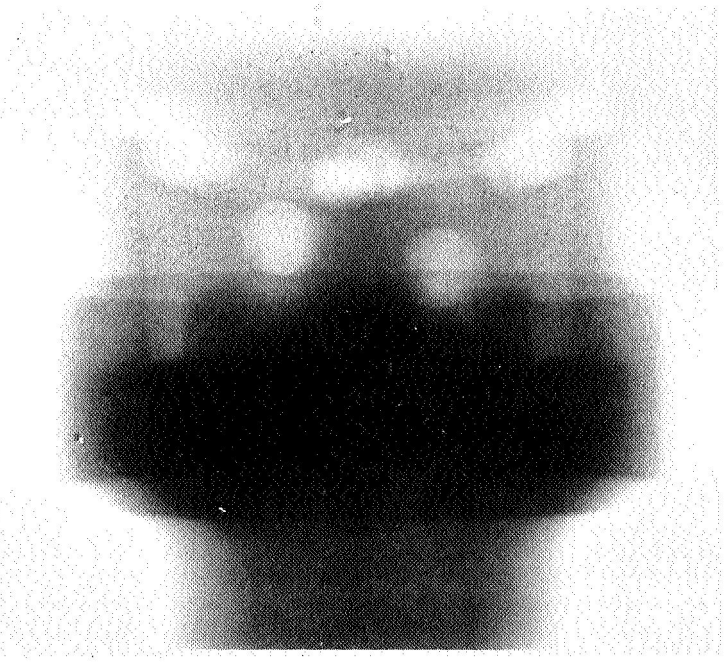

(b) Injector with steel tooling.

FIGURE I-41. RADIOGRAPHS OF HOT ISOSTATICALLY COMPACTED SUBSCALE NICKEL INJECTORS

Distortion of the fuel-channel tooling was about the same for both tooling materials.

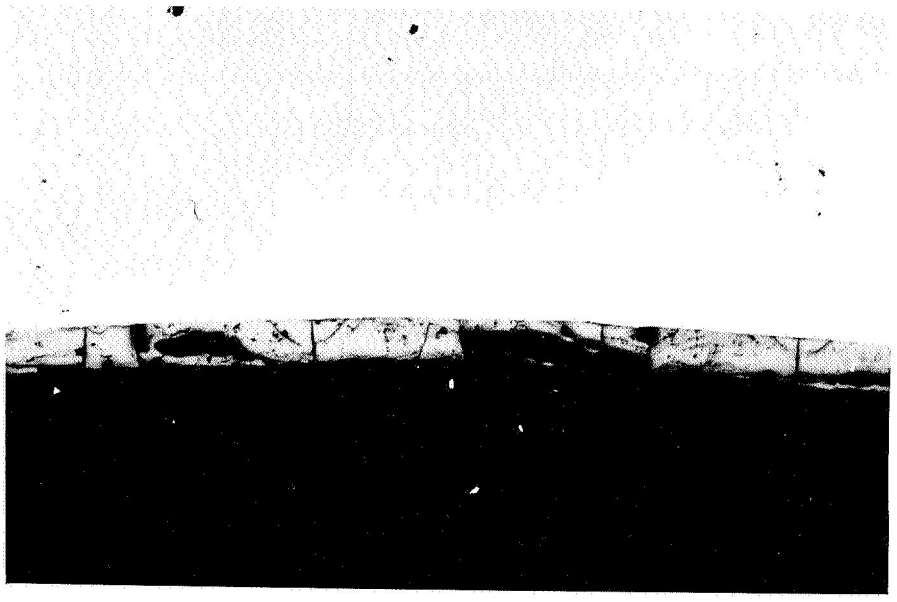

100X No. 3, As Polished 2D954

FIGURE I-42. ALUMINUM-NICKEL INTERFACE AFTER LEACHING ALUMINUM IN 8M NaOH

Attempts were thus made to find a technique to selectively remove the remaining brittle aluminide layer.

By washing the channels in 25 percent H_2SO_4 solution for several days, the NiAl compound was completely removed as shown in Figure I-43. Microhardness tests on the nickel near these surfaces indicated the nickel was not affected by aluminum alloying. Thus, only one disadvantage of aluminum remains, that of becoming soft or molten during hot-isostatic compaction. After completion of Task I, it appeared that to completely densify the nickel powder throughout the injector, a high compaction temperature and long soak time would be needed. Thus, for Task III studies at least, steel was preferred over aluminum.

Due to the low density regions in the subscale nickel injectors, no tensile tests were conducted on sections of the subscale nickel injectors. To verify that the nickel powder achieves acceptable mechanical properties with the process parameters used to fabricate the subscale injectors, solid cylindrical samples were fabricated from the N2-type nickel powder at the same conditions used to fabricate the subscale nickel injectors. Tensile bars were machined from this material and tested. The results of these tests are summarized in Table I-12 and show that the properties are comparable to wrought and annealed nickel.

Subtask I-C-2. Process Optimization

In the subscale copper baffles, a solid plate of OFHC copper inserted between the tooling prevented the tooling from moving inward, and good dimensional control was achieved. Fixturing was also successful in preventing movement of the tooling in the center portion of the baffle; however, near the sides the tooling was bent toward the frame. This end effect was caused by a gradient in pressure in the powder generated during compaction. Near the sides, the thin steel container was reinforced by the picture frame, and the powder directly under

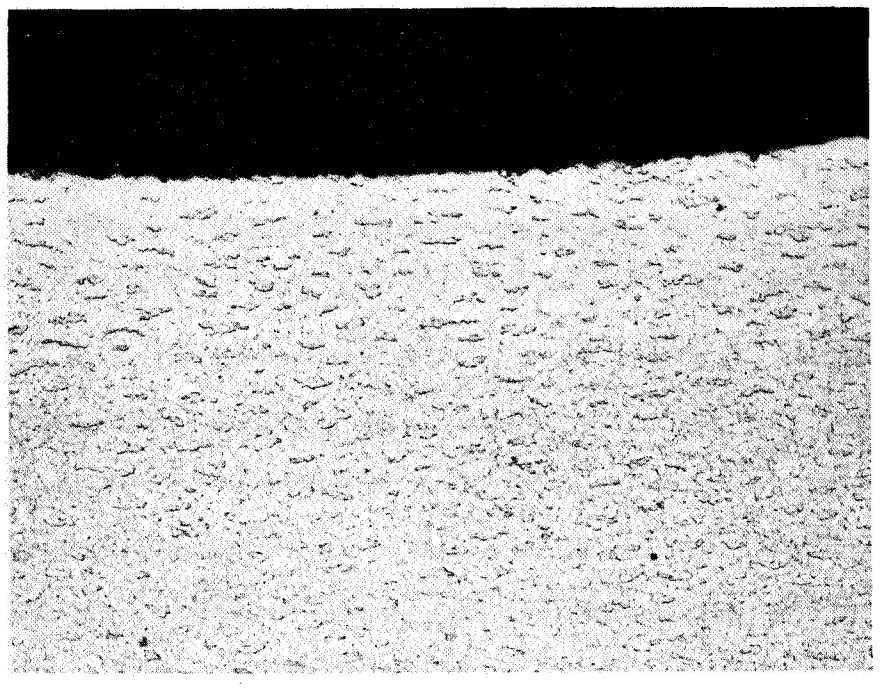

100X Etched 5D487

FIGURE I-43. NICKEL-ALUMINUM INTERFACE AFTER LEACHING IN 8MNaOH FOLLOWED WITH $25H_2SO_4$-$75H_2O$

Both intermetallic layers were completely removed by this leaching sequence.

TABLE I-12. COMPARISON OF MECHANICAL PROPERTIES OF HOT ISOSTATICALLY COMPACTED N2-TYPE NICKEL POWDER AND COMMERCIAL WROUGHT AND ANNEALED PRODUCTS

	N2 Nickel	Annealed Commercial Nickel
0.2% Offset Yield, psi	35,600	30,000
σ_{μ}, psi	64,500	70,000
Elongation, %	30	40
Red. in Area, %	24.5	--
E, 10^6 psi	32.2	32.0
Knoop Hardness, 100g	140	--
R_B Hardness, 100Kg	63	65

Note: Specimens were tested on Instron Testing Machine with cross-head speed of 0.005 in. per minute up to the 0.2 percent offset yield point, then cross-head speed was 0.05 in. per minute to fracture. All specimens were standard 1/4 in. gage diameter, 1.0 in. gage length, threaded end tensile bars.

this area was compressed to equivalent densities later than the powder in the center. The powder in the center regions thus had a tendency to move toward the sides where the density was slightly less. This end-effect and the tooling distortion that resulted from it was minimized by slanting the edges of the picture frame so that the container movement was not hindered in the area and by increasing the distance between the last piece of tooling and the edge of the baffle so that the end-effected area could be removed. Thus modifications were incorporated into the process to fabricate full-sized copper baffles and are described in detail in the section on Task II studies.

In the subscale nickel injectors, the fuel-channel tooling for the fuel channels was fixed with nickel pins with respect to the oxidized channel tooling to prevent rotation during vibratory packing and subsequent fabrication processes. The fixed positions were maintained satisfactorily by pinning; no rotation was observed. The fuel-channel tooling, however, experienced excessive distortion during hydropressing and hot-isostatic compaction. This was evident in radiographic examinations and in the sectioned components. This distortion was caused by tooling following the gross movement of powder above the fuel-channel tooling plate toward the less dense powder between this plate and the oxidizer-channel tooling. The fixturing of the nickel base plate and the oxidizer tooling with respect to the fuel tooling was designed to hold length-wise (axial) dimensions corresponding to those in the full sized injector. It was expected that the powder above the fuel tooling plate during compaction. However, as the powder above the fuel tooling plate densified, its ability to flow through this tooling was lessened and the fuel-channel tooling simply moved with the powder adjacent to it.

The oxidizer-channel tooling maintained good dimensional control and alignment during fabrication of the subscale injectors; the process optimization consisted solely of preventing distortion of the fuel-channel tooling. Two basic changes made in the design of the subscale injector to prevent this distortion were:

(1) Elimination of pinning and fixturing of the ox-channel tooling to the solid nickel retaining ring;

(2) Removal of edge restraints on the fuel-channel tooling by making the peripheral tooling ring out of hydropressed iron powder rather than solid low carbon steel.

During hot-isostatic compaction, the hydropressed iron ring was expected to compact the same as the nickel powder adjacent to the iron ring. This would allow the fuel-channel tooling piece to move freely without edge restraints. This changes are incorporated in the design sketch of the subscale injector shown in Figure I-44.

The tooling for the modified subscale nickel injectors was prepared from low carbon (1018) steel and from hydropressed iron powder. These pieces and other tooling parts are shown in Figure I-45. The only two parts made from solid nickel were the nickel base plate and the nickel inner retaining ring. The assembled modified subscale injector is shown in Figure I-46.

The nickel powder was vibratory packed around the assembled tooling pieces, and the subscale injectors were then placed in low carbon, thin walled, steel containers. Hydropressing of the nickel powder was unnecessary after the above changes in the design were made. Spun stainless steel lids were welded to the container and sealed by electron beam welding. Each container was pressure checked for leaks with 200 psi helium; no leaks were detected.

The subscale injectors were hot isostatically compacted at 1270 F and 10,000 psi for 3 hr.

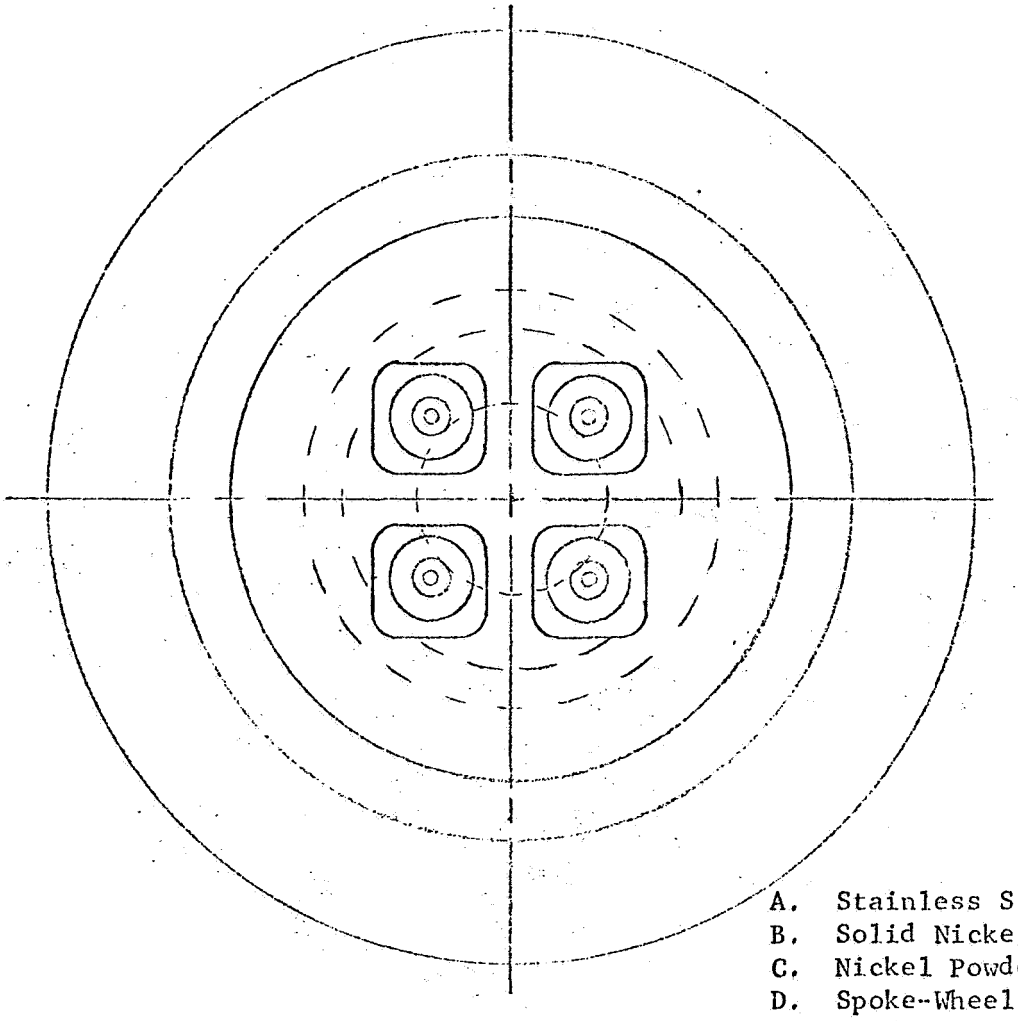

A. Stainless Steel Container
B. Solid Nickel Retaining Ring
C. Nickel Powder
D. Spoke-Wheel Tooling
E. Stud-Plate Tooling
F. Nickel Base Plate
G. Iron Powder Ring

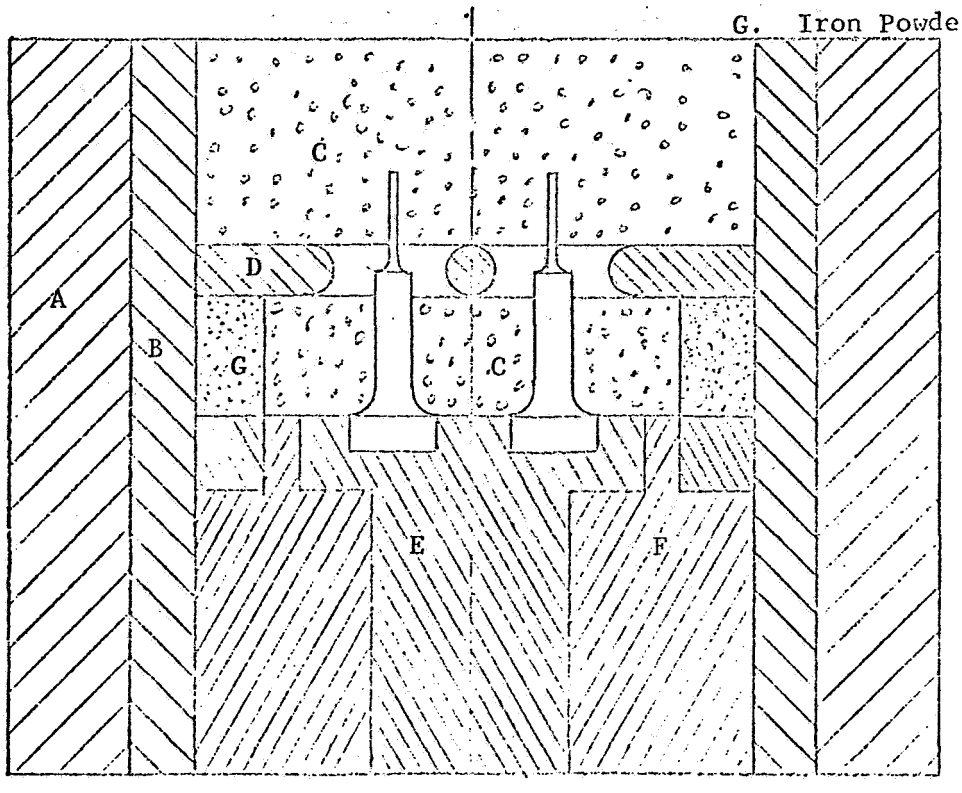

FIGURE I-44. SKETCH OF MODIFIED NICKEL INJECTOR DESIGN

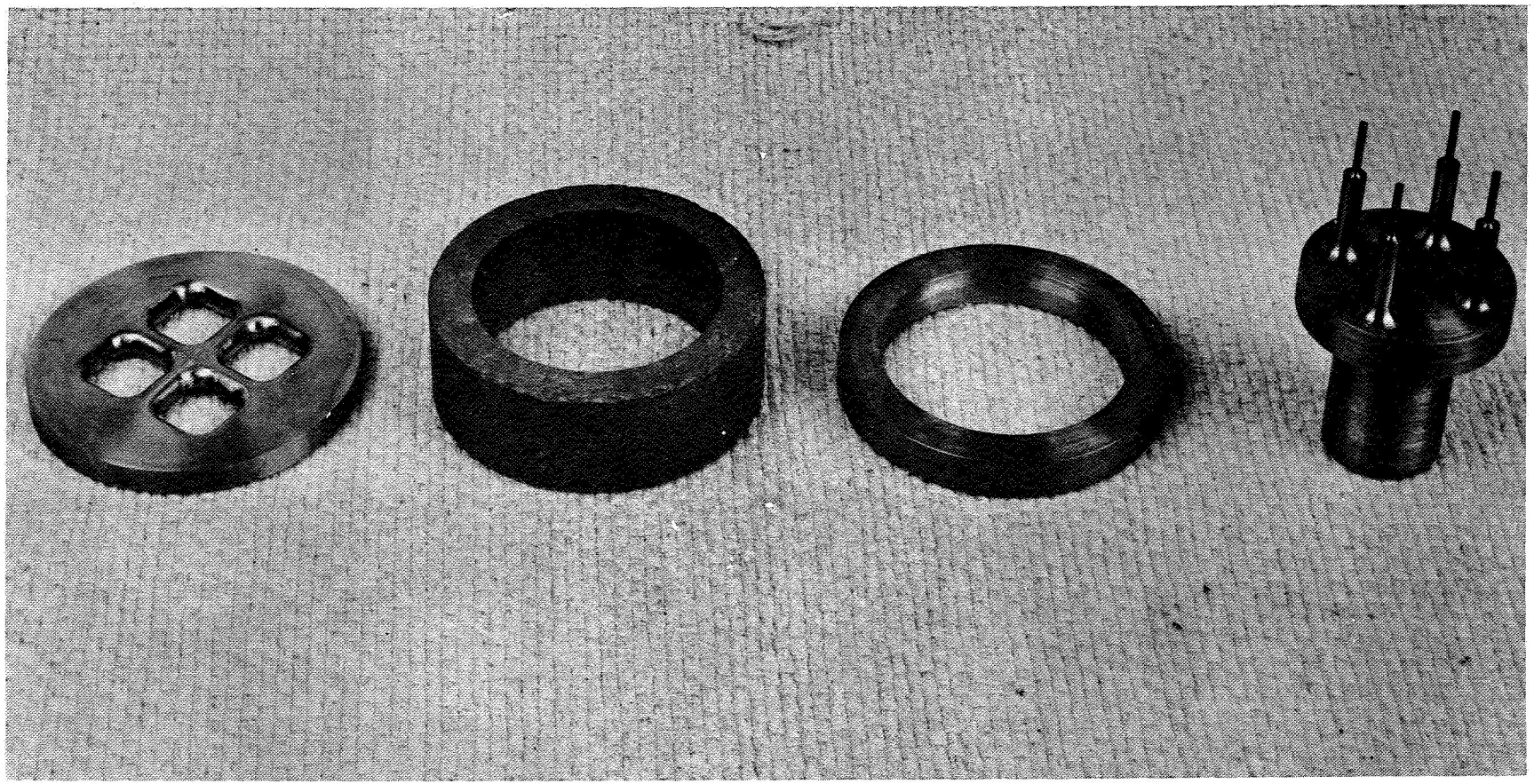

Fuel-channel tooling plate

Fuel-channel tooling ring of hydropressed iron powder

Fuel-channel tooling ring spacer insert

Ox-channel tooling

FIGURE I-45. ILLUSTRATION OF TOOLING USED IN MODIFIED DESIGN OF SUBSCALE NICKEL INJECTOR

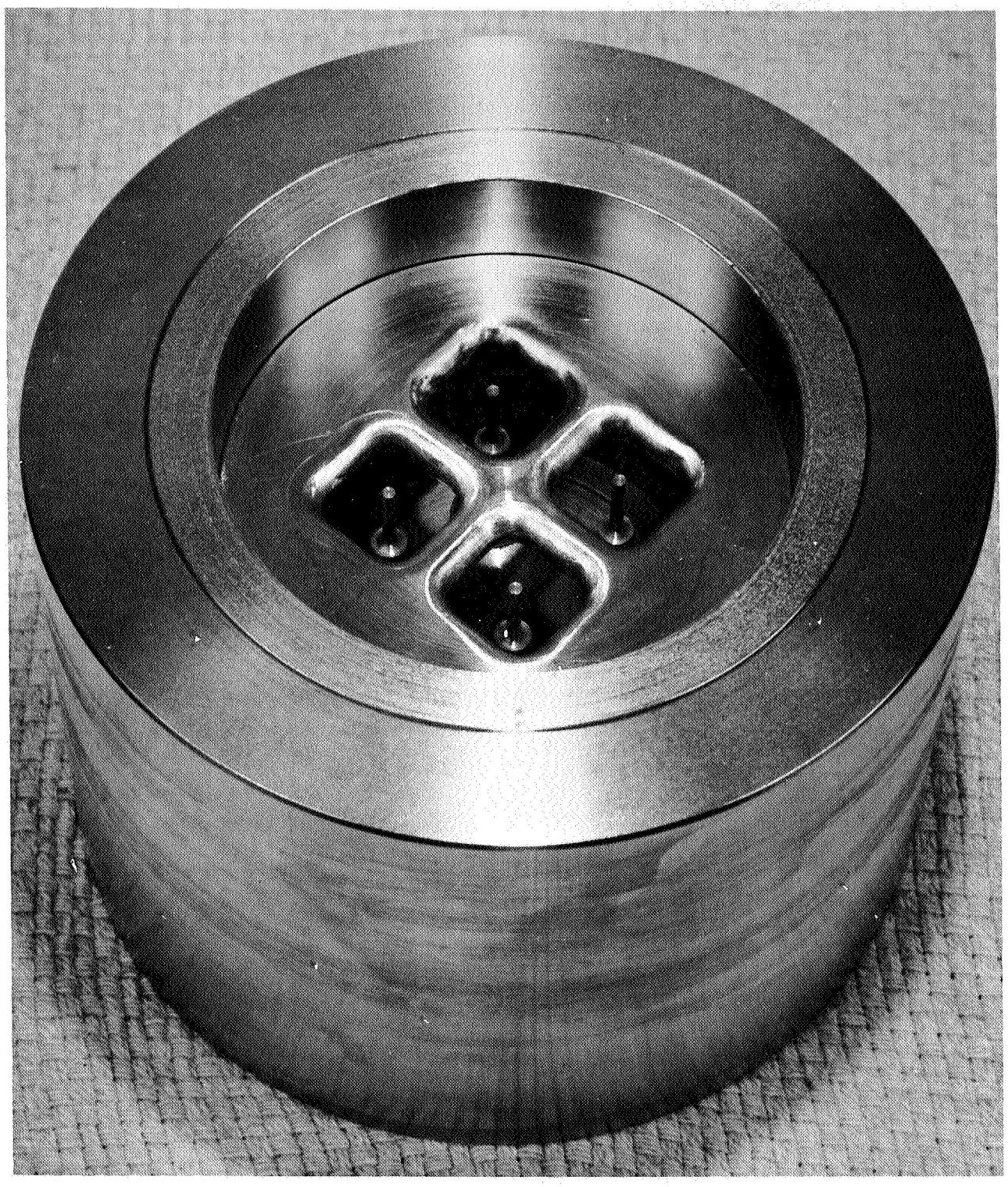

FIGURE I-46. ASSEMBLY OF MODIFIED SUBSCALE NICKEL INJECTOR

After the compaction cycle, the steel containers were removed and the steel tooling in the injectors was exposed by machining the nickel surfaces. The tooling was removed in $25H_2SO_4$-$75H_2O$ solution and the component was x-ray examined. The fuel-channel plate appeared to be slightly warped,but the warpage was considerably less than before. A void was detected at the top edge of the fuel channels and appeared to exist around the peripheral edge of the tooling. The radiographs are shown in Figure I-47.

One nickel injector was sectioned and examined visually and metallographically. A flow test was conducted on the other modified subscale injector. The fuel-hole channels were found to be free of any impediment to flow. The flow test also showed that the ox-hole channels were effectively separated from the fuel-hole channels. No interchannel leakage was detected. Figure I-48 is a macrograph of the sectioned subscale injector showing the dimensional control achieved by the tooling in the compacted nickel powder. The nickel powder was fully dense throughout as determined by metallographic examinations of the sectioned parts. Metallurgical bonds were achieved between the nickel powder and adjacent solid nickel parts. A typical region of the densified nickel powder is shown in Figure I-49. All passages appeared smooth and unimpeded, and the ox-hole channels were effectively separated from the fuel-hole channels. The iron ring fabricated from hydropressed iron powder had apparently achieved full density but bulged inward slightly during hot-isostatic compaction. The fuel channel cavity had a camber of 1/4 in. from the edge to the center of the piece. In the subscale injector specimens fabricated previously, this cavity had a camber of more than 1/2 in. from the edge to the center after hot-isostatic compaction of the nickel powder. The modified design considerably improved densification, bonding, and dimensional control, but it was apparent that to keep the fuel-

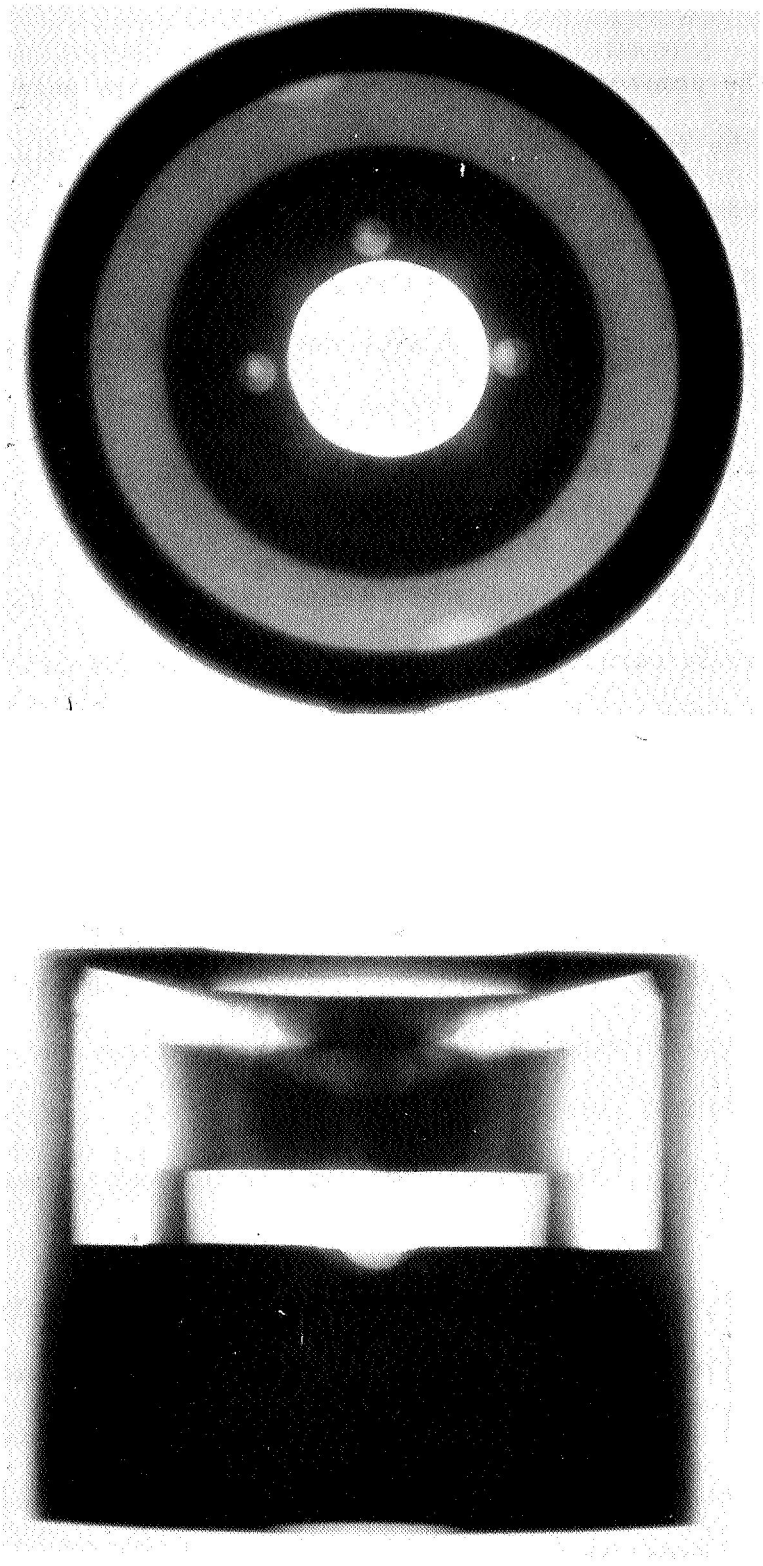

FIGURE I-47. RADIOGRAPHIC INSPECTION OF FLOW PASSAGES IN MODIFIED SUBSCALE INJECTOR AFTER TOOLING REMOVAL

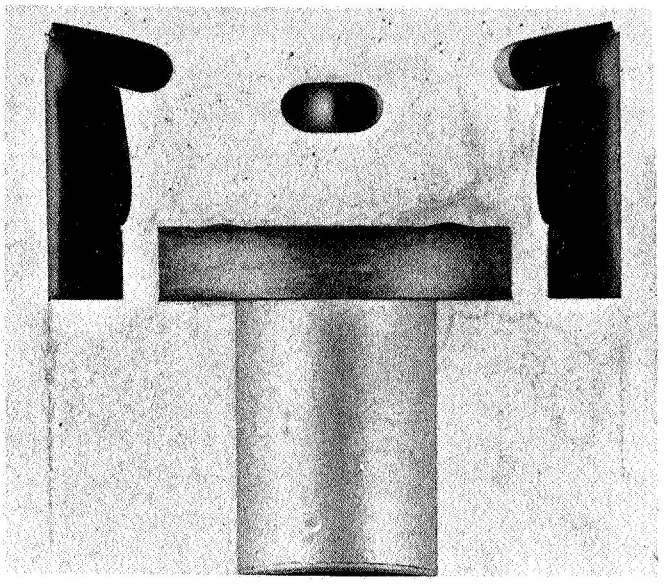

43712

FIGURE I-48. SECTIONED MODIFIED SUBSCALE INJECTOR

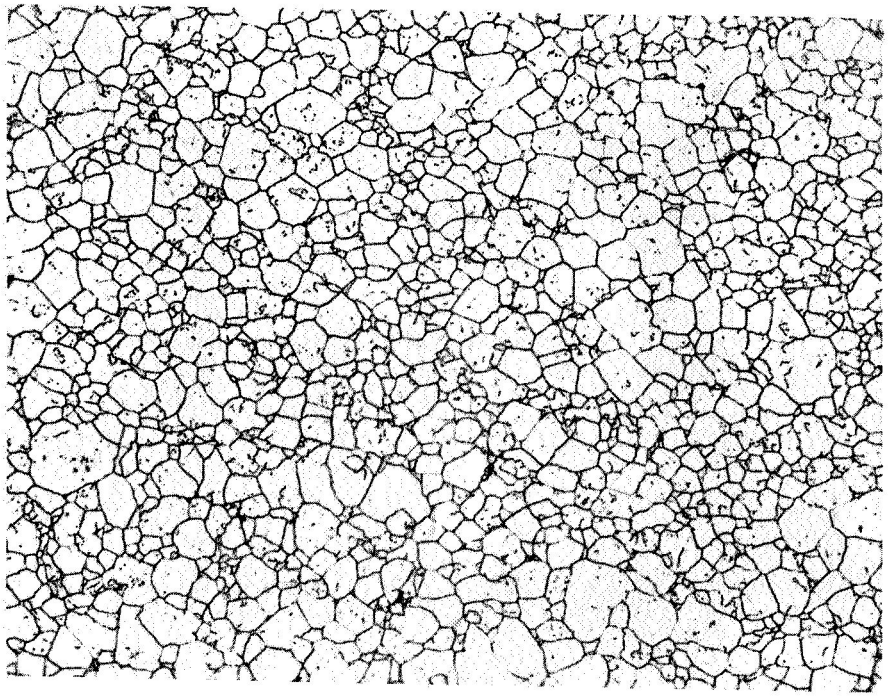

500X No. M1, Etched 4D985

FIGURE I-49. TYPICAL MICROSTRUCTURE OF DENSIFIED NICKEL POWDER IN MODIFIED SUBSCALE INJECTOR AFTER HOT-ISOSTATIC COMPACTION

channel tooling from bending beyond required tolerances, the nickel powder under and supporting this tooling piece should be as dense as possible before the remaining volume of powder and the fuel-channel plate were hot isostatically compacted.

Hardness tests were conducted on the sectioned component. Rockwell B indents were made on the various areas of dense nickel powder and the solid nickel parts. The results, given in the sketch of Table I-13, indicated that the nickel powder hardnesses were comparable to wrought and annealed nickel hardness, except in the region just above the ox-channel plate. In this region, the hardness was about 10 R_B points lower than the other dense regions. Results of metallographic examinations of the nickel powder in this particular region showed that some small porosity existed and caused the lower hardness values in this region.

Significant improvements were achieved in fully densifying the nickel powder and in controlling and minimizing the distortion of the fuel channel tooling, but to eliminate or reduce this distortion to within specified tolerances, the nickel powder surrounding the oxidizer-channel tooling had to be compacted to a sufficient density to prevent movement of the fuel-channel tooling. This was accomplished by modifying the fabrication procedures. First, the nickel powder surrounding the ox-channel tooling was to be densified to at least 95 percent of its theoretical density. The second and final step was to densify the nickel powder surrounding the fuel-channel tooling and simultaneously bond it to the already dense nickel around the ox-channel tooling. This technique is described in detail in the section on Task III studies.

TABLE I-13. RESULTS OF HARDNESS TESTS ON SECTIONED SUBSCALE NICKEL INJECTOR

Rockwell B, 100 Kg Load

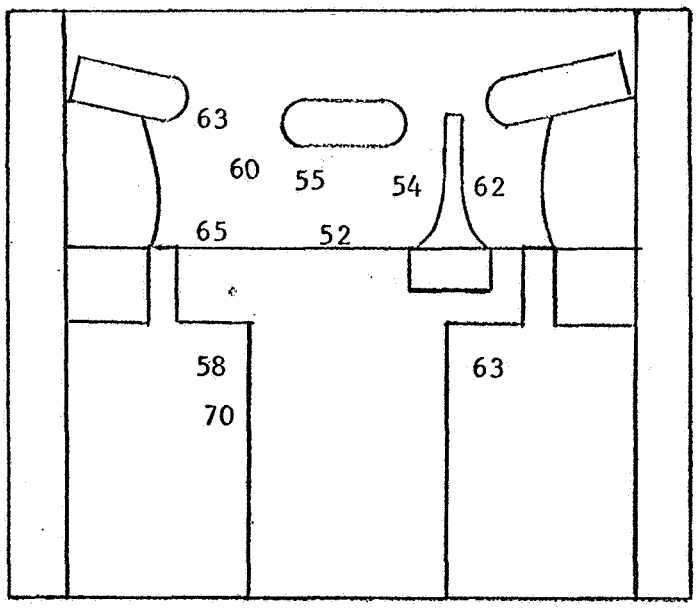

TASK II STUDIES: FABRICATION AND TESTING OF COPPER BAFFLE

The purpose of this task was to fabricate and test full-sized baffles from copper powder and having the design shown in Figure I-1. In Task I studies, subsize baffle test pieces were successfully fabricated by powder metallurgy techniques using borosilicate glass tooling. Copper powder was vibratory packed around glass tooling pieces, compacted to about 75 percent of theoretical density by cold hydropressing at 20,000 psi, and compacted to 100 percent of theoretical density by hot-isostatically compacting at 1000 F and 10,000 psi for 3 hr. The tooling was removed by selective leaching in a solution of HF acid, and the baffles were finished machined on the outside only and tested nondestructively and destructively. Changes in the frame design were required to prevent movement of the glass tooling during hot-isostatic compaction. In the subsize baffles, the tooling was positioned in close proximity of the frames and slight distortion of the tooling occurred during compaction due to the nonuniform and restrained compaction of powder near the frames. It was determined that this effect could be eliminated by chamfering the frame edges and by positioning the tooling out of the zone near the frames where this nonuniform powder compaction occurred.

Subtask II-A-1. Design of Tooling, Frames, Fixtures, and Baffles

Design modifications relocated the positions of the tooling with respect to the frame to improve the dimensional control of the glass tooling during hot-isostatic compaction.

The glass tooling pieces were prepared from 7052 borosilicate glass rods having the shape and dimensions shown in Figure II-1. To prevent glass breakage of the forked pieces during hydropressing, the void space between the legs of the fork shaped pieces were taken up with a solid copper centering piece. This centering fixture, shown in Figure II-2, was made long enough to extend and lock into steel picture frames. A solid copper base plate fixture, shown in Figure II-3, was prepared to maintain alignment of the fuel entrance holes. This solid fixture also assists in preventing glass plate distortion during compaction. The copper connecting rods, also shown in Figure II-3, were to be assembled in the glass plates and produce a bonded joint between the copper base plate and the copper centering fixture. The steel frames were machined from AM355 steel in four separate pieces shown in Figures II-4, -5, and -6. The AM355 age-hardenable stainless steel was chosen for its stiffness at room temperature and its yield strength and modulus at elevated temperatures. High stiffness at room temperature was needed to reduce the amount of bending during hydropressing at 20,000 psi to a level that assured that the glass would not be stressed to fracture. Then, during hot-isostatic compaction at temperatures of about 1200 F and pressures of 10,000 psi, the AM355 steel frames had adequate strength and a sufficiently high elastic modulus to prevent excessive deformation and bending of the tooling. The inner frame lengths provided about 1-1/4 in. of excess on each end to avoid end effects. This excess length maintained the tooling away from regions that were subjected to nonuniform and restrained powder compaction. As was shown in Task I studies, if the tooling is positioned in this region, near the frames, the tooling is distorted excessively.

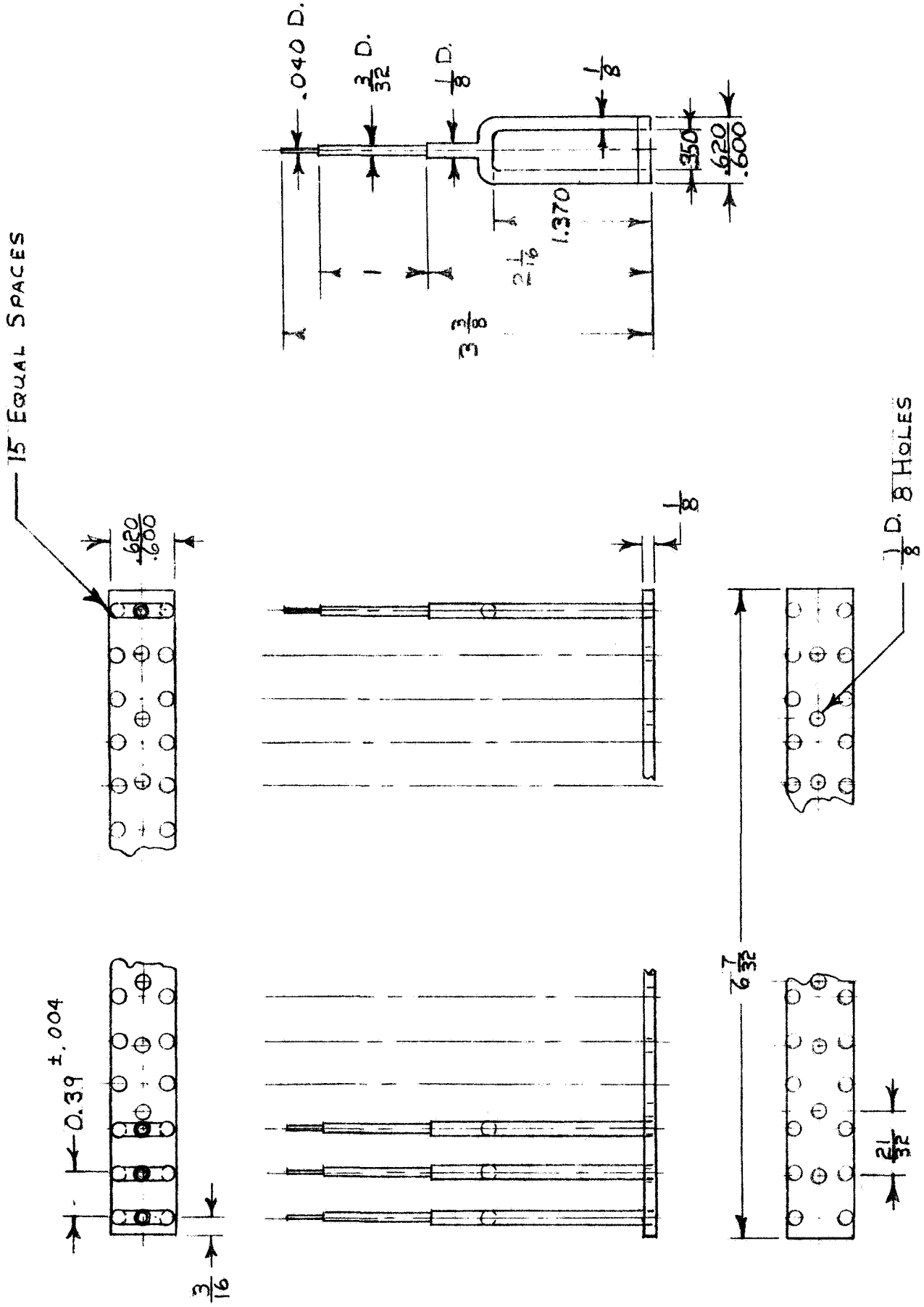

FIGURE II-1. BOROSILICATE GLASS TOOLING MANIFOLD DESIGN

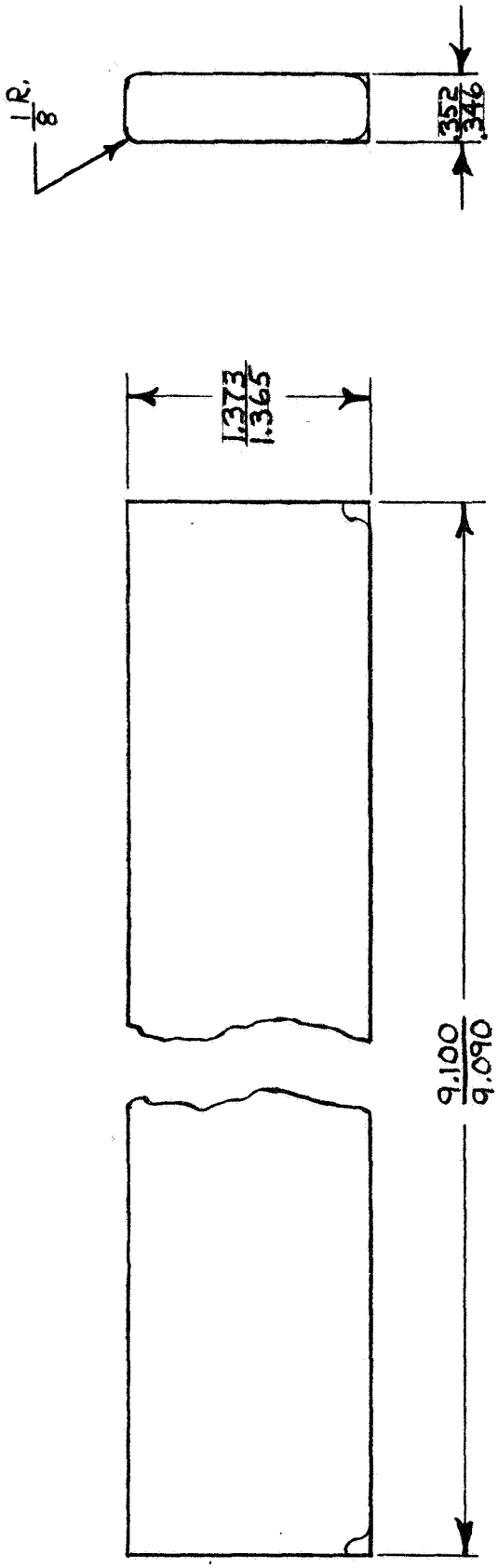

FIGURE II-2. OFHC COPPER CENTER BLOCK DESIGN

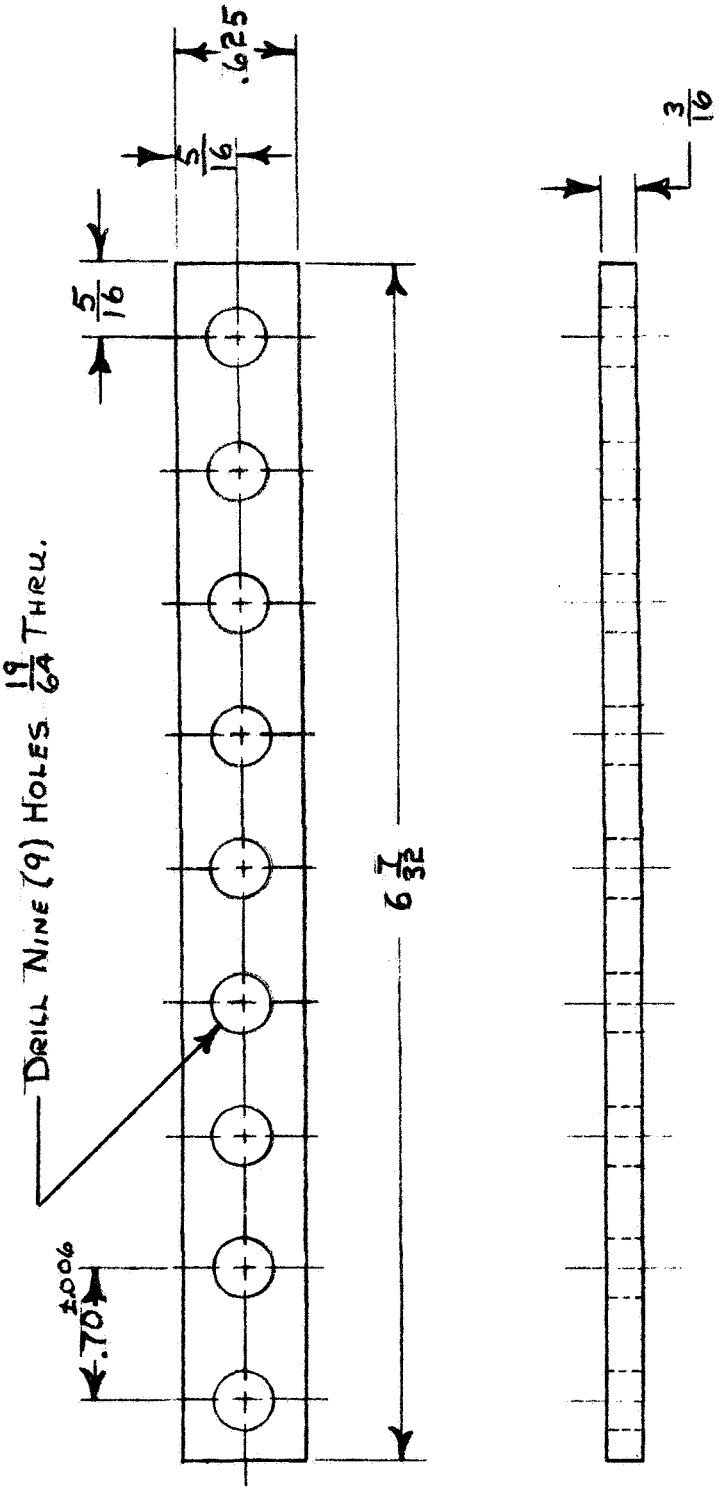

FIGURE II 3. OFHC COPPER BASE PLATE AND CONNECTING RODS DESIGN

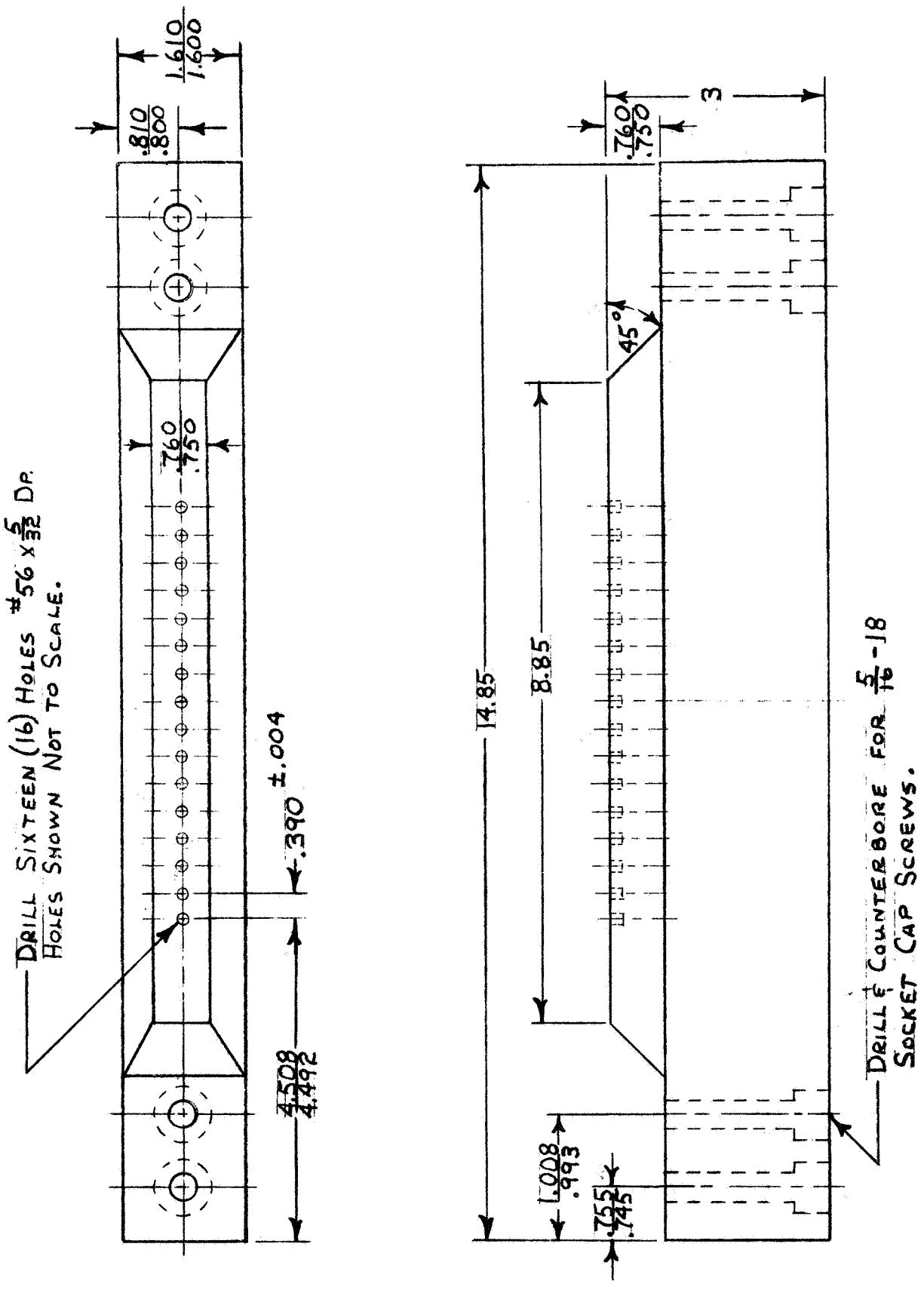

FIGURE II-4. DESIGN OF AM-355 STEEL FRAME - TOP

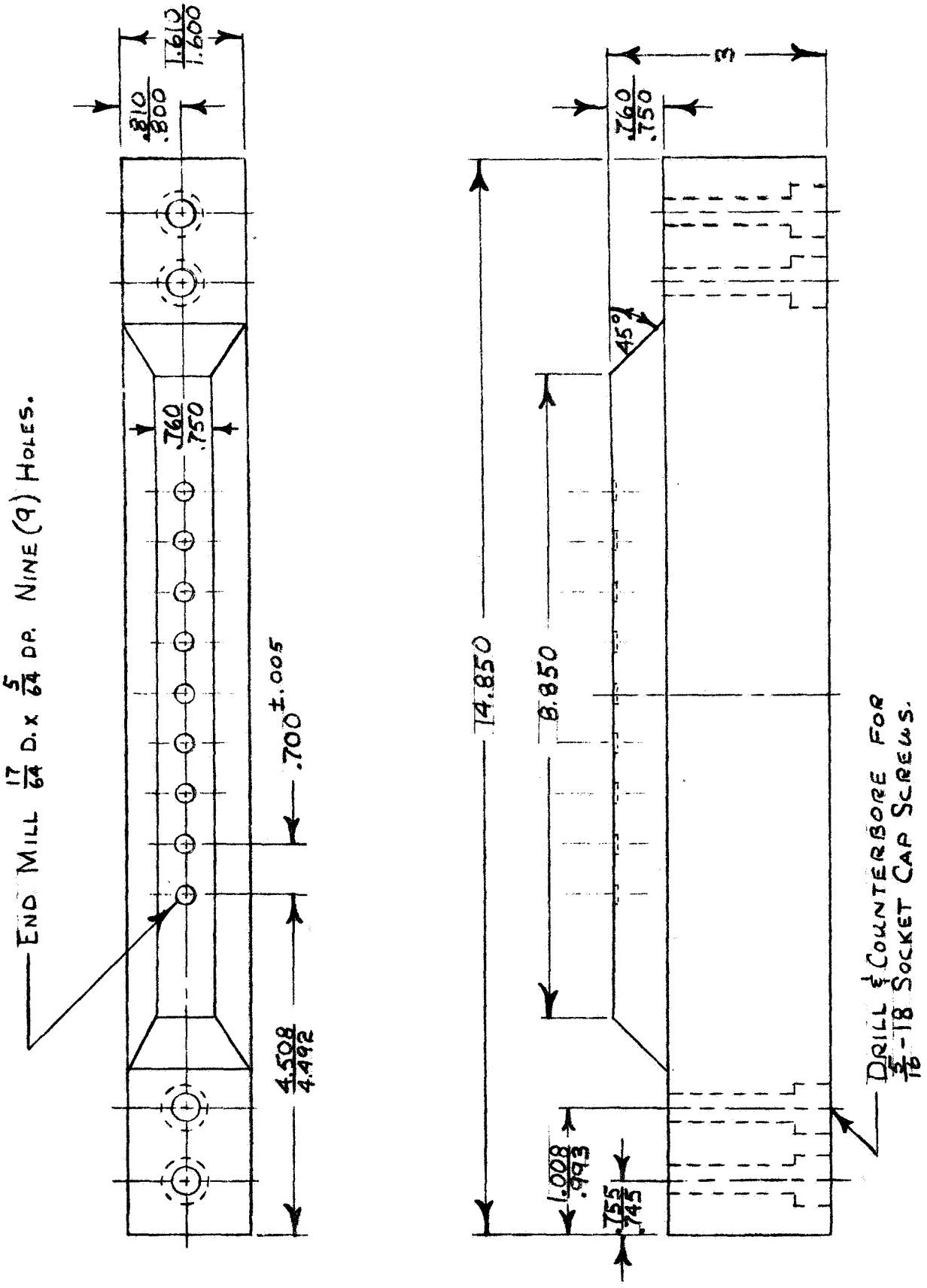

FIGURE II-5. DESIGN OF AM-355 STEEL FRAMES - BOTTOM

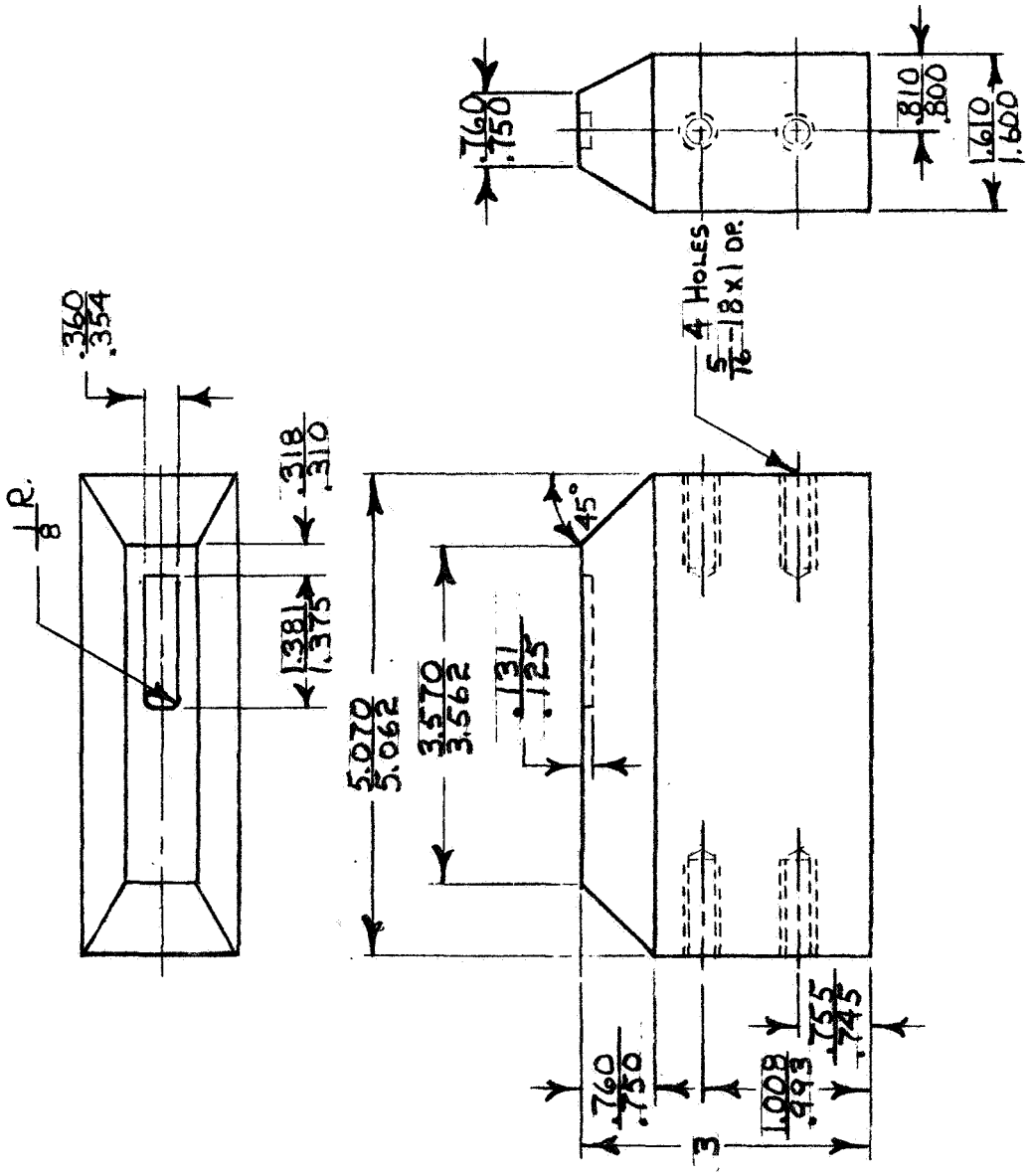

FIGURE II-6. DESIGN OF AM-355 STEEL FRAMES - ENDS

Subtask II-A-2. Fabrication of Copper Baffle Test Samples

The forked tooling pieces were fabricated from glass rods by heating and bending them over a graphite form block. The glass plate pieces were prepared from 3/16-in.-thick plates 6-1/4 in. square. Figure II-7 and Figure II-8 show the glass tooling parts before assembly. Wrought and annealed OFHC copper plate and rod were used to make the solid center bars, the connecting pins, and the base plates. The steel frames were fabricated from forged AM355 bar stock. The copper powder used was the C3-type powder selected in Task I, identified as ESPI grade K-1433, 3N5 pure, -100 mesh.

The assembled tooling, copper fixtures, and frame for Baffle No. 1 are shown in Figure II-9. Baffle No. 2, shown in Figure II-10, is basically the same with the exception that small copper braces were fitted over the forked glass parts to hold the small 0.040-in.-diameter stems and prevent breakage.

To facilitate vibratory packing of copper powder into the baffles and around the glass and solid copper parts, thick (1/2 in.) rubber plates were cut and taped to the faces of the baffle. These plates tapered out from the bottom to the top of the frames so that a 1/2-in. gap was left at the top on both sides of the frame to permit loading of the copper powder. After vibrapacking was completed, the gaps were plugged with thick rubber wedges, and the assembly was taped and sealed with Chem Rubber Fix Cement. The assembly was inserted into thin rubber bags (about 1/16 in. wall thickness), sealed, double bagged, and again sealed. Baffle No. 1 was then hydropressed at 20,000 psi.

After removing the bags and rubber plates, the copper was visually inspected. Baffle No. 1 appeared to have sufficient green strength and density for subsequent handling steps. The baffle was then x-ray inspected to determine

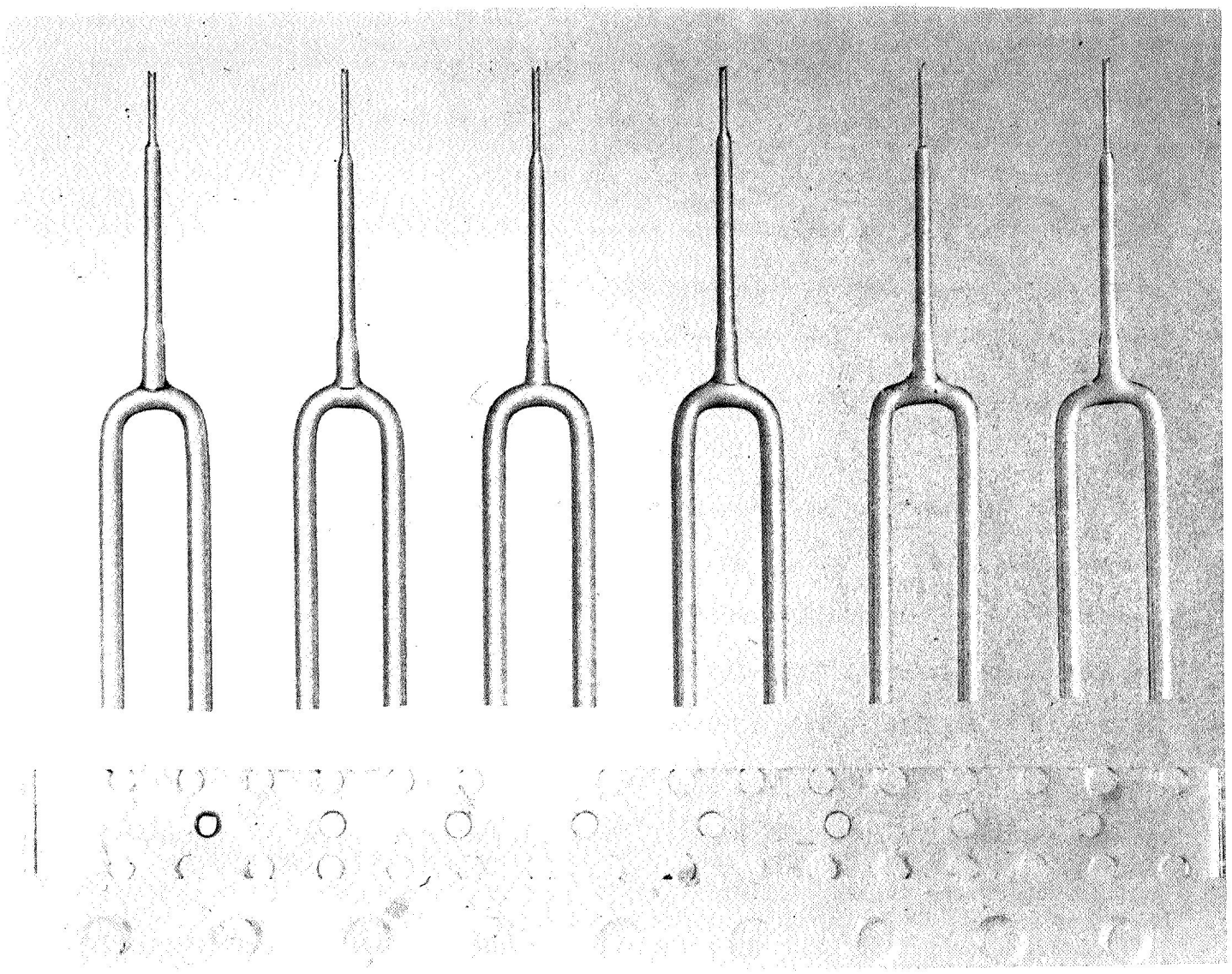

43208

FIGURE II-7. GLASS TOOLING PARTS FOR BAFFLES

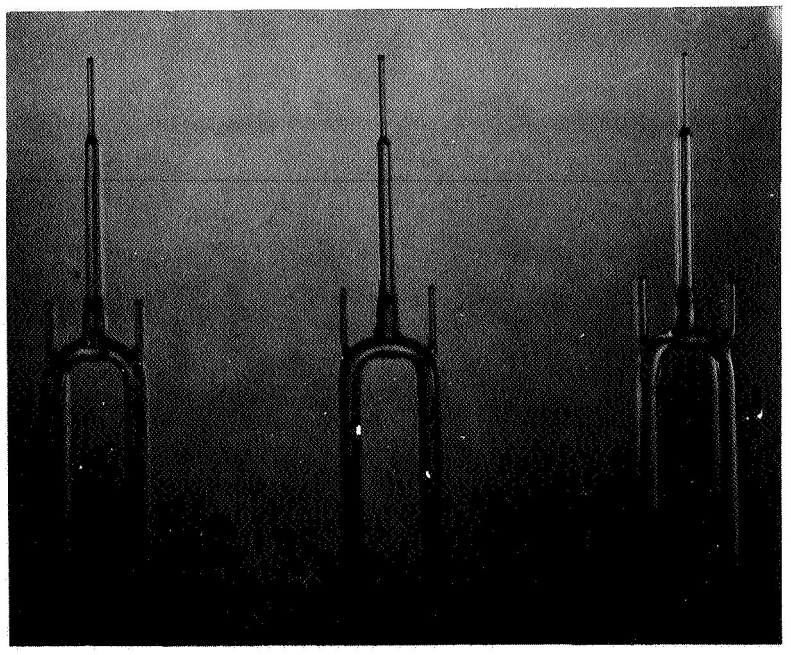

43346

FIGURE II-8. MODIFIED GLASS TOOLING PIECES FOR BAFFLE NO. 2

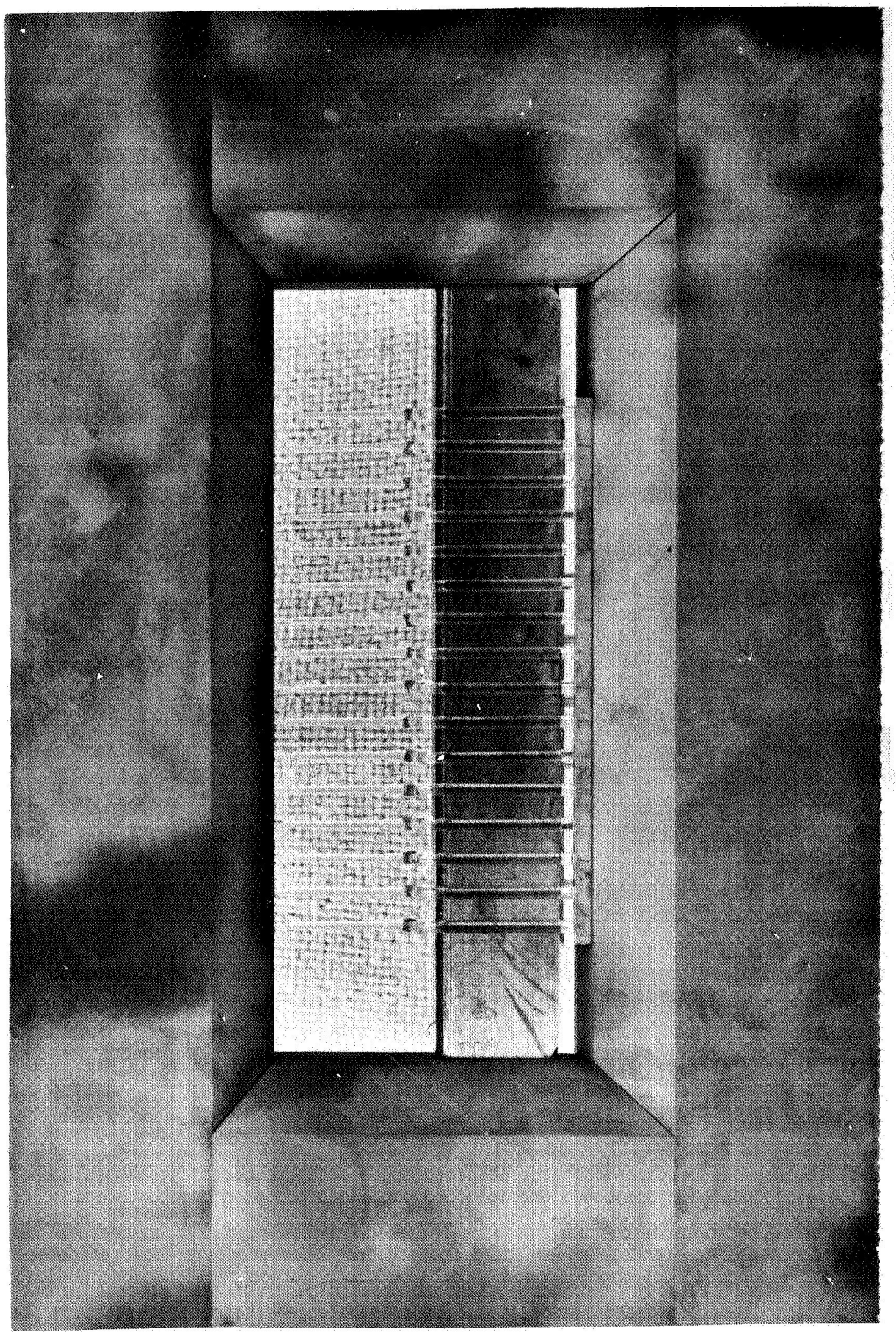

43217

FIGURE II-9. ASSEMBLED TOOLING, FIXTURES, AND FRAMES - BAFFLE NO. 1

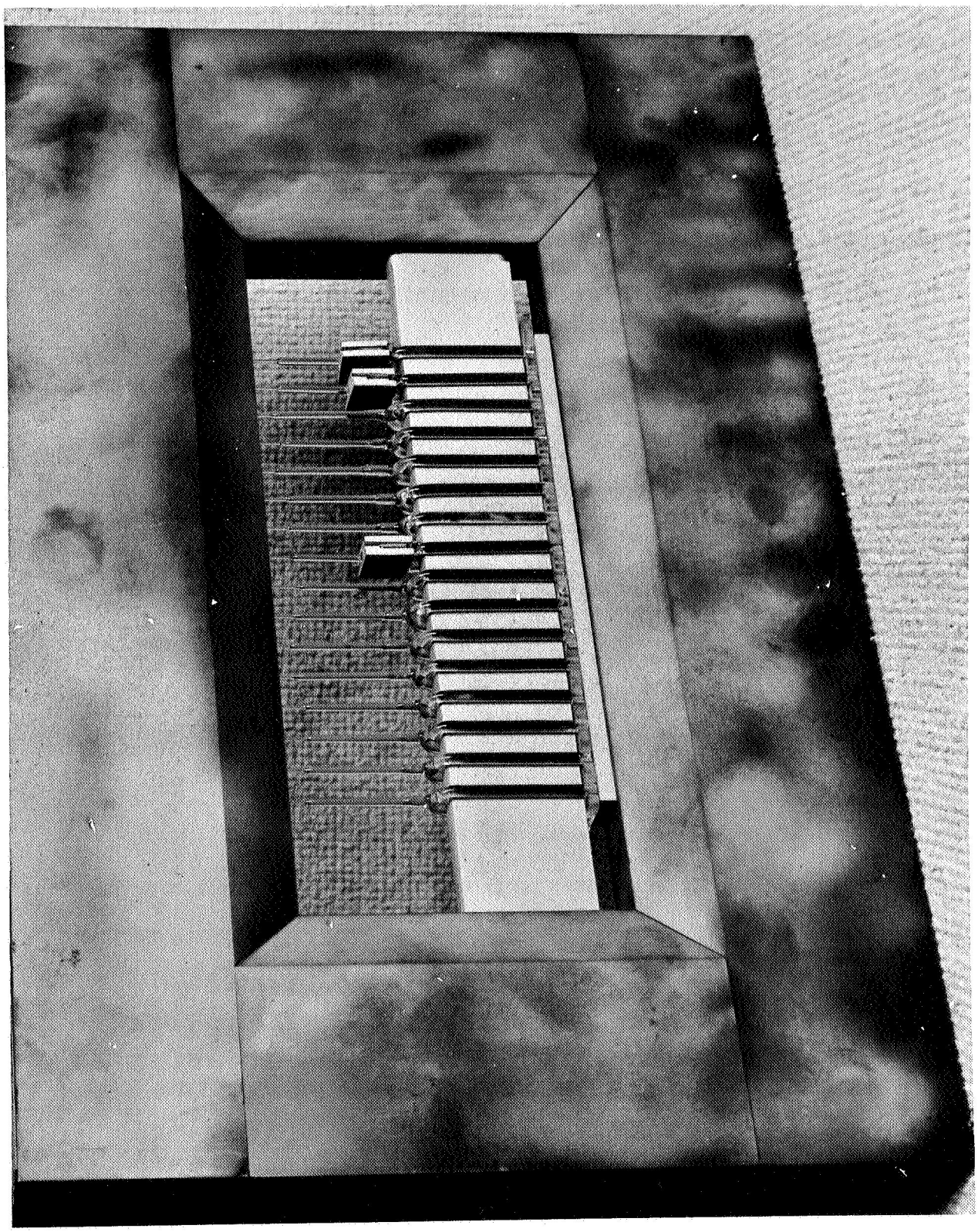

43483

FIGURE II-10. ASSEMBLED TOOLING, FIXTURES, FRAMES, AND STEM BRACES - BAFFLE NO. 2

the alignment and soundness of the glass tooling. As shown in Figure II-11, excellent dimensional location of the glass tooling pieces in the hydropressed specimen was maintained. No evidence of cracks in the glass pieces was found. There was evidence that bags leaked very late in the hydropressing cycle, but contamination was not severe. However, since any oil residue in the copper powder would outgas during hot-isostatic compaction and prevent complete densification of the powder, the part was canned and vacuum outgassed at 1200 F for 6 hr. The specimen was then cooled to room temperature, checked for leaks with a helium detector, evacuated, and sealed by forge welding the evacuation stem.

Baffle No. 2 was modified to prevent a recurrence of rubber bag leakage during hydropressing. Sharp corners and edges were filed and rounded off, all holes in the steel frames were plugged with metal filler, and rubber and felt pads were taped over the crevices of mating surfaces in the steel frames to prevent extrusion of the rubber bag into these crevices.

The baffle was then double sealed with rubber bags and hydropressed at 20,000 psi. No leaks occurred during hydropressing, and the copper was clean and bright and had sufficient green strength for subsequent handling. The radiograph in Figure II-12 shows that excellent dimensional alignment of the glass tooling was maintained in the second hydropressed baffle as well. Baffle No. 2 was then canned, evacuated, and outgassed at 1000 F for 4 hr. The baffle was cooled to room temperature under vacuum and sealed by forge welding the evacuation stem.

The two copper baffles were hot-isostatically compacted by preheating to 780 F with minimal pressure followed by densification at 1200 F and 10,000 psi for 3 hr. The variation of pressure and temperature with time during the autoclave cycle are tabulated in Table II-1. The containers on the baffles had shrunk and

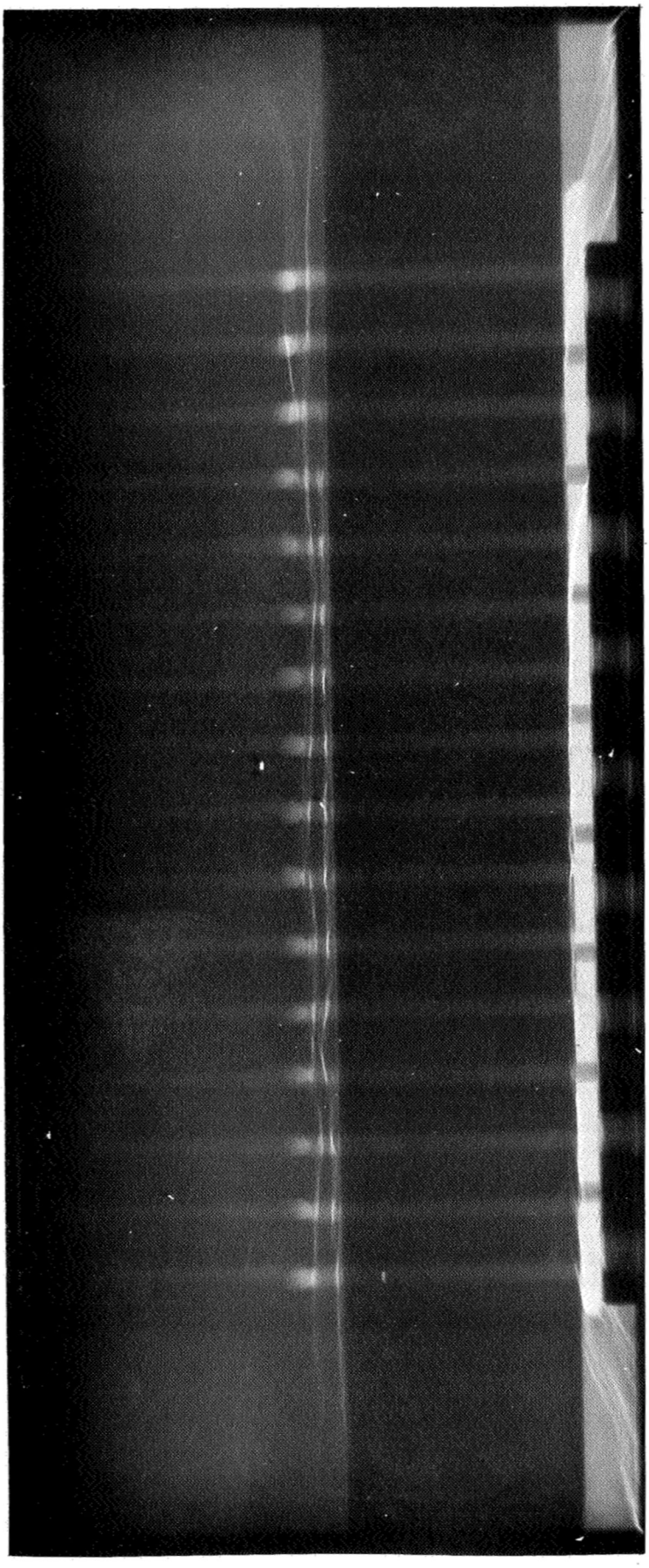

FIGURE II-11. RADIOGRAPH OF TOOLING AND FIXTURES IN HYDROPRESSED COPPER BAFFLE NO. 1

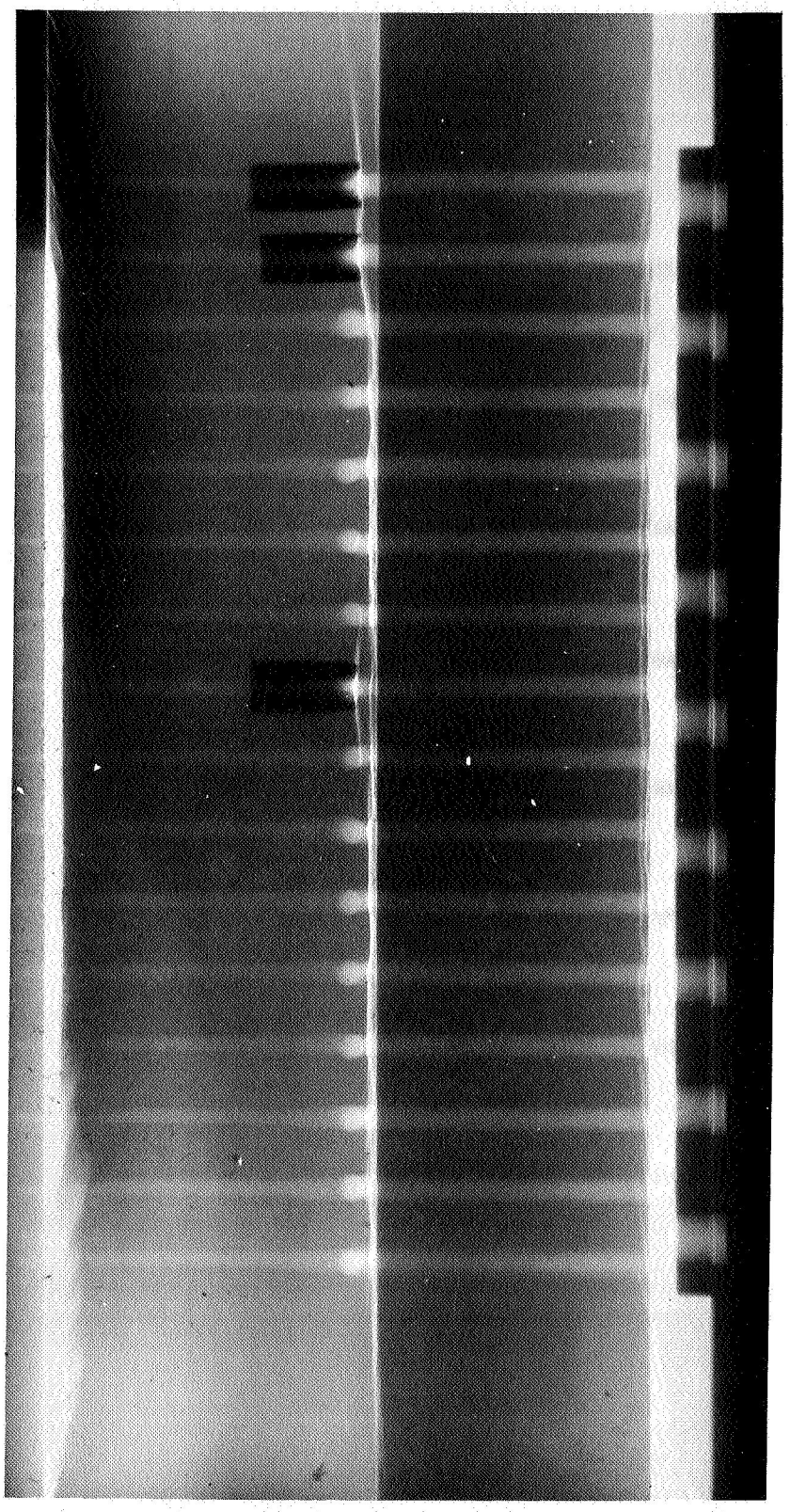

FIGURE II-12. RADIOGRAPH OF TOOLING AND FIXTURES IN HYDROPRESSED COPPER BAFFLE NO. 2

TABLE II-1. PRESSURE-TEMPERATURE-TIME PARAMETERS USED TO HOT ISOSTATICALLY COMPACT COPPER BAFFLES

Pressure, psi	Temperature, F	Time, hr:min	
150	RT	0:00	
150	683	1:15	
160	778	1:45	
2100	901	2:35	
8000	1125	3:40	
10,000	1209	4:25	3-hr hold period
10,000	1201	5:25	
10,000	1180	6:35	
10,000	1180	7:25	
Reduced	Power off, cooled slowly to RT	--	

compressed onto the copper powder, but leaks developed during the compaction cycle that caused the containers to bulge during the cooling cycle. A leak was found in each container in a corner region near the edge of the steel frames.

The containers were then removed and the copper was examined. The copper in Baffle No. 1 was bright and resistant to scratches. A piece of copper was sectioned from the excess on the end of the baffle and checked for density by water submersion techniques. The density of the sectioned piece from Baffle No. 1 was 8.64 g/cc or about 96 percent of theoretical density. The copper in Baffle No. 2 had a dull surface and appeared porous. A sectioned piece off an end was checked for density and determined to be 6.50 g/cc or 73 percent of theoretical density.

It was decided to proceed with the evaluation, testing, and inspection of Baffle No. 1 but to recan and recycle Baffle No. 2 to increase its density.

To prevent a recurrence of leaks during the hot-isostatic compaction cycle, the container for Baffle No. 2 was redesigned to reduce localized deformation at the corner regions of the steel frames. The welded container was checked for leaks, outgassed at 500 F for 3 hr, and sealed. Baffle No. 2 was then recycled by preheating to 800 F and hot-isostatically compacting at 1200 F and 10,000 psi for 3 hr. Visual inspection of the container afterwards, as shown in Figure II-13, indicated that the container remained gas tight and deformed evenly onto the copper powder. No leaks were detected in a post-compaction leak check. The container was removed and the copper inspected visually and by radiographic techniques. The copper surfaces appeared bright and dense. The density was found to be 8.81 g/cc or 98.3 percent of theoretical density.

After removing the steel frames, the baffles were machined on the ends and sides to remove excess copper and then placed in a solution of 67 percent HF -33 percent H_2O selectively remove the glass tooling.

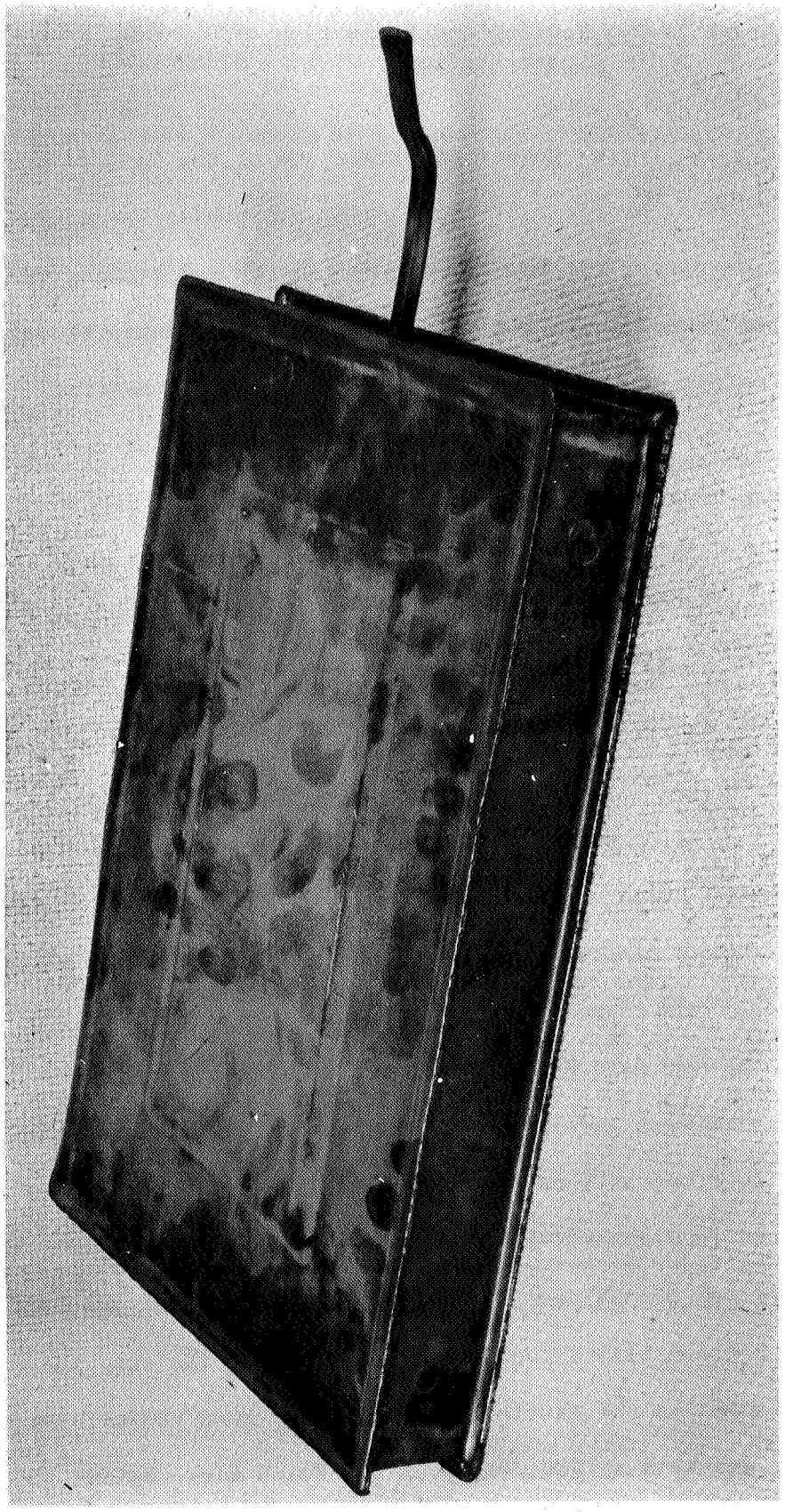

43713

FIGURE II-13. PHOTOGRAPH OF HOT-ISOSTATICALLY COMPACTED BAFFLE NO. 2 WITH STEEL CONTAINER INTACT

Subtask II-B. Testing and Evaluation of Copper Baffles

In Baffle No. 1 the copper powder at either end of the base of solid copper plate appeared slightly porous. At these ends, the powder was not strongly bonded to the solid copper plate. On the sides, the density and bonding was satisfactory. The copper powder in Baffle No. 2 was completely dense throughout. This was confirmed by density measurements on cut segments of the baffle.

X-ray photos of the baffles after hot-isostatic compaction were taken after the containers were removed but before the steel frames were disconnected. These are reproduced in Figures II-14 and II-15. Good alignment was maintained in the glass tooling parts of both baffles; no distortion or breakage could be detected in the tooling forks or in the small stems attached to the shoulders of the forks in Baffle No. 2. Extending the ends of the baffles successfully prevented distortion of the glass tooling at either end of the baffles. The glass plates at each end of the baffles were bent slightly due to overextension of the glass lengths beyond the solid copper base plate. This can be corrected in subsequent baffle fabrications simply by making the length of the glass plate coincide with the length of the copper base plate.

To accomplish the 700 psig hydrostatic pressure test, tooling was designed to seal the baffles with gaskets and clamp plates except for one inlet into the lower manifold section, as shown in Figure II-16. Equipment set up for the hydrotest is shown in Figure II-17. To insure that no air was trapped in the baffles, the fluid was pumped under a slight pressure through the baffle with the top open. After fluid flowed through each orifice at the top, the flat plate and gasket were clamped to the baffle. Attempts were made to increase the pressure to 700 psig and hold at 700 psig ± 10 psi for 5 min. Baffle No. 1 generated a leak through one side due to interconnected voids in the copper

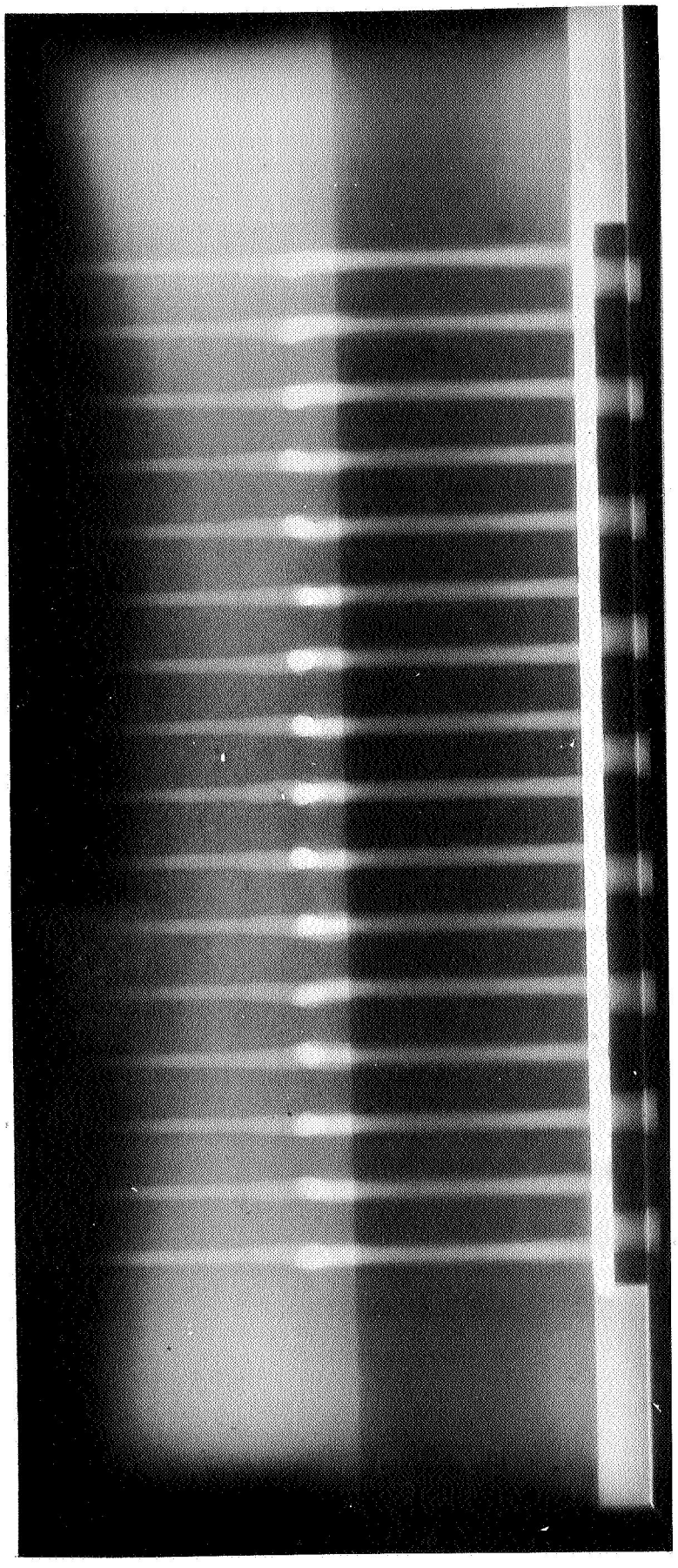

FIGURE II-14. RADIOGRAPH OF HOT-ISOSTATICALLY COMPACTED BAFFLE NO. 1

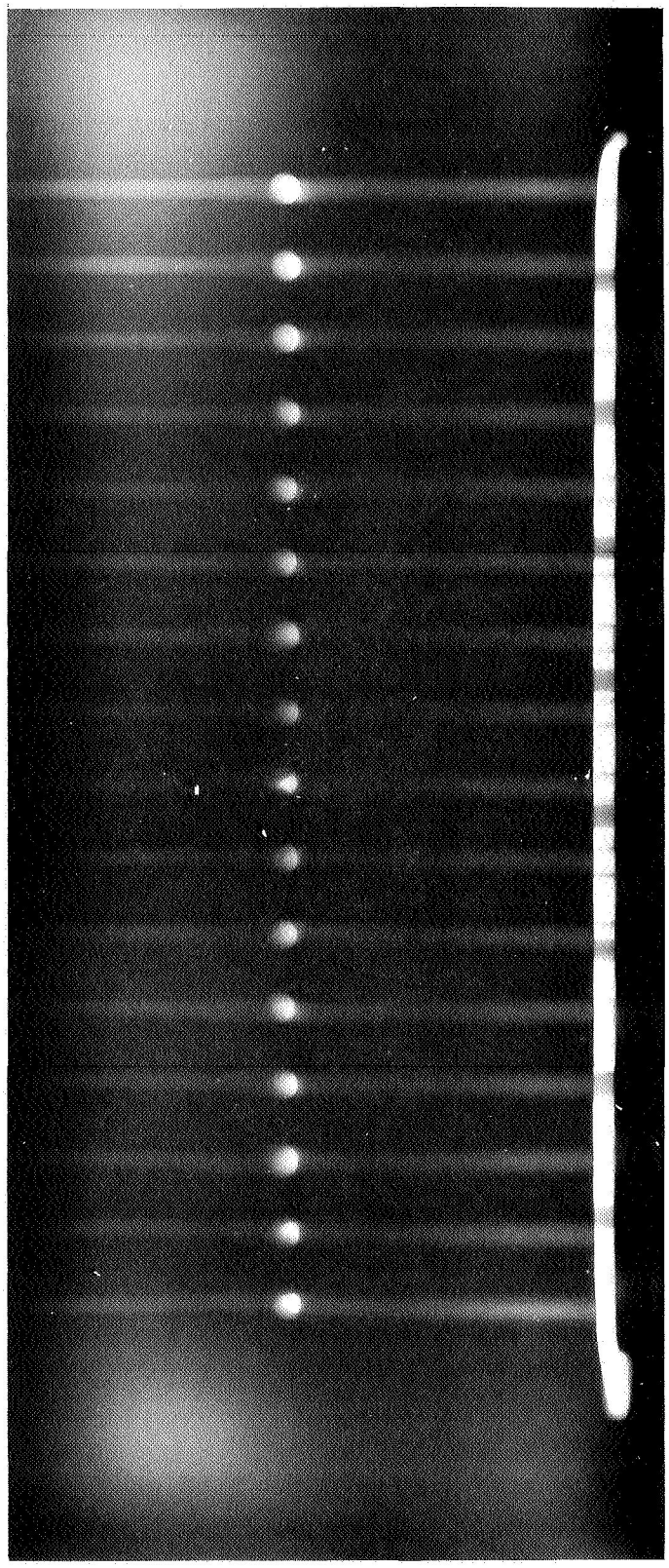

FIGURE II-15. RADIOGRAPH OF HOT-ISOSTATICALLY COMPACTED BAFFLE NO. 2

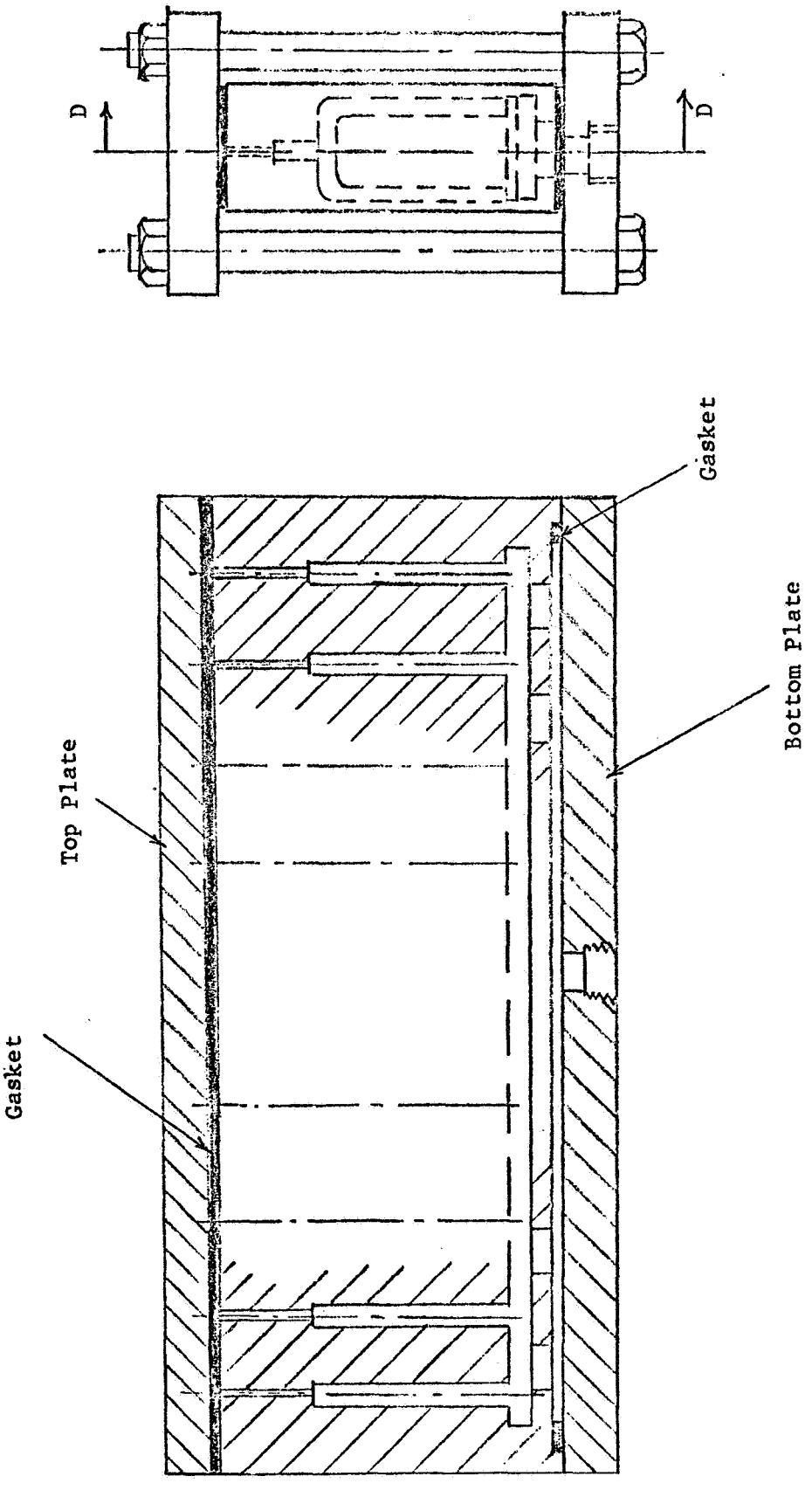

FIGURE II-16. SKETCH OF HYDROTEST FIXTURES

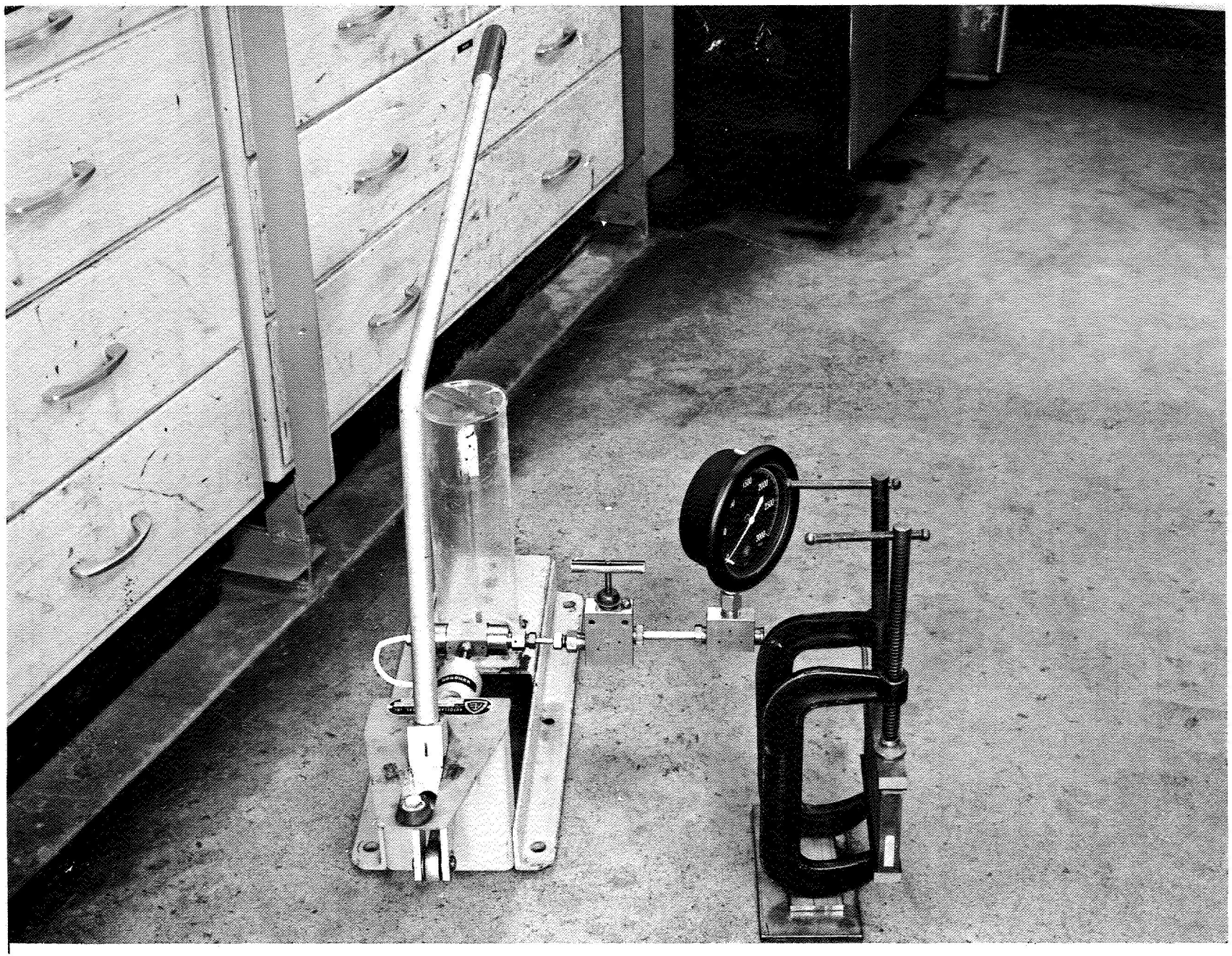

44063

FIGURE II-17. TEST SET-UP FOR HYDRAULIC PRESSURE TESTING OF COPPER BAFFLES

powder in this region. Baffle No. 2 tested satisfactorily at 700 psig ± 10 psi for 5 min and at 750 psig for shorter periods. Equipment set up for the flow tests and a typical flow rate test is shown in Figure II-18. Heights of water spouts were measured at three different flow rates. Angles of deflection from the center axis were measured. The results of the flow rate tests are tabulated in Table II-2. After nondestructive tests were completed, Baffle No. 1 was sectioned and examined. Macrostructures of the sectioned parts are shown in Figures II-19 and II-20. Near perfect alignment of the channels was maintained. All channels retained the dimensions, contour, and positions of the fabricated tooling to within ± 0.01 in. The orifices (exit holes) at the top contained an anomoly that affected flow through the channels. As seen in the figures, the orifices tended to "bell out" near the surface. This effect is probably due to a slight nonuniform reaction of the copper with the leaching solution. This defect can be corrected by making the baffle and the tooling in this region about 1/4 in. higher than the final dimension. The "bell effect" can then be removed after leaching is completed by machining off the excess 1/4 in. from the baffle height. Baffle No. 2 was sectioned across one of the channels that had been fabricated from modified tooling. A photograph of the sectioned piece is shown in Figure II-21. The alignment of the flow channels across the top of the baffle is shown to be straight and adequately controlled. Some misalignment during machining of the faces and sides is responsible for the "off-center" appearance of the flow channel in the sectioned face. A typical microstructure of the copper powder in Baffle No. 1 section is shown in Figure II-22 and that in Baffle No. 2 is shown in Figure II-23. Tensile tests were made on standard 1/8-in.-diameter tensile bars cut from end sections of each copper baffle, and the results are given in Table II-3. The copper powder in Baffle No. 1 had inferior mechanical properties due to its lower density. The mechanical properties of the copper in Baffle No. 2 are better than commercial products of wrought and annealed OFHC copper.

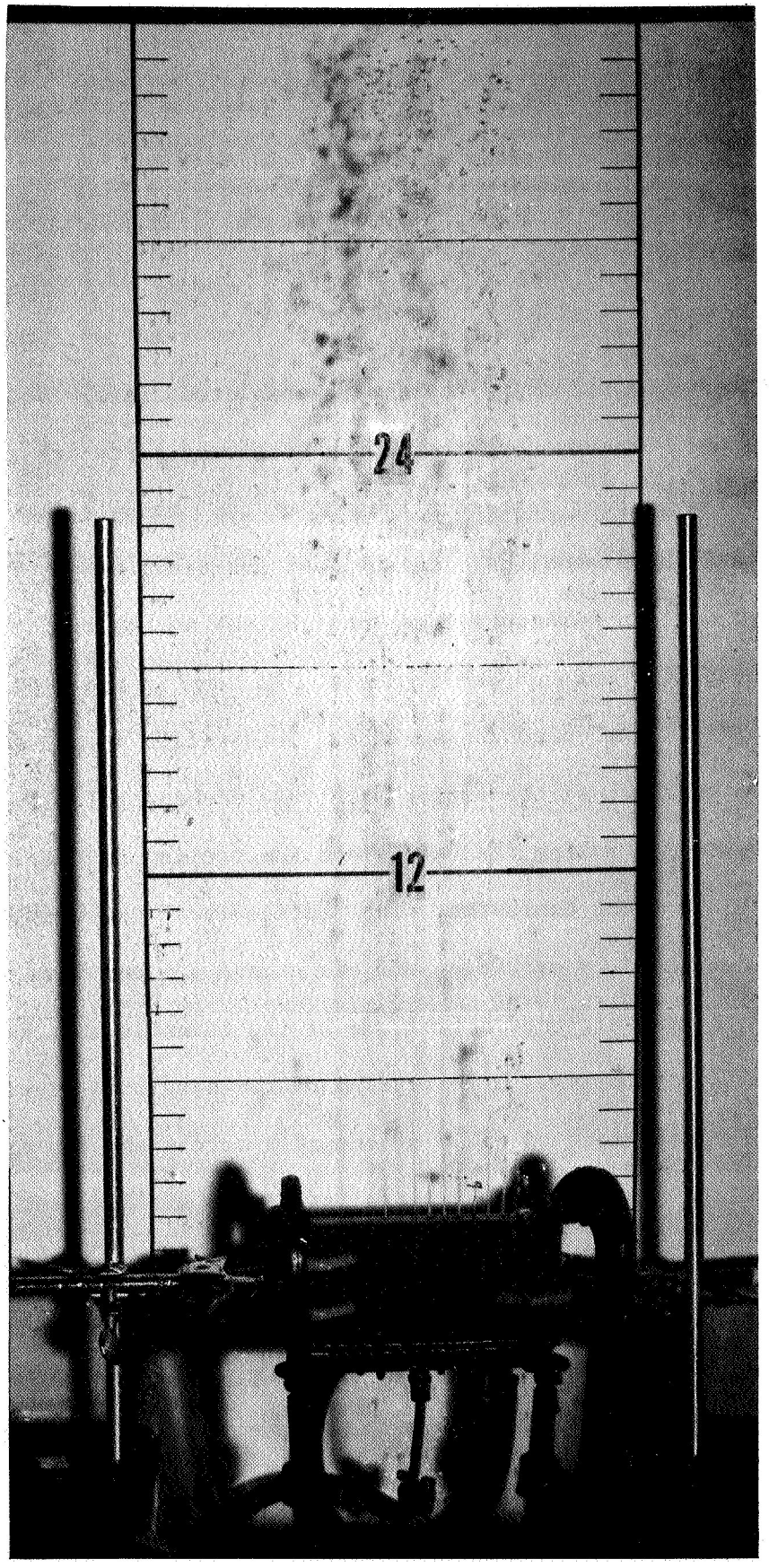

FIGURE II-18. FLOW-RATE TESTING OF COPPER BAFFLES

TABLE II-2. FLOW TEST DATA ON COPPER BAFFLES

	Height of Spout, in.															
Orifice No.	1	2	3	4	5	6	7	8	9	10	11	12	13	14	15	16
Flow Rate, Baffle No. 1																
Low	6.5	7	6.0	6.5	7.0	7.5	6.5	6.5	6.5	6.5	7.0	7.5	1.5	N(a)	N(a)	N(a)
Medium	11.5	12	11.0	11.5	11.0	11.5	11.5	11.0	11.0	3.0	11.5	13.5	3.0	N	N	N
High	17.5	18	16.5	17.0	16.5	16.5	17.0	16.5	16.5	4.5	16.5	19.5	4.0	N	N	0.5
Flow Rate, Baffle No. 2																
Low	9	9	8	8	9	9	N(a)	7	6	3	8	6	8	8	2	--(b)
Medium	15	15	15	15	15	16	N(a)	12	13	7(b)	14	10	13	12	5	--(b)
High	24	24	24	24	24	26	N(a)	18	22	11(b)	22	18	20	21	8	--(b)

	Maximum Displacement of Flow From Center Axes During Medium Flow Rate, degrees															
Orifice No.	1	2	3	4	5	6	7	8	9	10	11	12	13	14	15	16
Baffle No. 1	<1	<1	<2	<2	<1	<3	<2	<1	<1	<2	<5	<2	<2	N	N	N
Baffle No. 2	<1	<1	<1	<1	<1	<1	N	<1	<2	<3	<1	<1	<1	<1	<3	--(b)

N = No flow through orifice.

(a) One or two channels were blocked by glass particles that were not completely removed during leaching. Subsequent flushing of these channels and releaching in 67 percent HF removed these particles and produced satisfactory flow.

(b) Channel 16 in Baffle No. 2 was sectioned for destructive examination before flow tests were conducted.

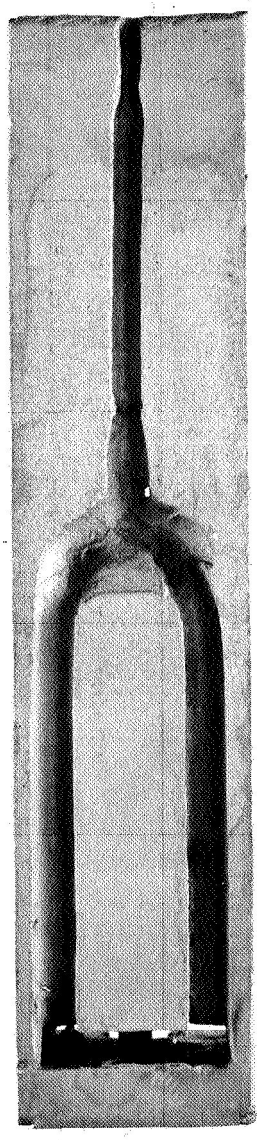

FIGURE II-19. MACROSTRUCTURE OF COPPER BAFFLE NO. 1 ALONG SECTION "B-B"

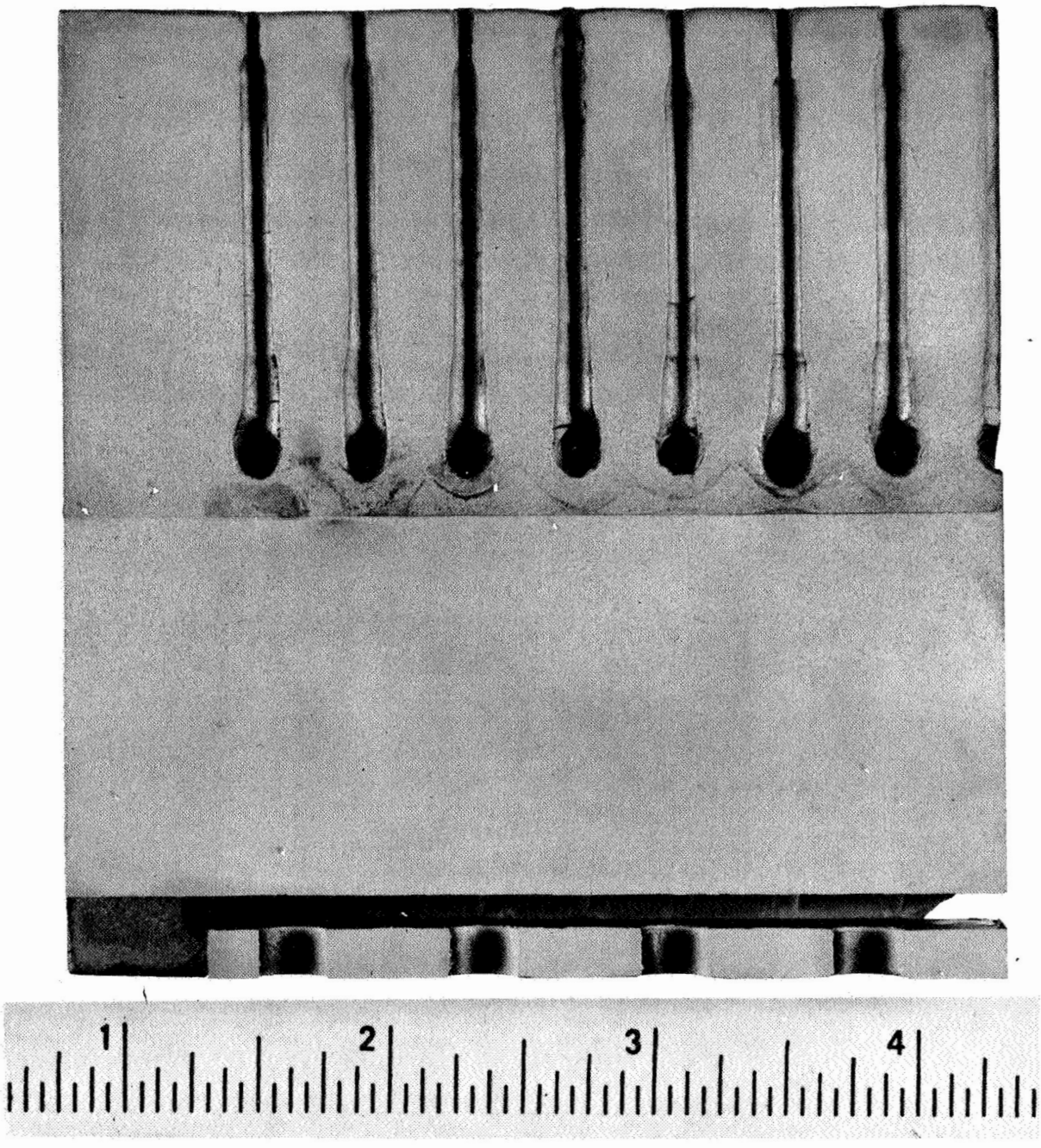

FIGURE II-20. MACROSTRUCTURE OF COPPER BAFFLE NO. 1 ALONG SECTION "D-D"

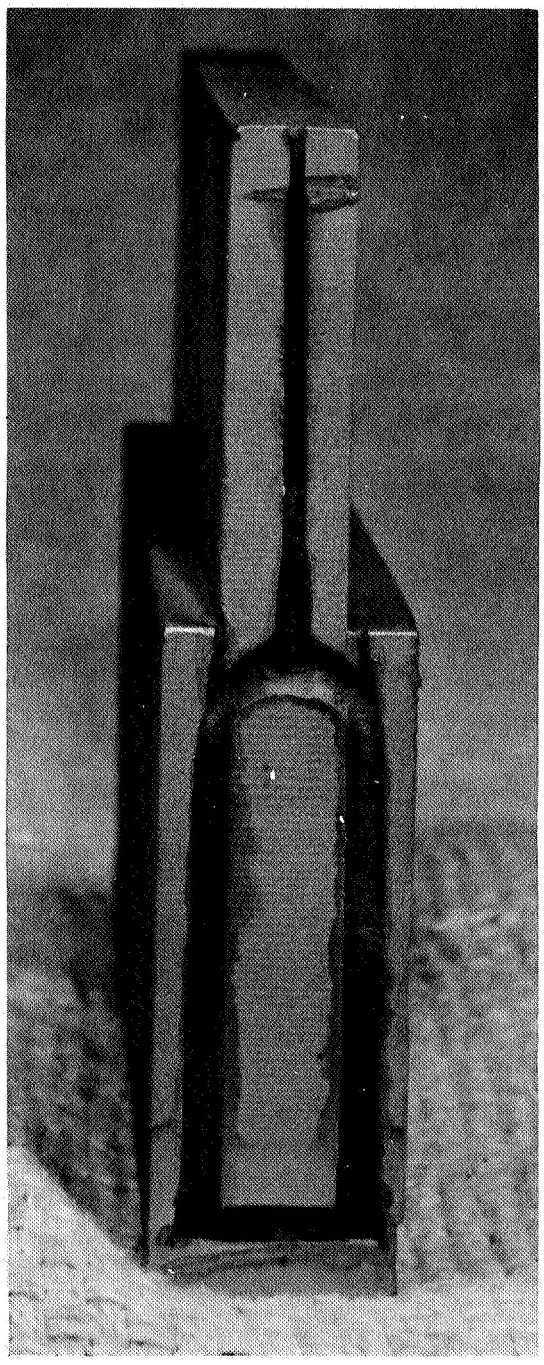

45265

FIGURE II-21. MACROSTRUCTURE OF COPPER BAFFLE NO. 2 ALONG SECTION "B-B"

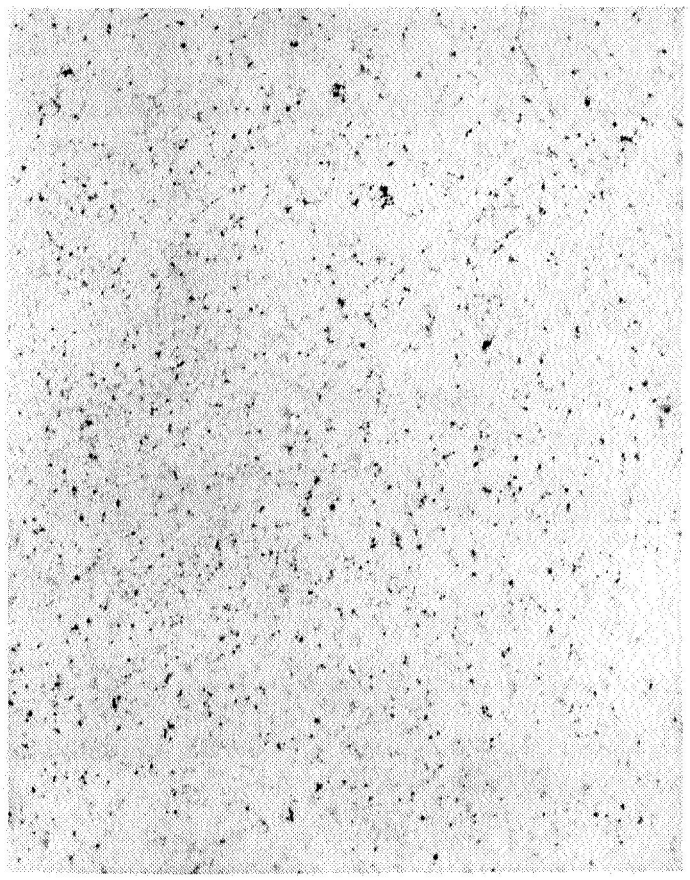

100X 5D544

FIGURE II-22. TYPICAL MICROSTRUCTURE OF COPPER (BAFFLE NO. 1) IN SECTION "D-D"

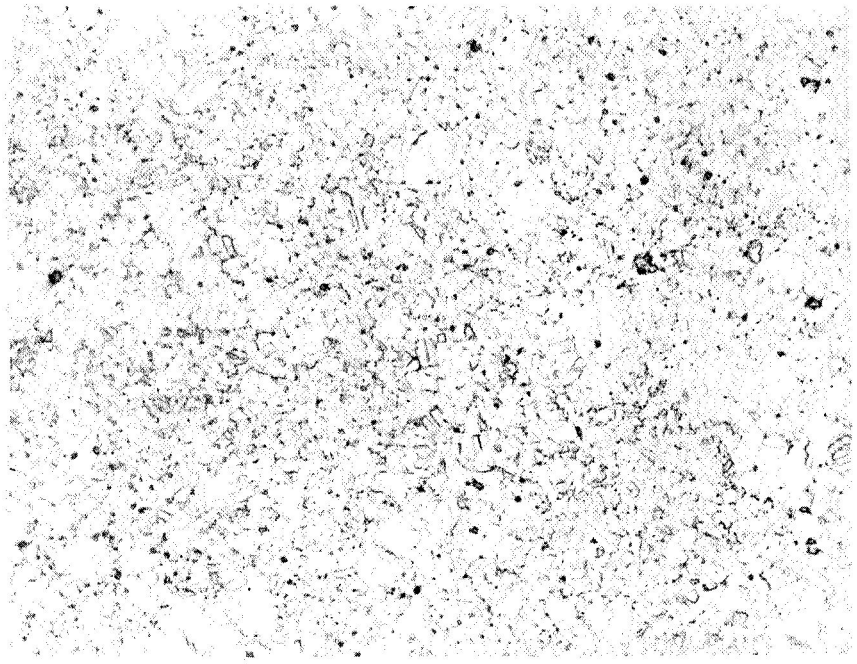

500X Etched 5D321

FIGURE II-23. MICROSTRUCTURE OF COPPER IN BAFFLE NO. 2 ALONG SECTION "B-B"

This photograph was taken in an area where the density was expected to be lowest. Even in this region, the porosity in Baffle No. 2 is very small. Note also the fine, uniform grain size in the microstructure.

TABLE II-3. RESULTS OF TENSILE TESTS ON END SECTIONS OF COPPER BAFFLES(a)

Baffle No.	Specimen No.	E, psi	0.2 Percent Offset Yield	psi, u	Percent Elongation	Percent R.A.
1	1	9.55×10^6	--	9,550	--	--
2	1	15.7×10^6	24,800	38,200	10.6(b)	48.3
2	2	17.1×10^6	24,600	38,300	14.2(b)	53.5
OFHC Copper(c)		17×10^6	10,000(d)	32,000	45	--

(a) Tensile test made at R.T. on ASTM standard 1/8 in. diameter tensile bars with cross-head speed of 0.005 in. per minute.

(b) Percent elongation was measured over total length of specimens which were 2-1/8 in. originally. If the elongation is taken over the effective gage length of 1/2 in., the percent elongation is 45 percent and 60.5 percent, and is equivalent to or higher in ductility than wrought and annealed commercial OFHC copper.

(c) Values taken from "Materials Engineering", mid-October, 1967-1968, (Materials Selector Issue), p 131.

(d) Yield point measured at 0.5 percent extension rather than 0.2 percent.

Densities and hardness were measured on localized sections of the baffles. The results of density tests are shown in Table II-4. Hardness tests were taken on Baffle No. 2 sections. These results are given in Table II-5. Dimensional analyses were conducted on sectioned parts of the baffles and the results are summarized in Table II-6.

TABLE II-4. RESULTS OF DENSITY MEASUREMENTS ON LOCALIZED SECTIONS OF BAFFLES

End-Sections (a)

Baffle No.	Section No.	Density, g/cc	Percent of Theoretical
1	E-1-L	7.12	79.5
1	E-1-S	7.77	86.7
2	E-1-L	8.89	99.2
2	E-1-S	8.84	98.7
2	E-2-L	8.80	98.2
2	E-2-S	8.87	99.0

Mid-Sections (b)

Baffle No.	Section No.(c)	Density, g/cc	Percent of Theoretical
1	M-1-A	7.45	83.1
1	M-1-B	8.24	92.0
1	M-1-C	8.12	90.8(d)
1	M-1-D	8.10	90.2(d)
1	M-2-A	7.50	83.4
1	M-2-B	8.05	90.0
1	M-2-C	8.10	90.2(d)
1	M-2-D	8.21	91.9(d)

(a) Each section was about 1-1/2 in. long, 1/4 in. wide, and 1/4 in. thick. The densities exclude the solid OFHC copper brace.

(b) Each section was about 3/4 in. long, 3/8 in. wide, and 1/4 in. thick.

(c) Numbers of sections are listed A through D according to their position from the "top" of the baffle in section B-B of NASA Drawing No. CF20868.

(d) The densities of the C and D mid-sections excluded the solid OFHC copper brace.

TABLE II-5. RESULTS OF HARDNESS TESTS ON SECTIONS OF BAFFLE NO. 2 (100 Kg R_B)

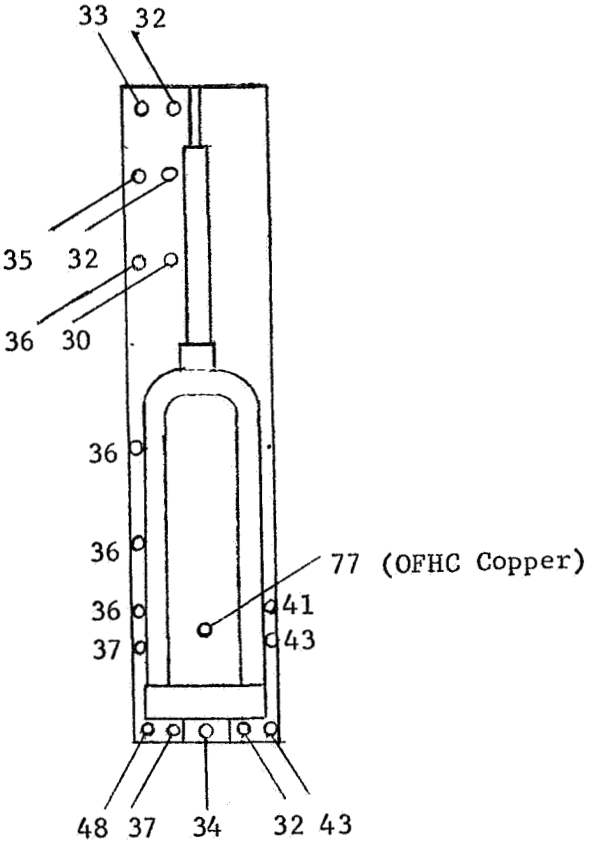

TABLE II-6. ANALYSIS OF DIMENSIONAL CONTROL AND ALIGNMENT OF INTERNAL FLOW CHANNELS IN COPPER BAFFLES

Section BB

(1) Top orifice diameter varied with length from 0.060 in. to 0.040 in. from the surface to about 0.2 in. below surface. This was apparently the cause for deflection of the spouts during the flow tests.

(2) Except for (1) above, the diameter of the channels were maintained to within ±0.01 in.

(3) The channel thickness at the junction was about 0.12 in. rather than the specified 0.07 in. since the glass tooling was fabricated with this dimension of 0.12 in. The contour of the cross-section was a curved passage with smooth transitions to the legs rather than a sharp corner passage with abrupt transition to the legs as given in NASA Drawing No. CF620868. These changes are considered to have a negligible effect on flow.

(4) Overall lengths and thickness were held to within ±0.01 in.

(5) The channels maintained nearly perfect alignment internally. No distortion, bending, or shifting of the tooling pieces was evident.

Section DD

(1) Top channels were spaced uniformly at 0.39 in. ± 0.01 in.

(2) Channel alignment (in vertical direction) varied less than 1 degree for 7 out of 8 channels inspected. One channel was very slightly distorted near the top and deflected from center by less than 3 degrees.

(3) The surfaces of the flow channels in both baffles were generally very smooth. In three channels of Baffle No. 1, a small protrusion of copper occurred about 1 in. from the top surface where the glass tooling apparently cracked and allowed a small amount of copper powder to extrude into the defect. The effect of the protrusion into the channel was minor. No such protrusions or other defects affecting the surface roughness were observed in the channels of Baffle No. 2.

TASK III STUDIES: FABRICATION AND TESTING OF SIMULATED NICKEL INJECTOR TEST PIECES

In Task I studies, several subscale nickel injectors were fabricated to develop the techniques, process parameters, testing methods, and the optimum tooling material for full size injectors to be fabricated in Task III. Two different tooling materials were selected for these experiments but low carbon (1018) steel was preferred over 1100-aluminum. During hot-isostatic compaction, the aluminum formed a nickel-aluminide compound which was found to prevent interdiffusion between nickel and aluminum. However, the aluminum becomes soft during hot-isostatic compaction and could produce distorted shapes in the tooling. Because of this disadvantage in using aluminum tooling, it was recommended that steel be the primary tooling material for the nickel injectors and that aluminum be a secondary choice. For other applications in which dimensional control is less rigid or in which higher compaction temperatures are not needed, aluminum tooling is to be preferred because of its much faster removal rate.

Distortion of the fuel-channel tooling in the subscale nickel injectors required additional studies to be undertaken. These experiments were described in Subtask I-C-2, Process Optimization. Subscale nickel injectors were fabricated and tested during this period using a modified tooling design. Distortion of the fuel-channel tooling was greatly reduced, and, by a slight change in fabrication techniques, it was expected that the distortion could be eliminated completely. Flow tests showed that no interchannel leaks existed between the ox-hole and fuel-hole channels of the subscale components. Destructive tests indicated that the nickel powder was compacted to theoretical density throughout the structure, that the mechanical properties were equivalent to wrought and annealed solid nickel products, and that the dimensions of the tooling were reproducible.

Subtask III-A-1. Design of Tooling, Plates, Containers, and Injectors

The tooling for the nickel injectors was prepared from 1018 carbon steel plate and rod. Only tooling for one quadrant and a single row across the diameter were provided in place of tooling for the full section. It was agreed that the quarter section and single row design would provide essentially the same information as a full design insofar as meeting the program objectives, that is, to demonstrate that engine hardware of this type could be fabricated from powder. The oxidizer channel tooling is shown in part in Figure III-1. The tooling pins and inserts shown in Figures III-2 and III-3 complete the tooling for the oxidizer channels. The pins were press-fit into the bored holes in the tooling plate. After the initial consolidation of nickel powder around the tooling pins and plate, the pins had small placement holes 0.068 in. diameter by 0.030 in. deep drilled into the top of each for insertion of the oxidizer channel tooling inserts.

The fuel channel tooling plates were also designed with just a quarter section and a line incorporating the tooling pins. This tooling piece is shown in Figure III-4. The 37 0.687 in. diameter through-holes provided spacing through which the oxidizer channel tooling pins projected. Fuel channel pins, shown in Figure III-5, were press-fitted into the hole spacings provided in the plate. The peripherally-located fuel channel tooling ring was produced with a steel ring shown in Figure III-6. This ring was welded to the plate and completed the tooling for the fuel-channels.

Since two consolidation cycles were planned for each injector test piece, two different sized hot-isostatic compaction containers were required. The container for the first cycle consisted of a 1018 steel seamless pipe 5.75 in. long and having a 12.5 in. OD and a 0.5 in. wall. The lids were cut and spun

NOTE: 125/ ALL OVER UNLESS OTHERWISE NOTED.

LIST OF MATERIAL				
ITEM	DWG. NO.	SIZE	NO. REQ'D.	TITLE – DESCRIPTION

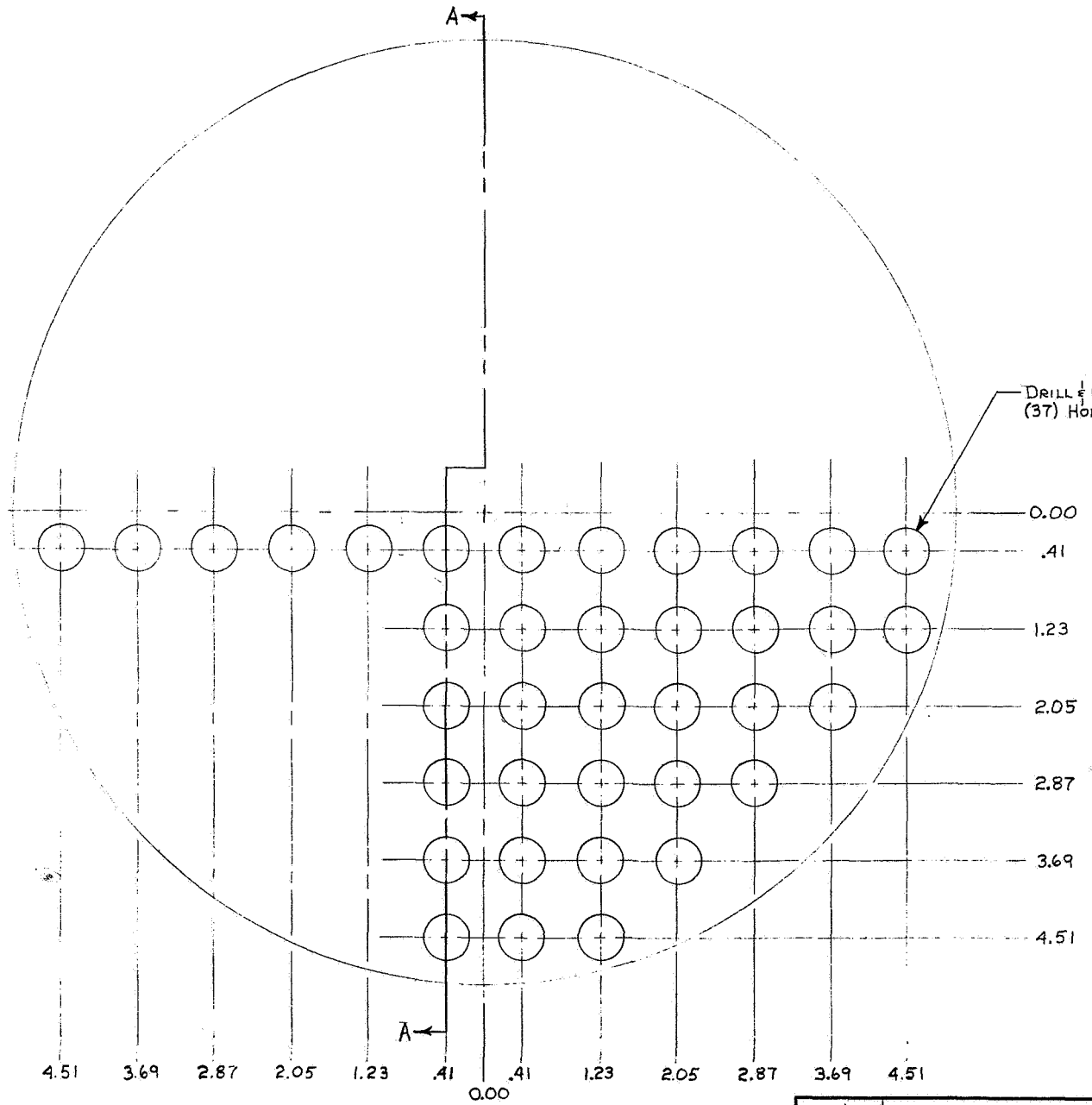

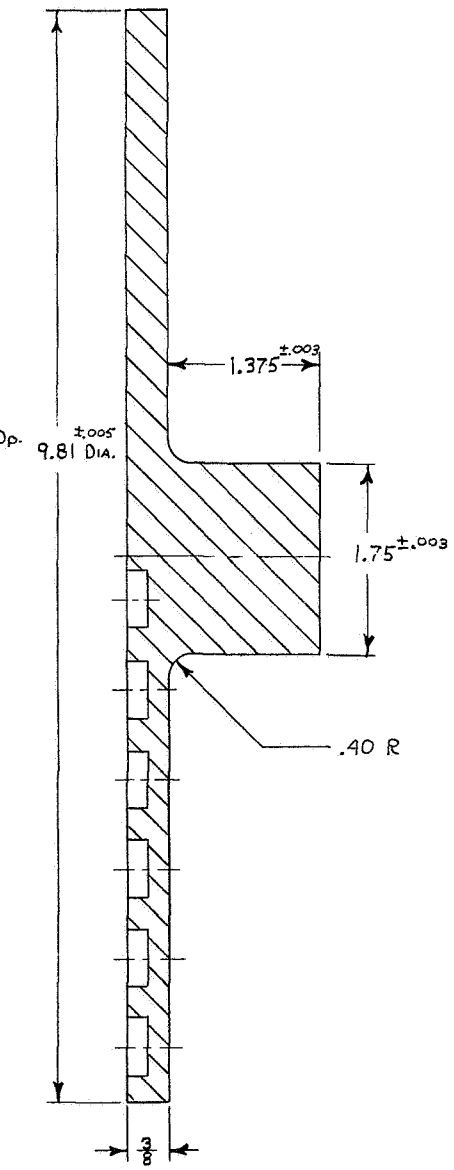

SECTION 'A-A'

ZONE	REV. LET.	REVISIONS	BY	DATE

MAT'L. (COMMERCIAL TOLERANCES APPLY): 1020 M/S PLATE

TOLERANCE UNLESS OTHERWISE NOTED: FRAC. ±; ANG. ±; DEC.

	DRAWN	CHECKED	PROJ. APP
BY	WLS		
DATE	11-18-68		
DIV.	765		

NEXT ASSY. | NO. REQ'D.

SCALE: FULL | K-G

ACCT. NO.

BATTELLE MEMORIAL INSTITUTE
505 KING AVE.
COLUMBUS 1, OHIO

TITLE: OX-CHANNEL TOOLING PLATE

DWG. NO.: FIGURE III-1 | C

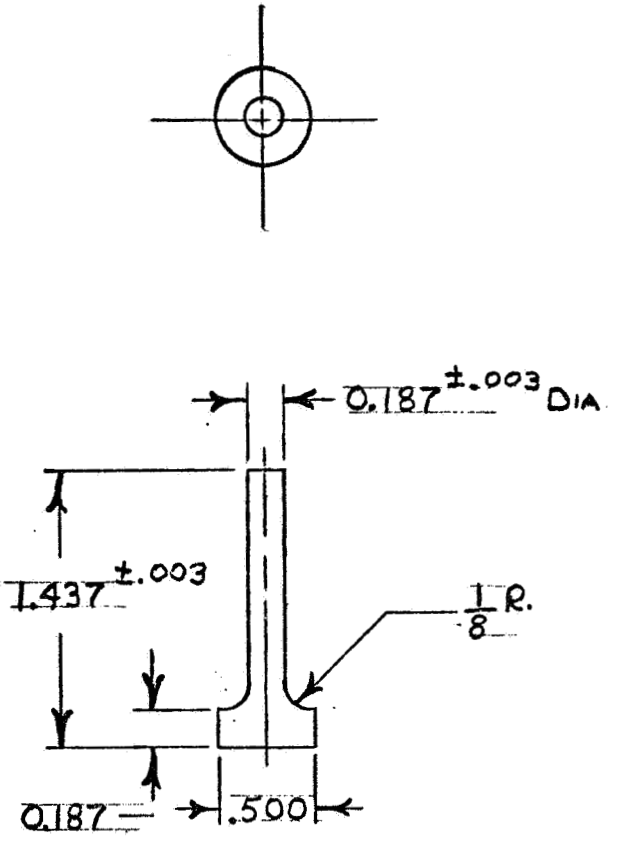

FIGURE III-2. OXIDIZER CHANNEL PIN

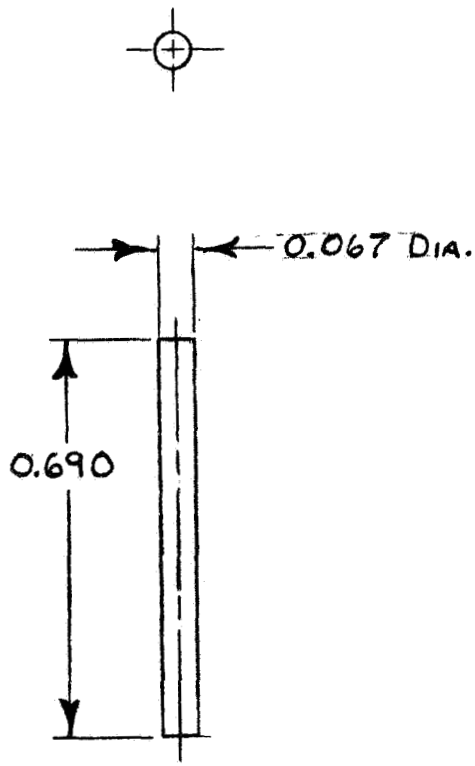

FIGURE III-3. OXIDIZER CHANNEL PIN INSERT

LIST OF MATERIAL				
ITEM	DWG. NO.	SIZE	NO. REQ'D.	TITLE – DESCRIPTION

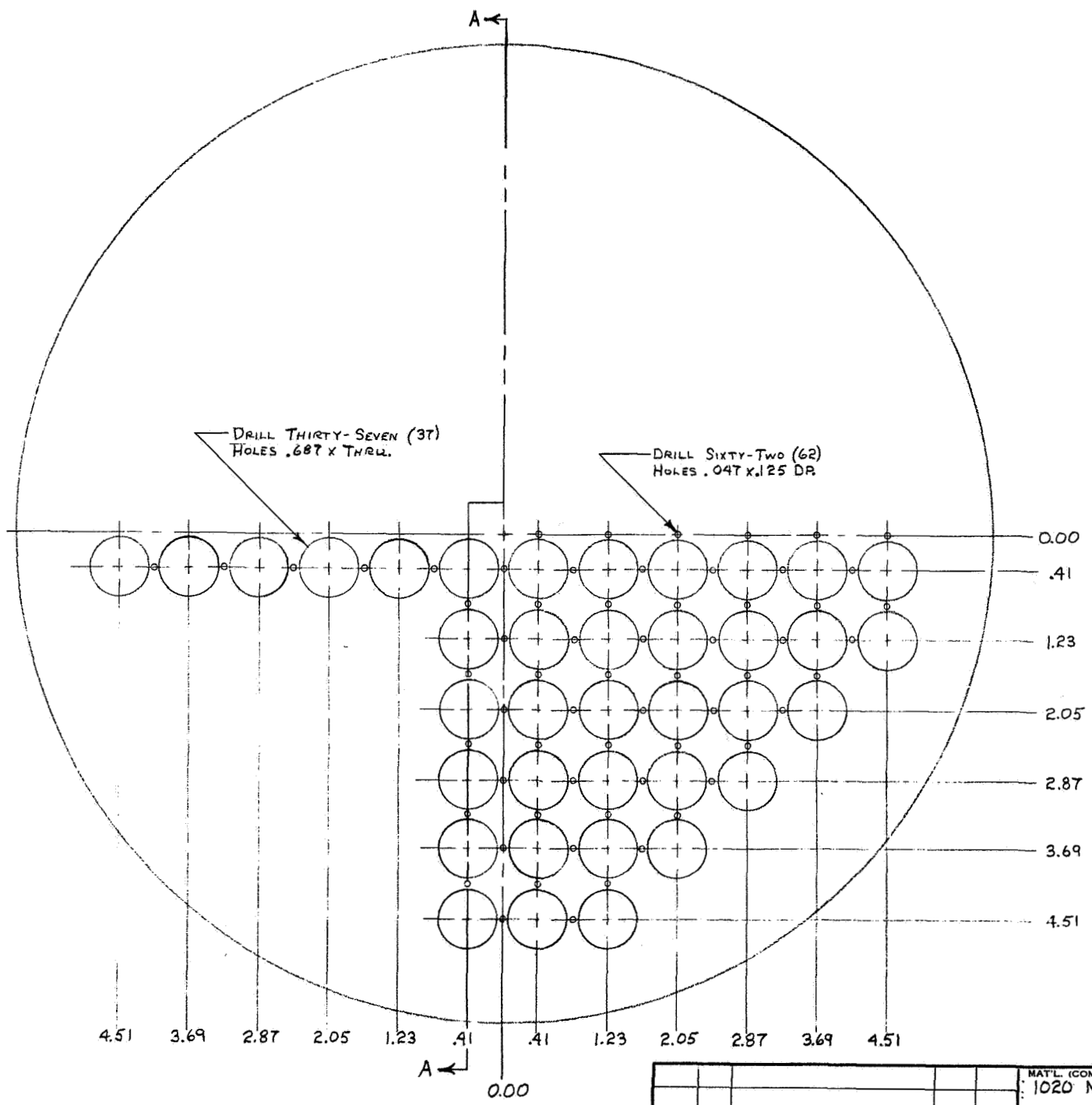

SECTION 'A-A'

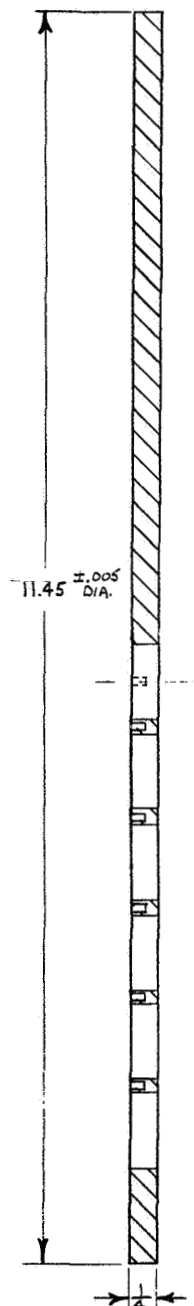

ZONE	REV. LET.	REVISIONS	BY	DATE

MAT'L. (COMMERCIAL TOLERANCES APPLY): 1020 M/S PLATE

BATTELLE MEMORIAL INSTITUTE
505 KING AVE.
COLUMBUS 1, OHIO

TOLERANCE UNLESS OTHERWISE NOTED			NEXT ASSY.	NO. REQ'D.
FRAC. ±	ANG. ±	DEC.		
	DRAWN	CHECKED	PROJ. APP.	
BY	WLS			
DATE	11-19-68			
DIV.	765			

TITLE: FUEL CHANNEL TOOLING PLATE

SCALE: FULL | K-G | ACCT. NO. | DWG. NO. FIGURE III-4 | C

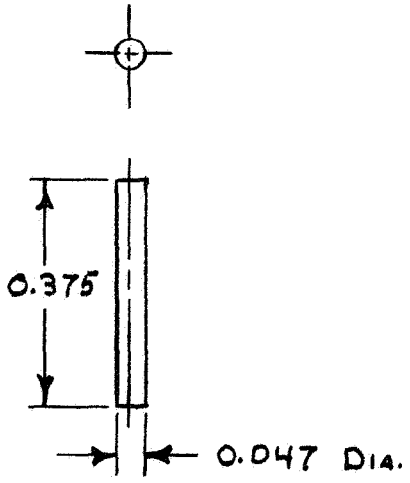

FIGURE III-5. FUEL CHANNEL PIN INSERT

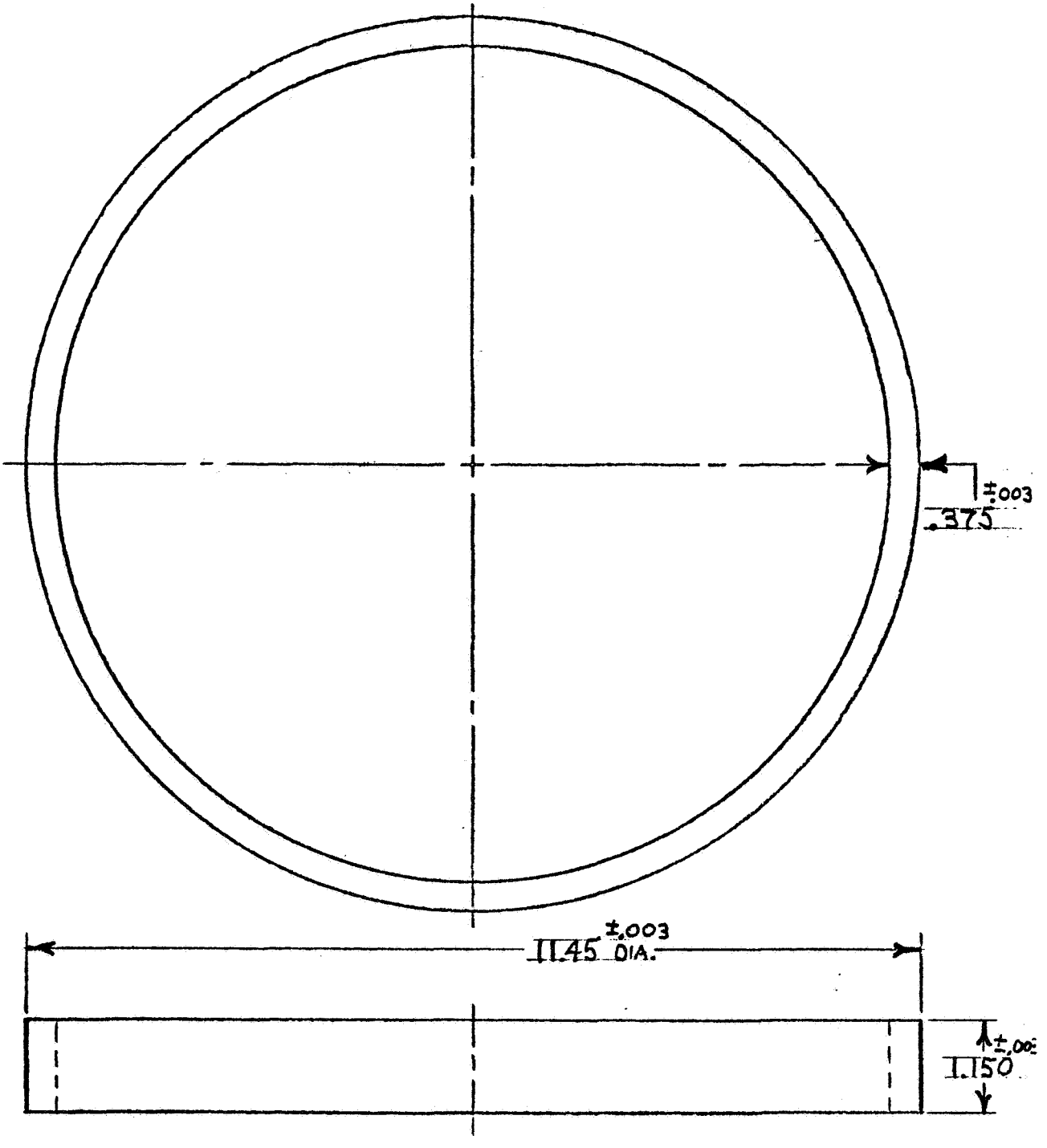

FIGURE III-6. FUEL CHANNEL TOOLING RING

from 0.050-in.-thick 304-type stainless steel sheet to fit the containers. The container for the second cycle was fabricated from 1018 steel pipe to a length of 5.25 in. and an OD of 16.2 in. and a wall of 0.25 in. The lids for each end were cut and spun from 0.050-in.-thick 304 stainless steel sheet to fit the container.

Solid nickel base plates having the dimensions in Figure III-7 were machined from Nickel 200 castings. The chemical analysis and mechanical properties are given in the vendor's test report, Figure III-8. The base plate provided dimensional reference for subsequent machining of the test pieces and also located the fixturing and centering of the various tooling parts.

The nickel powder used for Task III studies was similar to the N2-type powder which was judged to be optimum in Task I studies. The vendor's characterization of the powder, denoted hereafter as SF-grade powder, is given in Table III-1. A comparison of packing density, particle shape, and microstructure of the SF powder and the N2 powder showed that the SF grade vibratory packed to 57 percent of theoretical while the N2 grade vibratory packed to 65 percent of theoretical. The SF grade contained a coarser classification of sizes with few fines compared to the N2 grade and is the apparent cause for differences in vibratory-packed densities. Particle shapes and microstructure are compared in Figures III-9, -10, and -11. Other than the coarser classification and lesser surface roughness of the SF grade relative to the N2 grade, the two materials are equivalent.

Subtask III-A-2. Fabrication of Simulated Nickel Injector Test Pieces

The fuel-channel tooling plate shown in Figure III-12 is partially completed. The edges of the through holes were subsequently rounded to about

B

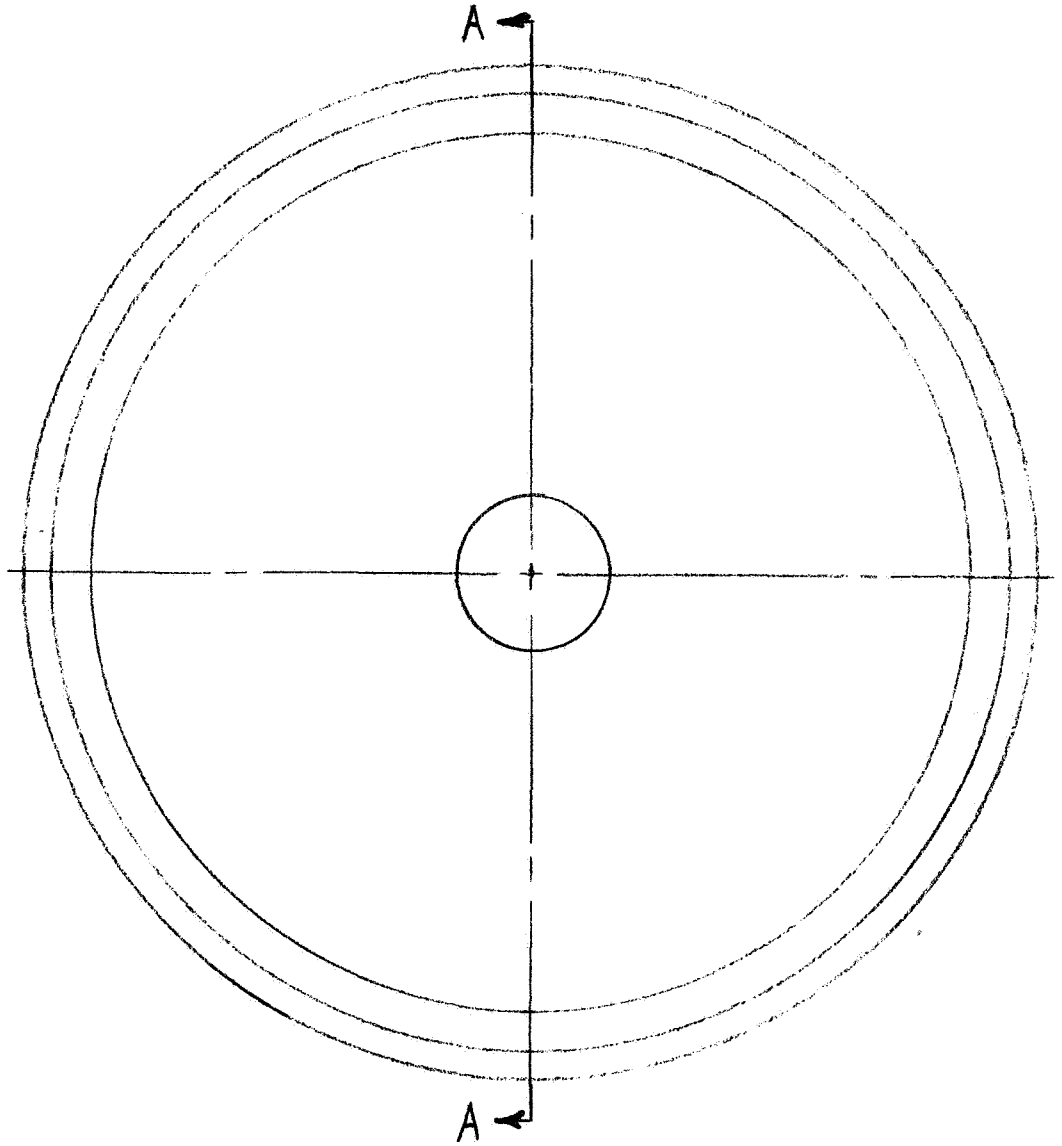

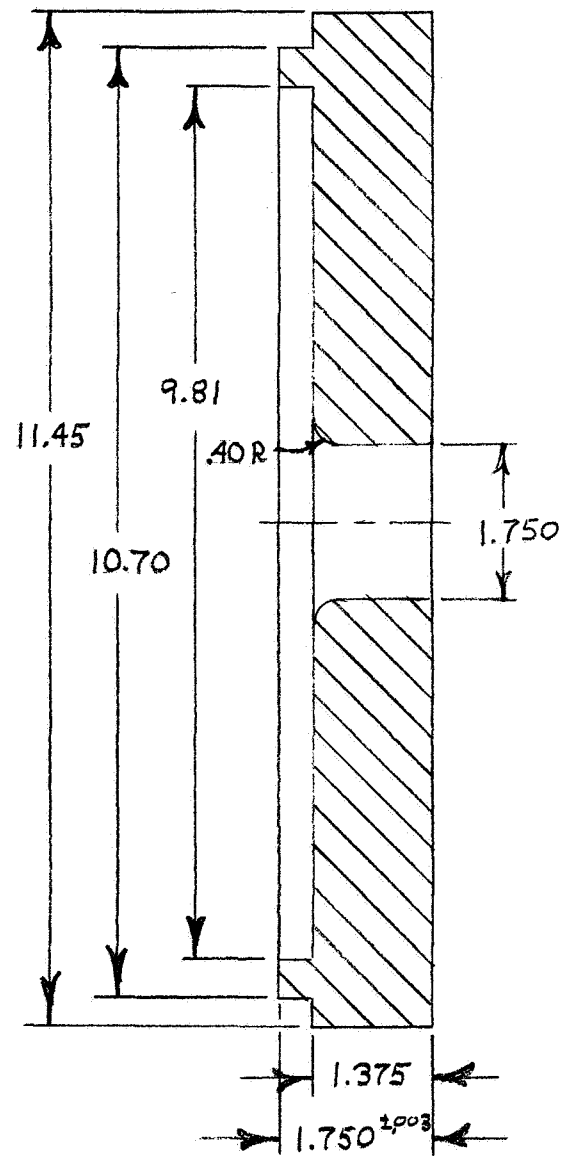

SECTION 'A-A'

NOTE: ALL DIMENSIONS ±.003.

ZONE	REV. LET.	REVISIONS	BY	DATE

MAT'L. (COMMERCIAL TOLERANCES APPLY)
NICKEL 200

TOLERANCE UNLESS OTHERWISE NOTED		
FRAC.	ANG.	DEC.
±	±	

	DRAWN	CHECKED	PROJ. APP.
BY	WLS		
DATE	11-25-68		
DIV.	765		

NEXT ASSY.	NO. REQ'D.

SCALE 1/2" = 1"

K-G

BATTELLE MEMORIAL INSTITUTE
505 KING AVE.
COLUMBUS 1, OHIO

TITLE
NICKEL BASE PLATE

ACCT. NO.

DWG. NO.
FIGURE III-7

B

HILLS CO.—10-5155—1000—10-68

FORM 40 REV. 9-66

TEST REPORT

☐ 901 PENNSYLVANIA AVE. PITTSBURGH, PA. 15233

☐ 5301 GRANT AVE. CLEVELAND, OHIO 44125

☒ 7640 REINHOLD DR. CINCINNATI, OHIO 45237

☐ 900 WILLIAMS AVE. COLUMBUS, OHIO 43212

☐ 946 KANE ST. TOLEDO, OHIO 43612

☐ 1109 S. PRESTON ST. LOUISVILLE, KY. 40203

☐ 1010 F. STREET CHARLESTON, W. VA. 25303

WILLIAMS AND COMPANY, INC.

"The House of Metals"

SOLD TO: Battelle Memorial Institute
505 King Ave.
Columbus, Ohio 43201

Date: 11-25-68
Customer's Order No: Y 3604
Williams and Company's Order No.: B018905-405

Item	Heat No.	Description	Specification
1	7058	Nickel 200 Plasma cut discs plate 12 " dia x 2"	Lukens Steel

CHEMICAL COMPOSITION

Item	Heat No.	C	Mn	P	S	Si	Cr	Ni	Fe	Cu	Al	Mg	Mo	Co
1	7058	.06	.25		.005	.10		99.51	.04	.01				

PHYSICAL COMPOSITION

Item	Heat No.	Ten. Str. Psi	Yield Psi	Elong. % - 2"	Red. Area %	Hrdns.	Grain Size			
1	7058	66,200	28,300	46		BHN 107				

Sworn to and subscribed before me
this 25 day of November 19 68

ORIGINAL NOTARIZED BY
[illegible] M. MOORE
NOTARY PUBLIC, HAMILTON COUNTY, OHIO

We hereby certify that the above data is a true copy of the data furnished us by the producing mill or supplier or of the data resulting from tests performed in approved laboratories and meets the requirements of the specification noted.

WILLIAMS AND COMPANY, INC.

By Douglas Stone

FIGURE III-8

TABLE III-1. CHARACTERIZATION OF NICKEL POWDER

Vendor: Sherritt Gordon Mines Limited

Grade: SS 150 x 325

Lot: No. 2

Apparent Density: 4.28 g/cc or 48 percent of theoretical

Flow Rate: 21.8 sec for 50 g

Chemistry:

Ni	Co	Cu	Fe	S	C	P
99.9(a)	0.106	0.010	0.006	0.025	0.008	nil

(a) Includes cobalt

Screen Analysis:

Mesh	Percent
+150	3.1
-150+170	12.2
-170+200	21.6
-200+250	17.7
-250+270	30.4
-270+325	11.2
-325	3.8

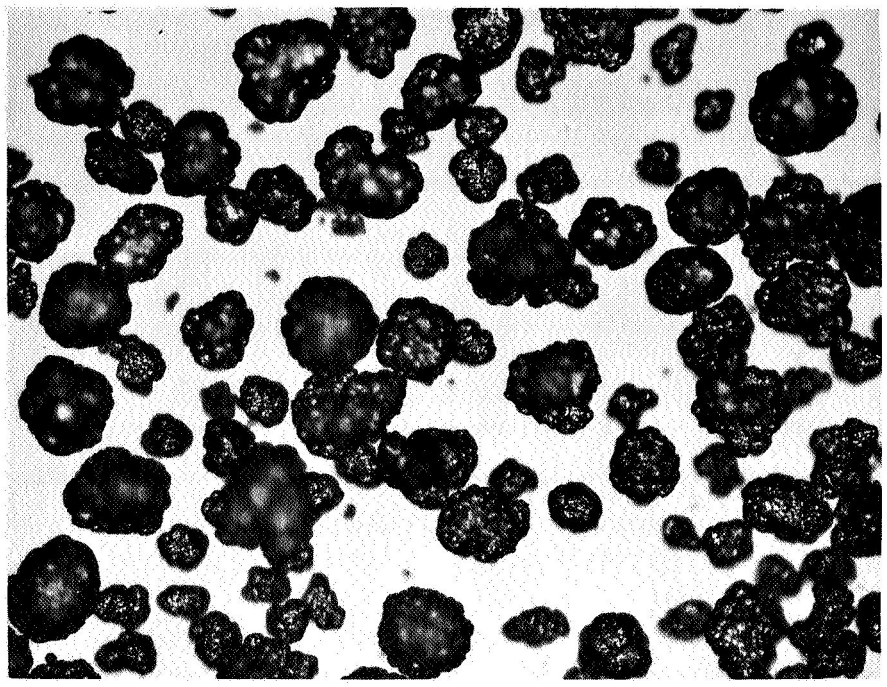

150X SF Grade 8D246

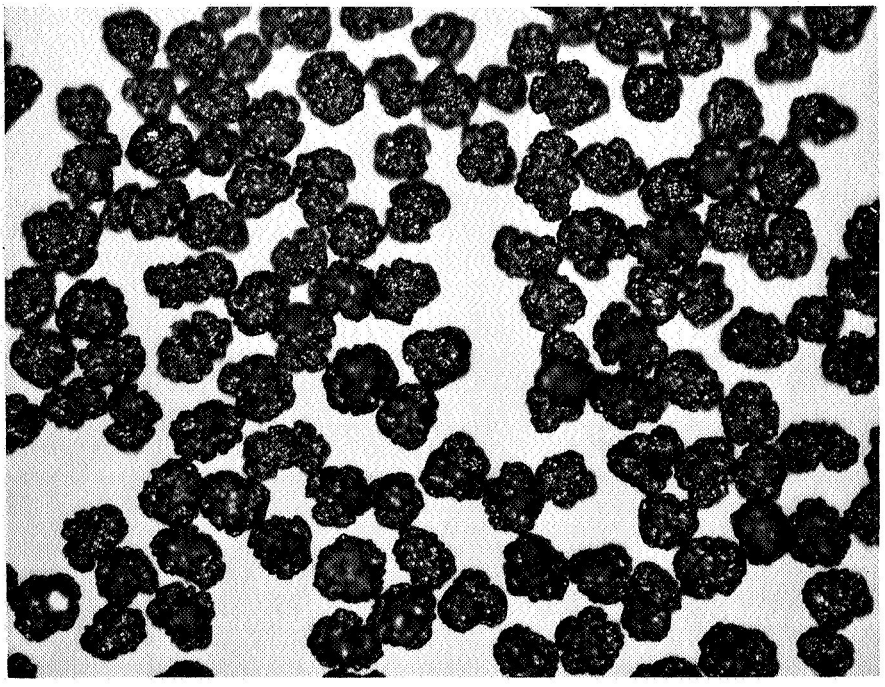

150X N2 Grade 8D247

FIGURE III-9. COMPARISON OF SURFACE AND PARTICLE SIZE IN TWO GRADES OF NICKEL POWDER

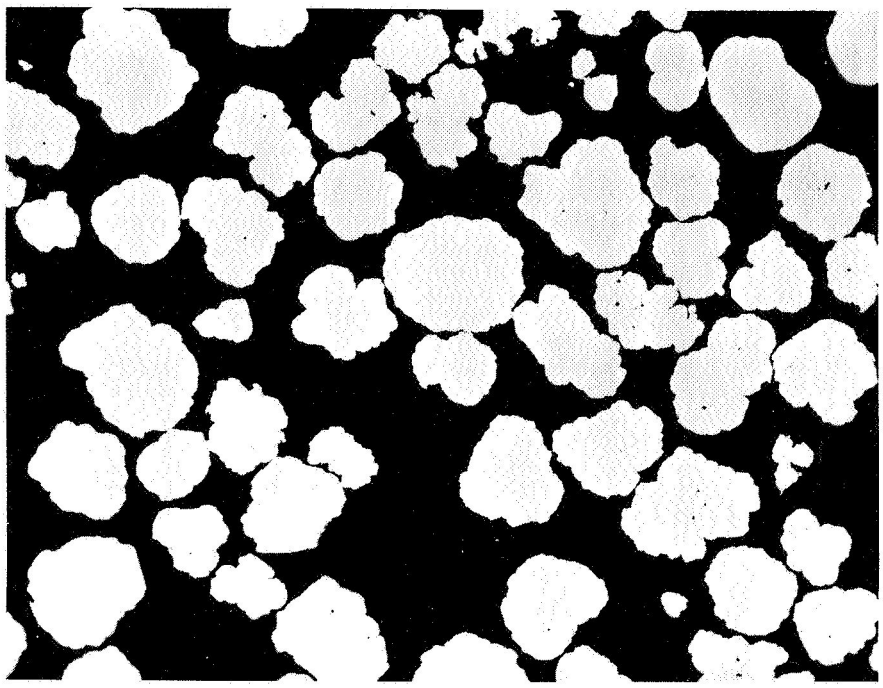

150X SF Grade 8D240

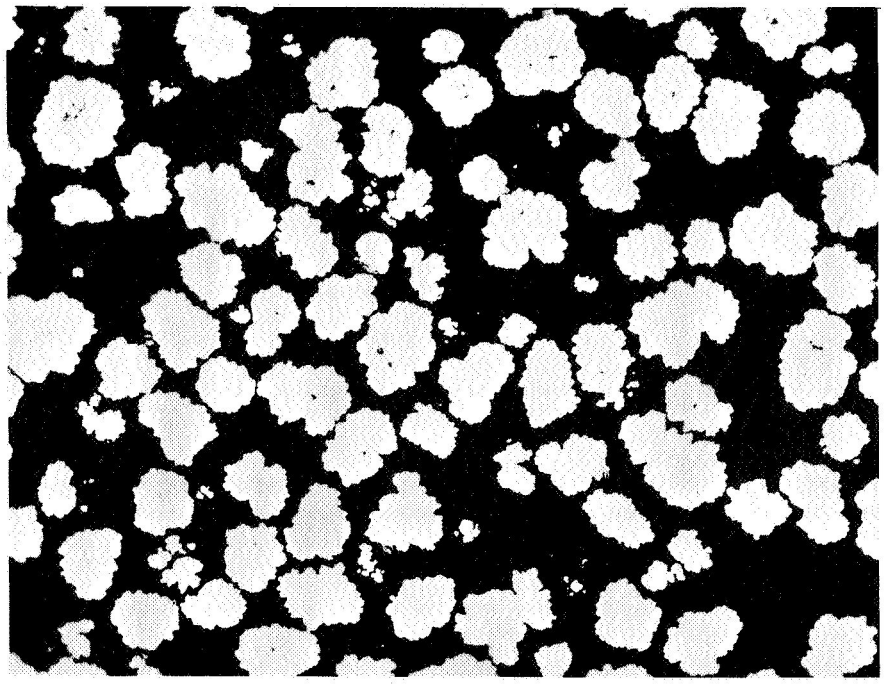

150X N2 Grade 8D241

FIGURE III-10. COMPARISON OF INTERPARTICLE POROSITY IN TWO GRADES OF NICKEL POWDER

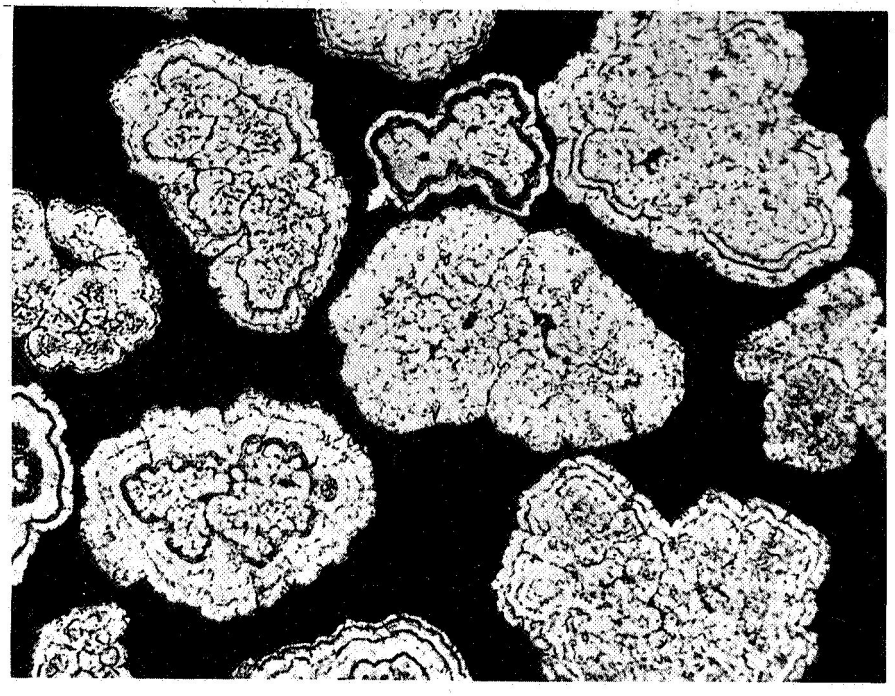

400X SF Grade 8D243

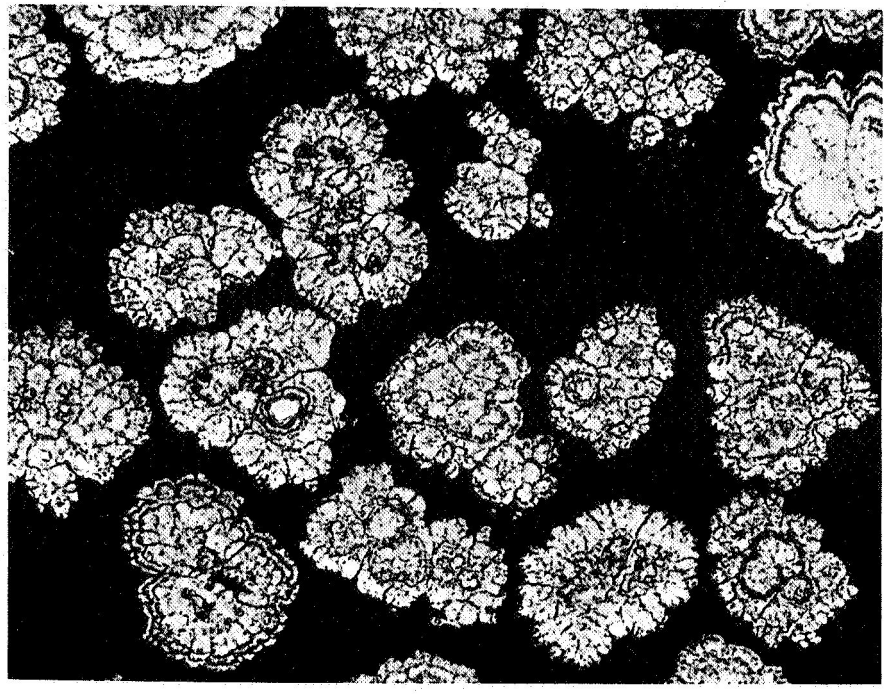

400X N2 Grade 8D244

FIGURE III-11. COMPARISON OF ETCHED MICROSTRUCTURES IN TWO GRADES OF NICKEL POWDER

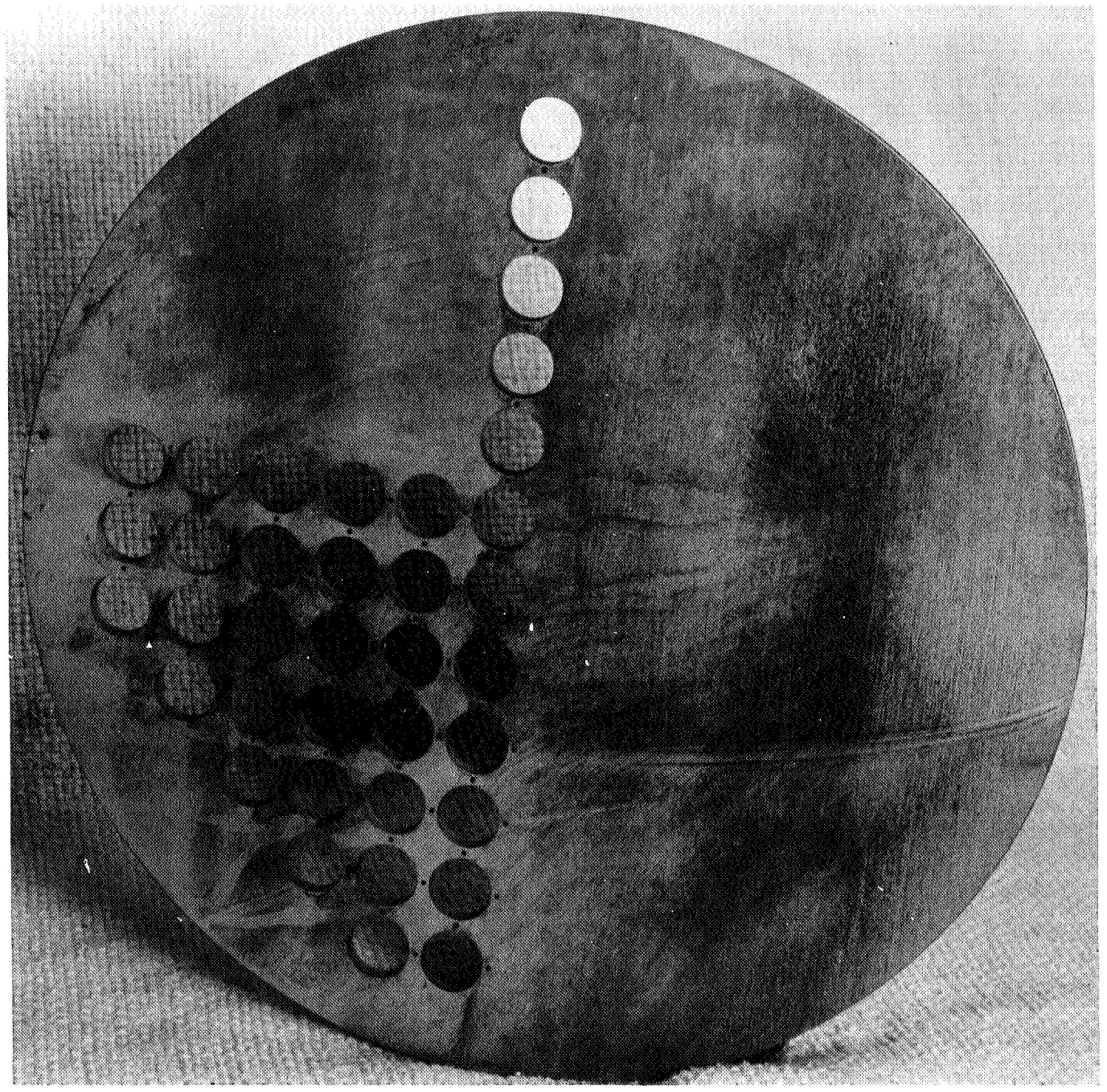

FIGURE III-12. PARTIALLY COMPLETED FUEL CHANNEL TOOLING PLATE

1/16-in. radius to simulate the hole channel shape in the final part. This machining step does not seem necessary, however, and could be eliminated without affecting the performance of the injector. The steel ring shown fabricated in Figure III-13 was welded to the fuel-channel tooling plate to fix the position of the plate and prevent slippage or rotation of the plate during compaction processes. The fuel-channel tooling pins were pressed in the holes allotted for the pins, and the completed fuel-channel tooling piece is shown in Figure III-14.

The ox-hole channel tooling plate is shown assembled with the tooling pins in Figure III-15. The tooling plate shaft on the back side was slip fitted into the nickel base plate hole shown in Figure III-16. For the first compaction cycle, the ox-channel tooling and nickel base plate were assembled in steel containers described in Subtask III-A-1. A 1/4-in. 304 stainless steel tube was welded to the top lids to facilitate leak checking and outgassing. The containers were then loaded and vibratory packed with about 45 lb of nickel powder and the lids were welded to the container. The container, tooling, and powder weighed about 100 lb, and to handle the specimen, eye bolt plates were welded to the sides of the container. The containers were checked for leaks with a helium leak detector. The containers were evacuated and heated to 600 F for 1 hr. The containers were sealed at less than 10^{-3} torr by forge welding the evacuation stems.

Two specimens were hot-isostatically compacted at about 1250 F and 10,000 psi for 3 hr. After the compaction cycle the containers were checked for leaks. One container, identified as Injector Specimen No. 2, contained a leak in the top lid. The leak was caused by a defect in the lid before the cycle started. The defect appeared to be a small indentation gouge in the lid surface originating probably from hitting or scuffing the surface with a hard, sharp instrument during handling. The defect was not detected before the cycle on the

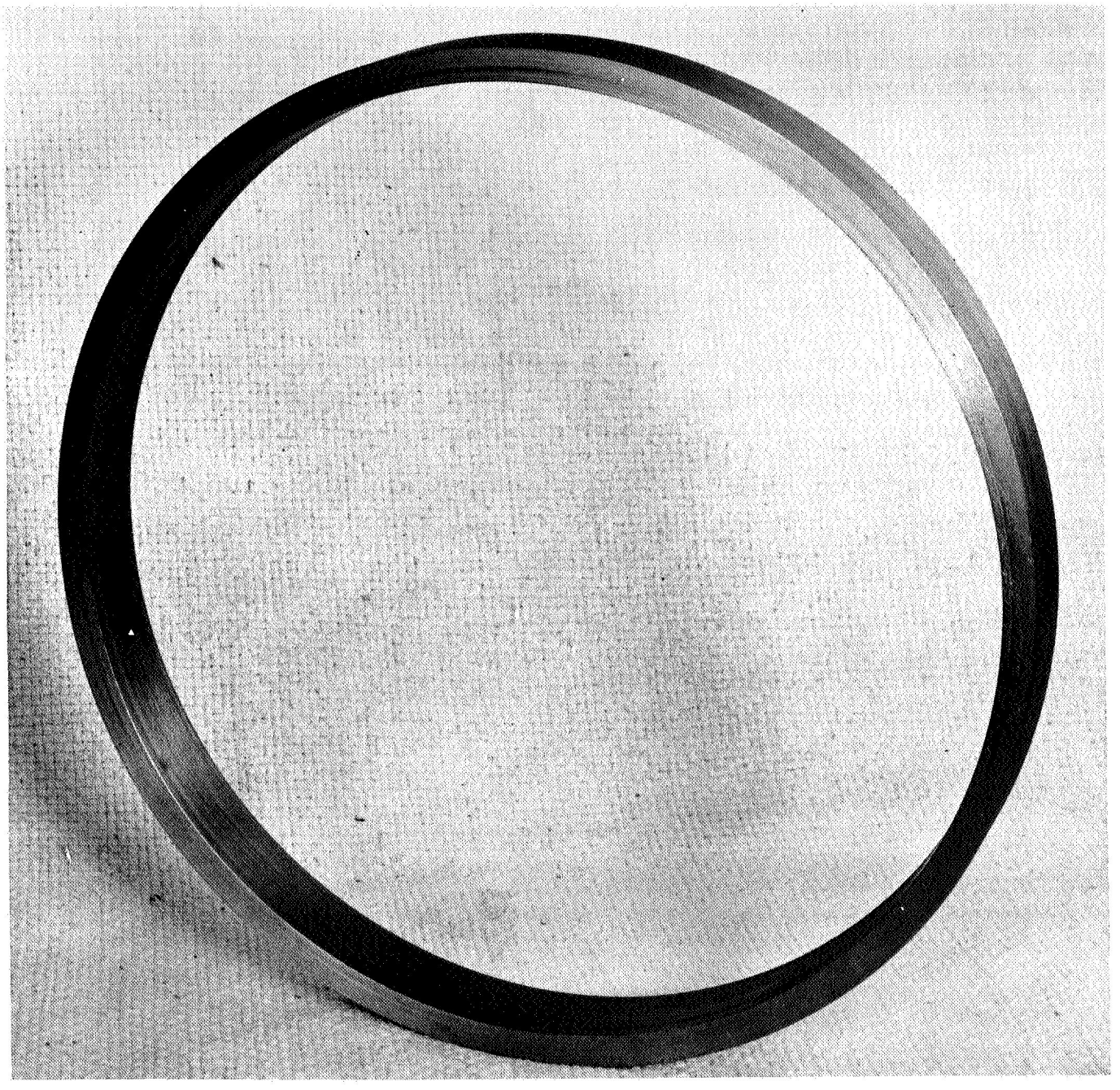

FIGURE III-13. STEEL RING FOR FUEL CHANNEL TOOLING

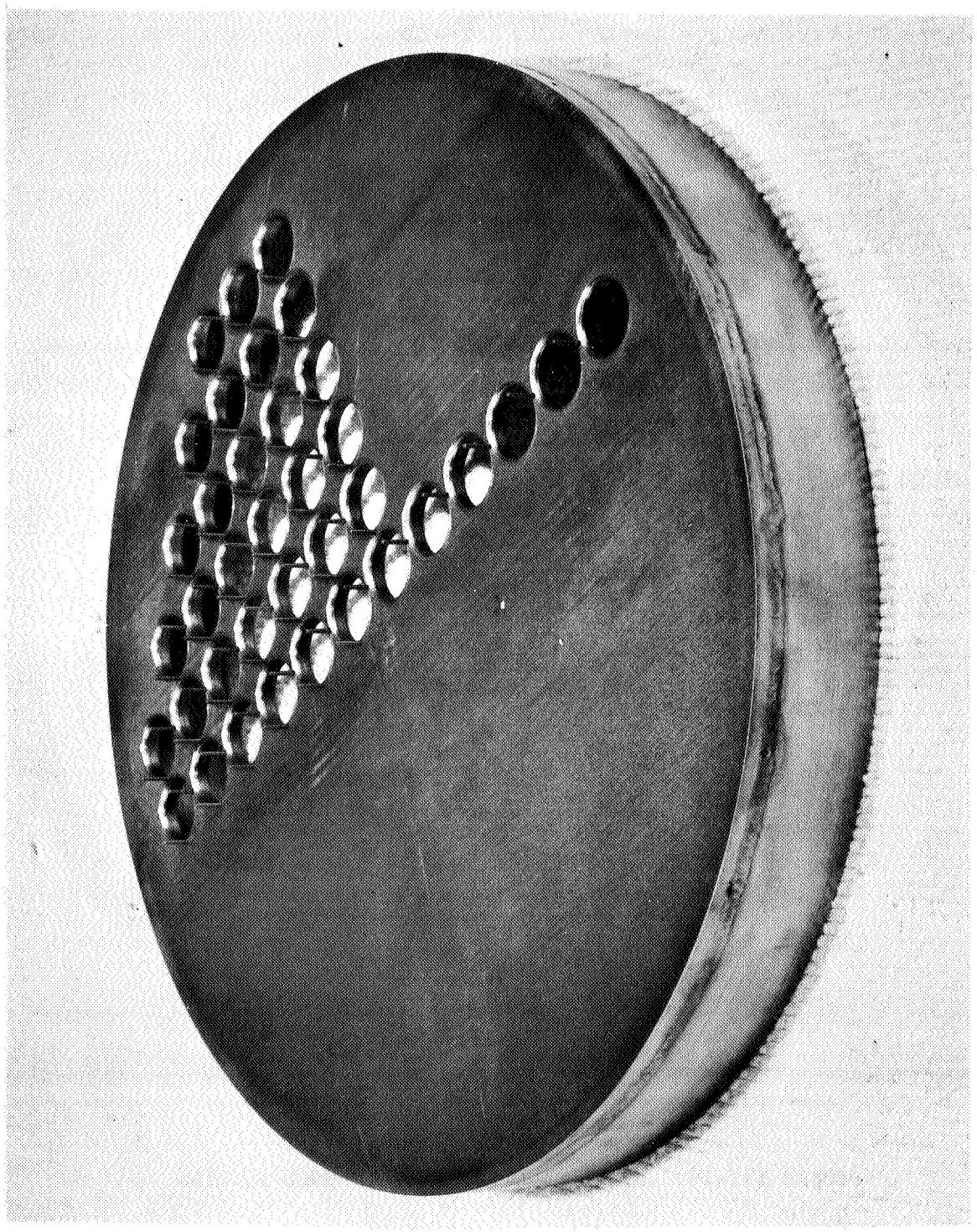

44968

FIGURE III-14. COMPLETED ASSEMBLY OF FUEL CHANNEL TOOLING

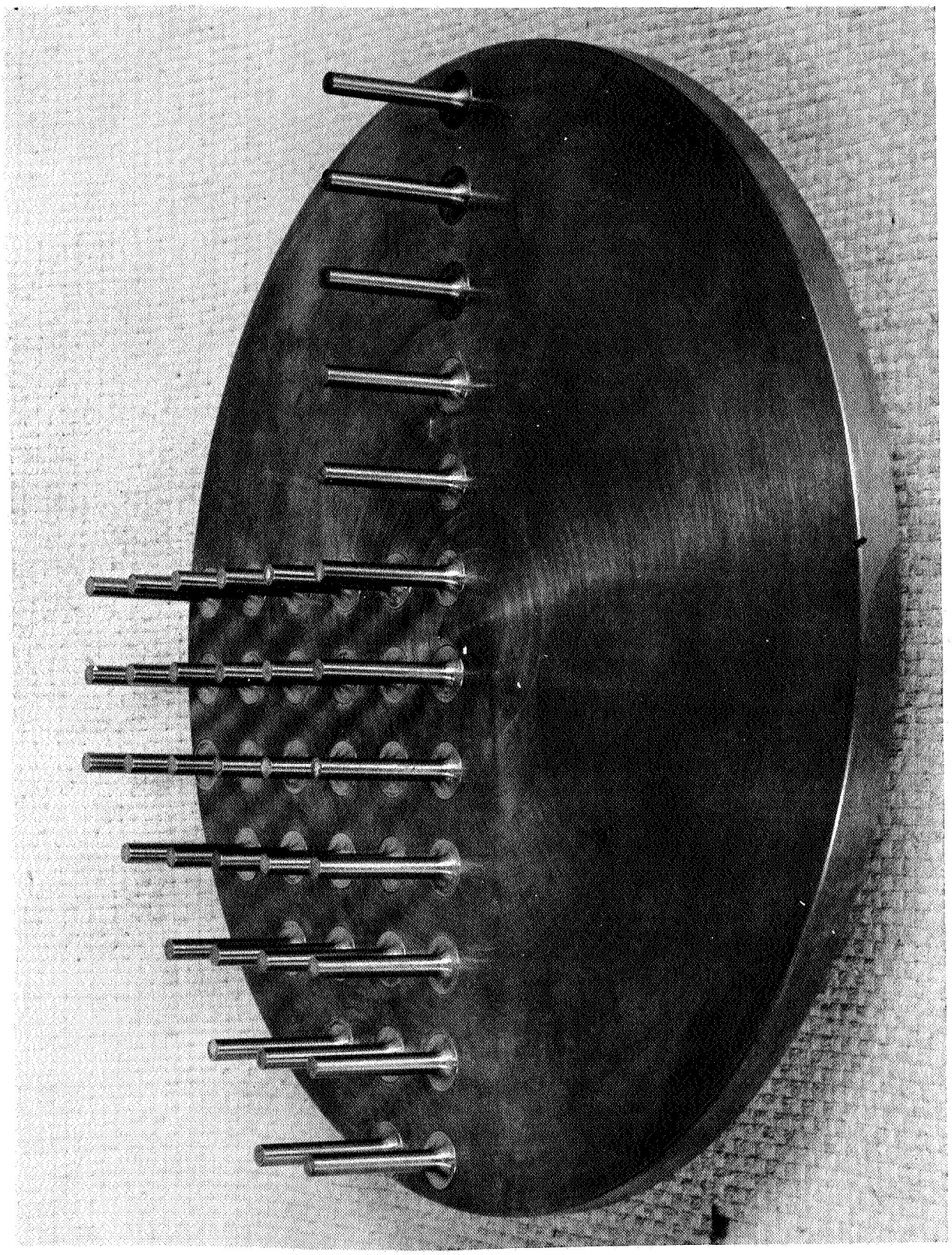

FIGURE III-15. OX-CHANNEL TOOLING

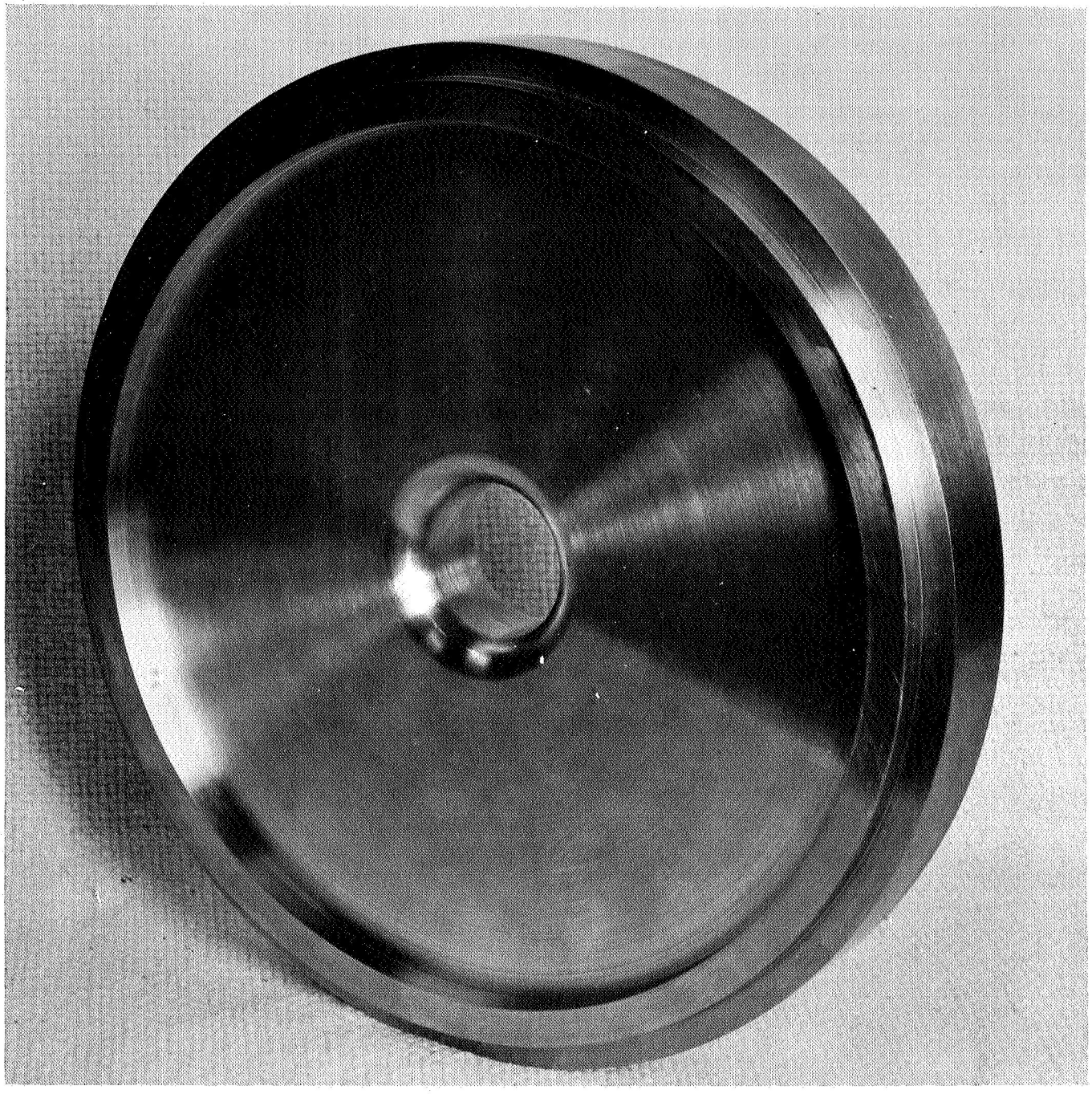

44743

FIGURE III-16. NICKEL BASE PLATE

helium leak detector since it did not penetrate through the lid. The other container, Injector Specimen No. 1, remained gas-tight during the compaction cycle, and is shown in Figure III-17. The defected lid on Injector No. 2 was machined off and a new lid welded to the container. The container was leaked checked, outgassed, sealed, and hot-isostatically compacted at 1250 F and 10,000 psi for 3 hr. In this recycle the container remained gas-tight and the nickel powder in the container was subsequently found to be densified.

The containers on both injector specimens were then machined off and the top surfaces faced down to the ox-channel tooling pins. This was necessary so that these pins might be located for the proper assembly and alignment of the fuel-channel tooling and also for insertion of the ox-channel pin extensions. The sides were turned down to 11.45 in. diameter, then a step cut made 0.375 in. deep and 1.15 in. long from the top surface. This step cut provided a seat for the fuel-channel tooling ring. The injector thus machined is shown in Figure III-18. The ox-channel pin extensions were inserted and extended 5/8 in. above the surface. The fuel channel tooling was then assembled by press fitting over the machined surfaces. One of the injectors with tooling assembled for the second compaction process cycle is shown in Figure III-19.

The assembled injectors were placed in the steel container prepared for the second compaction process cycle, nickel powder loaded into containers as shown in Figure III-20, and the containers welded with spun end lids. The containers were checked for leaks with a helium leak detector, evacuated and outgassed at 600 F for 3 hr. The evacuation stems were forge welded to seal the container at less than 5×10^{-3} torr. The two canned injector components were hot-isostatically compacted at about 1300 F and 10,000 psi for 3 hr.

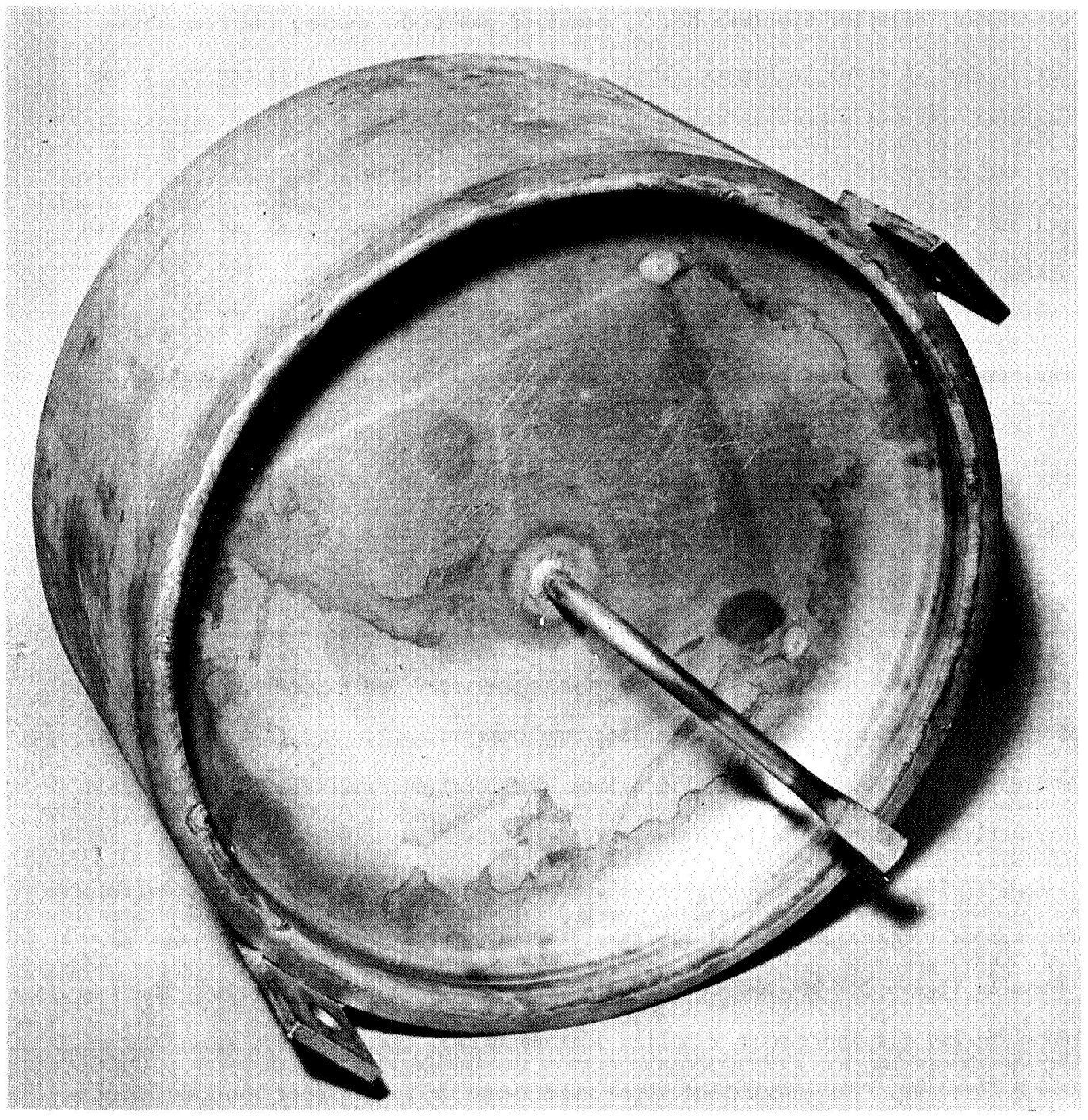

44810

FIGURE III-17. INJECTOR NO. 1 IN CONTAINER AFTER FIRST HOT-ISOSTATIC COMPACTION PROCESS CYCLE

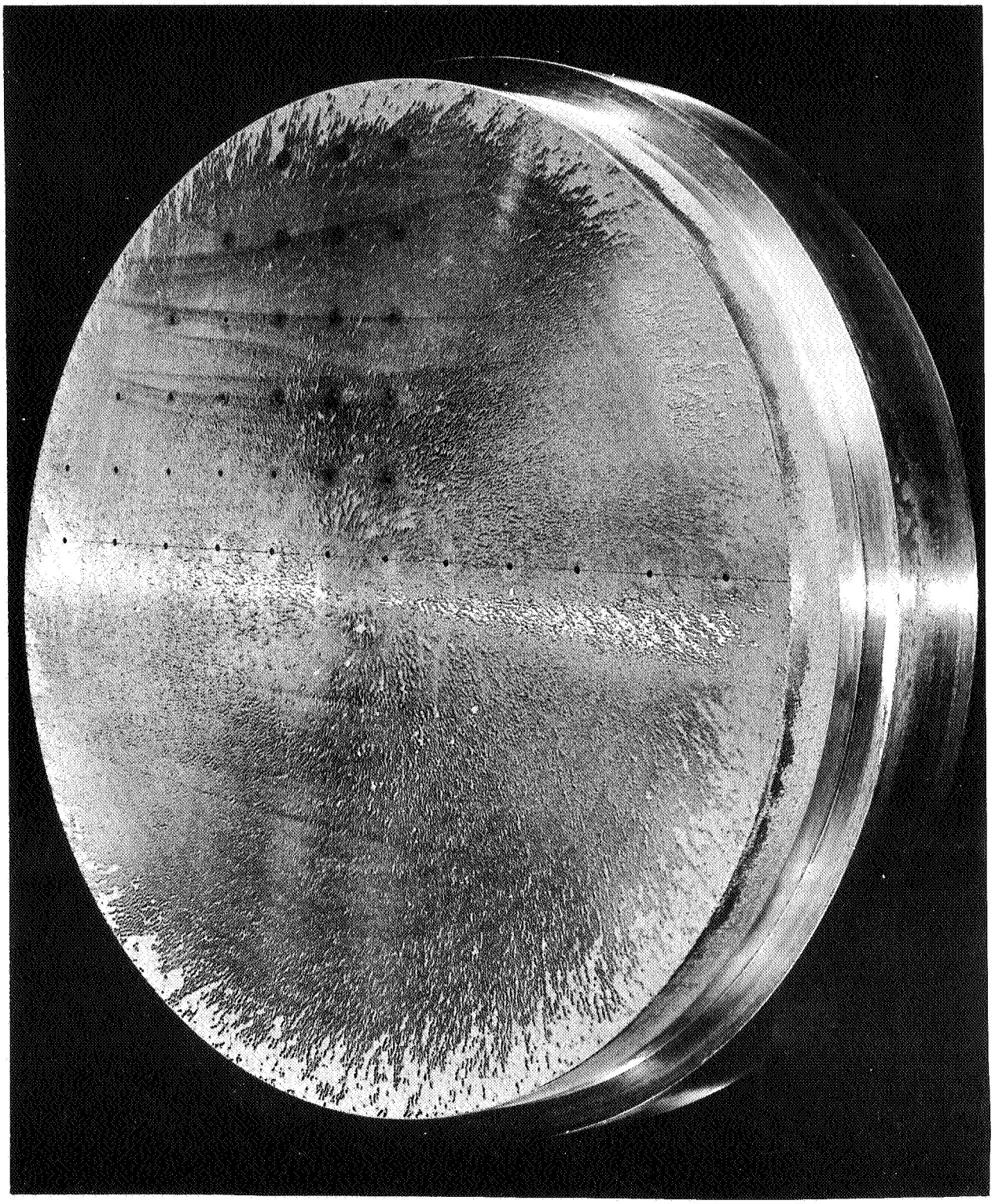

45144

FIGURE III-18. ROUGH MACHINED INJECTOR AFTER FIRST HOT-ISOSTATIC COMPACTION PROCESS CYCLE.

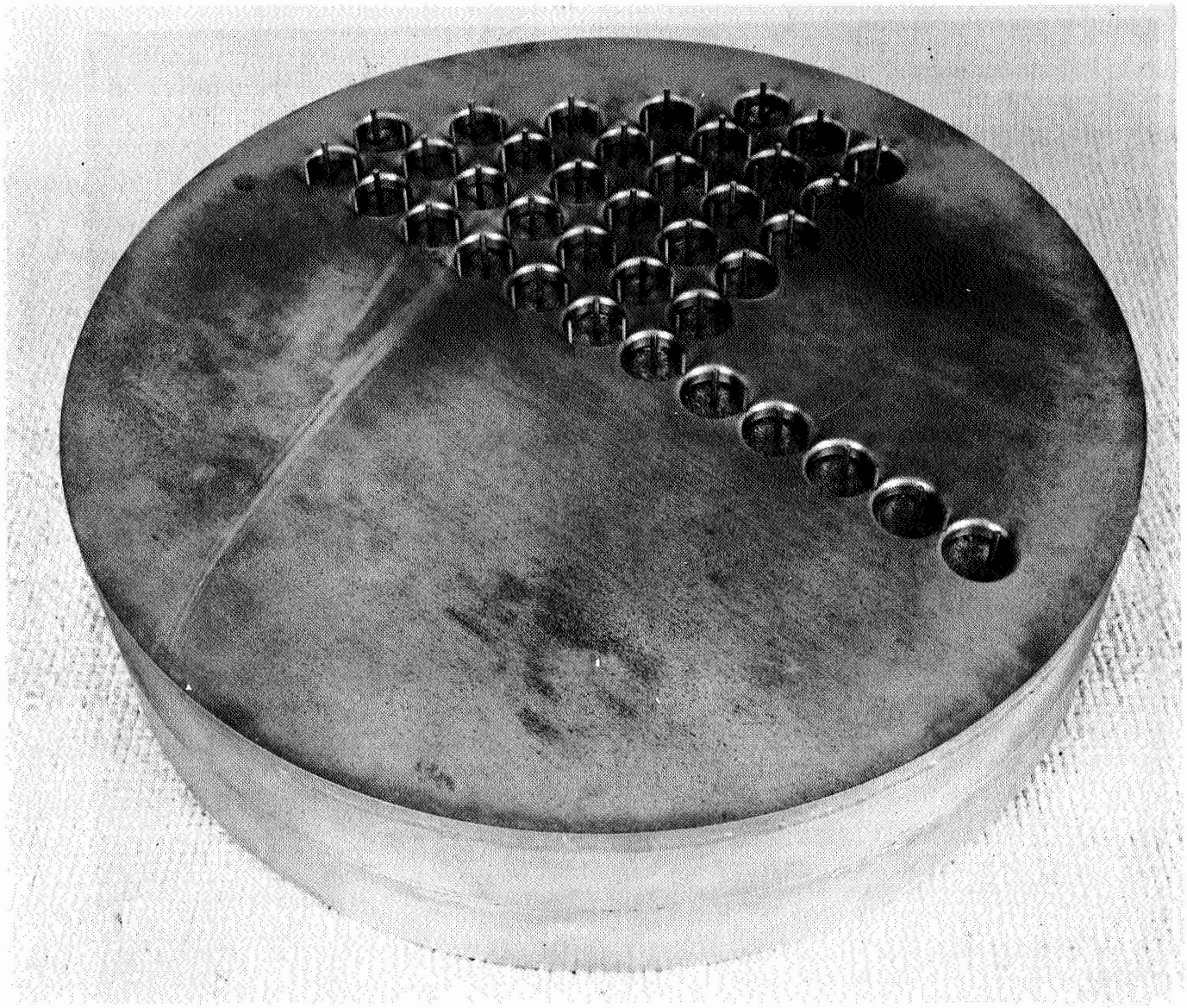

45149

FIGURE III-19. INJECTOR ASSEMBLED WITH FUEL-CHANNEL TOOLING

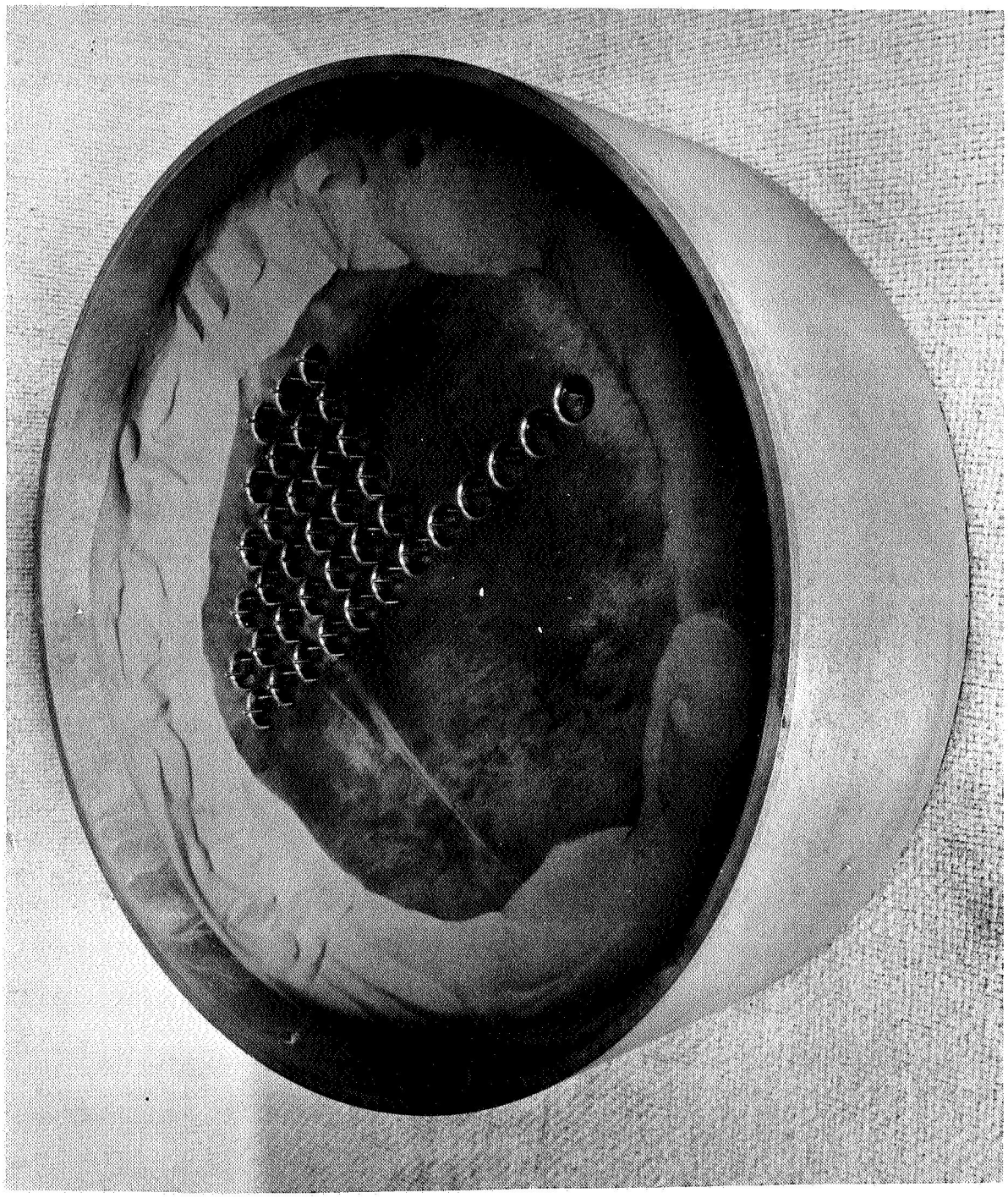

FIGURE III-20. LOADING OF INJECTOR TOOLING PIECES WITH NICKEL POWDER

After completion of the cycle, the containers on the two nickel injectors were examined and inspected for leaks. Both containers had deformed significantly, and the container on Specimen No. 1 showed a large amount of shrinkage in the side walls as indicated in Figure III-21. However, shrinkage was less than anticipated on the container for Specimen No. 2. Inert gas inspection was accomplished by cutting off part of the stainless steel evacuation stem, pressurizing the container internally with about 5 psi of argon gas, then soaking the container in a soapy water solution. A small leak was detected in the container lid on Specimen No. 1. It apparently occurred either late in the pressing cycle or by contraction of the lids during the cooling cycle. Several cracks were found by the same leak test method in the lid of Specimen No. 2, and these appeared to have formed early in the cycle since the nickel in the container was subsequently found to be porous and only partially densified. The top lid of Specimen No. 2 was removed by machining, and a new, thicker lid was welded to the container. The specimen was hot-isostatically compacted at 1400 F and 10,000 psi for 3 hr. The use of 1400 F rather than 1300 F was required in this recycle of Specimen No. 2 because in the past, when attempts were made to recycle a powder material at the same temperature as the initial hot-compaction cycle, the powder would not densify satisfactory. But by compacting at a higher recycle temperature, the density could be brought to the desired level. After the recycle, the container was examined both visually and by inert gas leak checks. The container was significantly deformed and no leaks were detected.

The containers on both injector specimens were removed by machining. The top surfaces were machined to expose the tooling pins, and leach holes were drilled into the sides to expose the fuel channel tooling ring. The ox-channel tooling was also exposed in the back face by virtue of the shaft on the back of the ox-channel tooling plate. A sectional view of injector specimen showing

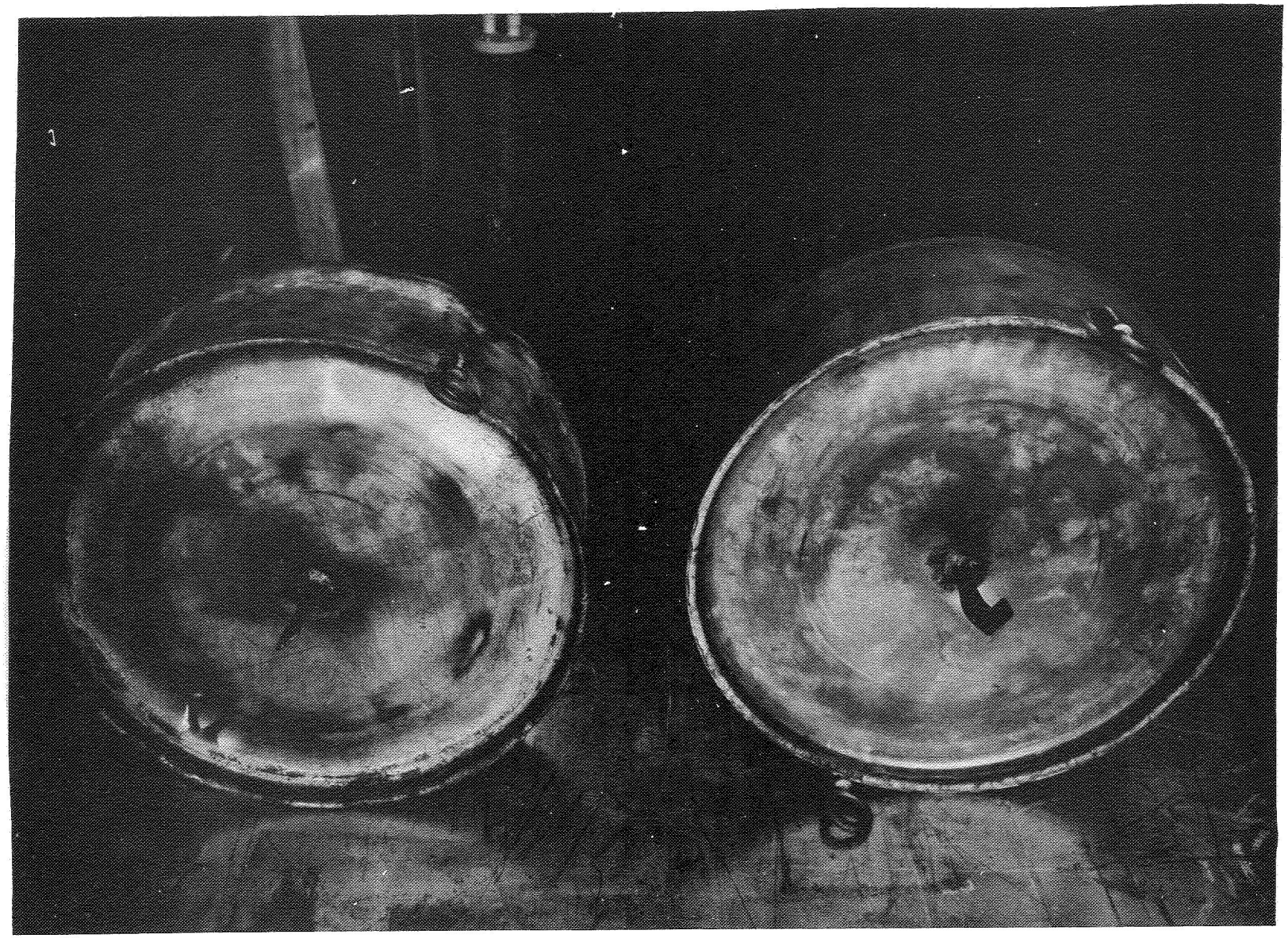

Injector No. 1 Injector No. 2

FIGURE III-21. INJECTOR COMPONENTS IN CONTAINERS AFTER THE SECOND HOT-ISOSTATIC COMPACTION PROCESS CYCLE

relative locations of the different pieces after the compaction processes are illustrated in the drawing of Figure III-22.

Removal of the steel tooling was accomplished by chemical leaching in a solution of 25 v/o H_2SO_4 - 75 v/o H_2O. The port holes on the sides and bottom were fitted with threaded pipe lengths, and these lengths were connected to plastic tubing. Several hundred gallons of the leaching solution were force-pumped and recycled into the tooling channels for a total of about 12 weeks. The fuel channel tooling was completely removed from both injectors in about 6 weeks. The ox-channel tooling, on the other hand, was more difficult to remove. An examination of Figure III-22 illustrates the problem. The fuel-channel tooling dissolved from the outer steel ring to the fuel-channel plate from four directions originating at the sides. Also, the removal of the fuel-channel tooling pins in the face was achieved quickly since these were only 1/4 in. long. The ox-channel tooling, however, was removed from just one direction, starting at the bottom face through the 1-47/64-in.-diameter port hole to the ox-channel tooling plate. The ox-channel pins were slowly removed because of their longer length. Also, as portions of the tooling were removed, it became increasingly difficult to force fresh acid into the channels and displace the used acid.

The steel tooling was completely removed from Injector Specimen No. 1 in all parts except for a few ox-channel pins on the sides and a small residue in the ox-channel plate. A significant amount of steel within the ox-channels remained in Specimen No. 2. Due to time limitations, it was decided to terminate the leaching process and proceed with nondestructive and destructive testing and evaluations. These tests are described in the following section. The injector component face after leaching is shown in Figure III-23.

LIST OF MATERIAL				
ITEM	DWG. NO.	SIZE	NO. REQ'D.	TITLE – DESCRIPTION

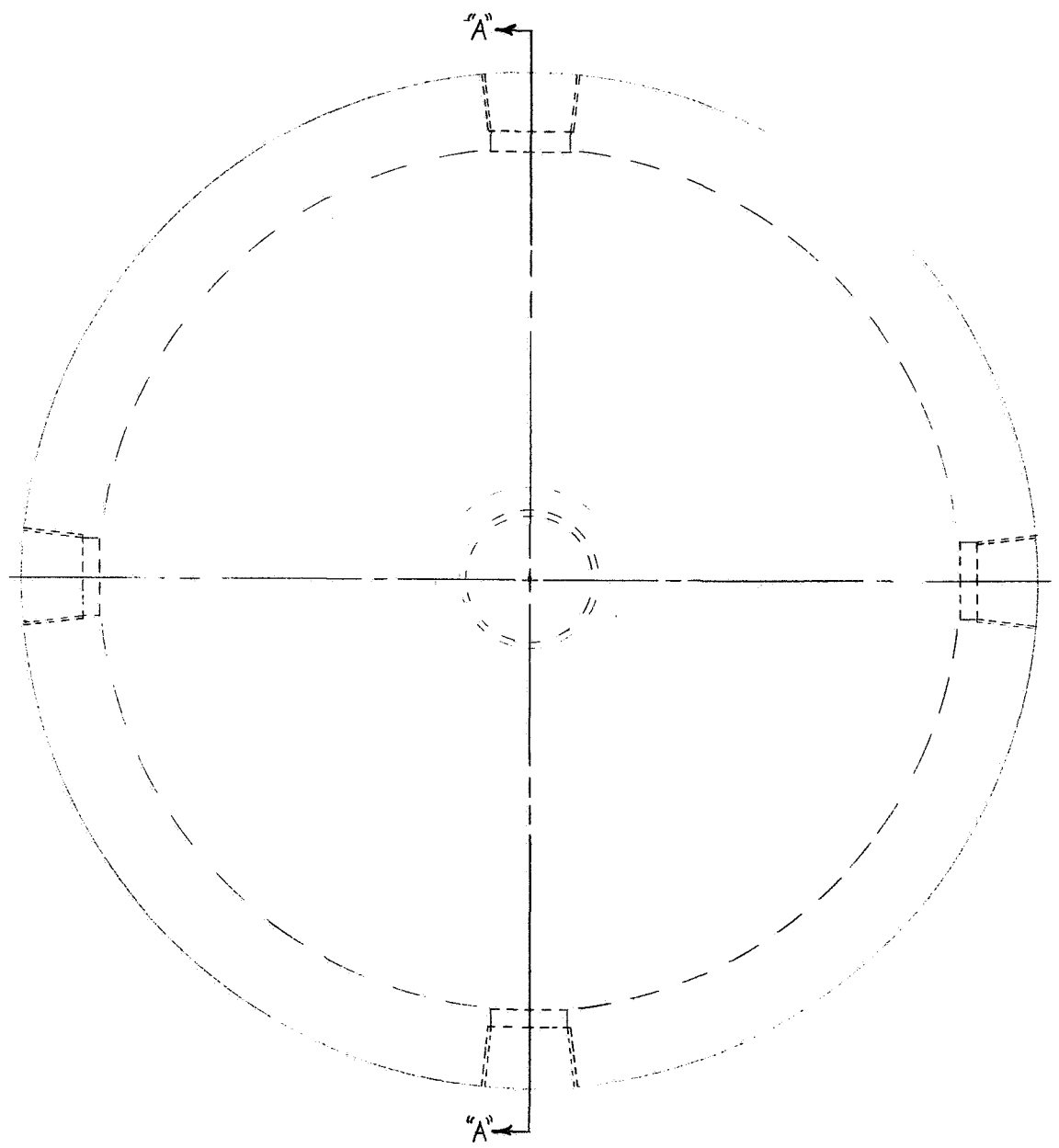

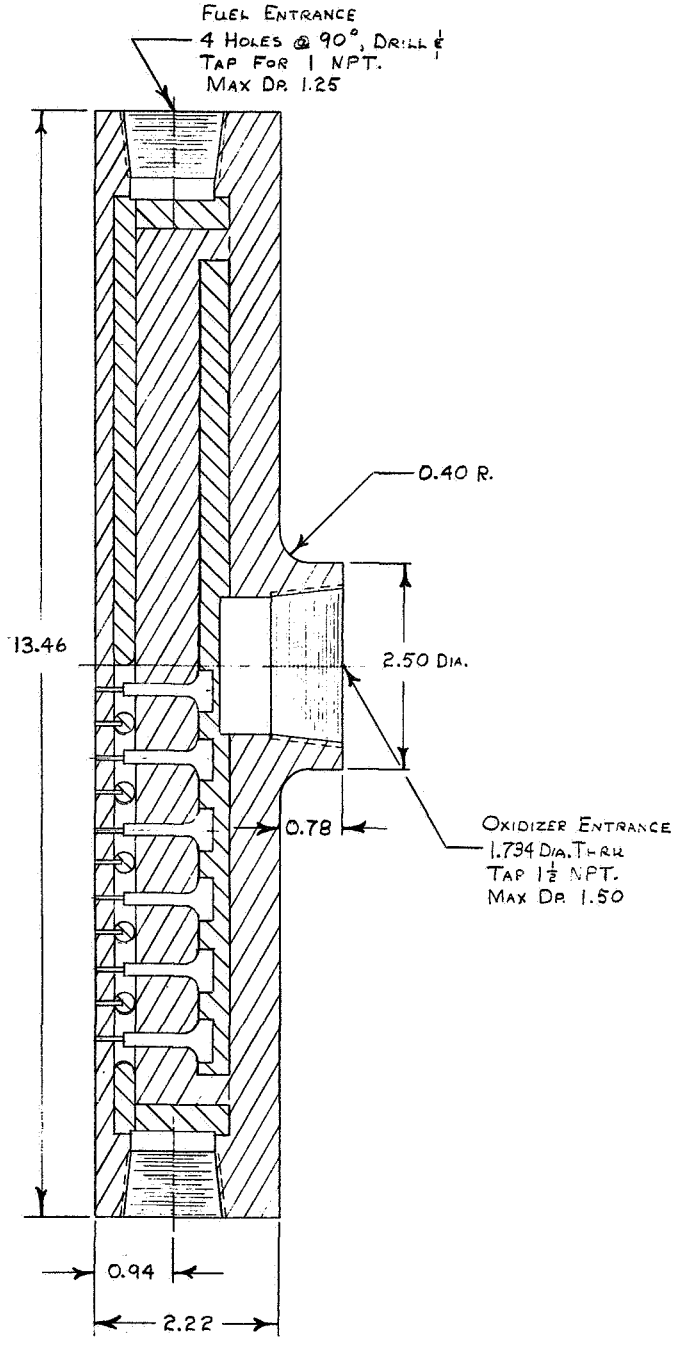

Section "A-A"

ZONE	REV. LET.	REVISIONS	BY	DATE

MAT'L. (COMMERCIAL TOLERANCES APPLY)

TOLERANCE UNLESS OTHERWISE NOTED: FRAC. ± ; ANG. ± ; DEC. 0.003

	DRAWN	CHECKED	PROJ. APP.
BY	WLS		
DATE	2-9-69		
DIV.	765		

NEXT ASSY. | NO. REQ'D.

SCALE: ¾" = 1" | K–G

BATTELLE MEMORIAL INSTITUTE
505 KING AVE.
COLUMBUS 1, OHIO

TITLE: Nickel Injector

ACCT. NO. | DWG. NO. Figure III-22 | C

46365

FIGURE III-23. INJECTOR COMPONENT AFTER LEACHING OF INTERNAL TOOLING

Subtask III-B. Testing and Evaluation of Simulated Nickel Injector Test Pieces

Nondestructive tests consisted of x-ray radiography, flow tests with water at three different flow rates, and helium leak testing for interchannel leaks.

The injectors were inspected periodically during the leaching operation to check on the progress of tooling removal. Figure III-24 is a radiograph of Injector No. 2 showing how leaching progressed in the early stages of tooling removal. The ox-channel tooling was removed from the center first, and the acid worked on the freshly exposed tooling from the center regions toward the periphery. The fuel channel tooling was removed from the sides, starting with the tooling ring, and the acid worked inward on the fuel-channel plate center regions. Figure III-25 shows Injector No. 1 after leaching had progressed about 4 weeks. Most of the fuel-channel tooling had been removed at this stage and many of the fuel-channel holes in the face were open. Most of the ox-channel tooling, however, had not been removed at this stage in the leaching operation although about 12 or 13 ox-channel holes (out of a total of 37) were open to the injector face.

The radiographs indicated that the tooling pins remained straight during the compaction processes and that the alignment of the fuel-channels with the ox-channels showed no change from the assembled alignment.

After leaching was terminated, the face of each injector was ground flat and smooth to provide a suitable surface on which to place sealing fixtures for the helium leak test. The sealing flange shown in Figure III-26 was fitted with a 1/8-in.-thick neoprene plate then clamped to the injector face plate to seal off the flow holes in the face. Both channel systems were then evacuated to effect and test the seal. One system, the fuel-channel system, was then back-filled with helium while the other system, the ox-channel system, was

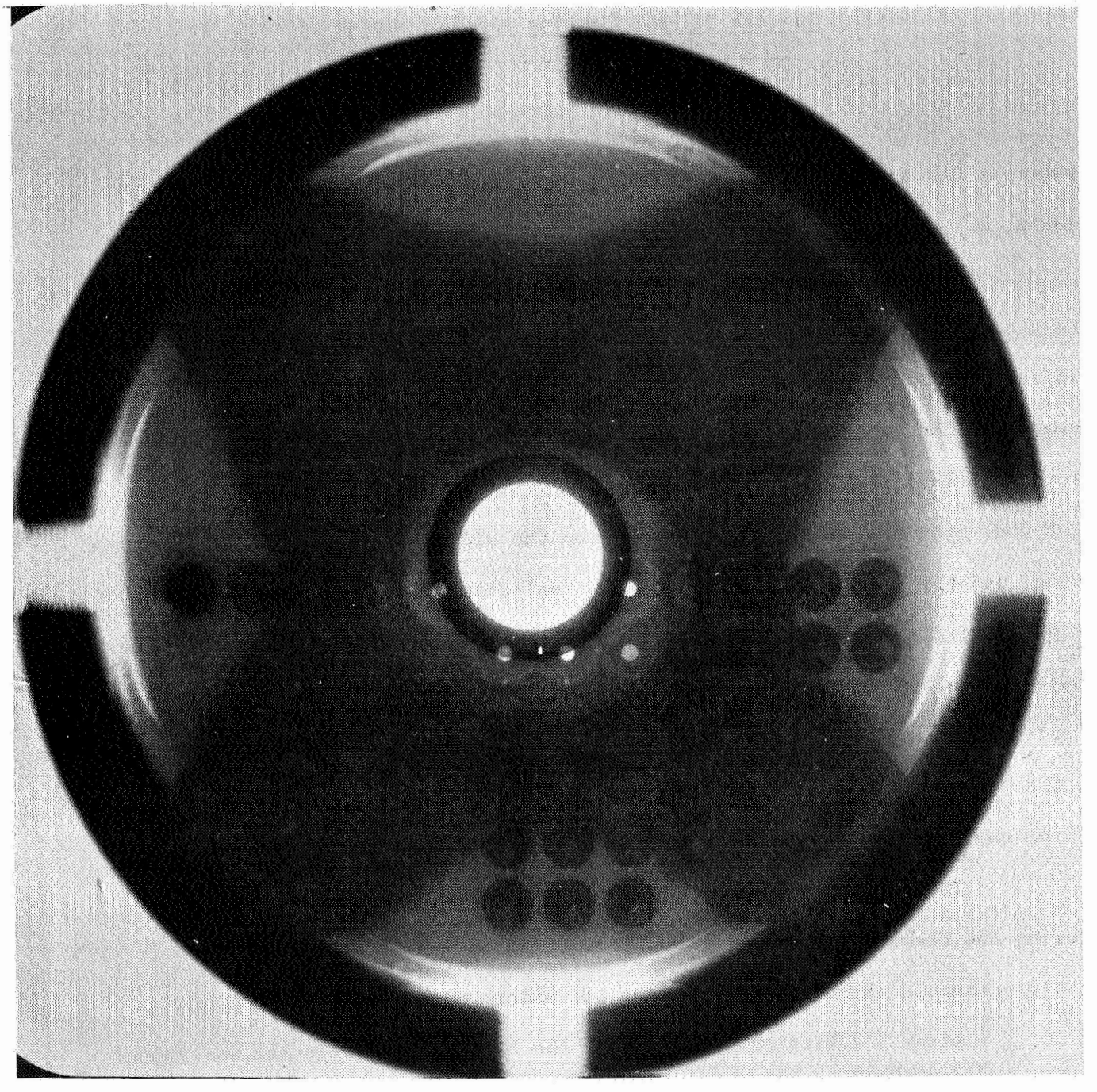

FIGURE III-24. RADIOGRAPH SHOWING PROGRESS OF LEACHING IN INJECTOR NO. 2 AT EARLY STAGE

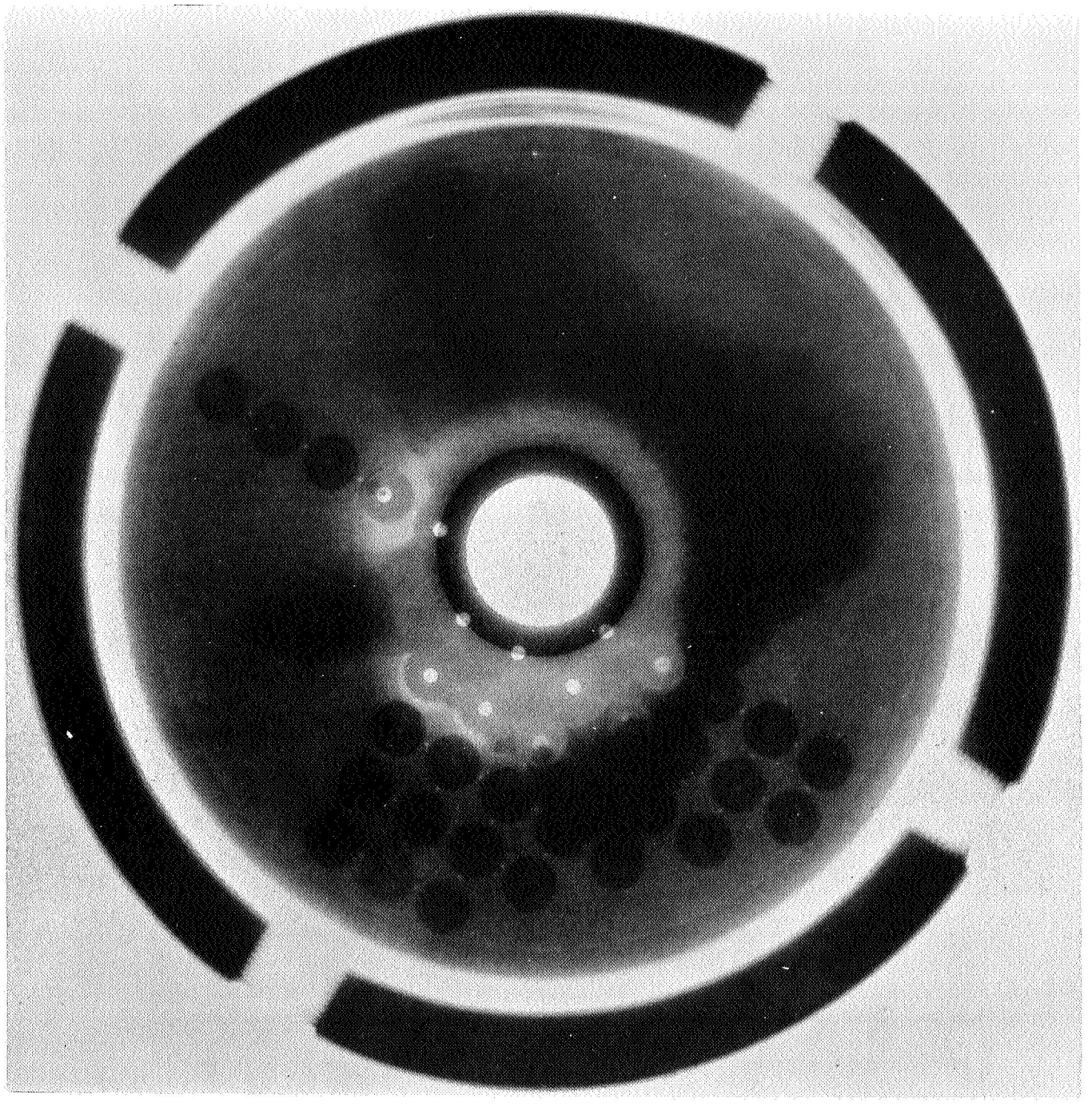

FIGURE III-25. RADIOGRAPH SHOWING PROGRESS OF LEACHING IN INJECTOR NO. 1 AT LATE STAGE

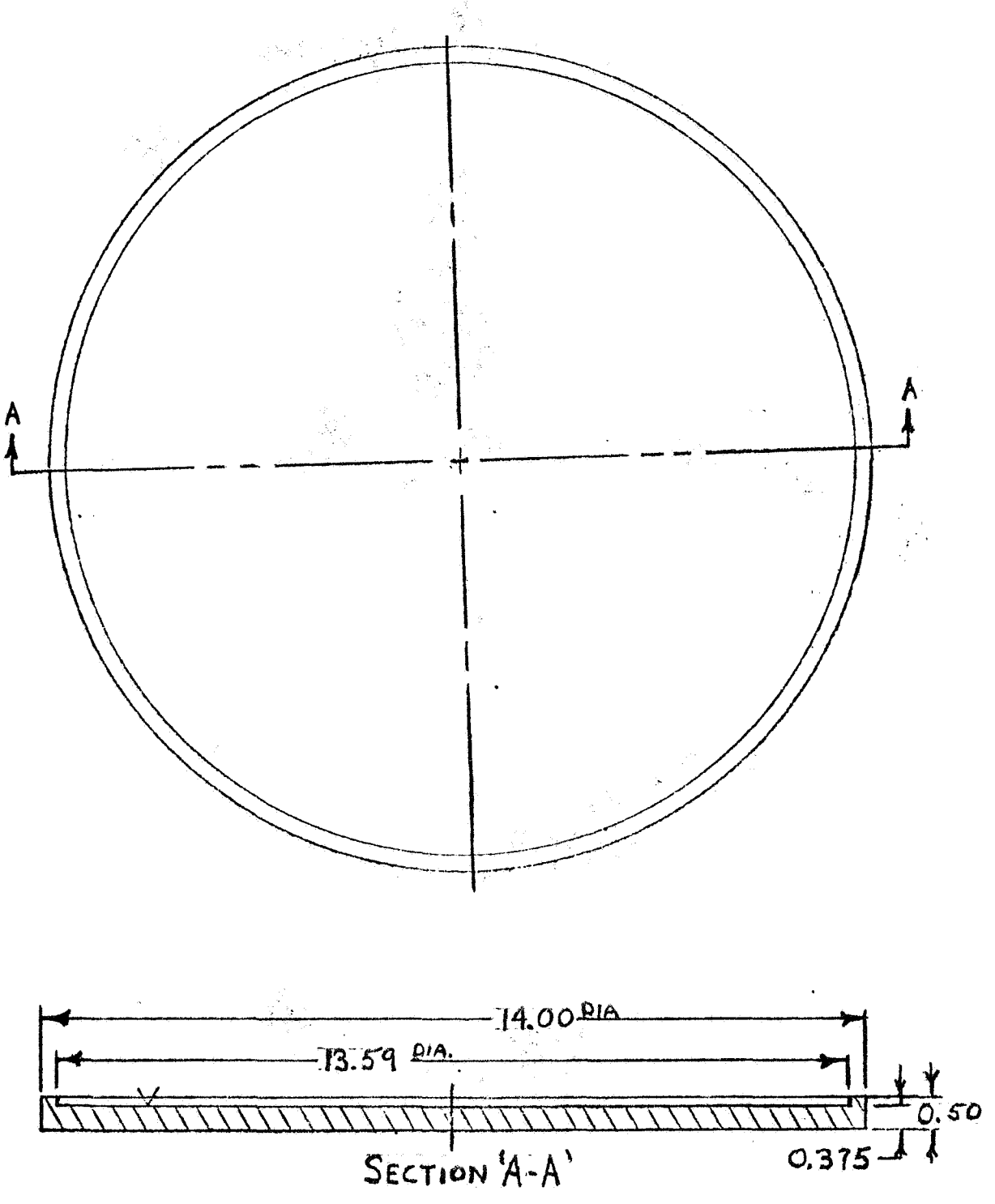

FIGURE III-26. LEAK TESTING FLANGE

evacuated through a helium leak detector. Helium penetrated into the ox-channel system in Injector No. 1 which was not fully dense. No leaks could be detected in Injector No. 2. The nickel in this specimen achieved full densification to at least 97 percent of theoretical density.

Flow tests were conducted on Injector No. 1 with water at three different flow rates. The flow channels and holes representing the fuel system ejected water without constriction through all 62 holes and at uniform heights above the injector face. The flow was perpendicular to the face in all cases. The flow channels and holes representing the oxidizer system ejected water without constriction in 31 of the 37 holes; the streams in the 31 nonconstricted holes were ejected exactly perpendicular to the face and at relatively uniform heights above the face of the injector. The constriction in 6 holes located at the edge of the injector was due to residue steel in the passageways. Flow tests were not conducted on Injector Specimen No. 2 because of obvious impediments to flow by residual tooling in sections of the flow channels.

Destructive testing was conducted on Injector No. 1 by cutting through sections "B-B" and "E-E" defined in Figure I-3. Density measurements on localized sections were conducted and these results are summarized in Table III-2. The microstructure in selected regions was examined to show the general structure. A typical microstructure is shown in Figure III-27. Hardness tests were conducted by traverses across surfaces of the sectioned pieces. The hardness test results are tabulated in Table III-3. Tensile bars were not fabricated from Injector No. 1 sections because of the obvious low density in the structure.

Inspection of the sectioned pieces for dimensional control and alignment of the internal flow channels provided the data tabulated in Table III-4. Macrographs of the sectioned pieces of Injector No. 1 are shown in Figures III-28 and -29.

TABLE III-2. DENSITY DETERMINATIONS IN NICKEL INJECTOR NO. 1

Position	Average Density	Percent of Theoretical
Center Region	8.13	91.3
Quadrant Containing Fuel Holes	7.80	87.7
Quadrant Away From Fuel Hole	7.57	85.0
Along Rim	8.14	91.5

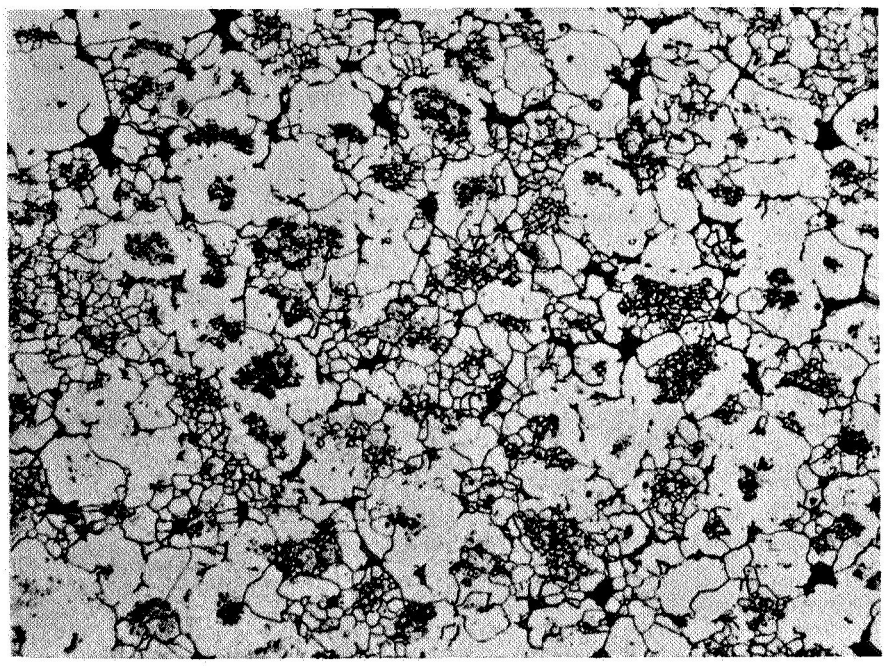

150X Etched 2E009

FIGURE III-27. MICROSTRUCTURE OF DENSIFIED NICKEL POWDER IN INJECTOR NO. 1

The nickel was about 90 percent in this specimen because of a leak that developed in the container during hot-isostatic compaction.

TABLE III-3. HARDNESS TEST RESULTS ON SECTIONS FROM INJECTOR NO. 1

Position	R_B (100 Kg load), Average of 5 Readings
Center Region	13
Quandrant with Fuel Holes	12
Along Rim	17
Overall Average	14.5

Low hardness values are a result of low density of compacted nickel powder in Injector No. 1. In components with adequately densified nickel powder, the R_B hardness is about 65.

TABLE III-4. SUMMARY OF DIMENSIONAL ANALYSES AND ALIGNMENT INSPECTION OF INTERNAL CHANNELS IN INJECTOR NO. 1

(1) Spacing of 0.82 in. between ox-hole channels was maintained to within ±0.02 in. except at sides. Ox-hole channels at sides were bent excessively due to pressure gradient in this area during hot-isostatic compaction.

(2) The low density in Injector Specimen No. 1 resulted in erosion of channels during tooling removal and vapor spray cleaning of surfaces for macrophotographs. Thickness of ox-hole channels measured on an adjacent section were 0.068 to 0.071 in. dia at the face. The fuel hole channels at the face were 0.047 to 0.049 in. in dia. Otherwise, channel dimensions internally were held to within ±0.015 in.

(3) The fuel-channel plate remained straight to within ±0.005 in. The ox-channel plate was straight with no detectable camber.

(4) Close alignment to within ±0.01 in. of the ox-hole channels with respect to the fuel-hole channels was maintained in the center regions. On the outer regions, the distortion of the ox-hole channels caused a misalignment from the specified location of about 0.2 in.

(5) Radial dimensions of the fuel-channel ring and overall diameter were held to within ±0.02 in. The overall height of the injector after machining the exterior surfaces was under specified dimensions by 0.2 in. The height of the injectors as-bonded was 3.12 to 3.18 in. but had to be reduced to expose the distorted ox-channel tooling pins on the sides.

(6) Surfaces of the channel cavities were smooth and showed no detectable impediments to flow except in several hole channels where the steel tooling in the small diameter holes was not completely leached out.

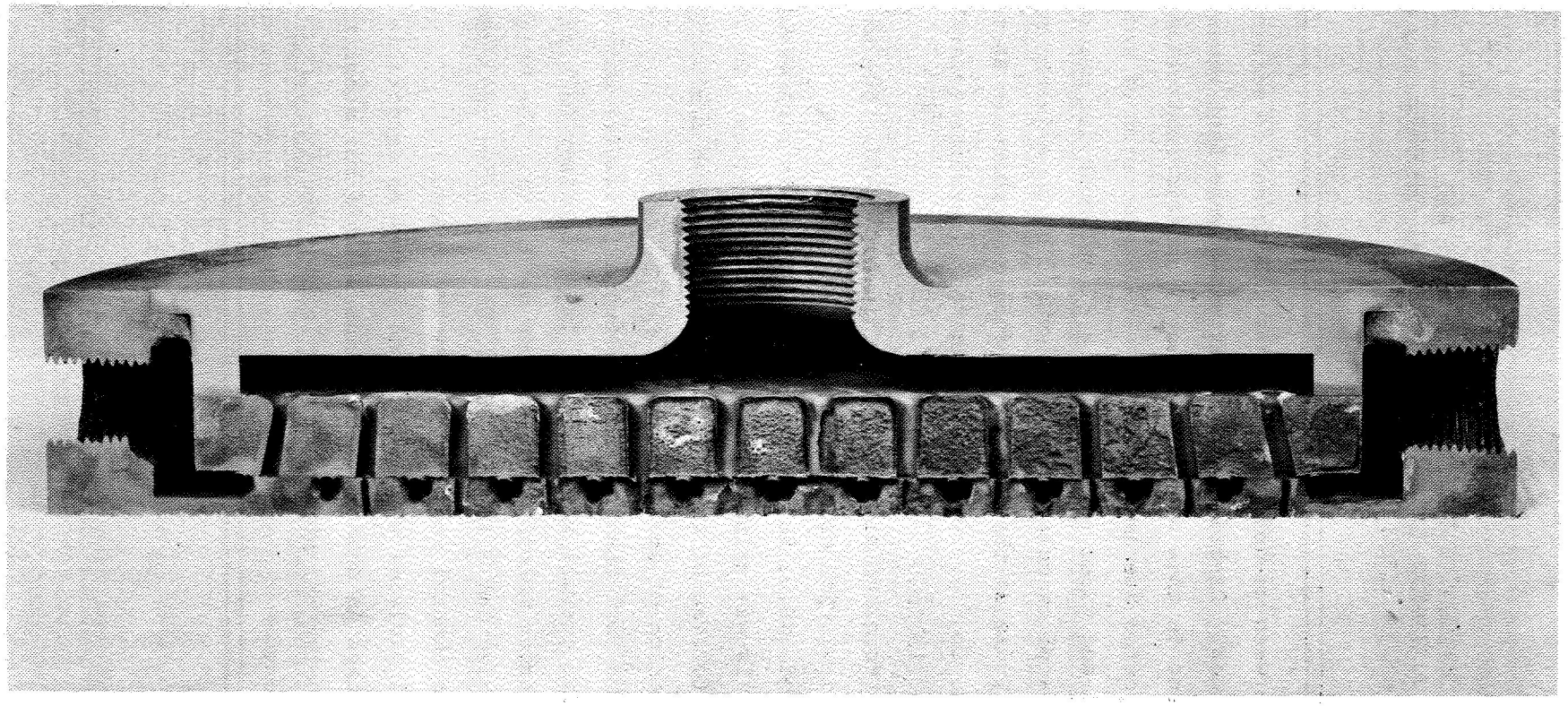

46630

FIGURE III-28. MACROSTRUCTURE OF SECTIONED INJECTOR NO. 1 ALONG SECTION PLANE "D-D"

The low density of the nickel in this specimen resulted in erosion of the channels during tooling removal and vapor spray cleaning of surfaces.

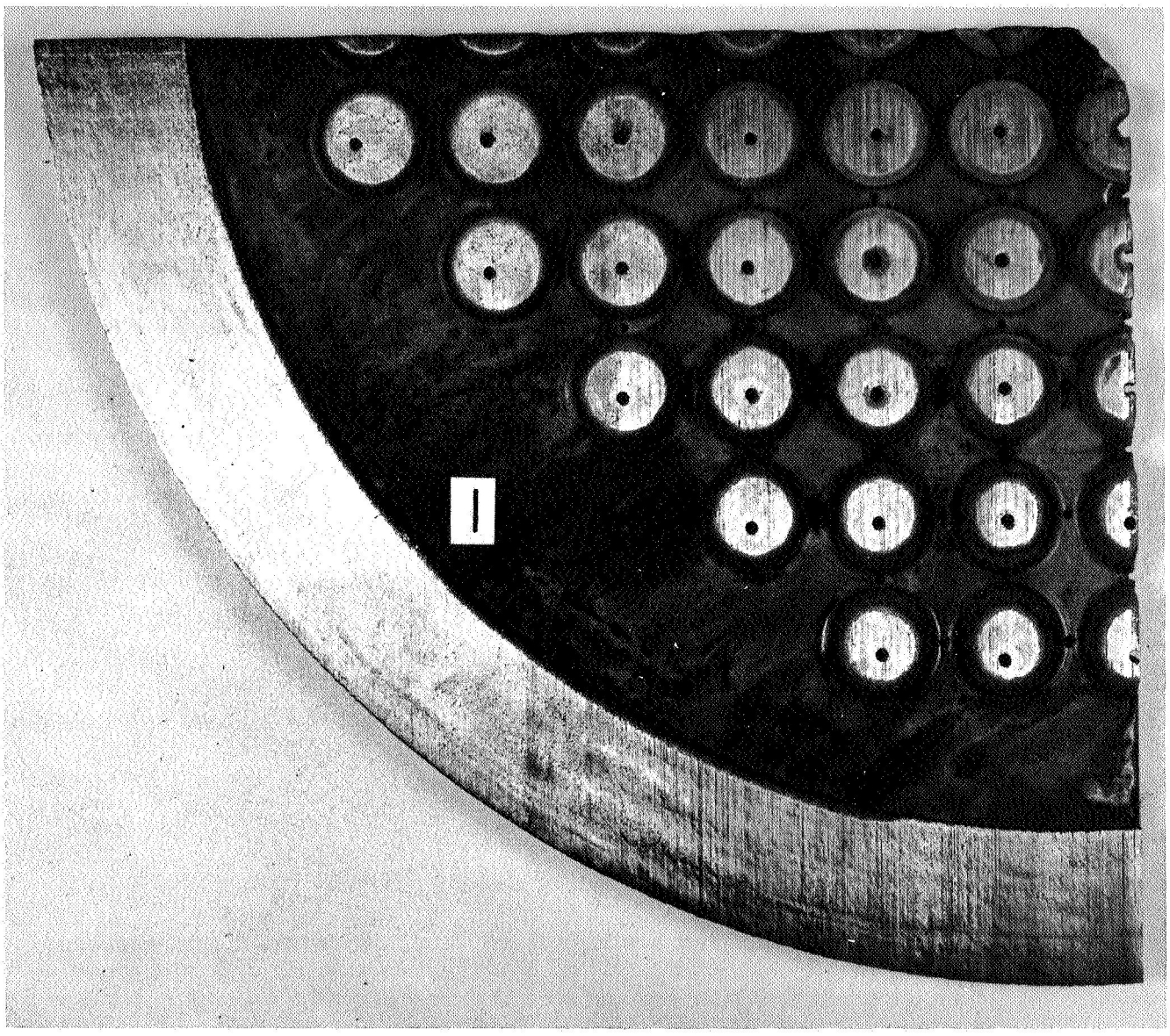

46701

FIGURE III-29. MACROSTRUCTURE OF SECTIONED NICKEL INJECTOR NO. 1 ALONG SECTION PLANE "E-E".

DISCUSSION OF RESULTS

Borosilicate glass was selected for the copper baffle tooling material because it had the best combination of properties for this application. Silica glass could not be selectively removed as quickly as borosilicate glass. The lead glass reacted with copper at 1000 F and left a rough surface in the flow channels. The borosilicate glass was stable at 1000 F and higher, did not react or interdiffuse with copper, and it left a smooth surface on the flow channels. Commercially pure aluminum required a diffusion barrier to prevent its alloying with copper; however, even with the chromium protective coating its use was limited to 1000 F. Above that temperature, the barrier deteriorated and resulted in extensive interaction between the copper and aluminum tooling. The borosilicate glass required no protective barrier and was useable to at least 1200 F. Low carbon steel was selected as a back-up tooling material for the copper baffles. While steel met all tooling requirements, it could not be removed from copper as quickly as the borosilicate glass.

Several other factors entered into the selection of the borosilicate glass as the optimum tooling material for the copper baffles. The glass could be formed and shaped to any desired configuration, and, for production purposes, casting of the tooling shapes into one or two integral pieces would be more economical than machining many separate pieces. Steel tooling had the advantage of maintaining precise dimensions during hot-isostatic compaction, but although the glass became soft at the compaction temperatures and could not retain its precise shape, the loss in precision was negligible. The only time that loss of tooling shape was significant was when the tooling reacted or alloyed excessively with the copper as did, for example, the lead glass and the chromium-coated aluminum tooling. Another factor that led to the choice of glass for the tooling was the

absence of residue products after leaching. Many potential tooling materials were eliminated because they left a residue of the products of chemical leaching. These products would have accumulated in the channels and possibly restricted or cut off the flow through the channels. The glass and steel materials could be removed from the baffle channels without any such accumulation.

Commercially pure aluminum, low carbon steel, and calcium were three materials that were selected for tooling in the nickel injectors. Low carbon steel was selected to make the tooling for full-scale simulated injectors, but the long times required to completely remove the steel from these components proved to be impractical. Otherwise, the steel was a satisfactory tooling material. It was compatible with nickel, left smooth surfaces on the flow channels, and could be selectively removed from the nickel. Aluminum was initially used with a chrome-coating for a diffusion barrier. This barrier coating was subsequently eliminated after it was determined that the nickel-aluminide intermetallics formed at the interface were effective in preventing gross reactions between the aluminum and nickel. The aluminum would have been used as the injector tooling material except for two factors. Densification of the nickel powder required that hot-isostatic compaction be conducted near the melting point of aluminum. Secondly, the brittle intermetallics formed at the nickel surfaces were considered possible sources of cracks during injector operation.

In the subscale injector specimens, the aluminum tooling deformed no more than steel tooling in corresponding parts of the specimens even though the aluminum was partially molten. The shape of the aluminum tooling was negligibly distorted. The shell of intermetallic compounds confined the aluminum and apparently contributed to maintaining its shape. However, the aluminum tooling was tried in only one subscale injector, and therefore there was no great assurance that the tooling shapes could be similarly reproduced. However, if this had been

the only objection to aluminum, a strong recommendation to make at least one full scale injector with aluminum tooling would have been justified.

The second objection to the use of aluminum tooling was the brittle aluminide layers retained on the channel surfaces after the aluminum was removed by leaching in 1N NaOH. Attempts were made to remove the aluminide layers but were not successful until after Task III was committed to the fabrication of full sized injectors with the steel tooling. The aluminum-rich aluminide layer was removed in 8N NaOH solution, and the nickel-rich aluminide layer was then removed in a 25 percent H_2SO_4 solution. Microhardness tests in the nickel near the interface showed no detectable change in hardness due to aluminum in solid solution with nickel. The amount of aluminum that is in solution with nickel is no more than 10 a/o ($\sim$ 5 w/o), and the whole Ni-Al solid solution region is contained within 0.001 in. of the interface. Thus, the only objections to the use of aluminum are: (1) it has not been used in a full scale injector and (2) a small amount of aluminum is in the solution with nickel near the interface.

Calcium was the third ranking tooling material for the nickel injectors. Its use was considered primarily because of the very fast reaction rates with tap water. The most serious objections to calcium were (1) the calcium had to be coated or encapsulated with a barrier layer to prevent reaction with the nickel during hot-isostatic compaction, and (2) calcium ingots were not available in suitable shapes to fabricate the tooling directly from the cast ingots. An iron or low carbon steel sheath proved to be an effective barrier. The real promise of calcium is in its use in the thicker parts of the tooling pieces, such as the tooling plates and the fuel-channel tooling ring. These parts could be fabricated from calcium metal, placed in a thin sheath of iron or steel, then assembled with other tooling parts fabricated from steel or aluminum. After compacting the

nickel powder around the tooling, the larger sections of the tooling can be removed very rapidly by exposing the calcium and removing it in water. This would cut down the leaching time to one-tenth compared to steel removal times and to one-half compared to aluminum removal times.

Dimensional control and alignment were factors that at first appeared to be dependent on the elevated temperature mechanical properties of the tooling material. These factors were subsequently found to be almost completely dependent on the fixturing and container design and independent of the tooling material properties. For example, the amount of bending observed in tooling pieces of three different materials within subscale baffle specimens was the same, regardless of the material. The bending in these specimens was due to anomalies in the powder flow during compaction, and not because any one tooling material had less resistance to deformation than the others. To keep the tooling in position and maintain satisfactory alignment within the powder during compaction, it was necessary to change only process procedures, the design of the fixture, the location of tooling with respect to the frames, or the container design, but not the tooling material. A typical case was the compaction of copper powder around the tooling in baffle components. Hydropressing was conducted at 20,000 psi primarily to prevent fracture of the glass tooling, but the steel and aluminum tooling deformed as much as the glass tooling during this compaction process. The glass simply cracked when it was deformed beyond its fracture strength while the aluminum and steel tooling pieces underwent permanent strain when deformed beyond the elastic limit. The amount of deformation was practically the same in each tooling material. Preventing this distortion, or at least reducing it to tolerable limits, required design changes that were common to all baffle components, regardless of tooling material. The position of the tooling within the powder had

to be aligned along a center plane that was symmetrical to the compaction direction. If the tooling was not placed within about 0.03 in. of this center plane, the tooling became warped during powder compaction. The tooling pieces near the frames were subjected to nonuniform powder flow from high density regions to low density regions. This nonuniform flow could not be eliminated, but the position of the tooling pieces could be moved out of and away from these regions. This was, in fact, the way distortion of tooling pieces in the full-scale baffle components was eliminated. A change in the tooling material would have accomplished little in this regard.

The selection of suitable temperatures, pressures, and times for hot isostatic compaction were initially based on results of hot pressing experiments conducted on copper and nickel powders. To reduce the number of experimental parameters, the pressure was fixed at 10,000 psi. Higher pressures could have been used if they had been required; the capability for higher pressures up to 15,000 psi exists so far as the fabrication of full-scale baffles and injectors is concerned. The lower temperature limit was that needed to produce a dense, metallurgically bonded structure. To densify and bond copper powder, a temperature of 1000 F was regarded as the lower limit with corresponding pressures of 10,000 psi and pressing times of at least 1 hr. Copper baffles containing glass tooling were actually compacted at 1200 F and 10,000 psi for 3 hr after determining that no adverse reactions occurred between the tooling and copper at these conditions. To densify and bond the nickel powder, a temperature of 1200 F was regarded as the lower limit with corresponding pressures of 10,000 psi and times of 3 hr. Subscale nickel injectors containing aluminum tooling were fabricated into dense, well-bonded structures at these conditions, and full size injector components with steel tooling were fabricated at 1300 F and 10,000 psi for 4 hr to dense, well-bonded structures. The temperature and time of compaction for the full sized

injectors were raised to insure that all parts of the massive structure were heated to at least the minimum conditions. The higher temperature limits were set by the tooling-base metal compatibility and the melting point of the tooling material. These higher temperatures were approached or slightly exceeded in the case of glass, which softens around 1200 F, of aluminum, which melts at about 1220 F, and calcium, which melts at about 1540 F but reacts with the base metals at lower temperatures.

The selection of the base metal powders for the copper baffles and nickel injectors was made after a large number of experiments had been performed relating powder properties to green strength, final density, final mechanical properties and microstructural characteristics. It was apparent after these tests that the most suitable powders for the fabrication of these components by hot-isostatic compaction techniques had the following common characteristics: (1) a high specific surface area, (2) a fine particle size, (3) small scatter in particle size distribution, and (4) low interparticle porosity. The first two properties produce hydropressed compacts with high green strength and enhance the rate of densification during hot-isostatic compaction. The latter two properties produce microstructures that have a uniform grain size with little or no porosity. Interparticle porosity in the loose particles is generally more difficult to remove than intergranular porosity, and while interparticle porosity would not result in interchannel leakage, such porosity does weaken the structure mechanically.

Two copper baffles were fabricated from powder having all of the four properties listed above. Although one baffle faired poorly in nondestructive and destructive testing because of high porosity, the cause of the low density (less than 90 percent of theoretical density) was not attributable to the powder but due to failure of the container enclosing the powder during the compaction

cycle. The second baffle fabricated from the same powder was successfully tested nondestructively and destructively. The copper in this baffle had mechanical properties that exceeded commercial wrought and annealed products. Its density was determined to be 98.8 ± 0.6 of theoretical. It is noted that this density agrees well with the predicted end-point densities calculated from the pressure-density curves for hot-pressed copper powder.

Two nickel injectors were fabricated from powder having just two of the four properties stipulated above. The specific surface area of the selected nickel powder was relatively low compared with other powders studied in the program, and its particle size was not as fine a grade as was available. However, its impurity content was much lower, the size distribution was more uniform, the interparticle porosity was practically nil, and the final microstructure and density in experimental fabrication cycles were better than those achieved with other nickel powders. Because of the larger particle size and low specific surface area, the selected nickel powder had little or no green strength after hydropressing at or below 30,000 psi. This proved to be no disadvantage because the hydropressing step was eventually eliminated completely. Hydropressing only contributed to tooling distortion, and the process for fabricating the injector had to be modified to eliminate the hydropressing cycle. The powder was loaded around the tooling, vibratory packed to about 57 percent of its theoretical density, then hot-isostatically compacted. The resultant density using the powder described above was better than 98 percent.

Several design changes were incorporated in the fixturing of tooling in the copper baffles to eliminate distortion and bending of the tooling. A modification in the process procedures was necessary to maintain dimensional control of

the tooling plates in the nickel injectors. In both cases, the changes were brought about by anomalies in the symmetrical loading of tooling in the powder and in the powder flow during compaction processes. Tooling distortion in the subscale copper baffles was due to restrictions in powder flow near the picture frames enclosing and fixing the tooling pieces. Tooling pieces located in this region tended to be pushed outward from the center regions as the powder in the central region densified and flowed into the less dense side regions. Also, if the powder around the tooling was loaded unequally on either side of the tooling during compaction the tooling tended to relocate along a plane that was symmetrical to the compacted powder surfaces but away from its proper location in the structure. Unequal loading of powder around the tooling could occur from several sources: (1) non-uniform vibratory packing densities; (2) unsymmetrical loading of powder adjacent to the tooling; and (3) dislocation of the tooling from its fixturing during loading or hydropressing.

The fuel-channel tooling plates in the subscale nickel injectors distorted because the plate was not symmetrically located with respect to the direction of powder flow. In the first attempt with subscale components, the fuel-channel tooling was fixed on its edge. Powder was loaded above and below this plate, and during compaction it was expected that the powder would flow through the void spaces in this plate and densify below as well as above the tooling plate. In fact, the powder did not flow through the voids. The tooling plate simply followed the flow pattern of the compacting powder. This in itself did not distort the plate. What contributed to the gross distortion was the edge fixturing of the tooling plate on the ring of low carbon steel. It was then reasoned that if the edge restraints were removed, the entire tooling plate would be free to move along with the powder during compaction. The tooling plate was thus placed on a ring of hydropressed iron powder. Some improvement was realized by this technique in the modified subscale nickel injectors, but the distortion

in tooling plate was still beyond tolerable limits. To eliminate the distortion in the fuel-channel tooling plates, the powder below the plate initially had to be compacted to a high density to provide an immoveable base upon which to assemble the fuel-channel tooling plate. The plate thus could not move any more than the dense powder below it. This procedure was adopted in Task III, and the fuel-channel locations in the full scale injectors were held to with ±0.01 in. of the specified dimensions.

Distortion of the ox-channel tooling pins was not encountered in the subscale nickel injectors but was detected during destructive testing of the full scale injector pieces. Several ox-channel tooling pieces near the rim of the injector bent outward, that is, away from the center. The cause of this distortion was similar to the tooling distortion in the subscale baffle components. Thick walled containers were used to enclose and seal the nickel powder. By comparison, the lids on the container were thin. During hot-isostatic compaction, the lids collapsed first and densified the powder adjacent to the lids. The thicker walls of the container did not collapse until later in the cycle. For a given pressure and temperature of compaction, the powder adjacent to the thick walls was less dense than the powder adjacent to the lids. This density gradient led to powder flow from the higher density regions to the lower density regions, and the ox-channel tooling pins located in the low density regions near the container wall tended to move along with the powder flow and bend outward. In regions away from the container wall, the powder flow was directed parallel to the ox-tooling pins and the pins remained straight. To prevent the pins near the container from bending, it is necessary only to reduce the wall thickness of the container. As shrinkage proceeds during hot-isostatic compaction, the powder adjacent to the wall will then compact to densities that are equivalent

to the densities of the powder adjacent to the lids. This will eliminate density gradients near the wall and will prevent tooling distortion.

Maintaining a gas-tight container around the large scale components during hot-isostatic compaction proved to be one of the problem areas that precluded successful fabrication and testing of two of the four component test pieces. Although the containers were carefully checked for pin-hole leaks and other defects in the welds and container materials, leaks developed during hot-isostatic compaction in several instances, but not from the same causes. In the first cycle with the baffle components, leaks developed in the corners of both containers where large localized deformation had occurred. One baffle was tested after this cycle but had more than 10 percent intergranular porosity in the copper matrix, and test results were unfavorable. The other baffle was recanned in a container that was designed to reduce localized deformation at the corners. This container remained gas-tight during the recycle, the copper powder compacted to very high densities, and the baffle responded very favorable during nondestructive and destructive testing.

The containers on the full scale injectors developed leaks from several sources. An indentation defect in the lid surface developed a leak in one container during the first compaction cycle. Large and localized deformation of the thin lid into a low density region near the container wall caused leaks to develop in the other container. In a subsequent cycle, a crack developed in the weld between the container wall and the lid. Inspection of the weld showed the weld bead in this area was put down without sufficient penetration. One of the injector components was tested even though a small leak had developed during the compaction cycle. It was felt the leak had developed late in the cycle after the nickel powder had achieved a sufficiently high density. However, this injector subsequently was found to have densities less than 92 percent of theoretical. The helium leak test for interchannel leakage detected apparent

leakage between the bi-propellant channels. The container around the second injector component remained gas-tight during the recycle and was successfully fabricated to densities of about 97 to 98 percent of theoretical. During the helium leak test, no interchannel leaks were detected in this injector component.

Selective removal of the internal tooling from fabricated components was not a problem that affected the performance or behavior of the components during nondestructive testing, but it did cause concern because of the long times required to completely remove all the tooling, particularly in the full scale injectors, and to a lesser extent in the full scale baffles. Leach tests showed that the glass in the baffles was removable at a rate of 0.019 in. per hr. The longest effective length of tooling in the baffles was slightly over 4 in. By leaching from both ends simultaneously, it was expected that the tooling could be completely removed in about 200 hr or less than 10 days. In one baffle, the glass was completely removed in about 17 days. In the second baffle, complete removal of the glass took three times as long. The slow leaching rate of glass in the second baffle was caused by partial closure of the channels. First, a number of the small diameter channels at the top of the baffle had been slightly, but further, reduced in diameter during hot isostatic compaction. This left an already small entrance even smaller for the leaching solution to penetrate, displace, and expel spent solution. The same problem occurred near the bottom entrances to the internal baffle channeling. Some of the copper powder had extruded into the small clearance gaps between assembled glass tooling pieces and partially closed off the flow channel. The constriction in the upper channels and the copper flashing partially closing off the lower channels were removed by injecting an etch solution for copper into the channels. The etchant opened up

the channels satisfactorily and removed 0.001 in. from the channel surfaces in the process. The removal of the remaining glass tooling was then completed within 3 additional days.

When it came to selectively removing the steel from fabricated components, the low carbon steel tooling in the nickel injectors presented a different problem. The removal rate for steel with 25 percent sulphuric acid solution was determined to be 0.008 in. per hr. The longest effective tooling length in the injector was estimated to be slightly greater than 5-5/8 in. for the ox-channel tooling system. The longest effective length of tooling in the fuel-channel tooling system was similar, about 5-7/8 in. However, the much shorter (1/4 in.) pin length in the fuel channels was removed rapidly, and central portions of this tooling plate were partially dissolved by the acid penetrating through the channel openings in the face. This reduced the effective fuel-channel tooling length to about 2 in. Due to the longer lengths of the pins in the ox-channel tooling (1-5/8 in.) the opening up of these holes through the face contributed little to reducing the effective tooling length to be leached. At best, this length could be reduced to 4 in. Thus, the fuel channel tooling was expected to be leached out within 250 hr or 11 days, while the ox-channel tooling was expected to take 500 hr or 21 days.

With the leaching apparatus used in the program, consisting of a rotary pump and centrifuge pump to recirculate the acid and force fresh acid solution into the channels, safety procedures dictated that the pumps be in operation only when attended by capable personnel. Because of cost considerations, the pumping operation was thus limited to a maximum of 10 hr per day. This provided an average of 180 hr of leaching time per month not including the time required to change and recharge the bath with fresh solution. Under these conditions, it was estimated that the fuel channel tooling could be removed in about 1-1/2 months while the ox-channel tooling would probably take about 2-3/4 months. In actuality,

the fuel-channel tooling was removed in about 2-1/2 months; the ox-channel tooling was taking about 3-1/2 months to remove completely, but leaching was terminated due to time limitations and in order to proceed to nondestructive and destructive testing.

With a suitable leaching apparatus that can be safely and economically operated 24 hr a day, the steel tooling in the nickel injectors can be completely removed in less than a month. This leaching time can be reduced considerably by (1) using aluminum tooling and removing it with 8 N NaOH solution, or (2) using calcium tooling enclosed in a steel shell for the larger sections of tooling and removing the calcium rapidly in tap water followed by removal of the remaining steel tooling shell and pins with the 25 percent H_2SO_4 solution.

CONCLUSIONS

(1) Full scale simulated rocket engine components containing intricate internal flow channels were successfully fabricated from powder around selectively removable tooling with close dimensional control. Nondestructive and destructive tests and evaluations gave very favorable results.

   (a) Pressure tests of the simulated copper baffle was successfully accomplished at hydrostatic pressures of 700 psi and higher for 5 min. The copper powder achieved densities higher than 98 percent of theoretical densities and mechanical properties that were equivalent or better than commercially pure wrought and annealed copper products.

   (b) Helium leak tests of the simulated nickel injector was accomplished with no detectable leakage between the bipropellant channel systems. The nickel powder achieved densities higher than 97 percent of theoretical density.

(2) Borosilicate glass had the best combination of properties for the tooling material used in simulated copper baffles. Low carbon steel can be used as an alternate tooling material.

(3) Low carbon steel had a reasonably good combination of properties for tooling in the nickel injector except for the slow leaching rate. The alternate tooling materials for the simulated nickel injector are (a) commercially pure aluminum, and (b) calcium. Aluminum and calcium can be selectively removed much faster than the steel tooling but are limited to the lower processing temperatures because of their melting points or adverse reactions with nickel.

(4) Dimensional control and alignment were found to be dependent only on the fixturing, the tooling location within the powder, and container design and independent of the mechanical properties of the tooling material.

(5) The most suitable powders for the fabrication of rocket engine components by hot-isostatic compaction had the following properties:

(a) a high specific surface area,

(b) a fine particle size,

(c) small scatter in the particle size distribution, and

(d) low interparticle porosity.

(6) Copper powder was compacted around the baffle tooling to 98.8 ± 0.6 percent of theoretical density by hydropressing at 20,000 psi followed by hot-isostatic compaction at 1200 F and 10,000 psi for 3 hr. The glass tooling remained dimensionally straight within ± 0.01 in. and retained adequate shape during the compaction processes.

(7) Nickel powder was compacted around the injector tooling to better than 97 percent of theoretical density by hot-isostatic compaction at 1300 F and 10,000 psi for 4 hr. The steel tooling for the fuel-channels remained dimensional straight to within ± 0.01 in. during the compaction processes. The steel tooling for the ox-channels remained straight except for a few tooling pins on the outer edge.

(8) Maintaining a gas-tight container around the simulated rocket engine components and preventing leaks from developing during hot-isostatic compaction of the powder caused unexpected difficulties, but the causes of leaks were found and corrected. Preventive measures include (a) helium leak checking of containers for small leaks, (b) inspecting the container and lids for surface defects and flaws, (c) redesigning of the container or loading scheme to prevent void spaces and preferentially low density regions adjacent to the container walls, and (d) controlling the welding

operation to ensure proper penetration and coverage of the weld along the container rim.

REFERENCES

(1) Smith, E. G., Materials Design and Fabrication Division, Battelle Memorial Institute, Unpublished Data.

DISTRIBUTION LIST FOR FINAL REPORT ON CONTRACT NAS3-11189

	Copies
National Aeronautics and Space Administration Lewis Research Center 21000 Brookpark Road Cleveland, Ohio 44135	
Attention: Contracting Officer, MS 500-313	1
Large Engine Technology Branch, MS 500-203	15
Technical Report Control Office, MS 5-5	1
Technology Utilization Office, MS 3-16	1
AFSC Liaison Office, MS 4-1	2
Library, MS 60-3	2
Howard W. Douglass, MS 500-203	1
John M. Kazaroff, MS 500-203	40
National Aeronautics and Space Administration Washington, D. C. 20546	
Attention: Code RPX	2
Code RPL	2
Scientific and Technical Information Facility P. O. Box 33 College Park, Maryland 20740	
Attention: NASA Representative Code CRT	6
National Aeronautics and Space Administration Ames Research Center Moffett Field, California 94035	
Attention: Library	1
C. A. Syvertson	1
National Aeronautics and Space Administration Flight Research Center P. O. Box 273 Edwards, California 93523	
Attention: Library	1
National Aeronautics and Space Administration Goddard Space Flight Center Greenbelt, Maryland 20771	
Attention: Library	1
National Aeronautics and Space Administration John F. Kennedy Space Center Cocoa Beach, Florida 32931	
Attention: Library	1
National Aeronautics and Space Administration Langley Research Center Langley Station Hampton, Virginia 23365	
Attention: Library	1
National Aeronautics and Space Administration Manned Spacecraft Center Houston, Texas 77001	
Attention: Library	1
National Aeronautics and Space Administration George C. Marshall Space Flight Center Huntsville, Alabama 35812	
Attention: Library	1
Keith Chandler, R-P & VE-PA	1
Jet Propulsion Laboratory 4800 Oak Grove Drive Pasadena, California 91103	
Attention: Library	1
Defense Documentation Center Cameron Station Alexandria, Virginia 22314	1
Air Force Rocket Propulsion Laboratory (RPR) Edwards, California 93523	1
Director (Code 6180) U. S. Naval Research Laboratory Washington, D. C. 20390	
Attention: H. W. Carhart	1
Air Force Aero Propulsion Laboratory Research & Technology Division Air Force Systems Command United States Air Force Wright-Patterson AFB, Ohio 45433	
Attention: APRP (C. M. Donaldson)	1
Aerojet-General Corporation P. O. Box 1947 Sacramento, California 95809	
Attention: V. Frick	1
Chrysler Corporation Space Division New Orleans, Louisiana 70150	
Attention: Librarian	1
General Electric Company Flight Propulsion Lab Department Cincinnati, Ohio 45215	
Attention: Library	1

DISTRIBUTION LIST
(Continued)

	Copies
Rocketdyne, A Division of North American Rockwell Corporation 6633 Canoga Avenue Canoga Park, California 91304 Attention: Library, Department 596-306	1
TRW, Incorporated TAPCO Division 23555 Euclid Avenue Cleveland, Ohio 44117 Attention: Library	1
United Aircraft Corporation Pratt & Whitney Division Florida Research and Development Center P. O. Box 2691 West Palm Beach, Florida 33402 Attention: Library	1
Mr. L. Jahnke General Electric Company Flight Propulsion Division Evandale, Ohio	2
Mr. Elmer Harbert Systems Research Laboratories, Inc. 500 Woods Drive Dayton, Ohio 45432	1
Mr. Edward D. Weisert North American Rockwell Corporation Rocketdyne Division 6633 Canoga Avenue Canoga Park, California 91304	2
Mr. A. J. Schulte Schulte Industries Company Box 756 Attleboro, Massachusetts 02703	1
Mr. R. E. Peebles, MS M-76 Materials Development Laboratory General Electric Company Cincinnati, Ohio 45215	2
Mr. W. A. Preston Fansteel Metallurgical Corporation 802 Spruce Lake Drive Harbor City, California 90710	2
Mr. W. E. Russell, MS 14-1 National Aeronautics and Space Administration Lewis Research Center 21000 Brookpark Road Cleveland, Ohio 44135	1
Mr. M. G. Ault, MS 105-1 National Aeronautics and Space Administration Lewis Research Center 21000 Brookpark Road Cleveland, Ohio 44135	1
Mr. R. L. Ashbrook, MS 49-1 National Aeronautics and Space Administration Lewis Research Center 21000 Brookpark Road Cleveland, Ohio 44135	1
Mr. Eugene W. Broache Defense Division Westinghouse Electric Corporation Baltimore, Maryland	1
Mr. C. F. Davies Composite Development Section Clevite Corporation 540 East 105th Street Cleveland, Ohio 44108	2
The Boeing Company Commercial Airplane Division Seattle, Washington Attention: Librarian J. F. Baisch D. F. Bulloch W. F. Spurr	1 1 1 1
Colt Industries Crucible, Incorporated Materials Research Center Box 988 Pittsburgh, Pennsylvania 15230 Attention: E. J. Dulis	1
University of California, Los Angeles 6532-B Boelter Hall Los Angeles, California 90024 Attention: Professor R. F. Bunshah	1

DISTRIBUTION LIST
(Continued)

	Copies
National Aeronautics and Space Administration Langeley Research Center Langley Station Hampton, Virginia 23365 Attention: Mr. Neal Kelly	1
The Budd Company 300 Commerce Drive Fort Washington, Pennsylvania 19036 Attention: R. C. Dethoff	1
General Dynamics Convair Division P. O. Box 1128 San Diego, California 92112 Attention: Mr. C. J. Kropp	1
The Franklin Institute Twentieth and Parkway Philadelphia, Pennsylvania 19103 Attention: Mr. H. W. Blakeslee	1
Mr. John C. Freche, MS 49-1 National Aeronautics and Space Administration Lewis Research Center 21000 Brookpark Road Cleveland, Ohio 44135	1
C & H 2525 Beech Daly Road Dearborn Heights, Michigan Attention: Nicholos Barbosa	1